PERSONALIZED MEDICINE FOR PATIENTS WITH ADVANCED CANCER

TOWARDS
TAILORED
ANTI-CANCER
TREATMENT

Salo N. Ooft

Personalized medicine for patients with advanced cancer

Towards tailored anti-cancer treatment

Salo N. Ooft

Personalized medicine for patients with advanced cancer

Towards tailored anti-cancer treatment

Gepersonaliseerde behandelstrategieën voor patiënten met uitgezaaide kanker

(met een samenvatting in het Nederlands)

Proefschrift

ter verkrijging van de graad van doctor aan de
Universiteit Utrecht
op gezag van de
rector magnificus, prof.dr. H.R.B.M. Kummeling,
ingevolge het besluit van het college voor promoties
in het openbaar te verdedigen op

dinsdag 29 september 2020 des middags te 2.30 uur

door

Salo Noël Ooft

geboren op 29 januari 1991
te Spijkenisse

ISBN: 978-94-6419-021-2
Cover: Ilse Modder | www.ilsemodder.nl
Lay-out: Ilse Modder | www.ilsemodder.nl
Printed by: Gildeprint, Enschede | www.gildeprint.nl

Promotor:
Prof. dr. E.E. Voest

Dit proefschrift werd (mede) mogelijk gemaakt met financiële steun van het Koningin Wilhelmina Fonds (KWF) en het Zwaartekrachtprogramma van het Nederlands Wetenschappelijk Orgaan (NWO)

TABLE OF CONTENTS

GENERAL INTRODUCTION AND OUTLINE OF THIS THESIS

GENERAL INTRODUCTION AND OUTLINE OF THIS THESIS

The central theme of precision medicine is designing effective therapeutic interventions for individual patients. In the era of countless treatment options and rising healthcare costs, there is a clear and unmet need to ensure a satisfactory trade-off between quality of life, healthcare costs and treatment efficacy. Currently, many anti-cancer therapies are designed to neutralize the effect of a single genetic mistake detected in the DNA of cancer patients: so-called "targeted therapies". Therefore, precision medicine in oncology has become nearly synonymous with DNA-sequencing. This is a rather one-dimensional approach to precision medicine and, as a consequence, most patient only marginally benefit from these novel treatment opportunities. A major reason for this is the context-dependency of oncogenic lesions among the thousands found in cancer genomes, and their significance for treatment outcome. Although problematic for targeted agents, this conceptual problem is even more pronounced for (combination) chemotherapies, because of their complex mechanisms of action.

Recent years have seen the adoption of novel technologies to study tumor biology, such as whole-genome sequencing and organoid culture. When cleverly combined with clinical studies and patient data, this creates an opportunity to approach the challenges of precision medicine from a new angle. In this thesis we confront the aforementioned challenges in several ways by integrative use of novel technologies, clinical studies and patient data, and propose several concepts to tailor anti-cancer treatment to individual patients.

In chapter 1 we review the current field of preclinical model systems of cancer and the development of (cancer) organoid technology, a novel culture method that allows for the establishment of tumors of individual patients in a dish. We also highlight one of the most exciting concepts: organoids as a tool for precision medicine by direct testing of drug sensitivity in patient-derived organoids (PDOs) and, thereby, providing treatment advice.

In chapter 2 we demonstrate in an observational, multicenter, clinical study the value of organoids to select metastatic colorectal cancer (mCRC) patients who benefit from certain types of chemotherapy. We develop predictive models based on organoid cultures of patient tumors, and demonstrate that *in vitro* drug sensitivity assays are excellent predictors for irinotecan-based regimens. An important observation is that the predictive value of organoids is not universal across different treatment regimens, as they fail to predict response to the combination of 5-FU and oxaliplatin (5-OX).

In chapter 3 we follow up on the question why organoids do not predict response to 5-OX *in vitro*. We hypothesized that *in vivo* models introduce several parameters that are absent *in vitro*, such as tumor stroma and systemic drug metabolism. We demonstrate that the correlation with clinical responses of patients does not improve when organoids are combined with immunocompromised mice (PDOX). Rather, we found that *in vitro* and *in vivo* drug responses of organoids to 5-OX are strongly correlated. We suggest that there is limited value for PDOX (and PDO) models in predicting clinical outcome to 5-OX.

In chapter 4 we identify two subgroups of mCRC patients, that either respond poorly or very well to a novel chemotherapeutic regimen, TAS-102 (Lon-surf). Through a combination of genomics and organoid drug assays we demonstrate that $KRAS^{G12}$ mutations predict lack of overall survival benefit on TAS-102. Conversely, in an exploratory analysis we found that patients with $KRAS^{G13D}$ mutant mCRC, an amino acid substitution just 1 codon apart from the G12 residue, have a particular poor prognosis when left untreated. However, these patients have pronounced overall survival benefit of TAS-102, which alleviates their poor prognosis. Because this hotspot mutation is tested in virtually every patient with mCRC, we foresee this precision medicine strategy can be readily implemented in clinical practice and expands on the number of effective treatment options available for mCRC patients.

In chapter 5 we apply organoid technology in a second clinical study. We set out to leverage organoids to propose additional treatment options for mCRC patients who have exhausted all other (standard-of-care) treatment lines. In a prospective, single-arm, single center feasibility trial we demonstrate that the application of organoids in this setting is rather challenging. We conclude that there is limited value for organoids in this phase 1 patient population due patient drop-out, because of a lower-than-expected culture success rate from biopsies, the poor condition of these patients and the absence of meaningful clinical responses. The observation that a strong effect in a culture dish does not necessarily translate into a clinically meaningful effect has important implications for the use of organoids in precision medicine and pre-clinical studies.

In chapter 6 we propose a new treatment strategy for non-small cell lung cancer (NSCLC) and CRC, by vertical blocking of 4 signaling nodes in the EGF-pathway. We demonstrate that multi low-dose (MLD) treatment can result in tumor control or reduction in multiple models, even ones that have previously progressed on EGFR-targeted therapy, which is common in NSCLC and CRC alike. Importantly, its modular approach can be readily applied in other tumor types and treatment settings.

In chapter 7 we discuss the concepts put forward in chapters 2-6 and their future outlook.

CHAPTER 1

TUMOR ORGANOIDS AS A PRE-CLINICAL CANCER MODEL FOR DRUG DISCOVERY

Fleur Weeber[1,#], Salo N. Ooft[1,#], Krijn K. Dijkstra[1], Emile E. Voest[1,2,3,4,5]

1. Department of Molecular Oncology; The Netherlands Cancer Institute; Amsterdam, Noord-Holland, 1066CX; The Netherlands
2. Department of Medical Oncology; The Netherlands Cancer Institute; Amsterdam, Noord-Holland, 1066CX; The Netherlands
3. Foundation Hubrecht Organoid Technology (HUB); Utrecht, Utrecht, 3584CM; The Netherlands
4. Cancer Genomics.nl; Utrecht, Utrecht, 3584 CG; The Netherlands
5. Lead contact

# Both authors contributed equally

Corresponding author: Emile E. Voest, MD/PhD (e.voest@nki.nl)

Cell Chemical Biology 2017 Sep 21;24(9):1092-1100

SUMMARY

Tumor organoids are three-dimensional cultures of cancer cells that can be derived on an individual patient basis with a high success rate. This creates opportunities to build large biobanks with relevant patient material that can be used to perform drug screens and facilitate drug development. The high take rate will also allow side-by-side comparison to evaluate the translational potential of this model system to the patient. These tumors-in-a-dish can be established for a variety of tumor types including colorectal, pancreas, stomach, prostate and breast cancer. In this review we will highlight what is currently known about tumor organoid culture, the advantages and challenges of the model system, compare it to other pre-clinical cancer models and evaluate its value for drug development.

CHALLENGES IN DRUG DEVELOPMENT

Costs of new anti-cancer drugs have surged over the past years due to, among others, the increasing complexity of clinical trials and regulatory requirements (Hay et al., 2014, Rubin and Gilliland, 2012). Meanwhile, the likelihood that a drug will reach market approval after entering phase 1 clinical testing has remained the same, and is significantly lower for anti-cancer drugs as compared to drugs in other disease areas (Hay et al., 2014, Rubin and Gilliland, 2012). When considering all indications in oncology, a mere 1 in 15 drugs that enters clinical development will reach FDA approval (Hay et al., 2014). While there are several factors that contribute to the low success rate from bench to bedside, one stands out: the translatability of pre-clinical cancer models to the patient. The difficulties of using model systems to predict drug efficacy in patients hamper not only general drug development pipelines, but also the advancement of companion diagnostics that can select subgroups of patients for treatment with molecularly targeted agents. In this review, we will discuss three-dimensional (3D) tumor organoid cultures, a novel pre-clinical model system in oncology which allows *ex vivo* propagation of tumors from individual patients. We will discuss the potential of this model system to facilitate drug discovery, and in comparison to cell lines and Patient-Derived Xenograft (PDX) models, highlight its pros and cons in the perspective of drug development.

TUMOR ORGANOIDS

Establishing the organoid culture system

Ex vivo culture of tumor cells from patients has been hampered in the past by low culture success and a limited proliferative capacity. The ability to perform long-term culture of primary colorectal cancer cells came from the fundamental discovery that healthy mouse intestinal stem cells could be propagated *in vitro* long-term using Wnt, R-spondin1, EGF and Noggin. (Sato et al., 2011, Sato et al., 2009, Clevers, 2016). Healthy intestinal stem cells formed crypt-villus-like structures in Matrigel and were able to generate all cell lineages of the gut upon withdrawal of particular medium components (Sato et al., 2011, Sato et al., 2009). Importantly, these cultures retained their normal genome over time (Sato et al., 2011, Sato et al., 2009, Behjati et al., 2014). Irrespective of its previous use to describe organogenesis experiments, the term 'organoids' was used, mainly because of the crypt-like architecture *in vitro* and the distinct resemblance to the in vivo situation (Sato et al., 2011, Sato et al., 2009, Clevers, 2016). Matrigel and a cocktail of essential stem cell growth factors, that were used to culture healthy mouse intestinal tissue, supplemented with a TGF-β receptor inhibitor (A83-01) and p38 MAPK inhibitor (SB202190), served as the basis for growth medium of healthy human intestine/colon, and eventually also for colorectal cancer organoids (Sato et al.,

2011). Subsequently, similar culture protocols were developed for healthy and malignant tissue of the pancreas (Boj et al., 2015), stomach (Bartfeld et al., 2015), prostate (Gao et al., 2014, Karthaus et al., 2014) and liver (Huch et al., 2013, Huch et al., 2015). The ability to culture patient-derived healthy and diseased cells was immediately recognized as a major breakthrough and holds potential for the transformation of biomedical research into more patient-focused approaches. Since the development of organoid culture protocols, several key papers have been published in which organoids have been used as a tool to broaden our basic understanding of cancer (Drost et al., 2015, Li et al., 2014, Matano et al., 2015, Nadauld et al., 2014). These and subsequent studies help to determine whether organoid cultures have the potential to improve drug development and clinical practice.

Culture of diverse tumor types with a high success rate

Van de Wetering et al. were the first to describe a collection of well characterized patient-derived organoids (van de Wetering et al., 2015). They report the successful culture of 20 matched healthy and tumor organoids derived from treatment-naive surgical resections with a ~90% success rate (van de Wetering et al., 2015). The unique achievement to culture tumor organoids with a nearly perfect success rate from individual primary colorectal cancers was unprecedented. Weeber et al. subsequently confirmed the feasibility to grow organoids from single 18G needle biopsy specimens of colorectal cancer metastases with a success rate of 71% (Weeber et al., 2015). Using a slightly modified protocol, Gao et al. succeeded in culturing organoids from metastatic prostate cancer tissue as well as from liquid biopsies (Gao et al., 2014). Thus far, this is the only published case in which organoid cultures from a blood sample succeeded, but may create new opportunities for minimally invasive methods to incorporate patient-derived tumor organoids in personalized medicine programs (Gao et al., 2014)". Boj et al. reported the successful culture of pancreatic adenocarcinoma organoids, a tumor type for which it is especially hard to establish cell lines, due to the large stromal component of the tumor (Boj et al., 2015)". Bartfeld et al. succeeded in culturing gastric organoids and used this to create a model system for *Helicobacter pylori* infection, elucidating the cascade of events that takes place after bacterial infection (Bartfeld et al., 2015, Bartfeld and Clevers, 2015)". The same culture conditions can also be used to culture gastric cancer organoids. In summary, organoid cultures can be established from a range of different tumor types, which paves the way for more successful drug development and precision medicine. Table 1 summarizes the success rates of establishing the various pre-clinical cancer models (organoid cultures, cell lines and PDX) of diverse tumor types.

PROOF OF CONCEPT: ORGANOIDS ARE A SUCCESSFUL TOOL FOR DRUG DEVELOPMENT IN CYSTIC FIBROSIS

Whereas the use of tumor organoids in cancer research, drug development and personalized medicine in oncology is still in its infancy, and validation studies to evaluate their potential as a model system are in progress, impressive proof of concept has already been shown for cystic fibrosis (CF) (Dekkers et al., 2016a, Dekkers et al., 2016b, Dekkers et al., 2013a, Dekkers et al., 2013b, Noordhoek et al., 2016)". Cystic fibrosis is a disease that is caused by specific mutations in the *CFTR* gene, which ultimately prevent localization of the CFTR protein to the plasma membrane (Dekkers et al., 2013b)". CFTR at the plasma membrane is necessary for homeostasis of fluids and electrolytes, and its absence results in an accumulation of viscous mucus in the gastrointestinal and pulmonary tract (Dekkers et al., 2013b)". Patients can suffer from persistent pulmonary infections, pancreatic insufficiency, malnutrition, and have a limited life expectancy (Dekkers et al., 2013b)". The pharmaceutical industry has developed small molecule inhibitors that can restore the function of mutant CFTR proteins by mutation-specific drug targeting. However, in clinical practice, these compounds have varying responses in patients, suggesting that more factors contribute to drug response than the genetic constitution of *CFTR* alone. Dekkers et al. have applied organoid culture conditions to rectal tissue of patients suffering from cystic fibrosis and have made the observation that forskolin (a cyclic AMP agonist) leads to swelling of healthy rectal organoids, but not of organoids from CF patients (Dekkers et al., 2013b)". This absence of forskolin-induced swelling in CFTR-deficient organoids could be reversed by CFTR-restoring compounds and has resulted in follow-up studies, where it was shown that this platform was very apt at predicting drug response in patients (Dekkers et al., 2016a, Dekkers et al., 2016b, Noordhoek et al., 2016)". Presently, rectal organoids of individual CF patients are used for drug discovery to identify novel, promising CFTR-restoring compounds, but also to determine which pre-existent small molecule inhibitor works best in the individual patient, especially those with rare uncharacterized *CFTR* mutations (Dekkers et al., 2016a, Dekkers et al., 2016b, Noordhoek et al., 2016)". Furthermore Vidovic et al. have used CRISPR/Cas9 technology in CF mutant organoids to genetically engineer and restore CFTR function (Vidovic et al., 2016)". Using rectal organoids from CF patients, Schwank et al. have also shown that the defective *CFTR* gene could be replaced by a functional copy using CRISPR/Cas9 (Schwank et al., 2013)". Since the complete lining of the gastrointestinal tract is affected, as well as other organ systems, this is presently not a viable treatment strategy for CF patients, but it does demonstrate that gene therapy in (gastro)-intestinal organoids is feasible.

In the field of cystic fibrosis, organoids have created a unique opportunity for drug development. The challenge ahead is now to employ tumor organoids in drug development.

However, whereas cystic fibrosis is a mono-genetic disease, cancer genetics is infinitely more complex. The practical and theoretical challenges of organoids in drug discovery for cancer will be discussed in the next paragraph.

CRITICAL APPRAISAL OF TUMOR ORGANOIDS COMPARED TO OTHER EXPERIMENTAL TUMOR MODELS

Genetic and phenotypic representation of original tumor

Organoid cultures offer great promise as a pre-clinical cancer model to improve drug development. First of all, organoid cultures closely recapitulate the genetic and morphological heterogeneous composition of the cancer cells in the original tumor (van de Wetering et al., 2015, Weeber et al., 2015). Van de Wetering et al. have shown that primary tumors that were put in culture gave rise to large numbers of different primary organoids (10-1000) suggesting that the heterogeneous composition of the original tumor was largely conserved (van de Wetering et al., 2015). The heterogeneous nature of the culture was also confirmed by transcriptome analysis of single organoids, which each gave rise to different expression profiles (van de Wetering et al., 2015). Histological analysis and DNA sequencing demonstrated a high concordance in morphology and mutational profile of the tumor organoids and matched patient tumor (van de Wetering et al., 2015). The mutational profile also showed a similar distribution when compared to the mutational spectrum for CRC included in the TCGA (The Cancer Genome Atlas), suggesting that in this set of 20 organoids the genetic diversity of CRC was captured (van de Wetering et al., 2015). Furthermore, RNA sequencing demonstrated that different subtypes of CRC could be cultured as organoids (van de Wetering et al., 2015). Weeber et al. have corroborated these findings for colorectal cancer, reporting that analysis of the original tumor and matched organoid cultures demonstrated a 90% concordance of somatic mutations, and a correlation between copy number profiles of 0.89 (Weeber et al., 2015). The most important observation however, was that none of the discordant findings affected driver genes, or concerned actionable events (Weeber et al., 2015). A similar observation was done by Fujii et al. who also report that no discordant mutations were found in drivers (Fujii et al., 2016). Schutte et al. have reported a high degree of genetic concordance between primary colorectal cancer and matched patient-derived colorectal cancer organoids, where only 3% of divergent mutations concerned relevant cancer genes (Schutte et al., 2017). Transcriptome analysis and subsequent unsupervised hierarchical clustering however identified three main molecular groups in patient material, as opposed to two main molecular groups for matched patient-derived tumor organoids (Schutte et al., 2017). Whereas this observation was similar in PDX, patient-derived tumor organoids also displayed unique expression of the stem cell marker ALDH1A1 and components of carbohydrate, steroid, retinoid and fatty acid

metabolism (Schutte et al., 2017). Boj et al. have found that their pancreatic adenocarcinoma organoid model reflected *in vivo* disease progression, based on transcriptomic and proteomic analyses of organoids established from tissue at different stages of malignant transformation (Boj et al., 2015). Duarte and Gogola et al. have generated mammary tumor organoids from genetically modified BRCA deficient mice "Duarte and Gogola et al. 2017; unpublished data". They have shown that copy number profiles of mammary tumor organoids better resembled the parental tumor than 2D cell lines derived from the same tumor "Duarte and Gogola et al. 2017; unpublished data".

Maintenance of heterogeneity in culture

The maintenance of tumor heterogeneity in culture is a factor that is often underestimated in genotype-phenotype relationships and likely a critical factor in the failure of many targeted agents (Russo et al., 2016, Turner and Reis-Filho, 2012). Whereas tumor organoids display genetic and phenotypic heterogeneity upon start of culture, it is not clear to what extent this heterogeneity is maintained over time (Fujii et al., 2016, van de Wetering et al., 2015, Weeber et al., 2015). It has been reported that early and late passage organoids displayed essentially the same mutation pattern (Schutte et al., 2017). We do know however, that particular oncogenic mutations can provide tumor cells with a competitive advantage over others *in vivo* and this is also imaginable *in vitro* (Snippert et al., 2014, Vermeulen et al., 2013). Barcode studies investigating clonal dynamics in tumor organoids cultures have not been conducted yet, but fluorescent labeling of tumor organoid cultures demonstrated that cultures were dominated by a single color after 30-40 days, indicating a drift towards clonality (Fujii et al., 2016). As with all cancer models, this aspect has to be taken in to account. Another aspect that can influence genetic composition of the organoids is the medium composition used for culture. For some CRC samples, standard culture medium appeared to be suboptimal for growth and required specific adaptations, such as culture under hypoxic conditions or removal of p38 MAPK inhibitors from the medium (Fujii et al., 2016). Examples that actually exploited condition-dependent clonal outgrowth of oncogenic mutations *in vitro* were demonstrated by Drost et al. and Matano et al. (Drost et al., 2015, Matano et al., 2015). Both research groups selected mutated clones by retracting medium factors such as Wnt, R-spondin1, EGF and Noggin (Drost et al., 2015, Matano et al., 2015). This suggests that deprivation of essential growth factors favors the outgrowth of mutant clones that can grow independent of one of these factors.

How is tumor heterogeneity maintained in other model systems? Gene expression analysis between solid tumors and corresponding cell lines have previously demonstrated significant differences (Stein et al., 2004, Szakacs and Gottesman, 2004). Also, cell lines often do not cover the full genetic spectrum of tumor types. Genetic analysis of both tumors and cell lines

have shown that common mutations can be preserved in cell lines, whilst rarer mutations are frequently not represented (Iorio et al., 2016). Classical cell line culture methods can also induce significant selection pressure on tumor cells: only cells that are able to grow in common culture conditions are able to survive. This can result in a misrepresentation of the original tumor and therefore non-physiological responses. It has been demonstrated in genetic barcode studies in cell lines that complexity is progressively lost (Porter et al., 2014). This suggests that a polyclonal pool of cells will turn into a multi- or monoclonal population over time. Interestingly, Porter et al. show that barcode complexity is better preserved when cell lines are subcutaneously injected in mice (Porter et al., 2014). This has important implications for cell lines and *in vitro* models in general and can partly explain the limited translational value of cell line data (Begley and Ellis, 2012, Stein et al., 2004, Szakacs and Gottesman, 2004). Firstly, it implies that the genetic composition and subsequent cell behavior *in vitro* can change over time. Secondly, it suggests that genetic diversity can be better preserved in favorable niches, such as the subcutaneous environment for PDX. To formally investigate clonal dynamics of tumor organoids after serial passaging, barcode studies, similar to those performed for PDX and cell lines, are warranted.

Drug response

Of course, whilst maintenance of genotypic and phenotypic features does inform us about the translational potential of these cancer models, correlating drug sensitivity data and clinical or genomic data is more informative. Whereas cell lines have many practical advantages and have long been the primary source to study drug responsiveness and find novel drug targets, the question has always remained if *in vitro* cell line findings translate to the clinic (Borst, 2012). Patient-Derived Xenografts (PDXs) closely recapitulate the genotype and phenotype of patient tumors at establishment (Hidalgo et al., 2014). Furthermore, intra-tumor clonal architecture is largely conserved in PDX after serial passaging (Bruna et al., 2016). The PDX approach has previously shown its high degree of translatability to the patient and provided an effective means to study resistance mechanisms and design novel treatment combinations. Bertotti et al. and Zanella et al. have demonstrated that HER2 or IGF2 overexpression attenuates the effect of cetuximab in CRC, resulting in novel treatment strategies to overcome unresponsiveness to cetuximab (Bertotti et al., 2011, Leto et al., 2015). Gao et al. performed high-throughput drug screening on ~1000 PDX with 62 treatments and demonstrated reproducibility as well as associations between genotype and drug response (Gao et al., 2015). PDX have also helped personalized medicine programs. Hidalgo and colleagues generated PDXs of individual patients and tested these against a range of clinically approved compounds and combinations. PDX-guided treatment resulted in an impressive 88% response rate (Hidalgo et al., 2011). Despite a small sample size, these successful efforts to directly select treatment for the individual patient underscore the translatability and

potential of PDX. But while significant successes have been achieved with PDX, this platform also has shortcoming as it does not lend itself for high throughput screens, is very costly, and it is a lengthy process to establish tumors in mice. Altogether these disadvantages make PDX less suited for drug discovery, but PDX do offer opportunities to confirm findings from high throughput *in vitro* studies.

How do tumor organoids compare to cell lines and PDX models? Studies examining drug sensitivity of organoids have thus far shown drug responsiveness in line with the molecular profile of the tumor. Van de Wetering et al. performed a drug screen with a panel of 83 compounds in colorectal cancer organoids, and demonstrated that loss-of-function *TP53* mutants were insensitive to MDM2 inhibition and *RAS* mutants resistant to EGFR inhibition. They also identified a potential treatment strategy for *RNF43* mutant colorectal cancer, as it was shown that *RNF43* mutant organoids are exquisitely sensitive to Wnt secretion inhibitors (van de Wetering et al., 2015). Gao et al. studied drug response in blood- and tissue- derived prostate cancer organoids, and also observed that it matched the expectations considering the molecular background of the tumor (Gao et al., 2014). An androgen-receptor (AR) amplified organoid line was significantly more sensitive to enzalutamide (an AR inhibitor), compared to wild type lines (Gao et al., 2014). Of course, medium components of the organoid culture model may significantly influence drug response to various compounds. For example, high concentrations of EGF may compete with EGFR inhibitors, and apoptosis inhibitors such as the p38 MAPK inhibitor could have a more general effect on drug response. Additionally, other extra-cellular factors derived from the tumor micro-environment might also contribute to discrepancies between the drug response of organoids, other model systems and the clinical response. Duarte and Gogola et al. describe the generation of mammary carcinoma organoids from BRCA-deficient mouse tumors, which show differential response to PARP inhibition "Duarte and Gogola et al. 2017; unpublished data". Interestingly, the authors describe a case in which organoids derived from an *in vivo* resistant tumor was sensitive *in vitro*, likely caused by a cell-extrinsic resistance mechanism "Duarte and Gogola et al. 2017; unpublished data". This suggests that in some cases the drug response of a mouse tumor can't be captured by tumor organoids, highlighting a shortcoming of the organoid platform. Additional studies comparing the drug response of organoids *in vitro* with organoids transplanted in mice, or the clinical response of a patient from which the organoids were derived, will shed light on the importance of this issue. Verissimo et al. showed the causal relationship between $KRAS^{G12D}$ and resistance to the combination of pan-HER and MEK inhibition (Verissimo et al., 2016). This combination led to a cell cycle arrest in $KRAS^{G12D}$ organoids, as opposed to cell death in $KRAS^{wt}$ tumor organoids (Verissimo et al., 2016). The addition of a BCL-2 inhibitor abrogated resistance to the combined pan-HER and MEK inhibition, which was also confirmed in a PDX model. This was especially interesting, as previous preclinical research using cell line models

had concluded the opposite. More specific, the combination of MEK and pan-HER inhibition was synergistic in *KRAS* mutant CRC and NSCLC cell lines (Sun et al., 2014). Based on these findings in cell lines, combined MEK and pan-HER inhibition is currently tested in patients with colorectal, lung and pancreatic cancer harboring a *KRAS* mutation. Results of these trials are still pending and might provide insight in the predictive value of these model systems.

Drug-genotype correlations

To investigate drug-genotype correlations, organoids pose a good platform for mechanistic studies. Several groups have successfully used CRISPR/Cas9 technology to investigate oncogenic transformation and model tumorigenesis (Drost et al., 2015, Li et al., 2014, Matano et al., 2015, Nadauld et al., 2014). Drost et al. and Matano et al. utilized CRISPR/Cas9 to study tumorigenesis by generating various combinations of mutated backgrounds in healthy organoids harbouring loss of APC, TP53 and/or SMAD4 and activating mutations in KRAS and PIK3CA (Drost et al., 2015, Matano et al., 2015). Duarte and Gogola et al. used CRISPR/Cas9 to investigate the mechanism behind PARP inhibitor response in BRCA1 deficient mammary tumors "Duarte and Gogola et al. 2017; unpublished data". These and other studies illustrate the ease of using organoids as a model system to study causal relationships, because organoids can be conveniently manipulated with state-of-the art technologies. This will facilitate studies investigating the influence of mono- or polygenetic events in relevant patient material.

The issue with numbers

There are large collections of PDX models to support drug testing in patient-derived tumors. Similarly, tumor organoids are excellently positioned to establish "living" biobanks with large numbers of different patient-derived organoid cultures. The importance of such a living biobank is highlighted in a review by Wilding and Bodmer who state that even in studies that have used an extensive number of cell lines in their drug screens, the exact numbers for each type of cancer, let alone a subtype, remain relatively low (Wilding and Bodmer, 2014). Taking into account the distribution of molecular characteristics within tumor types and drugs with small effect sizes, makes it nearly impossible to detect drug sensitivity patterns (Wilding and Bodmer, 2014). Of most tumor types we do not generally possess such a large collection of cell lines, and the enormous amount of time and resources that is related to working with PDX, prevents large scale screens using this model system (Wilding and Bodmer, 2014). Organoid libraries can be expanded to include considerable numbers of patients (>100), and can facilitate the identification of drug sensitivity profiles for small subsets of patients with significant results. In addition, organoids can be established from healthy tissue with a nearly perfect take rate (if there is enough starting material), enabling toxicity screening (to predict potential side-effects) as well as tumor drug sensitivity screening for the same patient.

Variable growth rate

A potential caveat for the use of organoids in drug development, that is also encountered in other *in vitro* models, is their variable growth rate. Variation in growth rate can confound pharmacological parameters such as IC50s from dose-response curves (Hafner and Niepel, 2016, Harris et al., 2016). Although inter- and intra-organoid growth variation can mask drug effects, new metrics have been proposed that correct for this confounding factor. By performing baseline and/or synchronous measurements in time, one can obtain a more accurate picture of the relative drug response of tumor cells (Hafner and Niepel, 2016). The growth rate inhibition metric (GR) and drug-induced proliferation rate (DIP) both incorporate these measurements in single metrics in order to better determine and compare drug-sensitivity *in vitro* (Hafner and Niepel, 2016, Harris et al., 2016). The potential value of these corrections can be illustrated by the obvious clinical response of *HER2*-amplified breast cancer patients to EGFR/HER2 inhibition, compared to patients with other breast cancer subtypes (Hafner and Niepel, 2016). This effect cannot be distinguished *in vitro* when comparing the IC50s of *HER2*-amplified cell lines with the IC50s of other breast cancer lines upon EGFR/HER2 inhibition (Hafner and Niepel, 2016), but only becomes apparent when corrected for the different growth rate of these cell lines.

Overgrowth of normal epithelial cells

A distinct challenge in the establishment of tumor organoids is the potential contamination with and subsequent overgrowth of normal epithelial tissue in the culture. Whereas in colorectal tumor organoids several "tricks", such as the modification of medium factors necessary for the ex vivo propagation of normal tissue, can be applied to remove normal organoids, in some other cultures this has proven to be more difficult. Cultures of primary prostate tumors have thus far failed to yield "pure" tumor organoids when derived from the primary prostate cancer. In lung cancer where field cancerization of the epithelial tract is a common phenomenon this may also prove to be a challenge (Karthaus et al., 2014). It is unclear why normal tissue has a growth advantage over tumor cells. An increased rate of apoptosis in cancer cells due to their genetically instable nature has been proposed as a possible explanation, but other factors such as culture supplements may also play a role (Karthaus et al., 2014).

Stromal and immune compartment

Even though tumor organoids are a closer, heterogeneous representation of an in vivo tumor than tumor cell lines, it remains a model system exclusively comprised of epithelial cells but lacking other cell types present in the tumor micro-environment. The tumor micro-environment may significantly (positively or negatively) affect drug response, which is an additional explanation for discrepancies between drug sensitivity *in vitro* and *in vivo*

(Junttila and de Sauvage, 2013). Co-culture of epithelial cells and stromal cells is possible and can promote growth of malignant or untransformed epithelial cells (Liu et al., 2012, Ootani et al., 2009). Furthermore, co-culture of mouse intestinal organoids with intraepithelial lymphocytes (IELs) is possible, and IELs were shown to be highly motile, dynamically entering and egressing from organoids (Nozaki et al., 2016). Stiffness of the extracellular matrix (ECM) affects organoid formation, differentiation and also drug response (Gjorevski et al., 2016, Liu et al., 2015). It will be important to further develop co-culture systems of human tumor organoids with stromal cell types to reconstitute an in vivo tumor. Although this could be achieved with commercially available cell lines, it is far more appealing to use cells from the same patient from whom the organoid is derived from. The latter approach has the advantage of capturing heterogeneity in the stromal compartment between patients, but may suffer from limitations in access to or expansion of such cells. Of note, while attempts to reconstruct the micro-environment *in vitro* may yield valuable new test systems, in some situations an in vivo model, such as PDX or genetically engineered mouse models (GEMM), may initially be more suitable.

Taken together, early studies have demonstrated the feasibility of growing tumor organoids from individual patients, have molecularly characterized organoid cultures at different levels and demonstrated the preservation of numerous characteristics between patient-derived tumor organoids and the original tumor. This has ignited great enthusiasm for the potential of this new technique to detect drug-genotype correlations and hence its use as a platform for drug discovery. What makes organoid technology very exciting however, is the potential to adequately assess the clinical relevance of *in vitro* findings. Cell lines and PDX for most tumor types have low to mediocre take or growth rates, preventing large scale comparison and calibration to the patient. Because organoids can be established on a single patient basis, we are able to compare the drug response of this model system to the patient, and if found representative, this could be used as a filter before embarking on clinical trials.

BIOBANKING EFFORTS AND VALIDATION STUDIES

Biobanking efforts

With the ability to create organoids from individual tumors, the gigantic clinical diversity of cancer can be introduced in the laboratory. Large efforts are therefore undertaken to make organoids available to the scientific community. The first is the establishment of a large collection of these cultures, the Hubrecht Organoid Technology (HUB) "living" biobank. The HUB is also part of the Human Cancer Models Initiative (HCMI) collaborating with The National Cancer Institute (NCI), Cancer Research UK, and the Wellcome Trust

Sanger Institute, to develop approximately 1,000 cancer cell models that better represent the hallmarks and diversity of human cancer. The HUB biobank collects and generates organoids of tumor tissue of patients with for example breast, colorectal, lung, pancreatic and prostate cancer. These cultures are then extensively analyzed by genome sequencing and expression profiling. Furthermore, baseline clinical data are also collected for every included patient, and all organoids undergo an extensive screen to analyze drug sensitivity to a vast array of anti-cancer drugs. This well-characterized library of cultures and corresponding clinical data has been created to aid basic research, find leads for new compounds, help explore novel therapeutic strategies, and is accessible to both industry and academia. However, the true value of tumor organoids in drug screening and precision medicine still needs to be determined. This will require an extensive comparison of the drug response of organoids *in vitro* with the response of the tumor in the patient.

If the use of tumor organoids as a clinical decision-making tool can be validated, two applications will be of great interest. First, to determine upfront the success of a treatment to avoid unnecessary side effects for patients and reduce costs of health care by limiting the use of expensive medication. Secondly, to support drug development in the setting of early clinical trials.

Comparing treatment response in vitro and of the patient

To evaluate if patient-derived tumor organoids recapitulate drug response in the patient, a large prospective observational cohort study has been initiated by our group. In this multicenter cohort study, the TUMOROID trial (NL49002.031.14), patients with metastatic colorectal, breast or non-small cell lung cancer are included before they start with standard of care treatment. The primary objective of this study is to determine whether standard of care treatment responses of organoids predict treatment responses of patients. Since metastases have genetically evolved over time all patients undergo a pre-treatment biopsy procedure of a metastatic lesion for organoid culture. Subsequently, clinical response data are collected and correlated with the in vitro organoid response. This test will first focus on establishing a high negative predictive value because this addresses one of the biggest challenges in the clinical care for patients: over-treatment with anti-cancer drugs. However, mimicking chemotherapy in vitro is not trivial, given vast differences in pharmacokinetics and drug dosing regimens between a patient undergoing treatment and an in vitro drug assay. Previous studies in cell lines have shown that timing and duration of drug exposure can be of significant influence for the measure of cytotoxicity *in vitro* (Fischel et al., 1998). Fischel and colleagues have shown that the type of fluorouracil exposure (continuous, mixed or short), as well as timing of oxaliplatin (before, during or after exposure to fluorouracil and folic acid) significantly altered drug sensitivity of the cells (Fischel et al., 1998). However, the

fact that tumor organoids can be cultured indefinitely provides the opportunity to modify various dosing schemes *in vitro* in such a way that it generates an approach where outcome matches clinical responses of patients.

Selecting treatment using patient-derived tumor organoids

Patient-derived tumor organoids can also be used to select individual patients for novel targeted therapies. The past decade, the pharmaceutical industry has developed a wide array of molecularly targeted agents. However, even though the target at which a particular drug acts is known (e.g. PI3K inhibitor), this does not necessarily mean that patients with a molecular alteration in the pathway (e.g. PIK3CA mutation) will be susceptible to this treatment (Voest and Bernards, 2016). To fully elucidate which targeted agents match which molecular profile, large and costly prospective biomarker studies and basket trials are needed. In general this contributes to the low success rate of drug development in oncology. A functional assay, such as patient-derived tumor organoids, may guide and improve drug development. Therapeutic agents are often discarded due to presumed inactivity, whilst it could also be that the drug was not tested in the appropriate patient group, because the drug in question has a small target population. To test whether patient-derived tumor organoids can help to select patients for targeted therapy, a prospective clinical proof of concept study has been initiated by our group (SENSOR study, NL50400.031.14 Eudract 2014-003811-13). Patients with metastatic colorectal cancer and NSCLC are recruited before they initiate their last standard of care (SOC) treatment line. Tumor biopsies are retrieved at inclusion, cultured as organoids, and tested for 8 different targeted treatments. When one of these agents is active *in vitro* the patient is offered this experimental treatment. If successful this approach may facilitate drug development. Taken together, these two studies will broaden our knowledge of this new technology, and will answer the question whether 3D organoid cultures can be translated to the patient setting. This paragraph is also summarized in figure 1.

To conclude, tumor organoids provide new opportunities for drug development. The ability to culture organoids from every individual patient and their close resemblance to the original tumors suggest that organoids hold the promise of a more representative and clinically relevant model system compared to cell lines for drug discovery and precision medicine.

Table 1 – Success rates of establishing pre-clinical cancer models for diverse tumor types

Tumor type	Success rate to establish:			References
	PDX	Cell lines	Organoid cultures	
Breast	3-21%	17-46%*	79-91%*	"Zhang et al. 2013" "Duarte and Gogola et al. 2017"
Colorectal	77%	10%	>90%, 71%#	"Dangles-Marie et al. 2007" "Weeber et al. 2015" "Van de Wetering et al. 2015"
Pancreas	54-100%	9%	75-83%	"Byrne et al. 2017" "Rückert et al. 2012" "Boj et al. 2016"
Prostate	39%^	7 cell lines established to date	15-20%#	"Lin et al. 2014" "Gao et al. 2014"

This table illustrates the reported success rates to establish pre-clinical cancer models for 4 tumor types. The pre-clinical cancer models incorporated in the table include organoid cultures, cell lines and PDX. Take rates in the table pertain to human primary tumors, unless otherwise specified. For some tumor types, culture protocols are currently further optimized. Derived from: * mouse tumors; # metastatic biopsy specimens; ^ primary tumors and metastases

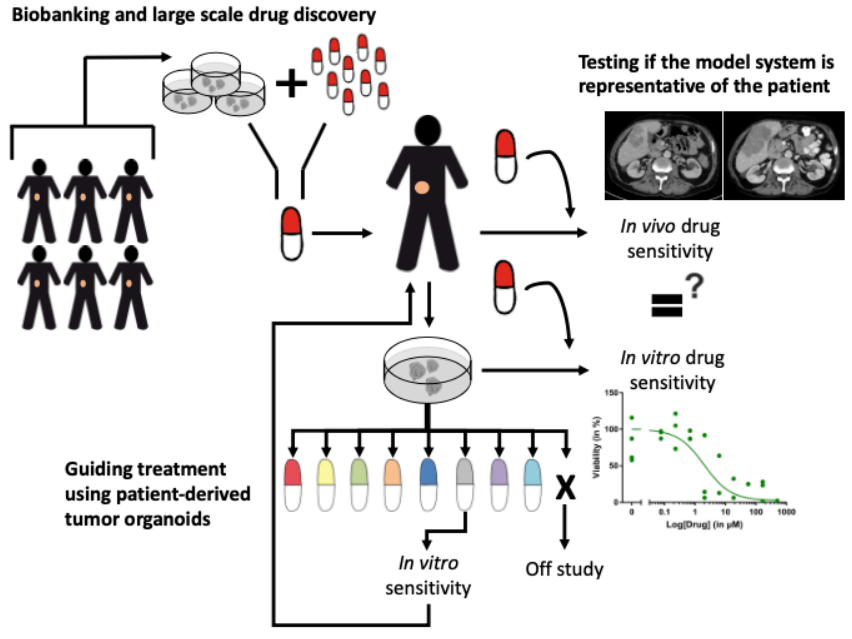

Figure 1 – Patient-derived tumor organoids and their applications

This figure summarizes the potential of patient-derived tumor organoids. Because of their high culture take rate, they can be used to establish large and well characterized biobanks that comprise the entire spectrum of molecular subtypes per tumor type. This can facilitate large scale drug screening efforts. Furthermore, organoids lend themselves for a drug sensitivity comparison to the individual patient responses because of their high take rates. Finally, patient-derived tumor organoids have the potential to select therapy for the individual patient, if there are no regular treatment options left.

SIGNIFICANCE

Drug development in oncology is hampered by the lack of representative model systems that can recapitulate all essential components of the patient's tumor. With the addition of a new technique, tumor organoid culture, to our repertoire of pre-clinical cancer models, it is important to evaluate the translational potential of this new model system. This model system has the potential to improve drug development by better discriminating, in an early stage, which drugs are effective, and for which indications, also serving as a selection assay in precision medicine. Here, we have reviewed current literature on organoid model systems and compared it to pre-existing models such as cell lines or PDX. We have also described the efforts that are currently ongoing to evaluate the clinical translatability of the organoid culture model and biobanking initiatives.

Author contributions

F.W., S.O., K.D., and E.V. were involved in the design of the manuscript, review and interpretation of the literature and writing of the manuscript.

Acknowledgements

We would like to thank Piet Borst from the Netherlands Cancer Institute for a critical review of the manuscript. Also, we would like to thank Alexandra Duarte and Ewa Gogola for access to their manuscript, which is currently under review, in order to incorporate their findings. The authors report no financial conflict of interest, however we would like to disclose that Emile Voest is co-founder of the HUB and former non-executive board member.

REFERENCE LIST

BARTFELD, S., BAYRAM, T., VAN DE WETERING, M., HUCH, M., BEGTHEL, H., KUJALA, P., VRIES, R., PETERS, P. J. & CLEVERS, H. 2015. In Vitro expansion of human gastric epithelial stem cells and their responses to bacterial infection. *Gastroenterology,* 148**,** 126-136 e6.

BARTFELD, S. & CLEVERS, H. 2015. Organoids as Model for Infectious Diseases: Culture of Human and Murine Stomach Organoids and Microinjection of Helicobacter Pylori. *J Vis Exp*.

BEGLEY, C. G. & ELLIS, L. M. 2012. Drug development: Raise standards for preclinical cancer research. *Nature,* 483**,** 531-3.

BEHJATI, S., HUCH, M., VAN BOXTEL, R., KARTHAUS, W., WEDGE, D. C., TAMURI, A. U., MARTINCORENA, I., PETLJAK, M., ALEXANDROV, L. B., GUNDEM, G., TARPEY, P. S., ROERINK, S., BLOKKER, J., MADDISON, M., MUDIE, L., ROBINSON, B., NIK-ZAINAL, S., CAMPBELL, P., GOLDMAN, N., VAN DE WETERING, M., CUPPEN, E., CLEVERS, H. & STRATTON, M. R. 2014. Genome sequencing of normal cells reveals developmental lineages and mutational processes. *Nature,* 513**,** 422-5.

BERTOTTI, A., MIGLIARDI, G., GALIMI, F., SASSI, F., TORTI, D., ISELLA, C., CORA, D., DI, N. F., BUSCARINO, M., PETTI, C., RIBERO, D., RUSSOLILLO, N., MURATORE, A., MASSUCCO, P., PISACANE, A., MOLINARO, L., VALTORTA, E., SARTORE-BIANCHI, A., RISIO, M., CAPUSSOTTI, L., GAMBACORTA, M., SIENA, S., MEDICO, E., SAPINO, A., MARSONI, S., COMOGLIO, P. M., BARDELLI, A. & TRUSOLINO, L. 2011. A molecularly annotated platform of patient-derived xenografts ("xenopatients") identifies HER2 as an effective therapeutic target in cetuximab-resistant colorectal cancer

445. *Cancer Discov,* 1**,** 508-523.

BOJ, S. F., HWANG, C. I., BAKER, L. A., CHIO, II, ENGLE, D. D., CORBO, V., JAGER, M., PONZ-SARVISE, M., TIRIAC, H., SPECTOR, M. S., GRACANIN, A., ONI, T., YU, K. H., VAN BOXTEL, R., HUCH, M., RIVERA, K. D., WILSON, J. P., FEIGIN, M. E., OHLUND, D., HANDLY-SANTANA, A., ARDITO-ABRAHAM, C. M., LUDWIG, M., ELYADA, E., ALAGESAN, B., BIFFI, G., YORDANOV, G. N., DELCUZE, B., CREIGHTON, B., WRIGHT, K., PARK, Y., MORSINK, F. H., MOLENAAR, I. Q., BOREL RINKES, I. H., CUPPEN, E., HAO, Y., JIN, Y., NIJMAN, I. J., IACOBUZIO-DONAHUE, C., LEACH, S. D., PAPPIN, D. J., HAMMELL, M., KLIMSTRA, D. S., BASTURK, O., HRUBAN, R. H., OFFERHAUS, G. J., VRIES, R. G., CLEVERS, H. & TUVESON, D. A. 2015. Organoid models of human and mouse ductal pancreatic cancer. *Cell,* 160**,** 324-38.

BORST, P. 2012. Cancer drug pan-resistance: pumps, cancer stem cells, quiescence, epithelial to mesenchymal transition, blocked cell death pathways, persisters or what? *Open Biol,* 2**,** 120066.

BRUNA, A., RUEDA, O. M., GREENWOOD, W., BATRA, A. S., CALLARI, M., BATRA, R. N., POGREBNIAK, K., SANDOVAL, J., CASSIDY, J. W., TUFEGDZIC-VIDAKOVIC, A., SAMMUT, S. J., JONES, L., PROVENZANO, E., BAIRD, R., EIREW, P., HADFIELD, J., ELDRIDGE, M., MCLAREN-DOUGLAS, A., BARTHORPE, A., LIGHTFOOT, H., O'CONNOR, M. J., GRAY, J., CORTES, J., BASELGA, J., MARANGONI, E., WELM, A. L., APARICIO, S., SERRA, V., GARNETT, M. J. & CALDAS, C. 2016. A Biobank of Breast Cancer Explants with Preserved Intra-tumor Heterogeneity to Screen Anticancer Compounds. *Cell,* 167**,** 260-274.e22.

CLEVERS, H. 2016. Modeling Development and Disease with Organoids. *Cell,* 165**,** 1586-97.

DEKKERS, J. F., BERKERS, G., KRUISSELBRINK, E., VONK, A., DE JONGE, H. R., JANSSENS, H. M., BRONSVELD, I., VAN DE GRAAF, E. A., NIEUWENHUIS, E. E., HOUWEN, R. H., VLEGGAAR, F. P., ESCHER, J. C., DE RIJKE, Y. B., MAJOOR, C.

J., HEIJERMAN, H. G., DE WINTER-DE GROOT, K. M., CLEVERS, H., VAN DER ENT, C. K. & BEEKMAN, J. M. 2016a. Characterizing responses to CFTR-modulating drugs using rectal organoids derived from subjects with cystic fibrosis. *Sci Transl Med,* 8**,** 344ra84.

DEKKERS, J. F., GOGORZA GONDRA, R. A., KRUISSELBRINK, E., VONK, A. M., JANSSENS, H. M., DE WINTER-DE GROOT, K. M., VAN DER ENT, C. K. & BEEKMAN, J. M. 2016b. Optimal correction of distinct CFTR folding mutants in rectal cystic fibrosis organoids. *Eur Respir J,* 48**,** 451-8.

DEKKERS, J. F., VAN DER ENT, C. K. & BEEKMAN, J. M. 2013a. Novel opportunities for CFTR-targeting drug development using organoids. *Rare Dis,* 1**,** e27112.

DEKKERS, J. F., WIEGERINCK, C. L., DE JONGE, H. R., BRONSVELD, I., JANSSENS, H. M., DE WINTER-DE GROOT, K. M., BRANDSMA, A. M., DE JONG, N. W., BIJVELDS, M. J., SCHOLTE, B. J., NIEUWENHUIS, E. E., VAN DEN BRINK, S., CLEVERS, H., VAN DER ENT, C. K., MIDDENDORP, S. & BEEKMAN, J. M. 2013b. A functional CFTR assay using primary cystic fibrosis intestinal organoids. *Nat Med,* 19**,** 939-45.

DROST, J., VAN JAARSVELD, R. H., PONSIOEN, B., ZIMBERLIN, C., VAN BOXTEL, R., BUIJS, A., SACHS, N., OVERMEER, R. M., OFFERHAUS, G. J., BEGTHEL, H., KORVING, J., VAN DE WETERING, M., SCHWANK, G., LOGTENBERG, M., CUPPEN, E., SNIPPERT, H. J., MEDEMA, J. P., KOPS, G. J. & CLEVERS, H. 2015. Sequential cancer mutations in cultured human intestinal stem cells. *Nature,* 521**,** 43-7.

FISCHEL, J. L., ETIENNE, M. C., FORMENTO, P. & MILANO, G. 1998. Search for the optimal schedule for the oxaliplatin/5-fluorouracil association modulated or not by folinic acid: preclinical data. *Clin Cancer Res,* 4**,** 2529-35.

FUJII, M., SHIMOKAWA, M., DATE, S., TAKANO, A., MATANO, M., NANKI, K., OHTA, Y., TOSHIMITSU, K., NAKAZATO, Y., KAWASAKI, K., URAOKA, T., WATANABE, T., KANAI, T. & SATO, T. 2016. A Colorectal Tumor Organoid Library Demonstrates Progressive Loss of Niche Factor Requirements during Tumorigenesis. *Cell Stem Cell,* 18**,** 827-38.

GAO, D., VELA, I., SBONER, A., IAQUINTA, P. J., KARTHAUS, W. R., GOPALAN, A., DOWLING, C., WANJALA, J. N., UNDVALL, E. A., ARORA, V. K., WONGVIPAT, J., KOSSAI, M., RAMAZANOGLU, S., BARBOZA, L. P., DI, W., CAO, Z., ZHANG, Q. F., SIROTA, I., RAN, L., MACDONALD, T. Y., BELTRAN, H., MOSQUERA, J. M., TOUIJER, K. A., SCARDINO, P. T., LAUDONE, V. P., CURTIS, K. R., RATHKOPF, D. E., MORRIS, M. J., DANILA, D. C., SLOVIN, S. F., SOLOMON, S. B., EASTHAM, J. A., CHI, P., CARVER, B., RUBIN, M. A., SCHER, H. I., CLEVERS, H., SAWYERS, C. L. & CHEN, Y. 2014. Organoid Cultures Derived from Patients with Advanced Prostate Cancer. *Cell.*

GAO, H., KORN, J. M., FERRETTI, S., MONAHAN, J. E., WANG, Y., SINGH, M., ZHANG, C., SCHNELL, C., YANG, G., ZHANG, Y., BALBIN, O. A., BARBE, S., CAI, H., CASEY, F., CHATTERJEE, S., CHIANG, D. Y., CHUAI, S., COGAN, S. M., COLLINS, S. D., DAMMASSA, E., EBEL, N., EMBRY, M., GREEN, J., KAUFFMANN, A., KOWAL, C., LEARY, R. J., LEHAR, J., LIANG, Y., LOO, A., LORENZANA, E., ROBERT MCDONALD, E., 3RD, MCLAUGHLIN, M. E., MERKIN, J., MEYER, R., NAYLOR, T. L., PATAWARAN, M., REDDY, A., ROELLI, C., RUDDY, D. A., SALANGSANG, F., SANTACROCE, F., SINGH, A. P., TANG, Y., TINETTO, W., TOBLER, S., VELAZQUEZ, R., VENKATESAN, K., VON ARX, F., WANG, H. Q., WANG, Z., WIESMANN, M., WYSS, D., XU, F., BITTER, H., ATADJA, P., LEES, E., HOFMANN, F., LI, E., KEEN, N., COZENS, R., JENSEN, M. R., PRYER, N. K., WILLIAMS, J. A. & SELLERS, W. R. 2015. High-throughput screening using patient-derived tumor xenografts to predict clinical trial drug response. *Nat Med,* 21**,** 1318-25.

GJOREVSKI, N., SACHS, N., MANFRIN, A., GIGER, S., BRAGINA, M. E., ORDONEZ-MORAN, P., CLEVERS, H. & LUTOLF, M. P. 2016. Designer matrices for intestinal stem cell and organoid culture. *Nature,* 539**,** 560-564.

HAFNER, M. & NIEPEL, M. 2016. Growth rate inhibition metrics correct for confounders in measuring sensitivity to cancer drugs. 13**,** 521-7.

HARRIS, L. A., FRICK, P. L., GARBETT, S. P., HARDEMAN, K. N., PAUDEL, B. B., LOPEZ, C. F., QUARANTA, V. & TYSON, D. R. 2016. An unbiased metric of antiproliferative drug effect in vitro. *Nat Methods,* 13**,** 497-500.

HAY, M., THOMAS, D. W., CRAIGHEAD, J. L., ECONOMIDES, C. & ROSENTHAL, J. 2014. Clinical development success rates for investigational drugs. *Nat Biotechnol,* 32**,** 40-51.

HIDALGO, M., AMANT, F., BIANKIN, A. V., BUDINSKA, E., BYRNE, A. T., CALDAS, C., CLARKE, R. B., DE JONG, S., JONKERS, J., MAELANDSMO, G. M., ROMAN-ROMAN, S., SEOANE, J., TRUSOLINO, L. & VILLANUEVA, A. 2014. Patient-derived xenograft models: an emerging platform for translational cancer research. *Cancer Discov,* 4**,** 998-1013.

HIDALGO, M., BRUCKHEIMER, E., RAJESHKUMAR, N. V., GARRIDO-LAGUNA, I., DE, O. E., RUBIO-VIQUEIRA, B., STRAWN, S., WICK, M. J., MARTELL, J. & SIDRANSKY, D. 2011. A pilot clinical study of treatment guided by personalized tumorgrafts in patients with advanced cancer

449. *Mol Cancer Ther,* 10**,** 1311-1316.

HUCH, M., BOJ, S. F. & CLEVERS, H. 2013. Lgr5(+) liver stem cells, hepatic organoids and regenerative medicine. *Regen Med,* 8**,** 385-7.

HUCH, M., GEHART, H., VAN BOXTEL, R., HAMER, K., BLOKZIJL, F., VERSTEGEN, M. M., ELLIS, E., VAN WENUM, M., FUCHS, S. A., DE LIGT, J., VAN DE WETERING, M., SASAKI, N., BOERS, S. J., KEMPERMAN, H., DE JONGE, J., IJZERMANS, J. N., NIEUWENHUIS, E. E., HOEKSTRA, R., STROM, S., VRIES, R. R., VAN DER LAAN, L. J., CUPPEN, E. & CLEVERS, H. 2015. Long-term culture of genome-stable bipotent stem cells from adult human liver. *Cell,* 160**,** 299-312.

IORIO, F., KNIJNENBURG, T. A., VIS, D. J., BIGNELL, G. R., MENDEN, M. P., SCHUBERT, M., ABEN, N., GONCALVES, E., BARTHORPE, S., LIGHTFOOT, H., COKELAER, T., GRENINGER, P., VAN DYK, E., CHANG, H., DE SILVA, H., HEYN, H., DENG, X., EGAN, R. K., LIU, Q., MIRONENKO, T., MITROPOULOS, X., RICHARDSON, L., WANG, J., ZHANG, T., MORAN, S., SAYOLS, S., SOLEIMANI, M., TAMBORERO, D., LOPEZ-BIGAS, N., ROSS-MACDONALD, P., ESTELLER, M., GRAY, N. S., HABER, D. A., STRATTON, M. R., BENES, C. H., WESSELS, L. F., SAEZ-RODRIGUEZ, J., MCDERMOTT, U. & GARNETT, M. J. 2016. A Landscape of Pharmacogenomic Interactions in Cancer. *Cell.*

JUNTTILA, M. R. & DE SAUVAGE, F. J. 2013. Influence of tumour micro-environment heterogeneity on therapeutic response. *Nature,* 501**,** 346-54.

KARTHAUS, W. R., IAQUINTA, P. J., DROST, J., GRACANIN, A., VAN BOXTEL, R., WONGVIPAT, J., DOWLING, C. M., GAO, D., BEGTHEL, H., SACHS, N., VRIES, R. G., CUPPEN, E., CHEN, Y., SAWYERS, C. L. & CLEVERS, H. C. 2014. Identification of Multipotent Luminal Progenitor Cells in Human Prostate Organoid Cultures. *Cell.*

LETO, S. M., SASSI, F., CATALANO, I., TORRI, V., MIGLIARDI, G., ZANELLA, E. R., THROSBY, M., BERTOTTI, A. & TRUSOLINO, L. 2015. Sustained Inhibition of HER3 and EGFR Is Necessary to Induce Regression of HER2-Amplified Gastrointestinal Carcinomas. *Clin Cancer Res,* 21**,** 5519-31.

LI, X., NADAULD, L., OOTANI, A., CORNEY, D. C., PAI, R. K., GEVAERT, O., CANTRELL, M. A., RACK, P. G., NEAL, J. T., CHAN, C. W., YEUNG, T., GONG, X., YUAN, J., WILHELMY, J., ROBINE, S., ATTARDI, L. D., PLEVRITIS, S. K., HUNG, K. E., CHEN, C. Z., JI, H. P. & KUO, C. J. 2014. Oncogenic transformation of diverse gastrointestinal tissues in primary organoid culture. *Nat Med,* 20**,** 769-77.

LIU, C., LIU, Y., XIE, H. G., ZHAO, S., XU, X. X., FAN, L. X., GUO, X., LU, T., SUN, G. W. & MA, X. J. 2015. Role of three-dimensional

matrix stiffness in regulating the chemoresistance of hepatocellular carcinoma cells. *Biotechnol Appl Biochem,* 62**,** 556-62.

LIU, X., ORY, V., CHAPMAN, S., YUAN, H., ALBANESE, C., KALLAKURY, B., TIMOFEEVA, O. A., NEALON, C., DAKIC, A., SIMIC, V., HADDAD, B. R., RHIM, J. S., DRITSCHILO, A., RIEGEL, A., MCBRIDE, A. & SCHLEGEL, R. 2012. ROCK inhibitor and feeder cells induce the conditional reprogramming of epithelial cells. *Am J Pathol,* 180**,** 599-607.

MATANO, M., DATE, S., SHIMOKAWA, M., TAKANO, A., FUJII, M., OHTA, Y., WATANABE, T., KANAI, T. & SATO, T. 2015. Modeling colorectal cancer using CRISPR-Cas9-mediated engineering of human intestinal organoids. *Nat Med,* 21**,** 256-62.

NADAULD, L. D., GARCIA, S., NATSOULIS, G., BELL, J. M., MIOTKE, L., HOPMANS, E. S., XU, H., PAI, R. K., PALM, C., REGAN, J. F., CHEN, H., FLAHERTY, P., OOTANI, A., ZHANG, N. R., FORD, J. M., KUO, C. J. & JI, H. P. 2014. Metastatic tumor evolution and organoid modeling implicate TGFBR2 as a cancer driver in diffuse gastric cancer. *Genome Biol,* 15**,** 428.

NOORDHOEK, J., GULMANS, V., VAN DER ENT, K. & BEEKMAN, J. M. 2016. Intestinal organoids and personalized medicine in cystic fibrosis: a successful patient-oriented research collaboration. *Curr Opin Pulm Med,* 22**,** 610-6.

NOZAKI, K., MOCHIZUKI, W., MATSUMOTO, Y., MATSUMOTO, T., FUKUDA, M., MIZUTANI, T., WATANABE, M. & NAKAMURA, T. 2016. Co-culture with intestinal epithelial organoids allows efficient expansion and motility analysis of intraepithelial lymphocytes. *J Gastroenterol,* 51**,** 206-13.

OOTANI, A., LI, X., SANGIORGI, E., HO, Q. T., UENO, H., TODA, S., SUGIHARA, H., FUJIMOTO, K., WEISSMAN, I. L., CAPECCHI, M. R. & KUO, C. J. 2009. Sustained in vitro intestinal epithelial culture within a Wnt-dependent stem cell niche. *Nat Med,* 15**,** 701-6.

PORTER, S. N., BAKER, L. C., MITTELMAN, D. & PORTEUS, M. H. 2014. Lentiviral and targeted cellular barcoding reveals ongoing clonal dynamics of cell lines in vitro and in vivo. *Genome Biol,* 15**,** R75.

RUBIN, E. H. & GILLILAND, D. G. 2012. Drug development and clinical trials--the path to an approved cancer drug. *Nat Rev Clin Oncol,* 9**,** 215-22.

RUSSO, M., SIRAVEGNA, G., BLASZKOWSKY, L. S., CORTI, G., CRISAFULLI, G., AHRONIAN, L. G., MUSSOLIN, B., KWAK, E. L., BUSCARINO, M., LAZZARI, L., VALTORTA, E., TRUINI, M., JESSOP, N. A., ROBINSON, H. E., HONG, T. S., MINO-KENUDSON, M., DI NICOLANTONIO, F., THABET, A., SARTORE-BIANCHI, A., SIENA, S., IAFRATE, A. J., BARDELLI, A. & CORCORAN, R. B. 2016. Tumor Heterogeneity and Lesion-Specific Response to Targeted Therapy in Colorectal Cancer. *Cancer Discov,* 6**,** 147-53.

SATO, T., STANGE, D. E., FERRANTE, M., VRIES, R. G., VAN ES, J. H., VAN DEN BRINK, S., VAN HOUDT, W. J., PRONK, A., VAN GORP, J., SIERSEMA, P. D. & CLEVERS, H. 2011. Long-term expansion of epithelial organoids from human colon, adenoma, adenocarcinoma, and Barrett's epithelium. *Gastroenterology,* 141**,** 1762-72.

SATO, T., VRIES, R. G., SNIPPERT, H. J., VAN DE WETERING, M., BARKER, N., STANGE, D. E., VAN ES, J. H., ABO, A., KUJALA, P., PETERS, P. J. & CLEVERS, H. 2009. Single Lgr5 stem cells build crypt-villus structures in vitro without a mesenchymal niche. *Nature,* 459**,** 262-5.

SCHUTTE, M., RISCH, T., ABDAVI-AZAR, N., BOEHNKE, K., SCHUMACHER, D., KEIL, M., YILDIRIMAN, R. & JANDRASITS, C. 2017. Molecular dissection of colorectal cancer in pre-clinical models identifies biomarkers predicting sensitivity to EGFR inhibitors. 8**,** 14262.

SCHWANK, G., KOO, B. K., SASSELLI, V., DEKKERS, J. F., HEO, I., DEMIRCAN, T., SASAKI, N., BOYMANS, S., CUPPEN, E., VAN

DER ENT, C. K., NIEUWENHUIS, E. E., BEEKMAN, J. M. & CLEVERS, H. 2013. Functional repair of CFTR by CRISPR/Cas9 in intestinal stem cell organoids of cystic fibrosis patients. *Cell Stem Cell,* 13**,** 653-8.

SNIPPERT, H. J., SCHEPERS, A. G., VAN ES, J. H., SIMONS, B. D. & CLEVERS, H. 2014. Biased competition between Lgr5 intestinal stem cells driven by oncogenic mutation induces clonal expansion. *EMBO Rep,* 15**,** 62-9.

STEIN, W. D., LITMAN, T., FOJO, T. & BATES, S. E. 2004. A Serial Analysis of Gene Expression (SAGE) database analysis of chemosensitivity: comparing solid tumors with cell lines and comparing solid tumors from different tissue origins. *Cancer Res,* 64**,** 2805-16.

SUN, C., HOBOR, S., BERTOTTI, A., ZECCHIN, D., HUANG, S., GALIMI, F., COTTINO, F., PRAHALLAD, A., GRERNRUM, W., TZANI, A., SCHLICKER, A., WESSELS, L. F., SMIT, E. F., THUNNISSEN, E., HALONEN, P., LIEFTINK, C., BEIJERSBERGEN, R. L., DI NICOLANTONIO, F., BARDELLI, A., TRUSOLINO, L. & BERNARDS, R. 2014. Intrinsic resistance to MEK inhibition in KRAS mutant lung and colon cancer through transcriptional induction of ERBB3. *Cell Rep,* 7**,** 86-93.

SZAKACS, G. & GOTTESMAN, M. M. 2004. Comparing solid tumors with cell lines: implications for identifying drug resistance genes in cancer. *Mol Interv,* 4**,** 323-5.

TURNER, N. C. & REIS-FILHO, J. S. 2012. Genetic heterogeneity and cancer drug resistance. *Lancet Oncol,* 13**,** e178-85.

VAN DE WETERING, M., FRANCIES, H. E., FRANCIS, J. M., BOUNOVA, G., IORIO, F., PRONK, A., VAN HOUDT, W., VAN GORP, J. & CLEVERS, H. 2015. Prospective derivation of a 'Living Organoid Biobank' of colorectal cancer patients. *Cell.*

VERISSIMO, C. S., OVERMEER, R. M., PONSIOEN, B., DROST, J., MERTENS, S., VERLAAN-KLINK, I., GERWEN, B. V., VAN DER VEN, M., WETERING, M. V., EGAN, D. A., BERNARDS, R., CLEVERS, H., BOS, J. L. & SNIPPERT, H. J. 2016. Targeting mutant RAS in patient-derived colorectal cancer organoids by combinatorial drug screening. *Elife,* 5.

VERMEULEN, L., MORRISSEY, E., VAN DER HEIJDEN, M., NICHOLSON, A. M., SOTTORIVA, A., BUCZACKI, S., KEMP, R., TAVARE, S. & WINTON, D. J. 2013. Defining stem cell dynamics in models of intestinal tumor initiation. *Science,* 342**,** 995-8.

VIDOVIC, D., CARLON, M. S., DA CUNHA, M. F., DEKKERS, J. F., HOLLENHORST, M. I., BIJVELDS, M. J., RAMALHO, A. S., VAN DEN HAUTE, C., FERRANTE, M., BAEKELANDT, V., JANSSENS, H. M., DE BOECK, K., SERMET-GAUDELUS, I., DE JONGE, H. R., GIJSBERS, R., BEEKMAN, J. M., EDELMAN, A. & DEBYSER, Z. 2016. rAAV-CFTRDeltaR Rescues the Cystic Fibrosis Phenotype in Human Intestinal Organoids and Cystic Fibrosis Mice. *Am J Respir Crit Care Med,* 193**,** 288-98.

VOEST, E. E. & BERNARDS, R. 2016. DNA-Guided Precision Medicine for Cancer: A Case of Irrational Exuberance? *Cancer Discov,* 6**,** 130-2.

WEEBER, F., VAN DE WETERING, M., HOOGSTRAAT, M., DIJKSTRA, K. K., KRIJGSMAN, O., KUILMAN, T., GADELLAA-VAN HOOIJDONK, C. G., VAN DER VELDEN, D. V., CUPPEN, E., VRIES, R. G., CLEVERS, H. & VOEST, E. E. 2015. Preserved genomic diversity in organoids cultured from biopsies of colorectal cancer metastases *J Natl Cancer Inst.*

WILDING, J. L. & BODMER, W. F. 2014. Cancer cell lines for drug discovery and development. *Cancer Res,* 74**,** 2377-84.

CHAPTER 2

PATIENT-DERIVED ORGANOIDS CAN PREDICT RESPONSE TO CHEMOTHERAPY IN METASTATIC COLORECTAL CANCER PATIENTS

Salo N. Ooft[1,10,†], Fleur Weeber[1,10,†], Krijn K. Dijkstra[1,10,#], Chelsea M. McLean[1,10,#], Sovann Kaing[1,10], Erik van Werkhoven[2], Luuk Schipper[1,10], Louisa Hoes[1,10], Daniel J. Vis[3], Joris van de Haar[1,3,10], Warner Prevoo[4], Petur Snaebjornsson[5], Daphne van der Velden[1,10], Michelle Klein[1,10], Myriam Chalabi[1], Henk Boot[6], Monique van Leerdam[6], Haiko J. Bloemendal[7], Laurens V. Beerepoot[8], Lodewyk Wessels[3,9,10], Edwin Cuppen[10,11,12], Hans Clevers[10,13,14], and Emile E. Voest[1,10,*].

[1]Department of Immunology and Molecular Oncology, The Netherlands Cancer Institute, 1066 CX Amsterdam, The Netherlands.

[2]Department of Biometrics, The Netherlands Cancer Institute, 1066 CX Amsterdam, The Netherlands.

[3]Department of Molecular Carcinogenesis, The Netherlands Cancer Institute, 1066 CX Amsterdam, The Netherlands.

[4]Department of Radiology, The Netherlands Cancer Institute, 1066 CX Amsterdam, The Netherlands.

[5]Department of Pathology, The Netherlands Cancer Institute, 1066 CX Amsterdam, The Netherlands.

[6]Department of Gastrointestinal Oncology, The Netherlands Cancer Institute, 1066 CX Amsterdam, The Netherlands.

[7]Department of Internal Medicine/Oncology, Radboud University Medical Center Nijmegen, 6525 GA Nijmegen, The Netherlands.

[8]Department of Internal Medicine, Elisabeth-Tweesteden Hospital, 5042 AD Tilburg, The Netherlands.

[9]Faculty of electrical Engineering, Mathematics and Computer Science, Delft University of Technology, 2628 CD Delft, The Netherlands.

[10]Oncode Institute, 3521 AL Utrecht, The Netherlands.

[11]Division Biomedical Genetics, Centre for Molecular Medicine, University Medical Centre Utrecht, 3584 CX Utrecht, The Netherlands.

[12]Hartwig Medical Foundation, 1098 XH Amsterdam, The Netherlands.

[13]Hubrecht Institute, Royal Netherlands Academy of Arts and Sciences and University Medical Centre Utrecht, 3584 CT Utrecht, Netherlands.

[14]Princess Maxima Center for Pediatric Oncology, 3584 CS Utrecht, The Netherlands.

*Correspondence to e.voest@nki.nl.

†,# These authors contributed equally to this work.

Science Translational Medicine 2019 Oct 9;11(513)

ABSTRACT

There is a clear and unmet clinical need for biomarkers to predict responsiveness to chemotherapy for cancer. We developed an in vitro test based on patient-derived tumor organoids (PDOs) from metastatic lesions to identify non-responders to standard-of-care chemotherapy in colorectal cancer (CRC). In a prospective clinical study, we show the feasibility to generate and test PDOs for sensitivity to chemotherapy.. Our PDO test predicted response of the biopsied lesion in more than 80% of patients treated with irinotecan-based therapies, without misclassifying patients who would have benefited from treatment. This correlation was specific to irinotecan-based chemotherapy, however, and the PDOs failed to predict outcome for treatment with 5-fluorouracil (5-FU) plus oxaliplatin. Our data suggest that PDOs could be used to prevent cancer patients from undergoing ineffective irinotecan-based chemotherapy.

INTRODUCTION

Chemotherapy is still considered the backbone of anti-cancer therapy and has improved the life expectancy of countless patients (*1, 2*). Unfortunately, a large fraction of patients does not benefit from this treatment, whilst still experiencing substantial side effects(*3–6*). Although genomics has greatly facilitated patient selection for targeted therapies, this has been unsuccessful for chemotherapy, in part due to its often incompletely understood and diverse mechanisms of action (*7–9*). A handful of clinical parameters can help provide prognosis, but the majority of proposed biomarkers are not currently used to predict chemotherapy treatment outcome in the clinic (*9–14*). Previous attempts to use patient material to determine treatment responsiveness have had limited success due to the long turnaround times, poor scalability, or low success rates of establishing patient cell lines or xenografts (*15, 16*). Taken together, personalized cancer treatment for chemotherapy is currently lacking, and new predictive assays to help match patients to treatments are highly needed.

PDOs are cultures of tumor cells that can be derived from individual patients with a high success rate and expanded indefinitely, and which recapitulate morphological and genetic features of the original tumor (*17–19*). Recent post-hoc studies suggest that PDOs may mirror clinical responses of individual patients to therapy (*20, 21*). We therefore embarked on a multi-center, prospective, observational clinical study to determine the feasibility and potential value of PDOs as a predictive test for chemotherapy treatment regimens for CRC patients. . The Tumor Organoids: feasibility to predict sensitivity to treatment in cancer patients (TUMOROID) study is a multi-center focused on regimens commonly used in CRC; patients received standard-of-care chemotherapy, including infusional 5-FU or capecitabine (oral pro-drug of 5-FU), in combination with either oxaliplatin (referred to as FO) or irinotecan (FI), or irinotecan alone. Bevacizumab was allowed in all treatments, but patients who received additional cetuximab or panitumumab were excluded. The primary objective was the development of an assay to accurately identify non-responders to chemotherapy. Non-responders were defined as patients with progressive disease after 3 cycles of chemotherapy according to the response evaluation criteria in solid tumors (RECIST) 1.1 (*22*).

RESULTS

Genetic and clinical characteristics of patients included in the TUMOROID study.

We included 61 patients in the trial, from whom 67 biopsies were taken and cultured as previously described (*19, 23*). Of the total 67 included biopsies, tissue retrieval was unsuccessful for 4 biopsies (Fig. 1A). Culture of 23 of the remaining 63 biopsies failed due to

no or too few tumor cells in the biopsy (n=14), quality control problem (n=6), or bacterial infection (n=3). Overall, we obtained a ~63% PDO culture success rate (40/63 cultures) across the whole study, which is in line with previous reports (*18–20*), and found that clinical parameters did not influence culture success (Fig. S1A). For 5 patients the culture succeeded, but the clinical response was not evaluable, and therefore the PDOs could not be used for in vitro-patient comparison of drug response. Of the resulting 35 PDOs, 16 were used to evaluate the PDO drug sensitivity for first line FO and 22 to second line FI or irinotecan (12 and 10 PDOs, respectively) (Fig. 1A). In most cases, the PDOs were established before the start of treatment. In rare cases, PDOs were established after progression on treatment (P27 and P28) or could also be used for testing response to multiple treatment outcomes because the patients were biopsied immediately after progression on first line treatment with FO and right before the start of second line treatment with irinotecan or FI (P2.2, 3.2, 4.2). Patient and tumor characteristics, clinical background, pathological parameters, genetic aberrations, and treatment history are presented in Fig. 1B and more elaborately in tables S1-3. We found that the frequency of known genetic drivers of CRC was similar between the first (FO) and second (FI/I) line treatment cohorts (Fig. 1B), and similar to a recent clinical sequencing study of metastatic CRC, suggesting that our study describes a representative population of patients (*24*). Clinical response data for each patient is depicted in Fig. 1C.

PDOs predict response to irinotecan monotherapy.

We first tested 10 PDOs from 10 patients treated with irinotecan (described in more detail in table S3). Five PDOs were derived from lesions that were classified as progressive disease (PD) and 5 from lesions that were classified as stable disease (SD) (Fig. 2A, depicted in more detail in fig. S2A). This distribution of responses is in line with larger studies using irinotecan (*6*). All PDOs were exposed to the active metabolite of irinotecan, SN-38, for 6 days, and each screen was repeated by a second person to determine inter-observer reproducibility (average Pearson's R = 0.947; range 0.796-0.996; fig. S2B). We calculated the drug-induced growth rate inhibition (GR) of each condition 6 days after drug exposure and fitted dose-response curves (DRCs) (Fig. 2B) (*25*). We quantified responses to SN-38 by calculating the GR_{50} and the area under the dose response curve (AUC_{DRC}), both of which are significantly different between PDOs generated from PD versus SD lesions (Mann-Whitney test p=0.0159 and p=0.0079, respectively; Fig. 2C and Fig. 2D). To reduce the number of organoids and data points required to test, we refined the drug assay by determining the concentration in the DRC at which the window of effect (or 'variance')of chemosensitivity was largest (fig. S3A). This strategy results in the elimination of drug concentrations for which the differential effect between PDOs was little. .). We found that 3.2 nM SN-38 yielded the largest window of effect and PDOs from SD patients were more sensitive than PDOs from PD patients when exposed to this concentration (Mann-Whitney test p=0.0159; Fig. 2E, fig. S3A). The receiver operating characteristic (ROC)-

curve generated from this window had an AUC of 0.96 (confidence interval 0.8427-1.1077; Fig. 2F), comparable to those generated based on GR_{50} and AUC_{DRC} (summarized in fig. 2G). We next aimed to develop a GR score-based classifier which accurately identifies non-responders to irinotecan, without misclassifying responders, and test its predictive performance using leave-one-out cross-validation (LOOCV; fig. S3B). The LOOCV resulted in correct classification of 80% of patients (empirical p=0.0061; fig. S3B). These data demonstrate that PDOs have predictive value for irinotecan monotherapy, which can be captured by exposure to a single concentration of SN-38 and application of a cut-off of GR>0.67. Such an assay required only ~5,000 cells, which could be generated and screened within about two weeks.

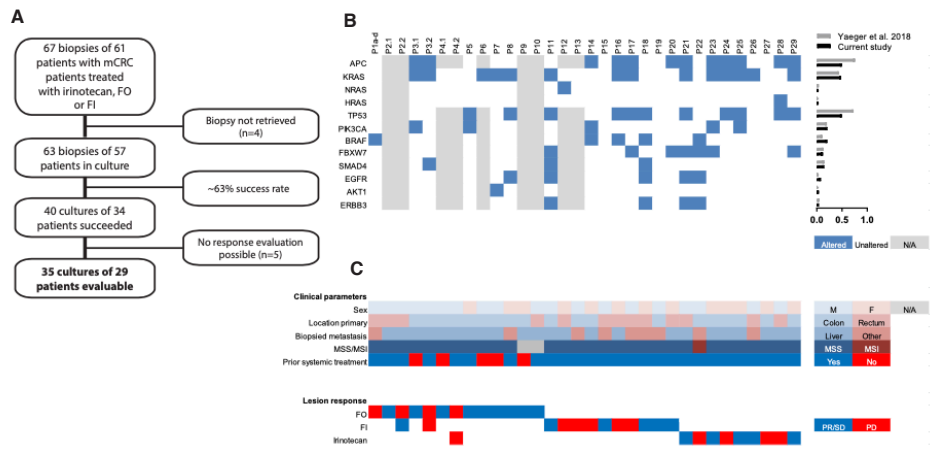

Fig. 1 Generation of PDOs from patients with metastatic CRC enrolled in the TUMOROID study.
(**A**) Flow chart indicating the number of patients with metastatic CRC included, the number of evaluable patients, reasons for non-evaluability, and the success rate of establishing cultures from patients. (**B**) Overview of all patients, corresponding mutations in genes commonly mutated in CRC, and clinical parameters (sex, primary location, biopsied metastasis, micro-satellite instability (MSI) status, and prior systemic treatment). Gray boxes indicate that data were not available. On the right side are bar graphs representing the fraction of samples with a genetic aberration identified per gene, plotted, and compared to Yaeger and colleagues (*24*). 'Altered' was defined as a given variant being predicted pathogenic by COSMIC. (**C**) Clinical responses of patients, indicated in either blue (PR/SD) or red (PD), on the relevant treatment indicated on the left. The clinical and genetic data are described in more detail in tables S1-3.

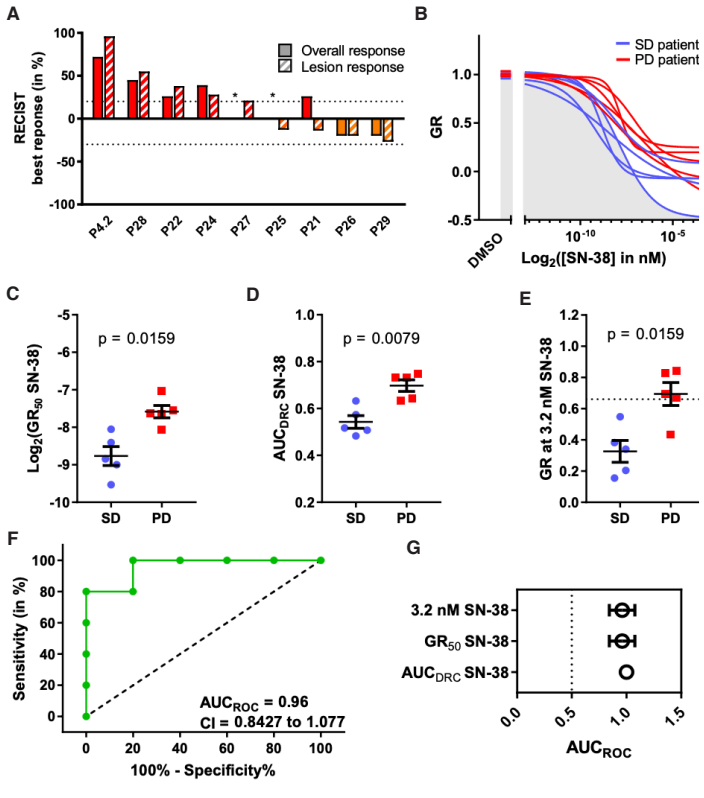

Fig. 2 PDO drug sensitivity predicts response to treatment with irinotecan.

(**A**) Waterfall plot of each patient's overall response and best response of the biopsied lesion in the irinotecan-treated PDO cohort. Red indicates progressive disease (PD) and orange stable disease (SD).* = new lesion(s). (**B**) Fitted dose-response curves (DRCs) of 10 PDOs exposed to SN-38 in vitro. Green lines represent PDOs derived from SD patients and red lines represent PDOs from PD patients. GR values represent in vitro sensitivity of PDOs to SN-38. The screen was plated in technical triplicate and performed twice, once each by 2 independent researchers. . Red indicates progressive disease (PD) and blue stable disease (SD) (**C**) Log2(GR_{50} SN-38) was interpolated from the fitted DRCs shown in panel B. Groups were compared using a two-tailed Mann-Whitney test. Dots/squares represent individual PDOs, horizontal bars represent the mean and error bars indicate standard error of the mean. (**D**) The area under the dose-response curve (AUC_{DRC}) was calculated by integrating the DRC of each PDO in panel B. Groups were compared using a two-tailed Mann-Whitney test. Dots/squares represent individual PDOs, horizontal bars represent the mean and error bars indicate standard error of the mean. (**E**) The data point with the largest window of effect (captured by the variance) was calculated (3.2 nM SN-38; Fig. S3A), and response was compared using a two-tailed Mann-Whitney test. (**F**) The data of panel E were plotted as an ROC curve. The dotted line represents an AUC_{ROC} of 0.5. , CI = confidence interval. (**G**) Summary graph of the AUC_{ROC}s and 95% CIs on the basis on the in vitro parameters GR_{50} and AUC_{DRC}.

PDOs predict response to 5-FU-irinotecan combination therapy.

Next, we attempted to construct a PDO-based classifier that would predict response to combination therapy. We also tested PDOs from 12 patients treated with FI (Fig. 3A, more details in fig. S4A). Again, the distribution of clinical responses was representative of distributions found in larger studies (6). Because FI is a combination chemotherapy of 2 drugs, we designed a drug matrix with a broad range of concentrations (fig. S4C). All 12 PDOs were screened in duplicate for response to FI (average Pearson's R = 0.922; range 0.819-0.991; fig. S4B), and responses were quantified by summing the GR values across the drug matrix to create a 'pan-matrix GR score' and then compared to the RECIST best response of the lesion (fig. S4D). We observed a pattern that closely mirrored the clinical responses: Five PDOs of patients with PD were resistant to FI in vitro, whereas seven PDOs derived from patients with PR/SD were sensitive to FI (P14 was derived from a patient with PD, but clustered with PDOs sensitive to FI; fig. S4D). Responses to the individual drugs 5-FU and SN-38 were not significantly different between PR/SD and PD lesions (fig. S4E). Most PDOs were either sensitive or resistant to both SN-38 and 5-FU, although there were two exceptions: P19 was resistant to 5-FU, but sensitive to SN-38, and P20 showed the opposite. These data suggest that in most cases 5-FU and irinotecan collectively contribute to the effect of FI and the correlation found in vitro (fig. S4F).

Analogous to the method described for the irinotecan monotherapy cohort, we refined the drug assay by determining the concentrations in the drug matrix at which the variance of in vitro chemosensitivity was largest (fig. S4C and S5A). This analysis identified 2 complementary rows and columns in the drug matrix with large windows of effect: 200 µM 5-FU as fixed concentration ('anchor') and a titration of SN-38, as well as 6.25 nM SN-38 as anchor and a titration of 5-FU (fig. S5A). For each PDO, we summed the 11 GR values within these 2 complementary dose response curves to create a GR score and found these to differ between PR/SD and PD patients (Mann-Whitney test p=0.0260; Fig. 3B and fig. S5A). Furthermore, a ROC based on this score produced an AUC of 0.89 (Fig. 3C), suggesting that PDOs may have predictive value for FI combination chemotherapy. Additionally, the 50% of PDOs that were most sensitive to FI in our assay had a significantly higher progression-free survival (PFS), indicating that in vitro sensitivity to FI is also associated with a longer response in the clinic (log-rank test p=0.0278; Fig. 3D). When compared to other in vitro endpoints, the combined DRCs performed as well as or better than 5-FU and SN-38 as single agents (summarized in Fig. 3E). Finally, for clinical implementation, the two complementary DRCs of the FI assay only required ~10,000 cells, which can be readily generated and screened within 21 days. This turnaround time is a marked improvement over the previously reported 2-6 months for other cell culture models and more similar to sequencing of gene panels such as the Memorial-Sloan Kettering IMPACT panel (21 days) or the turnaround times reported in precision medicine studies (I-PREDICT median time to start treatment: ~29 days) (*15*, *26*, *27*).

To assess the performance of the FI classifier, we first repeated the LOOCV for the FI data set and found that 83.3% of patients were correctly classified (empirical p=0.0017; fig. S5B). We then tested the classifier for FI combination therapy on the cohort of patients described above, which received irinotecan-monotherapy. All PDOs of the irinotecan cohort (Fig. 2A and fig. S2A) were exposed for 6 days to the complementary DRCs identified in the FI analysis above. When we applied the previously identified threshold of GR>0.46, we correctly classified 5/5 resistant patients and 4/5 sensitive patients (90% correct; Fisher's exact test p=0.0476) (Fig. 3F). Furthermore, the ROC curve generated from this GR score had an AUC_{ROC} of 0.84 (Fig. 3G). Together, these results demonstrate the predictive nature of our test in a second patient cohort.

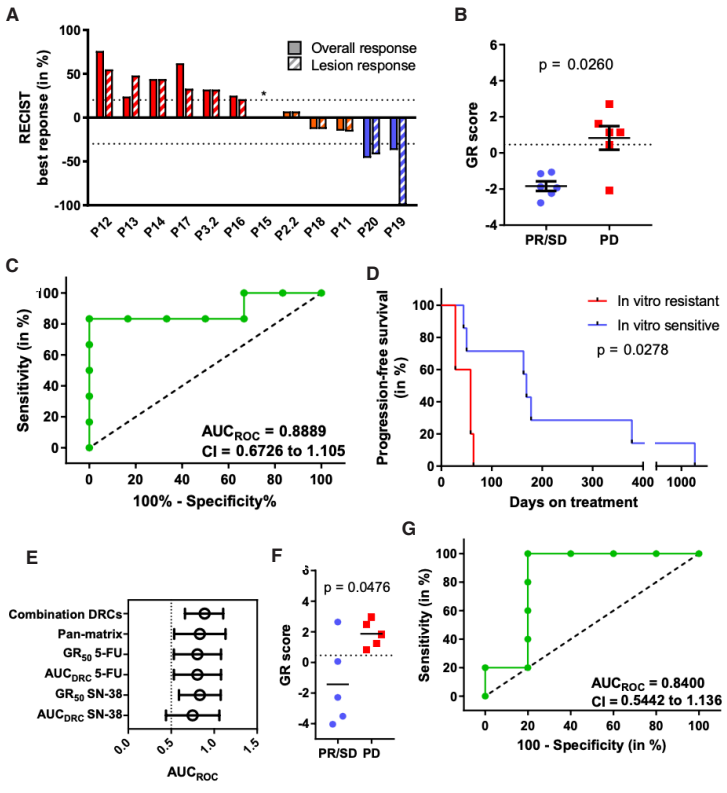

Fig. 3 PDO drug sensitivity predicts response to treatment with 5-FU/capecitabine and irinotecan. (**A**) Waterfall plot of each patient's overall response and best response of the biopsied lesion in the FI-treated PDO cohort. Red indicates progressive disease (PD), orange stable disease (SD) and blue partial response (PR). * = new lesion(s). (**B**) GR scores of FI-treated PDOs derived from lesions with PR/SD and PD. Scores of PR/SD (n=6) versus PD (n=6) patients were compared using a two-tailed Mann-Whitney test. The screen was plated in technical triplicate and performed 2 times, once each by independent researchers.

GR scores representing in vitro sensitivity of PDOs to FI were calculated by summing the 11 data points in the two complementary rows and colums in the drug matrix (fig. S5A). Dots/squares represent individual PDOs, horizontal bars represent the mean and error bars indicate standard error of the mean. (**C**) ROC curve of the FI cohort illustrating the potential to predict response. AUC_{ROC} = area under the receiver operating characteristic curve, CI = confidence interval. (**D**) Kaplan-Meier curve depicting the PFS of the 50% most-sensitive versus 50% most-resistant PDOs. Groups were compared using the Mantel-Cox log-rank test. (**E**) Summary of the area under the ROC curves (AUC_{ROC}) and 95% CI for lesion response, calculated on the basis of s in vitro parameters GR_{50} and AUC_{DRC}. **(F)** GR scores of irinotecan-treated PDOs derived from lesions with PR/SD and PD. The test developed using the FI set (described in panel B) was applied to the 10 PDOs from the patients in the irinotecan monotherapy cohort: All PDOs were exposed to the 11 concentrations identified in panel B, and GR scores representing in vitro sensitivity of PDOs to irinotecan were calculated analogous to the method described there. GR scores were compared to our threshold (GR>0.46, represented by the dotted line in the figure, as identified previously in panel B) to determine whether PR/SD (n=5) and PD (n=5) patients were correctly classified by this method. Groups were compared using a two-tailed Fisher-exact test. **(G)** The data of panel F plotted as an ROC curve.

PDOs do not predict response to 5-FU-oxaliplatin combination therapy.

We then performed similar experiments to test the predictive value of PDOs for FO chemotherapy using 16 PDOs derived from 10 patients (Fig. 4A; fig. S6A) (*22*). All samples were screened and analyzed as described above (inter-researcher reproducibility: average Pearson's R = 0.971; range 0.935-0.996; fig. S6B). In contrast to the irinotecan-based patient cohorts, we did not find a significant difference in PDOs generated from PD versus PR/SD lesions in response to any of the tested parameters (Fig. 4B; fig. S6C-D). Furthermore, no correlation with clinical response was found for the response to either the combination treatment or the individual drugs (summarized in fig. S6E). Consequently, the ROC curves showed no predictive value (Fig. 4C and D).

To analyze intra-patient differences in drug responses before treatment (P1a-d) or over the course of treatment (P2-4) we calculated response to FO and individual drug responses of PDOs Organoids were generated from multiple synchronous metastases of P1, as well as before and after treatment for P2-4. . In line with a previous study, we found that responses to individual agents can differ substantially between lesions in a single patient (P1a-d; fig. S7A and B (*21*). However, all 4 lesions were comparably sensitive to the FO combination (fig. S7C), which contrasts with the heterogeneous responses to single agents (fig. S7A and B, and summarized in S7F). For 3 patients, we profiled drug responses before treatment and upon clinical progression to FO (fig. S7E). P2.1 showed a considerable response to single agent 5-FU and oxaliplatin, and to the FO combination, which was partly diminished in P2.2 and mirrored

the clinical response of this patients (fig. S7E-H). This contrasts with P3 and P4, for whom only minor or modest changes between pre- and post-treatment cultures were found in response to single agent 5-FU and oxaliplatin, and to the FO combination (P3.1-P3.2 and P4.1-P4.2; fig. S7F-H). Moreover, baseline sensitivity to FO varied greatly between P1-3 (fig. S7C). These observations suggest that the current PDO culture/screening system does not recapitulate the responses of patients to FO in the clinic as it does for second-line irinotecan-based therapy.

We performed several calculations to control for underlying factors that might contribute to the discrepancy found between first (FO; AUC_{ROC} = 0.5) and second line (FI/I; AUC_{ROC} > 0.8) therapy response in vitro. We calculated the interaction (odds ratio) of clinical parameters or the presence of mutations in common CRC driver genes with clinical response (fig. SS8A and B) or with individual PDO responses to chemotherapy (fig. S8C and D,). We did not find a significant association with response or resistance, either clinical or in vitro, for any of these parameters.

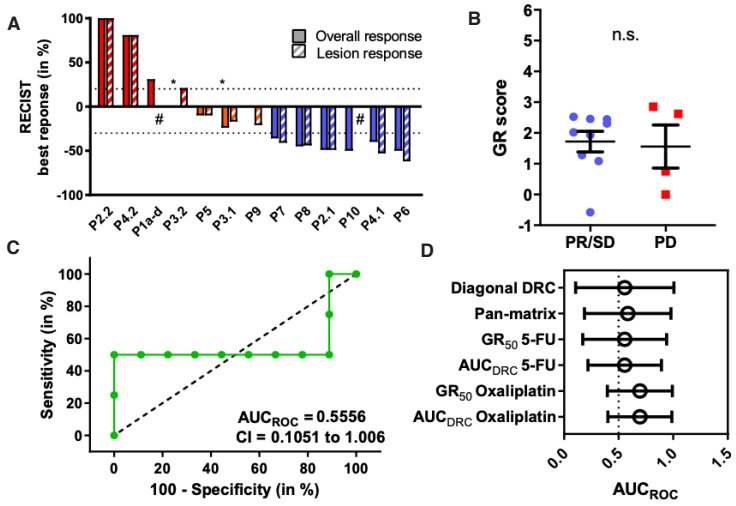

Fig. 4 PDO drug sensitivity does not predict response to treatment with 5-FU/capecitabine and oxaliplatin.

(**A**) Waterfall plot of the best lesion and overall responses in the FO-treated PDO cohort. Red indicates progressive disease (PD), orange stable disease (SD) and blue partial response (PR). * = new lesion(s). (**B**) GR scores of FO-treated PDOs derived from lesions with PR/SD and PD. Scores of PR/SD (n=13) versus PD (n=4) patients were compared using a two-tailed Mann-Whitney test. The screen was plated in technical triplicate and performed 2 times, once each by independent researchers. GR scores representing in vitro sensitivity of PDOs to FO were calculated by summing the 6 data points of equimolar concentrations of 5-FU and oxaliplatin to generate a GR score. Dots/squares represent scores for individual PDOs (except

for P1a-d, which are represented as the average of these 4 samples), horizontal bars represent the mean anderror bars thestandard error of the mean; n.s = not significant. (**C**) ROC curve of the FO cohort illustrating the potential to predict response. AUC_{ROC} = area under the receiver operating characteristic curve, CI = confidence interval. (**D**) Summary graph of the AUC_{ROC}s and 95% CIs calculated on the basis of various in vitro parameters GR_{50} and AUC_{DRC}.

DISCUSSION

The discrepancy between the predictive value of PDOs for irinotecan-based treatment and FO suggests that the sensitivity and necessary conditions of the test might differ across types of chemotherapy and underscores our limited knowledge with regards to the mechanism of action of chemotherapy, especially in combinations. Plausible explanations include the absence of stroma and an immune system in PDO cultures, which can dictate treatment outcome in various ways (*8*). Culture methods that at least partially retain the patient tumor micro-environment in vitro might provide a platform to overcome this hurdle and offer valuable insight into the multi-level interaction of 5-FU and oxaliplatin (*23*, *28*). Another important factor of the cost-effectiveness of PDO-based tests is the culture success. This might be further improved by obtaining multiple core biopsies, together with direct evaluation of the biopsies by a pathologist to identify samples with low cellularity, because we and others found this to be a major determinant of success (*20*). Another technical limitation of functional tests is that they cannot be 'rushed' as can be done for sequencing gene panels (*26*, *27*). These two points highlight the need to further increase the efficacy of PDO culture.

In summary, to date there are no predictive tests for responsiveness to standard-of-care chemotherapy in CRC. Our data support the use of PDOs as a predictive tool to prospectively identify patients with metastatic CRC who would not benefit from irinotecan-based palliative chemotherapy. We have demonstrated that it is clinically feasible to use PDOs to deliver a prediction on the outcome of irinotecan-based chemotherapy. Although encouraged by the data, we are mindful of several limitations to our study. Although we have performed analyses (LOOCV, data randomization, testing of the FI-assay in an irinotecan monotherapy cohort) to assess the strength of the data, the number of patients on which our initial test was designed is limited and the performances of the classifiers should be tested in independent cohorts of patients. However, we have now provided a foundation for confirmatory trials to validate and refine PDO-based tests and identify alternative treatments for patients unlikely to respond to irinotecan-based therapies (*20*, *21*). Our approach has the potential to prevent overtreatment with irinotecan in metastatic colorectal cancer patients and highlights the potential of PDOs as suitable tools for precision chemotherapy treatment.

MATERIALS AND METHODS

Study design

The TUMOROID study is a Dutch multi-center observational cohort study (NL49002.031.14). The objective of the study was to evaluate the potential and feasibility of PDOs to distinguish patients with and without response to standard-of-care treatment, and the primary objective is a standardized PDO-based test with an AUC_{ROC} of >0.7. and a high negative predictive value (the ability to exclude non-responders without withholding treatment to responders). The study was approved by the ethical review board of The Netherlands Cancer Institute. The protocol complies with the Declaration of Helsinki, Dutch law, and Good Clinical Practice. All patients provided written informed consent prior to any study-related procedures. Patients with metastatic CRC were accrued at the Netherlands Cancer Institute, Meander Medical Centre Amersfoort, and Elisabeth-TweeSteden Hospital Tilburg. Eligibility criteria included an Eastern Cooperative Oncology Group (ECOG) performance status of ≤2; measurable disease; feasibility of tumor biopsy for histologic analysis; and age of 18 years or older. Patients underwent biopsies before start of treatment with clinically approved regimens of capecitabine/5-FU combined with oxaliplatin/irinotecan (described below). In select cases, post-treatment biopsies were obtained upon clinical progression. Patients underwent CT scans at baseline and every 2 months to monitor response to treatment. Responses of the biopsied lesion were scored using RECIST 1.1(*22*).

Treatment

Patients were treated according to clinically approved regimens of irinotecan monotherapy or capecitabine/fluorouracil in combination with oxaliplatin or irinotecan. Bevacizumab was allowed in all regimens. Irinotecan monotherapy (350 mg/m²) was administered intravenously once every three weeks. Capecitabine plus oxaliplatin (CAPOX) was given in 3-week cycles; patients received capecitabine 1000 mg/m² orally twice a day on days 1-14 and oxaliplatin 130 mg/m² intravenously on day 1. 5-FU plus leucovorin plus oxaliplatin (FOLFOX) was given in cycles of 2 weeks; patients received oxaliplatin 85 mg/m², leucovorin 400 mg/m², and 5-fluorouracil (400 mg/m² as a bolus, 600 mg/m² in 22 hours) intravenously on day 1. On day 2, the patients received leucovorin 200 mg/m² and fluorouracil (400 mg/m² as a bolus, 600 mg/m² in 22 hours) intravenously. Capecitabine plus irinotecan (CAPIRI) was given in 3-week cycles, where patients received capecitabine 1000 mg/m² orally twice a day on day 1-14 and irinotecan 250 mg/m² intravenously on day 1. 5-FU plus leucovorin plus irinotecan (FOLFIRI) was given in cycles of 2 weeks; patients received irinotecan 180 mg/m², leucovorin 200 mg/m², and fluorouracil (400 mg/m² as a bolus, 600 mg/m² in 22 hours) intravenously on day 1. On day 2, the patients received leucovorin 200 mg/m² and fluorouracil (400 mg/m² as a bolus, 600 mg/m² in 22 hours) intravenously.

Patient material processing and organoid culture

One or two 18-gauge tumor biopsies were used for organoid culture and DNA sequencing. Biopsies were collected in Advanced Dulbecco's Modified Eagle's Medium with Nutrient Mixture F-12 Hams (Ad-DF) (Invitrogen; #12634), supplemented with 1% penicillin/streptomycin (Invitrogen; #15140-122), 1% HEPES (Invitrogen; #15630-056), and 1% GlutaMAX (Invitrogen; #35050) (hereafter referred to as Ad-DF+++). Biopsies were stored for a maximum of 24 hours at 4°C before being dissociated with sharp needles. Cells were counted, washed with Ad-DF+++, and cultured as previously described in CRC growth medium (*17*, *23*). We could generally expand these biopsies to an average of ~$2.0x10^5$ cells at the first split (around day 10). PDO cultures were checked for mycoplasma contamination every month using the MycoAlert Mycoplasma Detection Kit (Lonza). As part of quality control, PDOs were authenticated using a Taqman-based SNP array targeting 26 SNPs (Hartwig Medical Foundation). Identity scores of tumor DNA versus DNA obtained from healthy blood were computed as described elsewhere (*29*). PDOs with identity scores < 0.9 were discarded.

DNA-sequencing

Part of the biopsied material of each patient was used for routine clinical sequencing of a panel of cancer genes (Illumina TruSeq; *ABL1*; *AKT1*; *ALK*; *APC*; *ATM*; *BRAF*; *CDH1*; *CDKN2A*; *CSF1R*; *CTNNB1*; *EGFR*; *ERBB2*; *ERBB4*; *FBXW7*; *FGFR1; FGFR2*; *FGFR3*; *FLT3*; *GNA11*; *GNAQ*; *GNAS*; *HNF1A*; *HRAS*; *ADH1*; *JAK2*; *JAK3*; *KDR*; *KIT*; *KRAS*; *MET*; *MLH1*; *MPL*; *NOTCH1*; *NPM1*; *NRAS*; *PDGFRA*; *PIK3CA*; *PTEN*; *PTPN11*; *RB1*; *RET*; *SMAD4*; *SMARCB1*; *SMO*; *SRC*; *STK11*; *TP53*; *VHL*) or whole-genome sequencing (WGS) by the Hartwig Medical Foundation (HMF). Both libraries were prepared according to manufacturer's instructions (targeted sequencing: FC-130-1008; WGS: Truseq Nano LT; FC-121-4001-3) and sequenced on the Illumina MiSeq (panel) or HiSeqX paired-end 2x150 bp (WGS) platform. Analysis of the targeted panel was performed with Somatic Variant Caller v1.3 (Illumina). Analysis of the WGS data by the HMF was performed using their custom pipeline, which can be found online at BioRxiv/Github (*30*).

Drug screening

All drug screens were performed 2 times, once each by 2 independent researchers. PDOs were mechanically and enzymatically dissociated into single cells by incubating in TrypLE (Gibco, #12604-013) for 5-10 minutes, filtered, and re-plated to allow for formation of organoids over the course of 4 days. After 4 days, PDOs were collected, incubated with 2 mg/ml dispase II (Sigma #D4693) for 15 minutes to remove Geltrex, and counted using a hemocytometer and trypan blue. PDOs were resuspended in 1:2 Ad-DF+++:Geltrex at a concentration of 20 organoids/µl. Five µl/well of the suspension was dispensed in clear-bottomed, white-walled 96-well plates (Corning, #3707) using an automated repeat pipet and overlaid with 200 µl CRC growth medium. We generated 6-step, 4-fold drug matrices of 5-FU + oxaliplatin or 5-FU

+ SN-38 and 10-step, 2-fold single drug dose response curves in technical triplicate, covering physiological concentrations of 5-FU (5-FU C_{max} in patients = 1.7-2.4 µM; 5-FU range in vitro = 0.319-200 µM), SN-38 (C_{max} in patients ≈ 26 nM; SN-38 range in vitro = 0.195-100 nM), and oxaliplatin (oxaliplatin C_{max} in patients = 3.8-10.1 µM; oxaliplatin range in vitro = 0.319-200 µM) in patients using a Tecan D300e digital dispenser (*31–33*). Readouts were obtained at day 0 ('baseline') and at day 6 in the positive control (10 µM phenylarsine oxide), negative control, and the drug-treated wells. Quantification of cell viability was done by replacing the CRC medium with 50 µl Cell-TiterGlo 3D (Promega, #G9681) mixed with 50 µl Ad-DF+++ according to manufacturer instructions on an Infinite 200 Pro plate reader (Tecan Life Sciences).

Dose-response curve fitting and correlation analysis

For P1a-d, the results reported are the average of the 4 samples. In cases where lesion response could not be accurately measured (P1, P14, and P21), overall response was used. Growth rate (GR) values were calculated based on median luminescence values of day 0, untreated day 6, and drug-treated wells at day 6, using the method described in more detail elsewhere (*24*). For the FI cohort, the GR value of each data point in the whole drug combination matrix or 2 dose response curves (200 µM 5-FU anchor plus a titration of SN-38 combined with 6.25 nM SN-38 anchor and a titration of 5-FU) was summed to create a GR score for each PDO line. Z-scores used in the Kaplan-Meier curve were calculated as $(\mu-X)/\sigma$ (μ = mean; X = score; σ = standard deviation). Scores for response to combined FO in vitro were calculated based on the 1:1 ratio (the 'diagonal' in the combination matrix) of FO, again summing the GR value of each point to create an overall score. Curve fitting and estimation of GR_{50}s was done using the GRmetrics package v.1.8.0 in R (*34*). AUC_{DRC}s were inferred by integrating fitted curves. To analyse the reproducibility between drug screen 1 and drug screen 2, performed by 2 independent researchers, we calculated the Pearson's R and corresponding p-value using either the GR value of the 11 data points in the 2 complementary dose response curves identified as having the largest variance within our samples (FI set) or the GR value of the 36 data points in the full combination matrix (FO set) or all 10 data points in the DRCs (irinotecan monotherapy set). Correlation analyses, with associated p-values, were performed using the COR function in R

LOOCV and data randomization

To identify data points that had the largest variance within our samples in the irinotecan set, we calculated the variance for each of the 10 data points in the DRCs, across all 10 PDOs, in a leave-one-out setting. To set the threshold for the irinotecan classifier, we selected the GR score within our set of 10 samples that correctly classified all sensitive patients, while correctly classifying the maximum number of resistant patients (GR>0.76 classified as resistant; Fig. 2E).

To test the predictive performance of this threshold, we applied LOOCV and data randomization. Here, we used 9 samples as a training set to identify the data point with the highest variance, as described above. Next, we randomly reassigned our 10 GR scores among 5 sensitive and 5 resistant 'patients'. Using the GR scores of the 9 training samples, we set a threshold and used this cut-off to classify the 10th (validation) sample as either sensitive or resistant (fig. S4A and S4B). In this manner, tested samples were never used to determine the threshold. As with our empirically determined threshold, we set the threshold by selecting the highest GR score that correctly classified all sensitive patients within the test set of 9 PDOs, while correctly classifying the maximum number of resistant patients within the test set of 9 PDOs. Within each loop, the data randomization step was performed 120,000 times. This entire procedure was repeated 10 times in total, each time leaving out a different PDO. The p-value for our empirically determined threshold was calculated by dividing the number of cases where a randomly generated classifier threshold performed as well as, or better than, our empirically determined classifier threshold by the number of iterations executed ((p=R/I; p = p-value; R = number of times random data outperforms our classifier; I = number of iterations executed).

The analysis of the FI set was performed in a similar manner: We identified two complementary dose response curves that had the largest variance within our samples in the FI set by calculating the variance for each of the 36 data points in the full drug matrix, across all 12 PDOs, in a leave-one-out setting. To set the threshold for the FI classifier, we selected the GR score within our set of 12 samples that correctly classified all sensitive patients, while correctly classifying the maximum number of resistant patients (GR>0.46 classified as resistant; Fig. 3B).

To test the predictive performance of this threshold, we applied LOOCV and data randomization. Here, we used 11 samples as a training set to identify the two complementary DRCs with the highest variance, as described above. Then, for each of our 12 PDOs, the GR score was determined by summing the GR value of the 11 data points within these two complementary DRCs. Next, we randomly reassigned our 12 GR scores among 6 sensitive and 6 resistant 'patients'. Using the GR scores of the 11 training samples, we set a threshold and used this cut-off to classify the 12th (validation) sample as either sensitive or resistant (fig. S2A). In this manner, tested samples were never used to determine the threshold. As with our empirically determined threshold, we set the threshold by selecting the highest GR score that correctly classified all sensitive patients within the test set of 11 PDOs, while correctly classifying the maximum number of resistant patients within the test set of 11 PDOs. Within each loop, the data randomization step was performed 120,000 times. This entire procedure was repeated 12 times in total, each time leaving out a different PDO. The p-value for our

empirically determined threshold was calculated by dividing the number of cases where a randomly generated classifier threshold performed as well as, or better than, our empirically determined classifier threshold by the number of iterations executed.

Statistical analysis

Groups were compared using a Mann-Whitney test in case of continuous variables and Fisher's exact test in case of categorical values. Difference in PFS was calculated using the (Mantel–Cox test) log-rank test. Concordance between replicates was calculated using Pearson's R. All statistical tests were performed two-tailed in GraphPad Prism V7.03, with the exception of the correlation analysis which was done in R. P-values corrected for multiple testing using the Bonferroni correction when required, as mentioned in the figure legends. P-values <0.05 were considered significant.

Acknowledgments

We would like to acknowledge Chiara Cattaneo, Christina Stangl, Rene Bernards, Daniel Peeper, David Vredevoogd, Piet Borst, Hugo Snippert, Silvia Boj, Marc van de Wetering and Rene Overmeer for useful discussions and advice. We would like to acknowledge Stef van Lieshout and Ewart de Bruijn for performing authentication of PDOs and Suzanne van der Kolk, Judith Westra and Sandra Visser for help with patient inclusion. Rspondin-producing cells were a kind gift from C. Kuo (Stanford). Special thanks to Katarzyna Jozwiack and Karolina Sikorska for input on statistical analysis and Ben Morris and the Netherlands Cancer Institute Robotics and Screening Facility for advice on experimental design and all other research facilities at the NKI for their contribution and help. Furthermore, we would like to thank all participating centers, medical oncologists, and patients for contributing to the study.

Funding

This study supported by grants of the Koningin Wilhelmina Fonds (KWF; EV.**;** NKI2015-7732 and HUBR2014-7006) and the Nederlands Wetenschappelijk Orgaan (NWO gravitation program (EEV; 2012-2022; on behalf of the CancerGenomicsCenter.nl).

Author contributions

SNO and CMM designed and performed experiments, analyzed the data, and wrote the paper with input of all authors. FW coordinated the clinical trial. KKD contributed to the design and conceptual basis of the study. SK provided technical assistance in establishing, culturing, and expanding PDOs. EvW contributed to the statistical design. LH and LS provided assistance in coordinating the clinical trial. DJV assisted in analysis of the drug response data. JvdH contributed to the analysis. WP and PS provided radiological/pathological expertise. DvdV

provided assistance in coordinating the clinical trial. MK performed experiments. MC, HB, MvL, HJB, and LVB included patients. LW provided bioinformatics expertise. EC coordinated WGS. HC contributed to the design and conceptual basis of the study. EEV contributed to the (experimental) design and conceptual basis of the study, and supervised the overall execution of the study.

Competing interests

EEV is the medical director of the Netherlands Cancer Institute. EEV, SNO, FW, KKD and CMM have a filed patent related to the data in this manuscript. HC is an inventor of several patents regarding organoids culture. All other authors declare no competing interests.

Data and materials availability

All data needed to evaluate the conclusions in the paper are present in the paper and/or in the supplementary materials. Reagents obtained under material transfer agreement (MTA) are: Producer lines for conditioned medium of Wnt-3a, Noggin (Hans Clevers, Hubrecht Institute) and R-spondin-1 (Calvin Kuo, Stanford). Distribution of PDOs and deposition of DNA sequencing data in publicly available databases is regulated by the informed consent that participants to this study signed. If available**,** PDOs, clinical outcome, DNA sequencing data and safety data on a per patient level can be obtained through the Institutional Review Board of the Netherlands Cancer Institute (IRB@nki.nl). All other code and materials used in this manuscript are freely or commercially available.

List of supplementary materials

Fig. S1: Overview of clinical and genetic parameters in PDO cohorts.
Fig. S2: Overview of the irinotecan PDO-patient cohort.
Fig. S3: Development and cross-validation of an irinotecan-classifier.
Fig. S4: Overview of the 5-FU-irinotecan PDO-patient cohort.
Fig. S5: Development and cross-validation of a 5-FU-irinotecan-classifier
Fig. S6: Overview of the 5-FU-oxaliplatin PDO-patient cohort
Fig. S7: 5-FU-oxaliplatin drug responses of synchronous and paired metastases
Fig. S8: Interactions of clinical and genetic parameters with patients and PDO responses
Table S1: Characteristics and clinical history of all included patients in the TUMOROID study.
Table S2: Genetic and pathological characteristics of patients in the TUMOROID study.
Table S3: Chemotherapy, radiotherapy and surgery prior to the biopsy procedure.

REFERENCES AND NOTES

1. K. D. Miller *et al.*, Cancer treatment and survivorship statistics, 2016. *CA. Cancer J. Clin.* **66**, 271–289 (2016).
2. A. Grothey, D. Sargent, R. M. Goldberg, H.-J. Schmoll, Survival of patients with advanced colorectal cancer improves with the availability of fluorouracil-leucovorin, irinotecan, and oxaliplatin in the course of treatment. *J. Clin. Oncol.* **22**, 1209–14 (2004).
3. H. G. Prigerson *et al.*, Chemotherapy Use, Performance Status, and Quality of Life at the End of Life. *JAMA Oncol.* **1**, 778 (2015).
4. J. Cassidy *et al.*, XELOX (capecitabine plus oxaliplatin): active first-line therapy for patients with metastatic colorectal cancer. *J. Clin. Oncol.* **22**, 2084–91 (2004).
5. C. Tournigand *et al.*, FOLFIRI Followed by FOLFOX6 or the Reverse Sequence in Advanced Colorectal Cancer: A Randomized GERCOR Study. *J. Clin. Oncol.* **22**, 229–237 (2004).
6. M. T. Seymour *et al.*, Different strategies of sequential and combination chemotherapy for patients with poor prognosis advanced colorectal cancer (MRC FOCUS): a randomised controlled trial. *Lancet*. **370**, 143–152 (2007).
7. 714–726 (2013).na Holohan, Caitrio1. C. Holohan, S. Van Schaeybroeck, D. B. Longley, P. G. Johnston, Cancer drug resistance: an evolving paradigm. Nat. Rev. Cancer. 13, S. Van Schaeybroeck, D. B. Longley, P. G. Johnston, Cancer drug resistance: an evolving paradigm. *Nat. Rev. Cancer*. **13**, 714–726 (2013).
8. L. Zitvogel, L. Apetoh, F. Ghiringhelli, G. Kroemer, Immunological aspects of cancer chemotherapy. *Nat. Rev. Immunol.* **8**, 59–73 (2008).
9. C. J. A. Punt, M. Koopman, L. Vermeulen, From tumour heterogeneity to advances in precision treatment of colorectal cancer. *Nat. Rev. Clin. Oncol.* **14**, 235–246 (2017).
10. M. P. A. Ebert *et al.*, *TFAP2E–DKK4* and Chemoresistance in Colorectal Cancer. *N. Engl. J. Med.* **366**, 44–53 (2012).
11. C. G. Leichman *et al.*, Quantitation of intratumoral thymidylate synthase expression predicts for disseminated colorectal cancer response and resistance to protracted-infusion fluorouracil and weekly leucovorin. *J. Clin. Oncol.* **15**, 3223–3229 (1997).
12. C. Aschele *et al.*, Immunohistochemical Quantitation of Thymidylate Synthase Expression in Colorectal Cancer Metastases Predicts for Clinical Outcome to Fluorouracil-Based Chemotherapy. *J. Clin. Oncol.* **17**, 1760–1760 (1999).
13. M. J. Garnett *et al.*, Systematic identification of genomic markers of drug sensitivity in cancer cells. *Nature*. **483**, 570–575 (2012).
14. J. Barretina *et al.*, The Cancer Cell Line Encyclopedia enables predictive modelling of anticancer drug sensitivity. *Nature*. **483**, 603–607 (2012).
15. A. S. Crystal *et al.*, Patient-derived models of acquired resistance can identify effective drug combinations for cancer. *Science (80-.).* **346**, 1480–1486 (2014).
16. A. A. Friedman, A. Letai, D. E. Fisher, K. T. Flaherty, Precision medicine for cancer with next-generation functional diagnostics. *Nat. Rev. Cancer*. **15**, 747–756 (2015).
17. T. Sato *et al.*, Long-term expansion of epithelial organoids from human colon, adenoma, adenocarcinoma, and Barrett's epithelium. *Gastroenterology*. **141**, 1762–72 (2011).
18. J. Drost, H. Clevers, Organoids in cancer research. *Nat. Rev. Cancer*. **18**, 407–418 (2018).

19. F. Weeber *et al.*, Preserved genetic diversity in organoids cultured from biopsies of human colorectal cancer metastases. *Proc. Natl. Acad. Sci. U. S. A.* **112**, 13308–11 (2015).
20. G. Vlachogiannis *et al.*, Patient-derived organoids model treatment response of metastatic gastrointestinal cancers. *Science*. **359**, 920–926 (2018).
21. H. Tiriac *et al.*, *Cancer Discov.*, in press, doi:10.1158/2159-8290.CD-18-0349.
22. E. A. Eisenhauer *et al.*, New response evaluation criteria in solid tumours: Revised RECIST guideline (version 1.1). *Eur. J. Cancer*. **45**, 228–247.
23. K. K. Dijkstra *et al.*, Generation of Tumor-Reactive T Cells by Co-culture of Peripheral Blood Lymphocytes and Tumor Organoids. *Cell*. **0** (2018), doi:10.1016/j.cell.2018.07.009.
24. R. Yaeger *et al.*, Clinical Sequencing Defines the Genomic Landscape of Metastatic Colorectal Cancer. *Cancer Cell*. **33**, 125–136.e3 (2018).
25. M. Hafner, M. Niepel, M. Chung, P. K. Sorger, Growth rate inhibition metrics correct for confounders in measuring sensitivity to cancer drugs. *Nat. Methods*. **13**, 521–527 (2016).
26. A. Zehir *et al.*, Mutational landscape of metastatic cancer revealed from prospective clinical sequencing of 10,000 patients. *Nat. Med.* **23**, 703–713 (2017).
27. J. K. Sicklick *et al.*, Molecular profiling of cancer patients enables personalized combination therapy: the I-PREDICT study. *Nat. Med.* **25**, 744–750 (2019).
28. J. T. Neal *et al.*, Organoid Modeling of the Tumor Immune Microenvironment. *Cell*. **175**, 1972–1988.e16 (2018).
29. M. M. Y. Liang-Chu *et al.*, Human Biosample Authentication Using the High-Throughput, Cost-Effective SNPtraceTM System. *PLoS One*. **10**, e0116218 (2015).
30. P. Priestley *et al.*, Pan-cancer whole genome analyses of metastatic solid tumors. *bioRxiv*, 415133 (2018).
31. B. Reigner, K. Blesch, E. Weidekamm, Clinical Pharmacokinetics of Capecitabine. *Clin. Pharmacokinet.* **40**, 85–104 (2001).
32. M. A. Graham *et al.*, Clinical pharmacokinetics of oxaliplatin: a critical review. *Clin. Cancer Res.* **6**, 1205–18 (2000).
33. G. G. Chabot, Clinical Pharmacokinetics of Irinotecan. *Clin. Pharmacokinet.* **33**, 245–259 (1997).

SUPPLEMENTARY MATERIALS

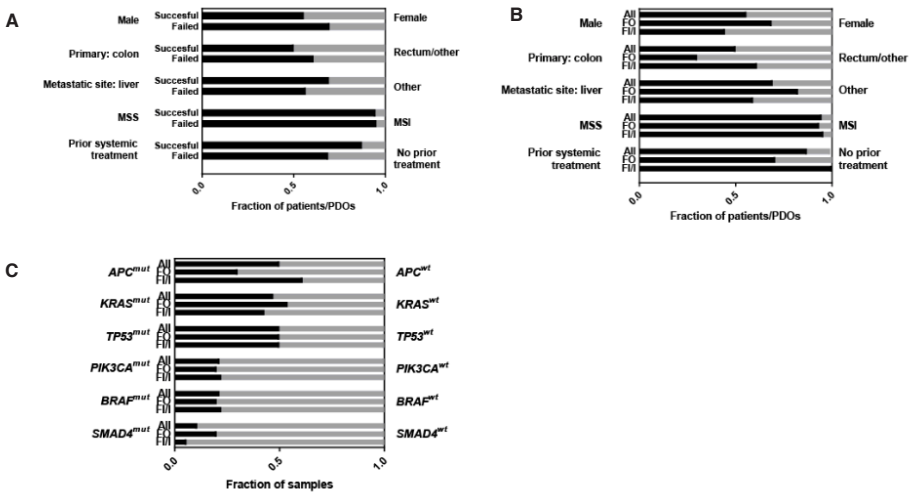

Fig. S1 Overview of clinical and genetic parameters in PDO cohorts.

(A) Bar graphs comparing clinical parameters between cohorts for which PDO establishment was or was not successful. MSS = microsatellite stable, MSI = microsatellite instable. (**B**) Bar graphs comparing clinical parameters between the first line 5-FU + oxaliplatin (FO) versus second line 5-FU + irinotecan/irinotecan alone (FI/I) cohorts versus all PDOs. (**C**) Bar graphs comparing frequencies of CRC drivers between the first line (FO) versus second line (FI/I) cohorts versus all PDOs.

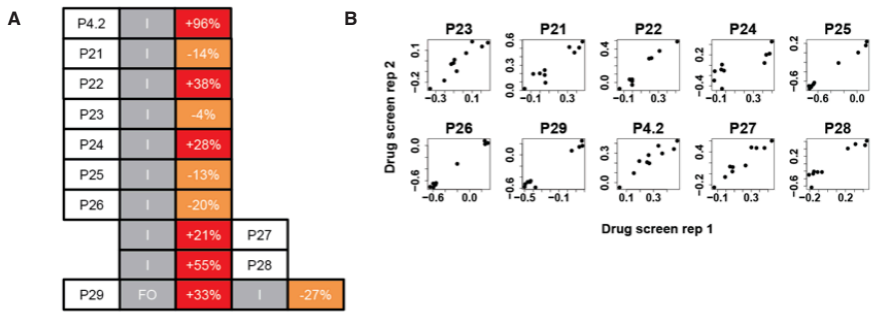

Fig. S2 Overview of the irinotecan PDO-patient cohort.

(A) The patient/sample number (p#), treatment (I = irinotecan, FO = 5-FU plus oxaliplatin), and subsequent response are presented. All patients were biopsied before start of treatment. Exceptions are P27 and P28, which were biopsied after the patient progressed on treatment. + or - indicates the percentage of tumor growth or shrinkage compared to the first evaluation (best response). **(B)** Correlation plot of

screen 1 versus screen 2 for all 10 PDOs, performed by independent researchers. For each PDO, the GR value of each of the 10 data points in the dose response curve was plotted, with the values from screen 1 on the x-axis and the values from screen 2 on the y-axis.

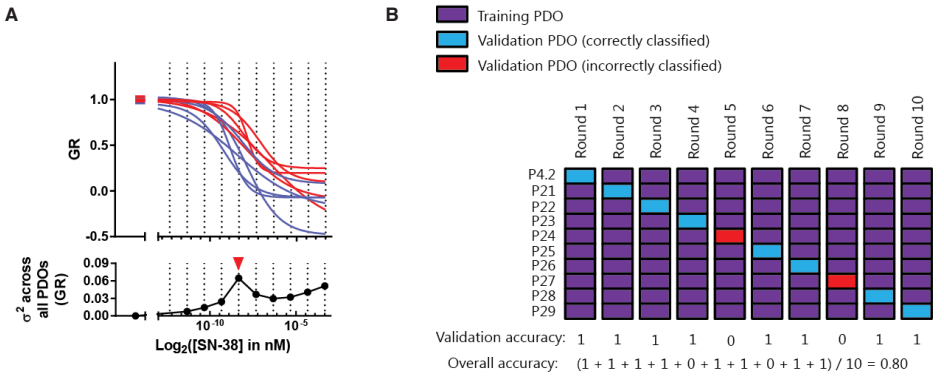

Fig. S3 Development and cross-validation of an irinotecan classifier.

(A) For all patients in the irinotecan cohort, we generated dose-response curves (DRCs) and compared these to the clinical response (top panel). For each data point in the DRCs, we calculated the variance (σ^2 on the y-axis, bottom panel) across all 10 PDOs, revealing data points that yield a large window of effect. We found that 3.2 nM SN-38 yielded the largest window of effect, as indicated by the red arrow. **(B)** To test whether our data were overfitted, we tested our prediction model in the context of a leave-one-out cross-validation (LOOCV). Briefly, we used 9 samples as a training set to identify data points with the highest variance, as described above in panel A. For all 10 PDOs, a GR score was then calculated based on this data point. Using the GR scores of the 9 training samples, we set a threshold and used this cut-off to classify the 10th (validation) sample as either sensitive or resistant. We set the threshold by selecting the highest GR score that correctly classified all sensitive patients within the test set of 9 PDOs, while correctly classifying the maximum number of resistant patients within the test set of 9 PDOs. This procedure was repeated 10 times in total, each time leaving out a different PDO. The percentage of total successful predictions over 10 repeats was then taken as a measure of overall accuracy.

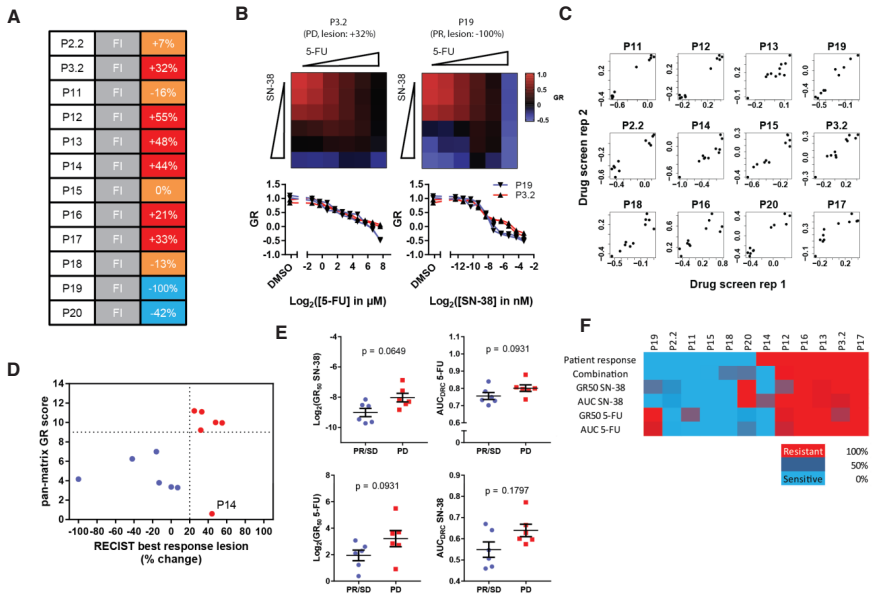

Fig. S4 Overview of the 5-FU-irinotecan PDO-patient cohort.

(A) The patient/sample number (p#), treatment (FI = 5-FU plus irinotecan), and subsequent response are presented. The position of the p# relative to the treatment and response indicates whether the biopsy was taken before treatment or at progression. **(B)** Correlation plot of screen 1 versus screen 2 for all 12 PDOs, performed by independent researchers. For each PDO, the GR value of each of the 11 data points in the 2 complementary dose response curves identified as having the largest variance within our samples was plotted, with the values from screen 1 on the x-axis and the values from screen 2 on the y-axis. **(C)** Representative results of the in vitro drug sensitivity screen. Top panels: Heatmaps representing the GR score for each of the 36 data points in the combination drug sensitivity matrix. P19 is a patient sensitive to FI treatment, whereas P3.2 is a patient resistant to FI treatment. Bottom panels: Single-agent dose response curves for 5-FU (left panel) and SN-38 (right panel). Both biological replicates of the screens are plotted. **(D)** Pan-matrix GR score was calculated by summing the 36 values of the data points in the full combination matrix as depicted in the top panel of fig. S4B. Pan-matrix GR scores were plotted on the x-axis versus RECIST best response of the biopsied lesion response on the y-axis. The dotted, vertical line represents the cut-off of the PR/SD and PD groups as defined by RECIST. The horizontal dotted line represents a test cut-off that could be applied to discriminate between PR/SD and PD patients when considering pan-matrix GR score as test metric. **(E)** For each panel, pharmacological parameters of PR/SD (n=6) versus PD (n=6) lesions were compared using the Mann-Whitney test. In the 2 panels on the left, the log base 2 of the GR_{50} of either 5-FU (top) or SN-38 (bottom) is graphed. In the 2 panels on the right, the AUC of either 5-FU (top) or SN-38 (bottom) is graphed. Dots/squares represent individual PDOs, and error bars indicate standard error of the mean. **(F)** Heatmap of in vitro drug responses and lesion responses per patient, summarizing fig. S4D and E. Blue indicates sensitive and red resistant.

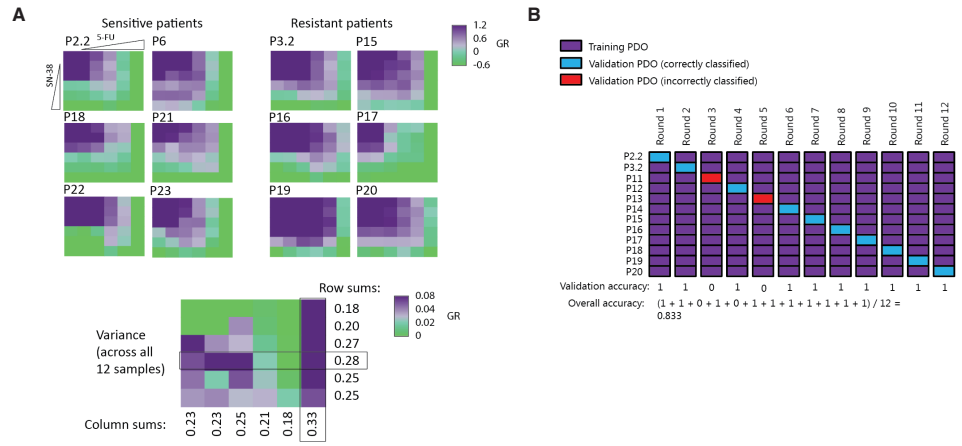

Fig. S5 Development and cross-validation of a 5-FU-irinotecan classifier.

(A) For all patients in the FI cohort, we generated drug matrices to evaluate the effect of 5-FU (horizontal), irinotecan (vertical), and all possible combinations of both drugs and compare this to clinical response (top panel). For each data point in the matrix, we calculated the variance across all 12 PDOs, resulting in a matrix that reveals what data points or part of the matrix yield a large window of effect. When we summed all rows and columns, we found that the last column and the fourth row yielded the largest window of effect (bottom panel). Based on these two combined dose-response curves, yielding 11 data points, we continued to develop our test for clinical response to FI. **(B)** To test whether our data were overfitted, we tested our prediction model in the context of a leave-one-out cross-validation (LOOCV). Briefly, we used 11 samples as a training set to identify DRCs with the highest variance, as described above in panel A. For all 12 PDOs, a GR score was then calculated from these DRCs. Using the GR scores of the 11 training samples, we set a threshold and used this cutoff to classify the 12^{th} (validation) sample as either sensitive or resistant. We set the threshold by selecting the highest GR score that correctly classified all sensitive patients within the test set of 11 PDOs, while correctly classifying the maximum number of resistant patients within the test set of 11 PDOs. This procedure was repeated 12 times in total, each time leaving out a different PDO. The percentage of total successful prediction over 12 repeats was then taken as a measure of overall accuracy.

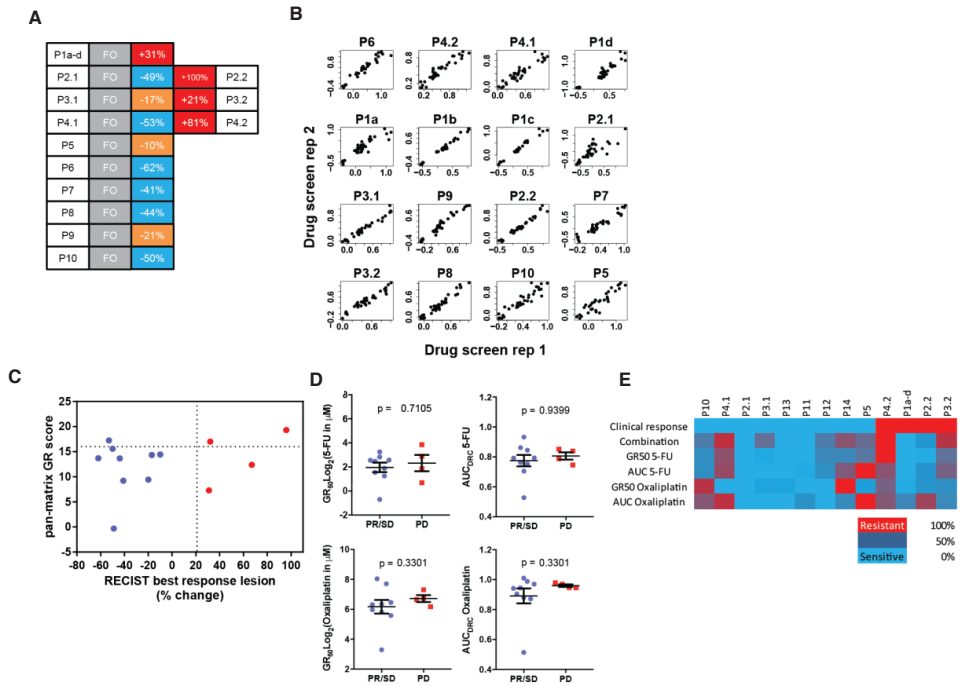

Fig. S6 Overview of the 5-FU-oxaliplatin PDO-patient cohort.

(A) The patient/sample number (p#), treatment (FO = 5-FU plus oxaliplatin) and subsequent response are presented. The position of the p# relative to the treatment and response indicates whether the biopsy was taken before treatment or at progression. For example, P2.1 was taken before the patient responded to FO treatment (-49%), and P2.2 was taken after progression on FO (+100%). **(B)** Correlation plot of screen 1 versus screen 2 for all 16 PDOs, performed by independent researchers. For each PDO, the GR value of each of the 36 data points in full combination matrix was plotted, with the values from screen 1 on the x-axis and the values from screen 2 on the y-axis. **(C)** Pan-matrix GR score was calculated by summing the 36 values of the data points in the full combination matrix. Pan-matrix GR scores were plotted against the RECIST best response of the biopsied lesion. The dotted vertical line represents the cut-off of the PR/SD and PD groups as defined by RECIST. The horizontal dotted line represents a test cut-off that could be applied to discriminate between PR/SD and PD patients when considering pan-matrix GR score as test metric. **(D)** For each panel, scores of PR/SD (n=13) versus PD (n=4) patients were compared using the Mann-Whitney test. In the 2 panels on the left, the log base 2 of the GR_{50} of either 5-FU (top) or oxaliplatin (bottom) is graphed. In the 2 panels on the right, the AUC of either 5-FU (top) or oxaliplatin (bottom) is graphed. Dots/squares represent individual PDOs (except for P1a-d, which are represented as the average of these 4 samples), and error bars indicate standard error. **(E)** Heatmap of in vitro drug responses and lesion responses per patient, summarizing fig. S6C and D. Blue indicates sensitive and red resistant.

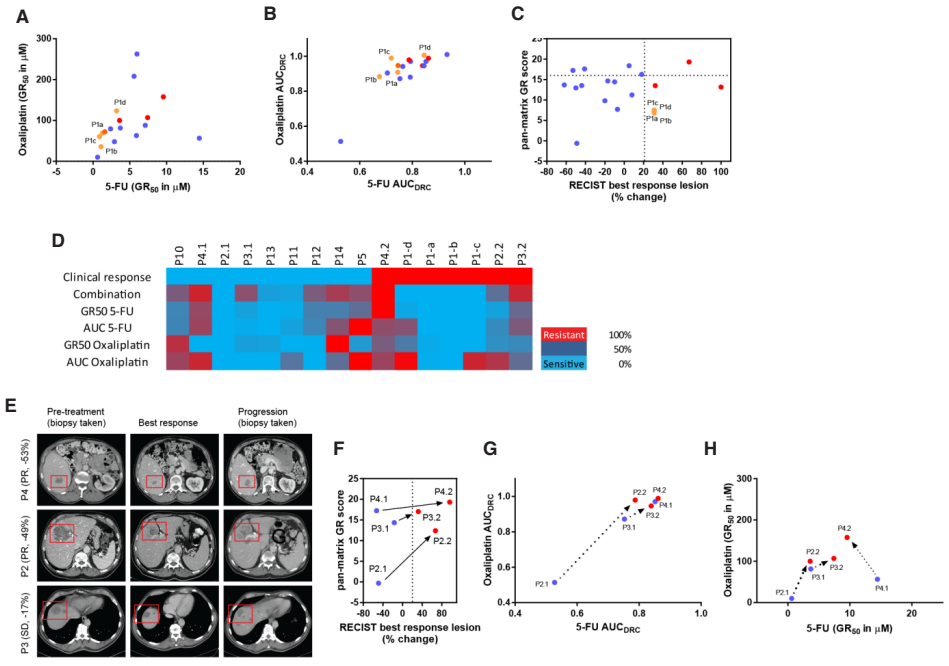

Fig. S7 5-FU-oxaliplatin drug responses of synchronous and paired metastases.

(**A**) Scatterplot of GR_{50} values of PDOs. (**B**) Scatterplot of AUC_{DRCs} values of PDOs. (**C**) Scatterplot of pan-matrix GR scores of all PDOs versus the RECIST best responses of the lesions. Blue dots represent PDOs with PR/SD and red dots with PD lesion responses. Blue dots represent responses of the 4 different lesions of P1a-d. (**D**) Heatmap of in vitro drug responses and lesion responses per patient, summarizing fig. S7A-C. Blue indicates sensitive and red resistant. (**E**) Representative CT scans of paired PDOs P2-4 before start of treatment, at best response, and at progression. The text on the left states the patient number, the RECIST response and the % shrinkage of the target lesion, which is indicated by the red box. (**F**) Dot plot of pan-matrix GR scores of P2-4 versus the RECIST best responses of the lesions. Arrows represent the change in drug sensitivity from before to after treatment. (**G**) Dot plot of AUC_{DRCs} values of P2-4. Blue dots represent pre-treatment and red dots post-treatment samples. (**H**) Dot plot of GR_{50} values of P2-4. Blue dots represent pre-treatment and red dots post-treatment samples.

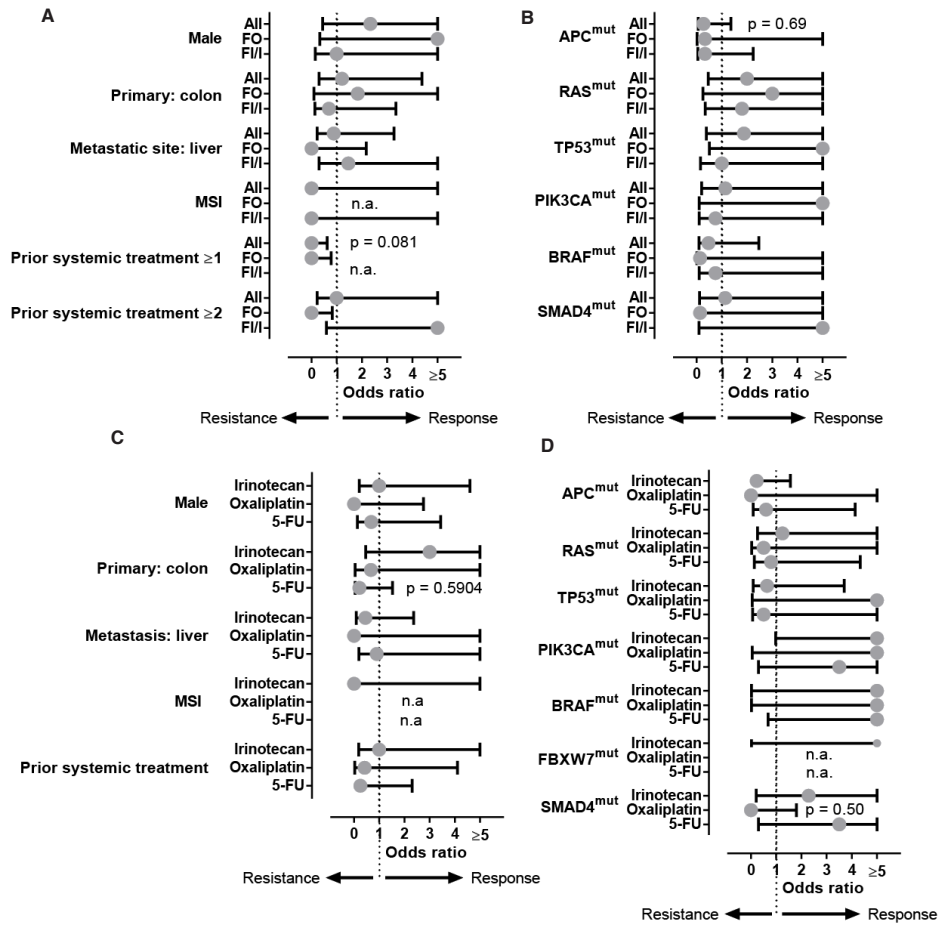

Fig. S8 The effect of clinical and genetic parameters on patients and PDO responses.

(**A**) Plot of clinical parameters and their association with lesion response or resistance, calculated over all samples or separately in the 1st (FO) and 2nd (FI/I) line cohorts. FO = 5-FU + oxaliplatin, FI/I = 5-FU + irinotecan. (**B**) Plot of genetic aberrations in common CRC drivers and their association with lesion response or resistance. (**C**) Plot of clinical parameters and their association with in vitro drug response to irinotecan, oxaliplatin, or 5-FU. (**D**) Plot of genetic aberrations in common CRC drivers and their association with in vitro drug response. Dots represent the odds ratio and the bars corresponding confidence intervals. Intervals that exceeded 6 were trimmed to ≥5 for readability. Odds ratios and p-values were computed using a two-tailed Fisher-exact test. Lowest Bonferroni-adjusted p-value of each panel were reported in the graph; n.a. = not available.

Table S1 Characteristics and clinical history of all included patients in the TUMOROID study.

PATIENT CHARACTERISTICS				
Study number	**Gender**	**Age at study entry**	**Age at diagnosis**	**Oncological medical history**
P1	M	67	64	-
P2.1	M	72	64	-
P2.2	M	73	64	-
P3.1	M	63	63	-
P3.2	M	63	63	-
P4.1	M	68	67	-
P4.2	M	69	67	-
P5	F	54	54	-
P6	M	72	72	-
P7	M	54	54	-
P8	F	58	55	-
P9	F	66	65	-
P10	M	78	77	-
P11	M	53	52	-
P12	F	49	47	-
P13	M	70	70	-
P14	F	47	45	-
P15	M	56	51	-
P16	F	62	61	-
P17	M	54	52	-
P18	F	33	34	-
P19	M	69	66	-
P20	F	55	54	-
P21	F	63	62	-
P22	F	65	64	Synchronous double tumor rectum and colon (2016); neuro-endocrine tumor appendix (2016)
P23	F	86	84	-
P24	F	30	29	-
P25	F	58	56	-
P26	M	56	55	-
P27	F	65	61	-
P28	M	52	51	-
P29	M	80	80	Prostate cancer (2011)

Table S2 Genetic and pathological characteristics of patients in the TUMOROID study. Part of each biopsy was used for pathological examination and targeted sequencing (performed on: P1, 2.1, 2.2, 4.1, 4.2, P6, P12, P13, P19, P29) or whole-genome sequencing (performed on: P3, 5-11, P14-18, P20-28), NOS = not otherwise specified, NA = not available/determined, '-' indicates no mutations found, * = truncation, fs = frameshift, sdv = splice-donor variant, MSS = microsatellite stable, MSI = microsatellite instable.

TUMOR CHARACTERISTICS					
Study number	**Localization**	**Differentiation**	**Genetic profile**		**Biopsied lesion**
			Mutations	MSI status	
P1	Rectum	Moderately	BRAF (V600E)	MSS	Skin
P2.1	Rectosigmoid	NA	-	MSS	Liver
P2.2	Rectosigmoid	NA	-	MSS	Liver
P3.1	Colon	Moderately	PIK3CA (G545L); KRAS (G12C); APC (T1493R)	MSS	Liver
P3.2	Colon	Moderately	APC (T1493R); KRAS (G12C); SMAD4 (R361C)	MSS	Liver
P4.1	Colon	NA	MEK1 (K57N)	MSS	Liver
P4.	Colon	NA	MEK1 (K57N)	MSS	Liver
P5	Colon	Poorly	PIK3CA (E110del); TP53 (p.R209fs)	MSS	Liver
P6	Colon	Moderately	KRAS (G12A)	MSS	Liver
P7	Colon	NA	AKT1 (E17K); KRAS (A146T)	MSS	Liver
P8	Colon	Undifferentiated	TP53 (V173L); KRAS (G13D); EGFR (G724V)	MSS	Lymph node
P9	Colon	Moderately	NA	NA	Liver
P10	Colorectal NOS	Moderately	NA	NA	Liver
P11	Colon	Moderately	KRAS (G12C); SMAD4 (Q245*); TP53 (R205D)	MSS	Liver
P12	Rectum	Moderately	NRAS (G12C)	MSS	Liver
P13	Colon	Poorly	MEK1 (Q56P)	MSS	Lymph node
P14	Colon	NA	APC (R1450*); BRAF (V600E); PIK3CA (E545K)	MSS	Liver
P15	Rectum	NA	-	MSS	Lymph node
P16	Rectum	Poorly	APC (G1288X); KRAS (G13A); BRAF (N594G); TP53 (E286K)	MSS	Breast
P17	Rectum	Moderately	FBXW7 (R465C); APC (R564*/P1439fs*34); KRAS (G12A); ERBB3 (E332K); TP53 (C141Y)	MSS	Liver
P18	Rectum	Moderately	PIK3CA (A38H); EGFR (A521L); PTCH1 (S1220T); TP53 (G294*); TP53 (G294*); SMAD4 (A537H)	MSS	Rectum
P19	Colon	Moderately	-	MSS	Omentum
P20	Rectosigmoid	Moderately	MSH2 (L92I); FBXW7 (G557V); APC (E1306*/E1353*); PALB2 (V425M); ARAF (D46N)	MSS	Liver
P21	Rectum	NA	KRAS (A146T); BARD1 (P182L); APC (P2216T/G1367*); CSF1R (A150C); MET (A426H); PTCH1 (A497T); TP53 (A175H)	MSS	Lung
P22	Colorectal NOS	NA	BRAF (V600E)	MSI	Peritoneum

Table S2 continued.

TUMOR CHARACTERISTICS					
Study number	**Localization**	**Differentiation**	**Genetic profile**		**Biopsied lesion**
			Mutations	MSI status	
P23	Colon	Well/moderately	PIK3CA (E545G); FBXW7 (R278*); KRAS (G12D); APC (S1411fs)	MSS	Liver
P24	Colon	Well/moderately	KRAS (G12C); APC (S1411fs); TP53 (R282W); ERK2 (Y263F); BRCA2 (T2662M); FANCA (L316V); TP53 (C238fs)	MSS	Liver
P25	Colon	Moderately	PIK3CA (G542K); KDS (A750P); APC (Q1429*); KRAS (G12V); TP53 (A161T/R110C)	MSS	Liver
P26	Rectum	Poorly	KRAS (G13D)	MSS	Lymph node
P27	Colon	Moderately	-	MSS	Liver
P28	Rectum	Well/moderately	HRAS (A59T); APC (E484*); TP53sdv; NF1 (R304*)	MSS	Liver
P29	Colon	Moderately	FBXW7 (G437E/R278*); APC (T1459fs); KRAS (A146V); TP53 (G245S)	NA	Liver

Table S3 Overview of the 3 cohorts and prior treatment and procedures.

CAP = Capecitabine, CAPOX = capecitabine + oxaliplatin, FOLFOX = infusional 5-FU + oxaliplatin. Addition of B = bevacizumab, * = also used in the FI cohort, # = also used in the irinotecan cohort, N/A = not available.

OVERVIEW OF THE COHORTS		SYSTEMIC TREATMENT AND PROCEDURES PRIOR TO BIOPSY			
Cohort	Study number	Treatment regimen	Surgery	Radiotherapy	Systemic treatment
			# of regimens		
5-FU + oxaliplatin	P1	CAPOX-B trametinib/panitumumab	1	2	3
	P2.1	CAPOX-B (adjuvant)	3	0	1
	P2.2*	FOLFOX	3	0	2
	P3.1	-	0	0	0
	P3.2*	CAPOX-B	0	0	1
	P4.1	-	3	0	0
	P4.2#	CAPOX-B	3	0	1
	P5	-	0	0	0
	P6	-	0	0	0
	P7	-	N/A	0	0
	P8	CAPOX (adjuvant)	1	1	1
	P9	-	1	0	0
	P10	Capecitabine	N/A	0	1
5-FU + irinotecan	P11	CAPOX-B	1	0	1
	P12	CAPOX-B (neoadjuvant)	1	1	1
	P13	CAPOX-B	0	0	1
	P14	CAPOX-B	0	0	1
	P15	CAPOX-B/panitumumab	3	1	2
	P16	CAP-B	N/A	2	1
	P17	CAPOX-B	0	1	2
	P18	CAPOX-B	0	0	1
	P19	CAPOX-B/panitumumab	1	1	2
	P20	FOLFOX-B	1	1	1
Irinotecan	P21	CAPOX	1	0	1
	P22	CAPOX	1	1	1
	P23	Capecitabine	1	0	1
	P24	CAPOX	0	0	1
	P25	FOLFOX	3	0	1
	P26	FOLFOX-B	1	1	1
	P27	Irinotecan	2	4	2
	P28	Irinotecan	1	1	2
	P29	CAP-B (intermittent treatment)	0	0	0

CHAPTER 3

IN VIVO MODELING OF METASTATIC COLORECTAL CANCER ORGANOIDS AND MATCHED CLINICAL RESPONSES OF PATIENTS

Salo N. Ooft[1,2], Fleur Weeber[1,2], Krijn K. Dijkstra[1,2], Sovann Kaing[1,2], Natalie Proost[2], Bas van Gerwen[3], Bjørn Siteur[3], Renske de Korte-Grimmerink[3], Chiara M. Cattaneo[1,2], Ji-Ying Song[4], Erik van Werkhoven[5], Henk Boot[6], Monique van Leerdam[6], Haiko J. Bloemendal[7], Myriam Chalabi[1,2,6], Marieke van de Ven[3,8], and Emile E. Voest[1,2,6,*].

Affiliations:

[1]Department of Molecular Oncology and Immunology, Antoni van Leeuwenhoek Hospital-The Netherlands Cancer Institute, Amsterdam, 1066 CX Amsterdam, The Netherlands.

[2]Oncode Institute, 3521 AL Utrecht, The Netherlands.

[3]Mouse Clinic for Cancer and Aging Research (MCCA), Preclinical Intervention Unit, Antoni van Leeuwenhoek Hospital-The Netherlands Cancer Institute, 1066 CX Amsterdam, The Netherlands.

[4]Department of Experimental Animal Pathology Antoni van Leeuwenhoek Hospital-The Netherlands Cancer Institute, Amsterdam, 1066 CX Amsterdam, The Netherlands.

[5]Department of Biometrics, Antoni van Leeuwenhoek Hospital-The Netherlands Cancer Institute, 1066 CX Amsterdam, The Netherlands.

[6]Department of Gastrointestinal Oncology, Antoni van Leeuwenhoek Hospital-The Netherlands Cancer Institute, Amsterdam, 1066 CX Amsterdam, The Netherlands.

[7]Department of Internal Medicine/Oncology, Radboud University Medical Center Nijmegen, 6525 GA Nijmegen, Netherlands

[8]Department of Molecular Pathology, Antoni van Leeuwenhoek Hospital-The Netherlands Cancer Institute, 1066 CX Amsterdam, The Netherlands.

*Corresponding author. Email: e.voest@nki.nl.

Cancer Research (submitted)

ABSTRACT

Organoid culture technology has been adopted with much enthusiasm in the field of translational oncology. Patient-derived organoids (PDOs) reiterate genetic, histological and clinical features of patient tumors, and have therefore become a versatile platform for cancer research. However, there are inherent drawbacks to the use of in vitro culture systems. We previously demonstrated that, in contrast to irinotecan-based regimens, the therapeutic effect of 5-FU + oxaliplatin (5-OX) was not recapitulated in vitro, likely owing to the reductive nature of culture systems. We hypothesized that patient-derived organoids xenografts (PDOX) are more suitable to study (systemic) effects of 5-OX, because it includes features absent in culture models, such as tumor stroma and systemic drug metabolism. To address this hypothesis, we subcutaneously injected PDOs in Foxn1nu mice and obtained an average take-rate of 95%. Mice were subsequently treated with 5-OX and in 6/9 cases treatment outcome was identical to the clinical response of corresponding patients. In 3/9 cases, however, patients experienced substantial clinical benefit, while PDOXs were resistant to 5-OX. Additional analysis showed that the use of PDOX models did not improve upon the limited correlation established earlier between patient and in vitro outcome (Cohen's β coefficient = 0.42 for in vitro versus 0.40 in vivo). Rather, the in vivo outcome strongly correlated to in vitro drug sensitivity (8/9 concordant; β = 0.72). Our data demonstrate that we can successfully model PDOs in vivo, but that there is limited use for mouse PDOX model systems in predicting clinical responses to 5-OX of patients.

INTRODUCTION

Patient-derived xenograft (PDX) models have been instrumental for cancer research because they allow propagation of human tumors in mice, including a (rudimentary) microenvironment, to study drug metabolism, and perform tumor imaging and drug testing. Drug sensitivity of PDXs can deviate significantly from cell lines, and they are therefore valuable to complement in vitro findings[1-3]. PDXs have also been shown to model patient responses to some forms of treatment in mice and can be used to prioritize treatment options for cancer patients in co-clinical trials, which further underscores their value for translational oncology[4,5]. Demonstrating a cytostatic or cytotoxic effect of a given drug in PDX models is therefore considered a strong supportive step of pre-clinical drug development and is often succeeded by phase 1/2 clinical studies. Both the United States and Europe have initiated large collaborative consortia, such as EuroPDX, to systematically gather and annotate PDX models as avatars for patient cohorts[6]. However, there are also technical limitations to PDX models such as time-to-establishment, costs, scalability, variable and biased engraftment, and mouse-specific tumor evolution[5,7]. And finally, there is an increasing call for reducing animal experimentation

Organoid culture technology has enabled the in vitro expansion of individual patient's tumors, allowing for pharmacological testing of tumors in a dish, thereby reducing the need for animal experiments[8,9]. Patient-derived organoids (PDOs) can be established from needle biopsies, and may complement cell lines and resource-intensive PDXs[10,11]. PDOs, like PDXs, recapitulate histological and genetic characteristics *in vitro* and can reinstate the histological features of individual patient tumors in vivo[9,12]. Importantly, for several treatments, PDO response correlated with clinical responses of patients[13-18]. PDOs have therefore been proposed as a means for precision medicine, although formal prospective studies still have to be performed to determine predictive value[13-18]. Current limitations of PDOs are low success rates of establishing PDOs from biopsies, artificial culture conditions, absence of tumor stroma, and possible overgrowth of normal epithelial cells from the site of origin[13,19,20].

We previously established a large collection of PDOs from metastatic colorectal cancer (CRC) matched with clinical responses as avatars for precision medicine. PDOs mirrored clinical responses to irinotecan and 5-FU + irinotecan *in vitro*, but not to the combination 5-FU + oxaliplatin (5-OX). Potential explanations may be the systemic effects of the 5-OX drug combination, the complex pharmacokinetics of oxaliplatin or medium-drug interactions[21]. The absence of tumor stroma may also be relevant[22]. Large comparative PDO-PDX studies described that drug sensitivity can differ significantly between PDOs and PDXs[23]. We therefore reasoned that patient-derived organoid xenografts (PDOXs) may harbor a different drug

sensitivity profile, because it incorporates several parameters not present *in vitro*, such as (hepatic) drug metabolism and the presence of tumor stroma, and could therefore improve upon the limited correlation of PDOs and patient drug responses to 5-OX reported in our previous study[16]. Here we established a PDOX cohort and systematically compared their drug responses to 5-OX and the clinical outcome of 9 patients on the same chemotherapy regimen to determine whether PDOXs (or potentially a combination of PDO and PDOX) can be used to predict treatment responses of patients.

RESULTS

First, we analyzed take rates and tumor outgrowth of subcutaneously injected PDOs of metastatic CRC derived from 10 individual patients in 10-12 *Foxn1*^{nu} mice per PDO line (6x10^5 cells/mouse; Fig. 1a), as these are commonly used for PDX and PDOX of mCRC modeling alike[5,16,23,24]. Across all PDOs we achieved an average engraftment rate of 95% (range 75-100%; Fig. 1b). On average, mice had established tumors of 200 mm^3 63 days (range 23-114 days) after the tumor cells were injected in the flank (Fig. 1c).

Because patients were included in the context of a prospective clinical study, the TUMOROID, we had clinical (response) data available of these 9 patients and the corresponding PDOs. Detailed genetic and clinical data are presented in table S1. All patients were treated with 5-OX and demonstrated a broad spectrum of clinical responses according to response evaluation criteria in solid tumours (RECIST) 1.1 metric: four had partial responses (TUM003, TUM009, TUM048, TUM055), 2 stable disease (TUM036, TUM038) and 3 PDOs were derived from patients with progressive disease (TUM009-2, TUM20-4, TUM052) on 5-OX in the clinic (Fig. 2a)[25]. We subsequently treated PDOXs with the maximum-tolerated dose (MTD) of 5-OX for 12 days. After treatment, tumors were allowed to re-grow until 1500 mm^3 (Fig. 1b).

Three PDOs were sensitive to 5-OX treatment: TUM038, TUM048 and TUM055, in line with the clinical response of the patients from which the organoids were derived (Fig. 2b). Treatment of PDOXs of three other patients with either partial response or stable disease, TUM003, TUM009 and TUM036 respectively, did not elicit a significant response (Fig. 2b). The PDOXs of patients with progressive disease, TUM009-2, -020-4 and -052, were all resistant to 5-OX (Fig. 2c). The outcome between clinical and PDOX drug response therefore correlated in 6/9 cases (Fig. 2d). To evaluate whether treatment of PDOXs led to a different conclusion on drug sensitivity than in vitro PDO treatment, we calculated the Cohen's kappa coefficient (β; a measure of agreement between two 'categories' with binary outcomes, corrected for chance) for outcome to 5-OX between patients, PDOs and PDOXs. We previously demonstrated only a

moderate agreement between *in vitro* and patient outcome (Fig. 2d-e; β = 0.42) and this did not improve with the use of PDOXs Fig. 2d-e; β = 0.40)[16]. This contrasts to the agreement between *in vivo* and *in vitro* outcome, which was concordant in 8/9 cases (Fig 2d-e; β = 0.73; only TUM020-4 deviated between both models). Collectively, our data suggest that PDOXs can successfully be established from PDOs. The presence of a rudimentary tumor micro-environment and systematic drug metabolism in the equation did not improve the correlation of patient and PDO drug responses suggesting that, at least in case of 5-OX treatment of mCRC, the use of subcutaneous PDOXs has limited added value to predict treatment outcome.

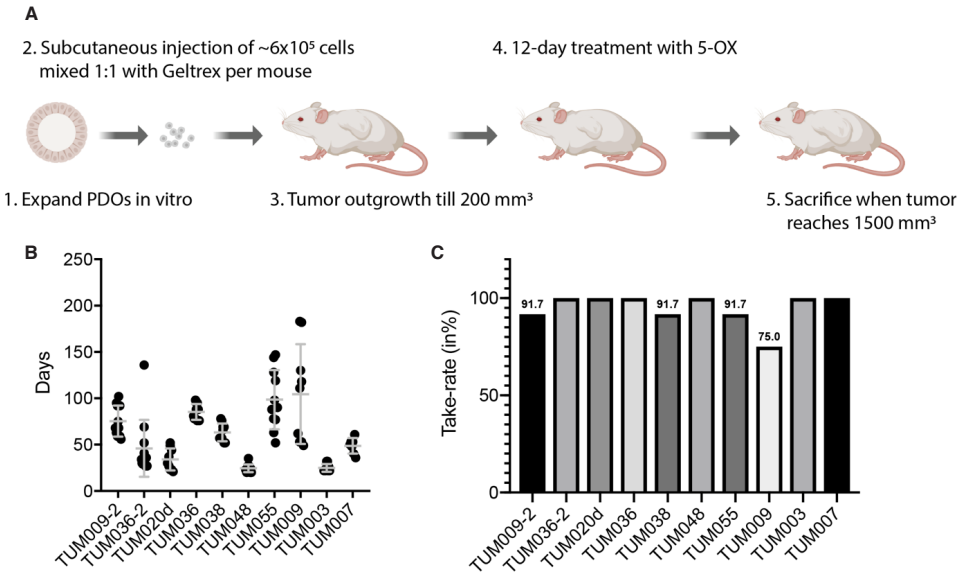

Fig. 1. Establishment of a PDOX cohort of patients included in the TUMOROID study.
(**A**) Outline of the experimental set-up to generate PDOX models. (**B**) Scatter plot indicating the number of days till tumors were established (defined as >200 mm^3). Dots represent individual mice, horizontal bars represent the mean, and error bars indicate the standard deviation (σ) (**C**) Bar graph representing take-rates of individual PDOs. For each organoid line we used 10-12 mice)

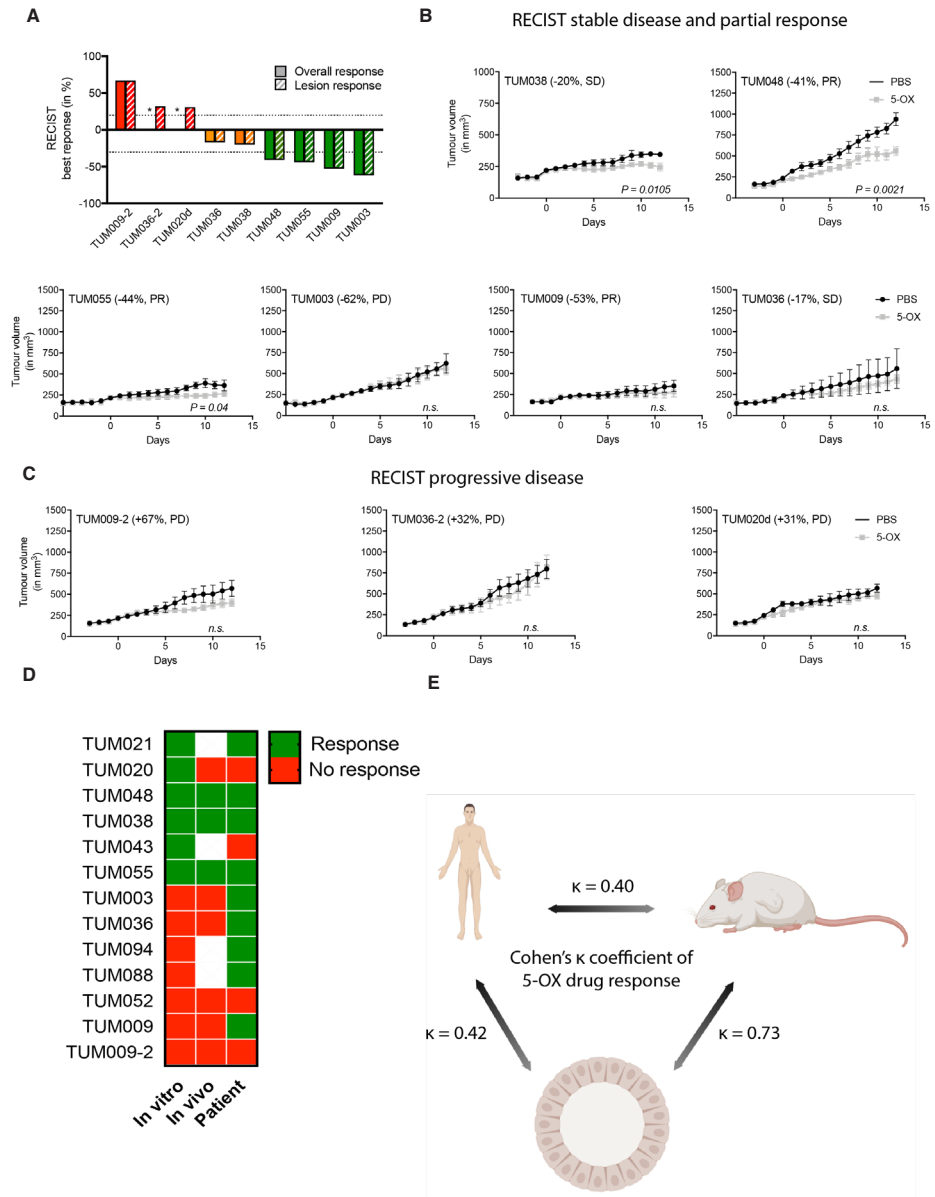

Fig. 2. PDOXs models do not improve the correlation with clinical responses of patients.

(**A**) Waterfall plot of the best lesion and overall responses in the FO-treated PDO cohort was adapted from Ooft, Weeber *et al.* 2019[16]. Red indicates progressive disease (PD), orange indicates stable disease (SD), and blue indicates partial response (PR). *, new lesion(s); #, lesion could not be measured. Treatment of PDOXs, derived from patients with SD or PR (**B**) or PD (**C**) in the clinic as depicted in the left top corner of each graph. Mice (n=5 or 6 per arm) were treated with PBS (black lines) or 5-FU (15 mg/kg, day 1-5 and 8-12) and oxaliplatin (10 mg/kg day 1 and 8; grey lines) starting when tumors reached 200 mm³. Data points

are plotted until the treatment was discontinued. Dots represent the mean, and error bars indicate the standard error of the mean (SEM). Arms were compared using the Students t-test and P-values below 0.05 were considered statistically significant. (**D**) Tumors that demonstrated a statistically significant difference between treatment arms were classified as 'response'. Tumors with non-significant differences between treatment arms were classified as 'no response'. RECIST classifications and continuous drug response data *of* Ooft, Weeber *et al.* 2019 were transformed into a binary response outcome for drug sensitivity (yes/no response to 5-OX; see the materials and methods for more details)[16]. (**E**) A schematic overview of the comparisons made from the data in panel D. Concordance between outcomes was calculated using Cohen's κ coefficient, in which 0 is no concordance and 1 perfect concordance.

DISCUSSION

In this study we generated PDOX models from PDOs to determine whether an in vivo model could recapitulate treatment outcome of 5-OX in patients where PDOs of the same patient failed to do so[16]. Our studies were performed in 10 PDOX models and we systematically compared clinical outcome of patients to drug responses of 9 PDOXs. We demonstrated a discordance between drug response of PDOXs to 5-OX and clinical outcome in patients. In contrast, the PDO and PDOX drug sensitivity profiles were strongly correlated.

In 3 cases we found PDOs to be completely resistant to 5-OX, both in vitro and in vivo, while patients experienced major clinical responses (TUM003, PR -63%;, TUM009, PR -53%). This is a very important finding and precludes the use of PDO(X)s in precision medicine approaches for 5-OX treatment, because withholding patients an effective treatment is not acceptable. In general, the effect we observed of 5-OX in mice was modest and inferior to tumor reductions in the patients. The observation that treatment of PDOs in vitro and in mice had a modest effect, even when treating at high- and MTD, also argues against a direct cytotoxic effect of 5-OX on tumor cells in these patients[16]. Anti-tumor immunity, instigated or amplified by chemotherapeutic treatment, has been well established by now and could perhaps be an essential factor in these patients and for this treatment regimen, as suggested earlier in syngeic mouse models[22,26-30].

Our current and prior findings discourage the use of 5-OX in combination with PDO(X) models and contradict a study of Ganesh et al, where a positive correlation between in vitro PDO and patient response to 5-OX was reported in a smaller set of 7 patients with rectal cancer[7]. Rectal cancer is a subtype of CRC with distinct clinical features, and standard-of-care also includes radiotherapy[17,31]. The authors report a correlation between *in vitro* drug sensitivity and matched clinical response of 7 patients to 5-OX. Two PDOs tested *in vivo* also showed

responses similar to the patient. A potential explanation for the observed difference in this small study could be the orthotopic engraftment of PDOs, which highlights a limitation of our study[17]. Other contributing factors between in vitro outcomes of our studies could be the use of rectal cancer PDOs and/or the use of 5-OX in a (neo)-adjuvant setting, while our studies concerned metastasized CRC and palliative treatment.

In conclusion, we have investigated whether PDOXs could overcome the limitations of PDOs in predicting clinical responses in patients treated with 5-OX but observed similar limitations as seen in PDOs. Although we had excellent take-rates in all cases PDOXs, responses to 5-OX did not correlate with clinical responses of patients. PDOXs did correlate to in vitro drug sensitivity (8/9 cases). We therefore conclude that in line with PDOs, PDOXs have limited value to model patient response to 5-OX. We caution against the use of PDO/PDOXs as a precision medicine tool without a careful analysis of the predictive value of these models using matched clinical treatment data.

3

MATERIALS AND METHODS

Organoid culture

Organoids were established in context of the TUMOROID (NL49002.031.14) and N14ITO (NL48824.031.14) studies[10,16]. The studies were approved by the ethical review board of the Netherlands Cancer Institute and the protocols comply with the Declaration of Helsinki, Dutch law, and Good Clinical Practice. All patients provided written informed consent before any study-related procedures. Biopsies were processed, cultured and frozen down as master and working biobanks at low passage as described previously[11,16,32]. Single vials of working biobanks were taken in culture approximately 3 weeks before the start of an experiment, depending on the growth speed and quality of the working biobank. PDOs were expanded in 10 cm plates, made single cell with TryplE (#12604-013, Gibco) on the morning of the subcutaneous injection, filtered through a 40 µm cell strainer and diluted to $6x10^5$/50 µl (352340, Corning). All master and working biobanks, and cultures were regularly tested for presence of mycoplasma (MycoAlert Mycoplasma Detection Kit; Lonza). Biobanks and subsequent PDOX tumors were subjected to quality control by single-nucleotide polymorphism (SNP) profiling (26 SNPs characterized by the Hartwig Medical Foundation) as previously described[16,32].

In vivo experiments

All animal studies were performed under the umbrella protocol, assigned by the Centrale Commissie Dierproeven (CCD) to the Antoni van Leeuwenhoek Hospital-Netherlands Cancer

Institute. The protocols were approved by the local Instantie voor Dierenwelzijn (IvD) and Dierexperimentencomissie (DEC). Eight-week-old BALB/c-nude (BALB/CAnN.Cg-*Foxn1*^{nu}) and NMRI-nude (NMRI-*Foxn1*^{nu}). Mice (M/F; at 10 weeks of age) were subcutaneously injected with 50 µl $6x10^5$ single cells mixed 1:1 with 50 µl Geltrex (#A1413202. Gibco) and tumors were allowed to establish (200 mm^3). Mice were randomized in two arms, and treated with the clinical formulation of 5-FU and oxaliplatin based on the dosing scheme of Fan et al. 2013[33]: 15 mg/kg 5-FU at day 1-5 and 8-12, and 10 mg/kg oxaliplatin at day 1 and 8, both intra-peritoneal or PBS. Tumor length and diameter were measured using a caliper and the tumor volume was calculated using the formula:

$$\frac{D \cdot d^2}{2}$$

D corresponds to the largest and d the smallest diameter (both in mm) of the tumor. Mice were sacrificed when tumors reached 1500 mm^3 or mice reached a humane endpoint.

3

(Statistical) analysis and representation

Groups were compared using the Student's t-test. P-values below 0.05 were considered statistically significant. Drug response data was derived from our prior study[16]. Cohen's β coefficient was calculated based on 2x2 tables of two outcomes (response or no response) per variable (in vitro, in vivo or patient). Initial RECIST measurements in the patient data set were converted to the binary outcome response and no response, as described earlier, but in short: complete and partial response or stable disease was considered 'response' and progressive disease 'no response'[16]. Response in the PDOX cohort was defined as a statistically significant difference in tumor growth in the 5-OX treatment arm compared to the PBS treatment arm, as defined *a priori* in the animal experiment work protocol. PDO drug response data was derived from Ooft, Weeber *et al*. 2019[16]. Response and no response in the in vitro data set was defined as the <50% most sensitive and >50% most resistant PDOs (calculated by pan-matrix GR scores, which is the sum of all the GR scores across the 5-FU and oxaliplatin drug matrix) as used before[16]. All graphs were generated in GraphPad Prism V7.03, with the exception of Fig. 1A, which was generated in Biorender.

Acknowledgments

We would like to thank the DEC, IvD and Preclinical Intervention Unit of the MCCA at the NKI for their technical support and/or input on the animal experiments. We would also like to thank all members of the Voest lab for discussing the experiments and results, and the Animal Pathology and Cryobase facilities at the NKI for their help collecting, processing and storing samples. Furthermore, we would like to thank all participating centers, medical

oncologists, and patients for contributing to the clinical study.

Author contributions

S.N.O designed the experiments, cultured organoids, analyzed the data and wrote the manuscript. F.W. coordinated the clinical study, included patients and contributed to the design of the study. K.K.D. established organoids and contributed to the design of the study. S.K. established organoids and generated biobanks. N.P., B.W., B.S., R.d.G., and C.C. performed mouse experiments. J.S provided expertise on animal pathology. E.v.W contributed to the statistical analysis. H.B., M.v.L., H.J.B. M.C. included patients. M.v.d.V contributed to the design of the experiments and supervised in vivo experiments. E.V. proposed the concept and designed and supervised the overall execution of the study.

REFERENCES

1 Gao, H. *et al.* High-throughput screening using patient-derived tumor xenografts to predict clinical trial drug response. *Nature medicine* **21**, 1318-1325, doi:10.1038/nm.3954 (2015).

2 Mainardi, S. *et al.* SHP2 is required for growth of KRAS-mutant non-small-cell lung cancer in vivo. *Nature medicine* **24**, 961-967, doi:10.1038/s41591-018-0023-9 (2018).

3 Johnson, J. I. *et al.* Relationships between drug activity in NCI preclinical in vitro and in vivo models and early clinical trials. *British journal of cancer* **84**, 1424-1431, doi:10.1054/bjoc.2001.1796 (2001).

4 Fiebig, H. H. *et al.* Development of three human small cell lung cancer models in nude mice. *Recent results in cancer research. Fortschritte der Krebsforschung. Progres dans les recherches sur le cancer* **97**, 77-86, doi:10.1007/978-3-642-82372-5_8 (1985).

5 Hidalgo, M. *et al.* Patient-derived xenograft models: an emerging platform for translational cancer research. *Cancer discovery* **4**, 998-1013, doi:10.1158/2159-8290.Cd-14-0001 (2014).

6 Scannell, J. W., Blanckley, A., Boldon, H. & Warrington, B. Diagnosing the decline in pharmaceutical R&D efficiency. *Nature reviews. Drug discovery* **11**, 191-200, doi:10.1038/nrd3681 (2012).

7 Ben-David, U. *et al.* Patient-derived xenografts undergo mouse-specific tumor evolution. *Nature genetics* **49**, 1567-1575, doi:10.1038/ng.3967 (2017).

8 Sato, T. *et al.* Long-term expansion of epithelial organoids from human colon, adenoma, adenocarcinoma, and Barrett's epithelium. *Gastroenterology* **141**, 1762-1772, doi:10.1053/j.gastro.2011.07.050 (2011).

9 van de Wetering, M. *et al.* Prospective derivation of a living organoid biobank of colorectal cancer patients. *Cell* **161**, 933-945, doi:10.1016/j.cell.2015.03.053 (2015).

10 Weeber, F., Ooft, S. N., Dijkstra, K. K. & Voest, E. E. Tumor Organoids as a Pre-clinical Cancer Model for Drug Discovery. *Cell chemical biology* **24**, 1092-1100, doi:10.1016/j.chembiol.2017.06.012 (2017).

11 Weeber, F. *et al.* Preserved genetic diversity in organoids cultured from biopsies of human colorectal cancer metastases. *Proceedings of the National Academy of Sciences of the United States of America* **112**, 13308-13311, doi:10.1073/pnas.1516689112 (2015).

12 Fujii, M. *et al.* A Colorectal Tumor Organoid Library Demonstrates Progressive Loss of Niche Factor Requirements during Tumorigenesis. *Cell stem cell* **18**, 827-838, doi:10.1016/j.stem.2016.04.003 (2016).

13 Sachs, N. *et al.* A Living Biobank of Breast Cancer Organoids Captures Disease Heterogeneity. *Cell* **172**, 373-386.e310, doi:10.1016/j.cell.2017.11.010 (2018).

14 Tiriac, H. *et al.* Organoid Profiling Identifies Common Responders to Chemotherapy in Pancreatic Cancer. *Cancer discovery* **8**, 1112-1129, doi:10.1158/2159-8290.Cd-18-0349 (2018).

15 Vlachogiannis, G. *et al.* Patient-derived organoids model treatment response of metastatic gastrointestinal cancers. *Science (New York, N.Y.)* **359**, 920-926, doi:10.1126/science.aao2774 (2018).

16 Ooft, S. N. *et al.* Patient-derived organoids can predict response to chemotherapy in metastatic colorectal cancer patients. *Science translational medicine* **11**, doi:10.1126/scitranslmed.aay2574 (2019).

17 Ganesh, K. *et al.* A rectal cancer organoid platform to study individual responses to chemoradiation. *Nature medicine* **25**, 1607-1614, doi:10.1038/s41591-019-0584-2 (2019).

18 Yao, Y. *et al.* Patient-Derived Organoids Predict Chemoradiation Responses of Locally Advanced Rectal Cancer. *Cell stem cell* **26**, 17-26.e16, doi:10.1016/j.stem.2019.10.010 (2020).

19 Sachs, N. *et al.* Long-term expanding human airway organoids for disease modeling. *The EMBO journal* **38**, doi:10.15252/embj.2018100300 (2019).

20 Gao, D. *et al.* Organoid cultures derived from patients with advanced prostate cancer. *Cell* **159**, 176-187, doi:10.1016/j.cell.2014.08.016 (2014).

21 Graham, M. A. *et al.* Clinical pharmacokinetics of oxaliplatin: a critical review. *Clinical cancer research : an official journal of the American Association for Cancer Research* **6**, 1205-1218 (2000).

22 Galluzzi, L., Buque, A., Kepp, O., Zitvogel, L. & Kroemer, G. Immunogenic cell death in cancer and infectious disease. *Nature reviews. Immunology* **17**, 97-111, doi:10.1038/nri.2016.107 (2017).

23 Schutte, M. *et al.* Molecular dissection of colorectal cancer in pre-clinical models identifies biomarkers predicting sensitivity to EGFR inhibitors. *Nature communications* **8**, 14262, doi:10.1038/ncomms14262 (2017).

24 Pauli, C. *et al.* Personalized In Vitro and In Vivo Cancer Models to Guide Precision Medicine. *Cancer discovery* **7**, 462-477, doi:10.1158/2159-8290.Cd-16-1154 (2017).

25 Eisenhauer, E. A. *et al.* New response evaluation criteria in solid tumours: revised RECIST guideline (version 1.1). *European journal of cancer (Oxford, England : 1990)* **45**, 228-247, doi:10.1016/j.ejca.2008.10.026 (2009).

26 Ghiringhelli, F. *et al.* Activation of the NLRP3 inflammasome in dendritic cells induces IL-1beta-dependent adaptive immunity against tumors. *Nature medicine* **15**, 1170-1178, doi:10.1038/nm.2028 (2009).

27 Ciampricotti, M., Hau, C. S., Doornebal, C. W., Jonkers, J. & de Visser, K. E. Chemotherapy response of spontaneous mammary tumors is independent of the adaptive immune system. *Nature medicine* **18**, 344-346; author reply 346, doi:10.1038/nm.2652 (2012).

28 Voorwerk, L. *et al.* Immune induction strategies in metastatic triple-negative breast cancer to enhance the sensitivity to PD-1 blockade: the TONIC trial. *Nature medicine* **25**, 920-928, doi:10.1038/s41591-019-0432-4 (2019).

29 Tesniere, A. *et al.* Immunogenic death of colon cancer cells treated with oxaliplatin. *Oncogene* **29**, 482-491, doi:10.1038/onc.2009.356 (2010).

30 Obeid, M. *et al.* Calreticulin exposure dictates the immunogenicity of cancer cell death. *Nature medicine* **13**, 54-61, doi:10.1038/nm1523 (2007).

31 Liu, Y. *et al.* Comparative Molecular Analysis of Gastrointestinal Adenocarcinomas. *Cancer cell* **33**, 721-735.e728, doi:10.1016/j.ccell.2018.03.010 (2018).

32 Dijkstra, K. K. *et al.* Generation of Tumor-Reactive T Cells by Co-culture of Peripheral Blood Lymphocytes and Tumor Organoids. *Cell* **174**, 1586-1598.e1512, doi:10.1016/j.cell.2018.07.009 (2018).

33 Fan, C. W. *et al.* Cancer-initiating cells derived from human rectal adenocarcinoma tissues carry mesenchymal phenotypes and resist drug therapies. *Cell death & disease* **4**, e828, doi:10.1038/cddis.2013.337 (2013).

SUPPLEMENTARY FILES

Table S1. Clinical, genetic and pathological annotation of PDOs in this study.

Part of each biopsy was used for pathological examination and targeted sequencing (performed on: TUM020d, -009, -009-2, -003 and -007) or whole-genome sequencing (performed on: TUM036, -036-2, 048), NA = not available/determined, '-' indicates no mutations found, MSS = microsatellite stable, MSI = microsatellite instable, CAPOX = capecitabine + oxaliplatin, FOLFOX = infusional 5-FU + oxaliplatin. Addition of B = bevacizumab.

	PATIENT CHARACTERISTICS		**TUMOR CHARACTERISTICS**					**REGIMENS PRIOR TO BIOPSY**
Study number	Gender	Age at study entry	Localization	Differentiation	Genetic profile		Biopsied lesion	Treatment regimen
					Mutations	MSI status		
TUM020d	M	67	Rectum	Moderately	BRAF (V600E)	MSS	Skin	CAPOX-B; Irinotecan-B; Trametinib/ Panitumumab
TUM036	M	63	Colon	Moderately	PIK3CA (G545L); KRAS (G12C); APC (T1493R)	MSS	Liver	No prior treatment
TUM036-2	M	63	Colon	Moderately	APC (T1493R); KRAS (G12C); SMAD4 (R361C)	MSS	Liver	CAPOX-B
TUM009	M	68	Colon	NA	MEK1 (K57N)	MSS	Liver	No prior treatment
TUM009-2	M	69	Colon	NA	MEK1 (K57N)	MSS	Liver	CAPOX-B
TUM003	M	72	Colon	Moderately	KRAS (G12A)	MSS	Liver	No prior treatment
TUM048	M	54	Colon	NA	AKT1 (E17K); KRAS (A146T)	MSS	Liver	No prior treatment
TUM055	F	58	Colon	Undifferentiated	TP53 (V173L); KRAS (G13D); EGFR (G724V)	MSS	Lymph node	CAPOX (adjuvant)
TUM038	F	66	Colon	Moderately	NA	NA	Liver	No prior treatment
TUM007	M	70	Colon	Poorly	MEK1 (Q56P)	NA	Lymph node	CAPOX-B

CHAPTER 4

CODON-SPECIFIC KRAS MUTATIONS PREDICT OVERALL SURVIVAL BENEFIT OF TAS-102 IN METASTATIC COLORECTAL CANCER

Joris van de Haar[1,2,3*], Salo N. Ooft[1,3*], Louisa R. Hoes[1,3], Takayuki Yoshino[4], Eric van Cutsem[5], Robert J. Mayer[6], Lodewyk F.A. Wessels[2,3,7], Emile E. Voest[1,3]

1. Division of Molecular Oncology & Immunology, The Netherlands Cancer Institute, Amsterdam, 1066 CX, the Netherlands.
2. Division of Molecular Carcinogenesis, The Netherlands Cancer Institute, Amsterdam, 1066 CX, the Netherlands.
3. Oncode Institute, The Netherlands Cancer Institute, Amsterdam, 1066 CX, the Netherlands.
4. Department of Gastroenterology and Gastrointestinal Oncology, National Cancer Center Hospital East, Kashiwa, Japan
5. University Hospitals Gasthuisberg, Leuven, Belgium; Clinical Digestive Oncology, KU Leuven, Leuven, Belgium.
6. Department of Medical Oncology, Dana-Farber Cancer Institute and Harvard Medical School, Boston, Massachusetts.
7. Faculty of EEMCS, Delft University of Technology, Delft, 2628 CD, the Netherlands.

* Co-first author.

New England Journal of Medicine (submitted)

ABSTRACT

Background

Recently, the chemotherapeutic trifluridine/tipiracil (FTD/TPI) has been approved for the treatment of late-stage metastatic colorectal cancer (mCRC). We aimed to identify genomic biomarkers for outcome of FTD/TPI treatment in mCRC.

Methods

Whole genome sequencing was performed on a discovery cohort of mCRC patients who received FTD/TPI as part of their regular treatment. Somatic genomic variants were tested for association with time on treatment and overall survival (OS). We further supported our findings using *in vitro* drug testing on patient-derived mCRC organoids (PDOs) and a re-analysis of the global, double-blind, placebo-controlled phase 3 RECOURSE trial.

Results

In the discovery cohort (n=37), KRAS codon G12 ($KRAS^{G12}$) mutations –but not other KRAS mutations– were the only genomic drivers significantly associated with shorter time on treatment (FDR=0.0040) and shorter OS (FDR=0.021). $KRAS^{G12}$ mutant PDOs were consistently more resistant to FTD/TPI than $KRAS^{G13}$ mutant and $KRAS^{WT}$ PDOs (n=11, P=0.0043). In the RECOURSE study, FTD/TPI did not prolong OS as compared to placebo in $KRAS^{G12}$ mutant patients (n=279, HR=0.97, 0.73–1.20, P=0.85). In the population as a whole (n=800), $KRAS^{G12}$ mutations were predictive of reduced OS benefit of FTD/TPI vs placebo (interaction P=0.0017), also after adjustment for all ten prognostic factors pre-specified by the RECOURSE study team (interaction p=0.017). In sharp contrast, the $KRAS^{G13}$ mutant subgroup showed a strong OS benefit of FTD/TPI vs placebo (n=60, unadjusted HR=0.29, 0.15–0.55, P<0.001; adjusted HR=0.20, 0.092–0.45, P<0.001). In this group, the OS benefit of FTD/TPI was significantly more pronounced as compared to the $KRAS^{G12}$ mutant population (unadjusted interaction p<0.001, adjusted interaction p<0.001) and the $KRAS^{WT}$ population (unadjusted interaction p=0.020, adjusted interaction p=0.036). For patients with $KRAS^{G13}$ mutant tumors, the median OS in the FTD/TPI arm was three times longer as compared to the placebo arm (8.7 vs 2.9 months, respectively).

Conclusions

Among patients with late-stage metastatic colorectal cancer, $KRAS^{G12}$ mutations were associated with the absence of clinically relevant overall survival benefit of FTD/TPI treatment. In contrast, this chemotherapy led to the strongest improvement of overall survival in patients with $KRAS^{G13}$-mutated tumors, followed by those with $KRAS^{WT}$ tumors who had intermediate benefit.

INTRODUCTION

Chemotherapy is a cornerstone of anti-cancer treatment. For metastatic colorectal cancer (mCRC), systemic treatment consists of the chemotherapeutics 5-FU/capecitabine, oxaliplatin and irinotecan, supplemented with EGFR- or VEGF-targeting agents[1]. More recently, the standard-of-care treatment options were expanded with the chemotherapeutic FTD/TPI (Lonsurf), a combination of trifluridine (FTD), a nucleoside analogue, and tipiracil (TPI), a thymidine phosphorylase inhibitor[2-4]. These treatment regimens have jointly improved overall survival of mCRC patients[1,3,5,6].

Precision medicine based on genomic biomarkers is broadly applied to select patients for targeted cancer therapies. In mCRC, KRAS hotspot mutations are considered to be the most important genomic biomarkers, as they are used in daily clinical practice to predict clinical resistance to the EGFR-targeting antibodies[7-9]. KRAS mutations are found in 44% of mCRC patients, of which mutations at codon G12 ($KRAS^{G12}$; observed in 28% of patients) and G13 ($KRAS^{G13}$; 8% of patients) are the most frequent (**Fig. 1A**)[10]. In general, clinical guidelines do not discriminate between KRAS mutations at different codons, although they have different biochemical properties[11,12], display tissue-specific and treatment-induced mutational patterns[13], and have retrospectively been shown to differentially impact anti-EGFR treatment outcome[13-16].

For chemotherapies, however, there are few genomic biomarkers. Due to the wide usage of chemotherapies and their often limited response rates, such biomarkers are a clear and unmet need. In mCRC, a prime example is the recently approved FTD/TPI treatment with a disease control rate of 44%[3]. To identify genomic biomarkers for this chemotherapy, we analyzed whole genome somatic profiles of a mCRC patient cohort that received FTD/TPI, as well as patient-derived organoid (PDO) drug screens and data from the double-blind, placebo-controlled phase 3 RECOURSE trial. We show that codon-specific KRAS mutations strongly predict overall survival benefit of FTD/TPI in mCRC, enabling genomics-based precision medicine for this chemotherapeutic.

METHODS

Patients

Discovery Cohort

The large, publicly available, real world-dataset with clinical annotation and whole genome sequencing by the Hartwig Medical Foundation (HMF) was used as a discovery cohort[17]. All patients who received FTD/TPI as part of their standard-of-care treatment for metastatic

colorectal cancer were identified in May 2018 (**Table S1**). Data collection was approved by the Medical Ethical Committee of the University Medical Center Utrecht and was conducted in accordance with the Declaration of Helsinki. All patients provided written informed consent for paired tumor-normal whole genome sequencing and collection of clinical characteristics for correlative biomarker discovery.

RECOURSE Trial Cohort

The RECOURSE trial design has been previously described in detail[3]. Briefly, the RECOURSE trial was a double blind, randomized, placebo-controlled, international phase 3 trial, comparing FTD/TPI plus best supportive care to placebo plus best supportive care. Heavily pretreated, refractory metastatic colorectal cancer patients (n=800) were randomly assigned, in a 2:1 ratio, to receive FTD/TPI or placebo. Within this process, patients were stratified based on KRAS status (mutant yes/no), time between first diagnosis of metastases and randomization (<18 months vs. ≥18 months), and geographical region (Japan or the United States, Europe, and Australia). Data cutoff was at the 571st death.

MSKCC Colorectal Cancer Cohort

Somatic mutation data were downloaded from the cBioportal for cancer genomics (http://cbioportal.org/msk-impact) on August 8th, 2017. All samples with 'GeneralTumorType' = 'Colorectal Cancer' were included (**Table S1**).

TCGA Colorectal Cancer Cohort

Somatic mutation data were obtained from The Cancer Genome Atlas (TCGA) Research Network (http://cancergenome.nih.gov/). Mutation calls of TCGA's final project, the PanCanAtlas, were downloaded from Synapse (syn7824274) on September 18th, 2017. Only patients with available Consensus Molecular Subtypes (CMS) were considered (**Table S1**).

Endpoints

For the discovery cohort, overall survival (OS) data and duration of FTD/TPI treatment were used as endpoints to assess FTD/TPI treatment outcome. For the validation cohort, we obtained data from the RECOURSE trial, of which OS was the primary endpoint. Secondary endpoints were progression-free survival (PFS), response rate, rate of disease control, and safety. In the re-analysis of the RECOURSE trial data presented here, we used OS and PFS as primary and secondary endpoints, respectively, as prespecified in a formal data request before access to the data was granted.

Bioinformatics analysis

For the discovery cohort, whole genome sequencing of tumor-normal pairs and bioinformatics

analysis were performed by HMF as previously described[17], with some additional data filtering (see **Appendix 1** for details).

Candidate biomarker selection

The procedure for the selection of candidate biomarkers is described in **Appendix 2**. All candidate biomarkers occurring in at least 5 patients in the discovery cohort were tested for association with treatment outcome. **Table S2** provides a comprehensive overview of the frequencies of all candidate biomarkers identified in our cohort.

Statistical analysis

Median time on treatment, OS and PFS were calculated using the Kaplan-Meier method. Hazard ratios (HRs) and corresponding 95% confidence intervals and p-values were estimated from Cox regression models. Multivariate Cox regression was used to adjust for all prognostic factors pre-specified by the RECOURSE study, except KRAS mutation status. These included: time since diagnosis of first metastases (<18 months vs ≥18 months), geographical region (Japan vs the United States, Europe, and Australia), sex, ECOG performance status, primary site of the disease (colon vs rectum), disease refractory to fluoropyrimidine (as part of last prior regimen), prior use of regorafenib, number of prior regimens (2, 3, or ≥4), and number of metastatic sites (1-2 vs or ≥3). None of these variables were found to be predictive of FTD/TPI benefit in the RECOURSE Trial[3]. Baseline characteristics were compared by Fisher's exact test for categorical variables with two levels and by c^2 test in the case of >2 levels. All reported p-values are two-sided. RECOURSE trial data-based survival analyses were performed on the intention-to-treat population. All RECOURSE trial data-based analyses and end points were prespecified in a formal data request before access to the data was granted. Used statistical packages as specified in **Appendix 3**.

Organoid culture and drug assays

Patient Derived Organoids (PDOs) were cultured, expanded and assayed as previously described[18]. We used 5 $KRAS^{G12}$-mutated (#1 $KRAS^{G12V}$, #2 $KRAS^{G12S}$, #3 $KRAS^{G12C}$, #4 $KRAS^{G12A}$, #5 $KRAS^{G12A}$), 4 $KRAS^{G13D}$- mutated (#6 $KRAS^{G13D}$, #7 $KRAS^{G13D}$, #8 $KRAS^{G13D}$, #9 $KRAS^{G13D}$), and 2 $KRAS^{WT}$ (#10 $KRAS^{WT}$, #11 $KRAS^{WT}$) PDOs (**Table S3** for details). Trifluridine (#S1778, Selleckchem) was reconstituted in DMSO at a stock concentration of 50 mM. PDOs were exposed for 11 days to 2-step, 9-fold dilution of trifluridine (range: 0.319 to 200 uM). Culture medium and trifluridine were refreshed every 3-4 days.

TCGA Consensus Molecular Subtypes

Colorectal cancer Consensus Molecular Subtypes (CMS) for TCGA colorectal cancer tumors were obtained from the original publication[19].

RESULTS

Identification of codon-specific KRAS mutations as biomarkers for FTD/TPI treatment outcome

We first employed a publicly available, real-world discovery cohort of the Hartwig Medical Foundation (HMF), comprising 37 mCRC patients who received FTD/TPI as part of their standard-of-care. Whole genome sequencing was available and used to identify the somatic genomic alterations driving the growth of each patient's tumor[17]. In total, ten genomic drivers occurred in at least five patients and were tested as candidate biomarkers for treatment outcome (**Table S2, Appendix 2**).

After correction for multiple hypothesis testing, the $KRAS^{G12}$ mutation (the most frequent KRAS hotspot mutation, n=20) was the only biomarker for treatment discontinuation that attained statistical significance (hazard ratio [HR] for treatment discontinuation, 4.59, 95% confidence interval [CI], 1.97–10.7, Benjamini-Hochberg false discovery rate [FDR]=0.0040; threshold for significance: FDR<5%; **Fig. 1B, Table S4**). When OS was used to define treatment outcome, $KRAS^{G12}$ mutations were again the only biomarker reaching statistical significance robust to FDR correction (HR for death, 3.38, 95% CI, 1.56–7.33, Benjamini-Hochberg corrected FDR=0.021; **Fig. 1C, Table S5**). Thus, in the discovery cohort, patients with $KRAS^{G12}$ mutations remained on FTD/TPI treatment for a shorter period of time and had shorter OS as compared to patients without these mutations. This suggests that $KRAS^{G12}$ mutations may either be negatively prognostic or predictive for outcome of FTD/TPI treatment in mCRC.

We next performed an in-depth analysis of the different KRAS mutations in the discovery cohort. In total, 20 out of 37 (54%) patients harbored $KRAS^{G12}$ mutations, 4 (11%) had KRAS mutations at other codons ($KRAS^{Q61}$: 2 patients [5%], $KRAS^{P34}$: 1 patient [3%], $KRAS^{A146}$: 1 patient [3%]), and 13 (35%) patients had $KRAS^{WT}$ tumors (**Fig 1D**). None of the patients with $KRAS^{G12}$ mutations remained on treatment for more than 3 months, and the time on treatment in this group was significantly shorter as compared to patients with $KRAS^{WT}$ tumors (HR for treatment discontinuation, 3.51, 95% CI, 1.47–8.41, P=0.0048; **Fig. 1E**). This translated into significantly shorter OS for patients with $KRAS^{G12}$ mutations as compared to patients without KRAS mutations (HR for death, 3.32, 95% CI, 1.40–7.87, P=0.0065; **Fig. 1F**). Interestingly, the time on treatment for $KRAS^{G12}$-mutated patients was also remarkably shorter as compared to the small group (n=4) of patients with $KRAS^{Other}$ mutations (HR for treatment discontinuation, 13.6, 95% CI, 1.75–105, P=0.013; **Fig. 1E**). When comparing the OS of these two groups, an insignificant trend was observed in favor of patients with $KRAS^{Other}$ mutations (HR for death, 3.31, 95% CI, 0.96–11.5, P=0.059; **Fig. 1F**). Thus, our analyses on the discovery cohort suggests that specifically $KRAS^{G12}$ mutations, and not other KRAS mutations, are negatively prognostic

or predictive for FTD/TPI treatment outcome in mCRC.

Next, we tested mCRC organoids for their responsiveness to trifluridine, the cytotoxic component of FTD/TPI. $KRAS^{G12}$-mutated patient-derived organoids (PDOs; n=11; See **Table S3** for details) were consistently more resistant to trifluridine *in vitro* than $KRAS^{WT}$ and $KRAS^{G13D}$-mutated PDOs (Wilcoxon rank-sum test P=0.0043; **Fig. 1G-H**). These findings could not be explained by differences in PDO growth rates (**Fig. S1).**

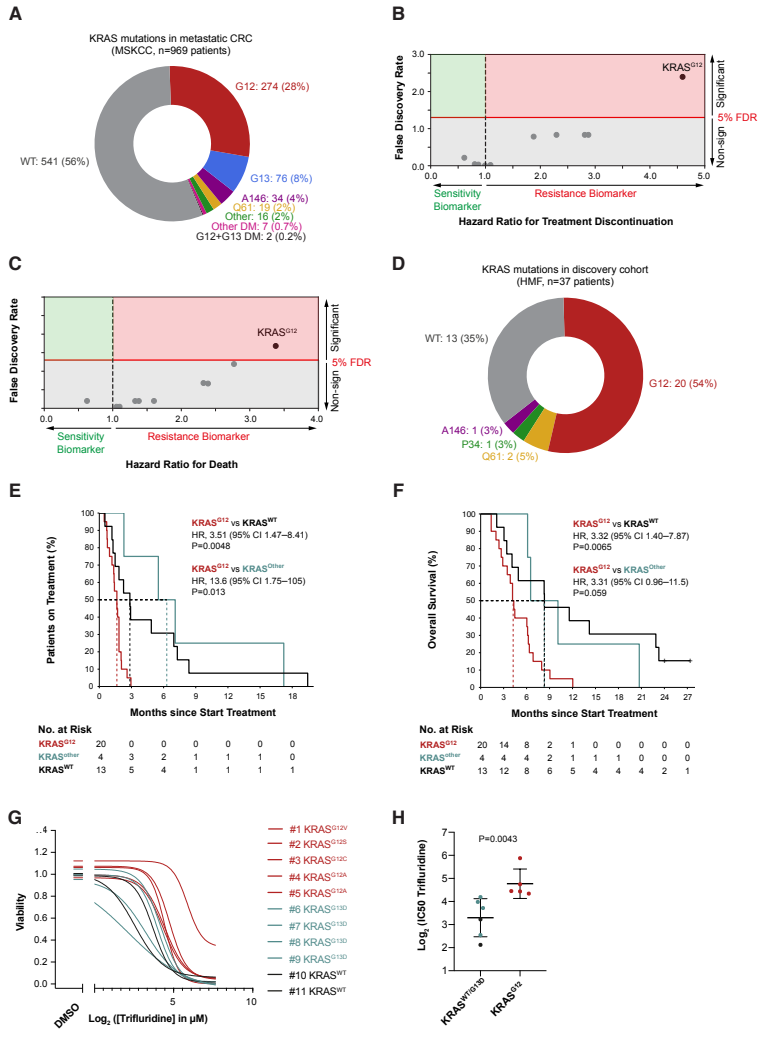

Figure 1. Associations of codon-specific KRAS mutation status with clinical and *in vitro* FTD/TPI treatment outcome in mCRC.

A. Codon-specific KRAS mutation frequencies in mCRC (MSKCC cohort[10]).

B. A dot plot showing the associations of candidate genomic biomarkers to time on FTD/TPI treatment in the discovery cohort (n=37). The hazard ratio for treatment discontinuation for patients with the candidate biomarker vs those without is plotted against the Benjamini-Hochberg-corrected false discovery rate (FDR). The red line indicates the 5% FDR significance threshold.
C. As panel B, but for overall survival (n=37).
D. Codon-specific KRAS mutation frequencies in the discovery cohort.
E. Time on FTD/TPI treatment in the discovery cohort, stratified based on KRAS mutation status. $KRAS^{Other}$ comprises all patients with KRAS mutations other than $KRAS^{G12}$.
F. Overall survival in our discovery cohort, stratified based on KRAS status. $KRAS^{Other}$ comprises all patients with KRAS mutations other than $KRAS^{G12}$.
G. Dose response curves of patient-derived mCRC organoids harboring different KRAS mutations exposed to a concentration range of trifluridine *in vitro*.
H. Half maximal inhibitory concentrations (IC50; log_2) for trifluridine of patient-derived mCRC organoids, stratified based on codon-specific KRAS mutation status. Colors encode the codon-specific KRAS mutation status, as in G. Two-sided Wilcoxon rank-sum test P-value is shown.

WT: wild type; DM: double mutation; FDR: false discovery rate

Codon-specific KRAS mutations and survival in the RECOURSE study

To further validate our findings, we employed data from a large, independent clinical cohort, the RECOURSE study[3]. Briefly, this international, randomized, double-blind, placebo-controlled, phase 3 study assigned 800 heavily pre-treated CRC patients to receive either FTD/TPI or placebo, in a 2:1 ratio. Approximately half of the patients (n=393) were $KRAS^{WT}$, whereas the other half (n=407) were KRAS mutant ($KRAS^{M}$). In this study, KRAS mutation status (mutated yes/no) was not significantly associated with reduced OS or PFS benefit of FTD/TPI vs placebo, but codon-specific analyses were not performed[3,4].

From our data, we hypothesized that $KRAS^{G12}$ mutant patients have reduced survival benefit from FTD/TPI, and that the survival benefit observed in the full $KRAS^{M}$ population in the RECOURSE trial was in fact driven by patients with $KRAS^{other}$ mutations. To assess this, we pre-specified three study objectives in our RECOURSE trial data request. The primary objective was to assess OS benefit of FTD/TPI (the primary end point of the RECOURSE trial) specifically in $KRAS^{G12}$-mutated CRC. Secondary objectives were analyses on associations of other KRAS codon-specific mutations to OS benefit of FTD/TPI vs placebo, and associations of all KRAS codon-specific mutations to PFS benefit of FTD/TPI vs placebo.

For 367 out of 407 (90%) patients with KRAS mutated tumors in the RECOURSE trial, codon-specific mutation status was available. Of these, 279 (76%) had $KRAS^{G12}$ mutations, 60 (16%) had

$KRAS^{G13}$ mutations, 21 (5.7%) had $KRAS^{G12/13}$ double mutations, and 7 (1.9%) had other mutations (the true percentage of patients with other mutations was likely higher, as their assessment was only broadly implemented later[8]). Thus, the RECOURSE trial data provided us with reasonably sized subgroups to study the effects of $KRAS^{G12}$ and $KRAS^{G13}$ (mono)mutations on treatment outcomes with FTD/TPI in mCRC. Throughout this work, we consider patients with $KRAS^{G12/13}$ double mutations as a distinct subgroup.

When comparing baseline characteristics between $KRAS^{G12}$ mutant, $KRAS^{G13}$ mutant, and $KRAS^{WT}$ patients in the RECOURSE trial, we found that those with KRAS mutations generally had more recent diagnoses of metastatic disease, tended to be less heavily pretreated, and were more often refractory on fluoropyrimidine as part of the last prior regimen (**Table 1**). All these factors were balanced between the $KRAS^{G12}$ and $KRAS^{G13}$ mutant populations. Between these two groups, the only significant difference was that patients with $KRAS^{G13}$ mutations originated less often from Japan (**Table 1**).

Table 1. Baseline characteristics of patients in the RECOURSE trial intention-to-treat population, stratified based on codon-specific KRAS mutation status.

Two-sided p-values are for comparisons between codon-specific KRAS mutation status-based subgroups, by Fisher's exact test for categorical variables with two classes, and c^2 test for categorical variables with more than two classes.

						P-Value			
Characteristic	**All (n=800)**	**$KRAS^{G12}$ (n=279)**	**No $KRAS^{G12}$ (n=521)**	**$KRAS^{G13}$ (n=60)**	**$KRAS^{WT}$ (n=393)**	**G12 vs. No G12**	**G12 vs. G13**	**G12 vs. WT**	**G13 vs. WT**
Age									
<65	448 (56)	167 (60)	281 (54)	30 (50)	212 (54)	0.12	0.19	0.13	0.58
≥65	352 (44)	112 (40)	240 (46)	30 (50)	181 (46)				
Sex									
Female	309 (39)	116 (42)	193 (37)	26 (43)	143 (36)	0.22	0.86	0.20	0.32
Male	491 (61)	163 (58)	328 (63)	34 (57)	250 (64)				
Region									
Japan	266 (33)	103 (37)	163 (31)	13 (22)	134 (34)	0.12	**0.025**	0.46	0.075
United States, Europe, and Australia	534 (67)	176 (63)	358 (69)	47 (78)	259 (66)				
ECOG performance score									
0	448 (56)	169 (61)	279 (54)	34 (57)	212 (54)	0.062	0.66	0.097	0.78
1	352 (44)	110 (39)	242 (46)	26 (43)	181 (46)				
Primary site of disease									
Colon	499 (62)	179 (64)	320 (61)	39 (65)	234 (60)	0.49	1.0	0.23	0.48
Rectum	301 (38)	100 (36)	201 (39)	21 (35)	159 (40)				
Time from diagnosis of metastases									
<18 mo	166 (21)	76 (27)	90 (17)	21 (35)	57 (15)	**0.0013**	0.27	**<0.001**	**<0.001**
≥18 mo	634 (79)	203 (73)	431 (83)	39 (65)	336 (85)				
No. of prior regimens									
2	140 (18)	78 (28)	62 (12)	21 (35)	33 (8)	**<0.001**	0.34	**<0.001**	**<0.001**
3	173 (22)	74 (27)	99 (19)	11 (18)	73 (19)				
≥4	487 (61)	127 (46)	360 (69)	28 (47)	287 (73)				
Refractory to fluoropyrimidine as part of last prior regimen									
Yes	455 (57)	207 (74)	248 (48)	43 (72)	166 (42)	**<0.001**	0.75	**<0.001**	**<0.001**
No	345 (43)	72 (26)	273 (52)	17 (28)	227 (58)				
Prior use of regorafenib									
Yes	144 (18)	44 (16)	100 (19)	8 (13)	70 (18)	0.25	0.84	0.53	0.47
No	656 (82)	235 (84)	421 (81)	52 (87)	323 (82)				
No. of metastatic sites									
1–2	477 (60)	171 (61)	306 (59)	32 (53)	236 (60)	0.50	0.31	0.75	0.33
≥3	323 (40)	108 (39)	215 (41)	28 (47)	157 (40)				
Treatment									
FTD/TPI	534 (67)	185 (66)	349 (67)	40 (67)	262 (67)	0.87	1.0	0.93	1.0
Placebo	266 (33)	94 (34)	172 (33)	20 (33)	131 (33)				

We then investigated the prognostic effects of codon-specific KRAS mutations by analyzing OS in the placebo arm. We found that $KRAS^{G12}$-mutated and $KRAS^{WT}$ patients had similar OS in the placebo arm (**Fig. S2**). Interestingly, placebo-treated patients with $KRAS^{G13}$ mutations had remarkably shorter OS than those with $KRAS^{G12}$ mutations (HR=2.50, 95% CI, 1.47 to 4.25, P<0.001; **Fig. S2**), also after adjustment for all prognostic factors prespecified in the RECOURSE trial (HR=2.43, 95% CI, 1.33–4.45, P=0.0039; **Fig. S2**). $KRAS^{G13}$-mutated patients also had significantly shorter OS as compared to $KRAS^{WT}$ patients in unadjusted analysis (HR=2.05, 95% CI, 1.23–3.39, P=0.0056; **Fig. S2**), but significance was lost in adjusted analysis (HR=1.73, 95% CI, 0.97–3.11, P=0.064; **Fig. S2**). Thus, patients with $KRAS^{G13}$ mutations had relatively short OS in the placebo arm of the RECOURSE trial, suggesting that $KRAS^{G13}$ mutations (but not $KRAS^{G12}$ mutations) are a negative prognostic factor in heavily pre-treated mCRC.

We then assessed our primary objective. Within the $KRAS^{G12}$-mutated subgroup (n=279), we found no significant OS benefit of FTD/TPI vs placebo (HR=0.97; 95% CI, 0.73–1.20, p=0.85; **Fig. 2A**, upper left). Within the population as a whole (n=800), $KRAS^{G12}$ mutations were significantly associated to reduced OS benefit of FTD/TPI vs placebo (unadjusted interaction p=0.0017, adjusted interaction p=0.017; **Fig. 2B**). Furthermore, we did not find evidence for OS benefit of FTD/TPI vs placebo in subgroups of $KRAS^{G12}$-mutated patients stratified based on the specific type of mutation-induced amino acid change (**Fig. S3**). Thus, in line with our results on the discovery cohort, we found that FTD/TPI does not lead to a clinically relevant prolongation of OS in mCRC patients with $KRAS^{G12}$-mutations. In addition, we conclude that this is based on a negative predictive (rather than prognostic) effect.

As reported by Mayer *et al.*[3], the median OS benefit of FTD/TPI in the full RECOURSE trial population was 1.8 months. After excluding patients with $KRAS^{G12}$ mutations, this increased to 2.7 months (**Fig. 2**). Cox regression analysis showed a pronounced OS benefit of FTD/TPI in the patient group without $KRAS^{G12}$-mutations (n=521, HR=0.55; 95% CI, 0.44–0.67, P<0.001; **Fig. 2A**, upper right).

We next addressed our first secondary objective and analyzed the treatment effect of FTD/TPI in patients with (prognostically poor) $KRAS^{G13}$-mutated tumors. In sharp contrast to the $KRAS^{G12}$-mutated population, the $KRAS^{G13}$-mutated population showed a clear OS benefit in the FTD/TPI arm vs. placebo arm (HR=0.29; 95% CI, 0.15–0.55, P<0.001; **Fig. 2A**, lower left). This remained significant in a model adjusted for all prognostic factors pre-specified in the RECOURSE trial (HR=0.20; 95% CI, 0.092–0.45, P<0.001; **Fig. 2B**). The median OS in the FTD/TPI arm was three times longer as compared to the placebo arm (8.7 vs 2.9 months, respectively; **Fig. 2**). Thus, $KRAS^{G13}$ mutations mark mCRC patients with clear OS benefit of FTD/TPI.

Given the convincing OS benefit of FTD/TPI in the $KRAS^{G13}$-mutated population, we wondered how this compared to patients with $KRAS^{G12}$-mutant or $KRAS^{WT}$ tumors. An analysis on the population with either $KRAS^{G12}$ or $KRAS^{G13}$ mutations showed that the OS benefit of FTD/TPI is significantly more pronounced in patients with $KRAS^{G13}$-mutated CRC as compared to those with $KRAS^{G12}$-mutated disease (unadjusted interaction P<0.001, adjusted interaction P=0.0070, respectively; **Fig. 2B**). The OS benefit of FTD/TPI in the $KRAS^{G13}$ population was also significantly more pronounced as compared to the $KRAS^{WT}$ population (unadjusted interaction P=0.020, adjusted interaction P=0.036; **Fig. 2**). Thus, these analyses indicate that $KRAS^{G13}$ mutations are, in sharp contrast to $KRAS^{G12}$ mutations, positively predictive for OS benefit on FTD/TPI therapy in mCRC.

As our second secondary objective, we assessed KRAS codon-specific associations to PFS benefit of FTD/TPI. Prolonged PFS in the FTD/TPI arm was observed for all three major subgroups: $KRAS^{G12}$-mutated (HR = 0.50; 95% CI, 0.38–0.65, P<0.001; **Fig. 2B**), $KRAS^{G13}$-mutated (HR = 0.31; 95% CI, 0.16–0.58, P<0.001; **Fig. 2B**) and $KRAS^{WT}$ subgroups (HR = 0.47; 95% CI, 0.37–0.59, P<0.001; **Fig. 2B**). These findings remained significant in adjusted analyses ($KRAS^{G12}$: HR = 0.45, 95% CI, 0.34–0.59, P<0.001; $KRAS^{G13}$: HR = 0.35, 95% CI, 0.17–0.71, p=0.0036; $KRAS^{WT}$: HR = 0.47, 95% CI, 0.37–0.60, P<0.001; **Fig. 2B**). PFS benefit of FTD/TPI did not significantly differ between the 3 subgroups (interaction P>0.2 for all pairwise comparisons; **Fig. 2B**). Thus, the $KRAS^{G12}$-mutated population showed a similar PFS benefit of FTD/TPI vs placebo as compared to $KRAS^{G13}$-mutated and $KRAS^{WT}$ populations, although this did not translate into prolonged OS in the former population.

In the $KRAS^{G12+13}$ double mutant population (n=21), no significant OS benefit in the treatment vs placebo arm was observed (HR=0.87; 95% CI, 0.32–2.34, p=0.78). The small subgroup size and hence limited statistical power limits definitive conclusions.

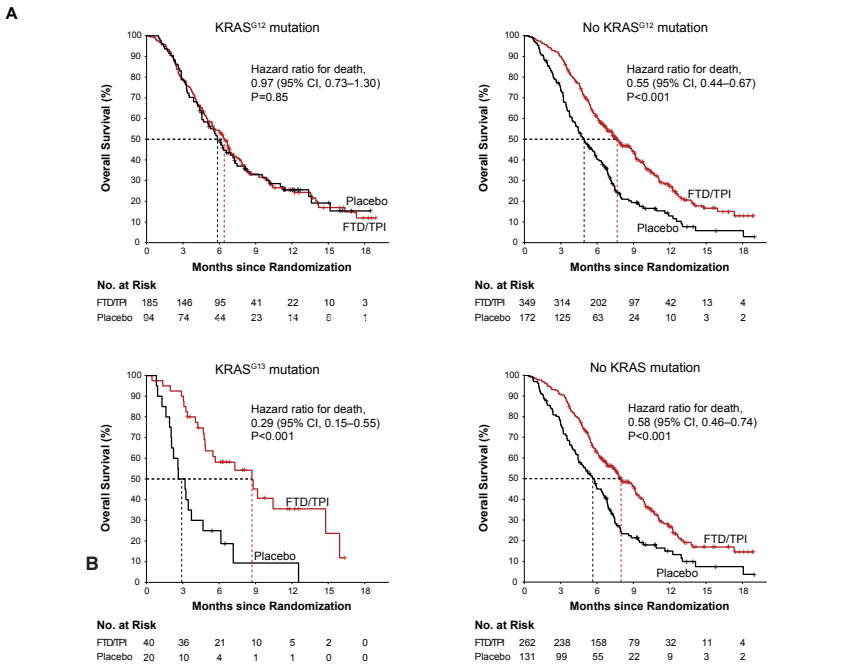

B

Analysis and Subgroup	Patients (n) FTD/TPI, Placebo	Median Survival (95% CI), mo FTD/TPI	Placebo	Hazard Ratio (95% CI)	P-value	P-value for Interaction		
Overall survival								
Unadjusted								
KRAS^{G12} mutation	185, 94	6.4 (5.4–7.2)	5.8 (4.7–7.3)	0.97 (0.73–1.30)	0.85	0.0017	<0.001	0.0083
No KRAS^{G12} mutation	306, 154	7.7 (6.8–8.9)	4.9 (4.2–5.9)	0.55 (0.44–0.67)	<0.001			
KRAS^{G13} mutation	40, 20	8.7 (5.5–NA)	2.9 (2.1–6.1)	0.29 (0.15–0.55)	<0.001	0.020		
No KRAS mutation	262, 131	8.0 (7.3–9.2)	5.7 (4.5–6.8)	0.58 (0.46–0.74)	<0.001			
Adjusted								
KRAS^{G12} mutation	185, 94	6.4 (5.4–7.2)	5.8 (4.7–7.3)	0.89 (0.66–1.19)	0.43	0.017	0.0070	0.079
No KRAS^{G12} mutation	306, 154	7.7 (6.8–8.9)	4.9 (4.2–5.9)	0.56 (0.45–0.70)	<0.001			
KRAS^{G13} mutation	40, 20	8.7 (5.5–NA)	2.9 (2.1–6.1)	0.20 (0.09–0.45)	<0.001	0.036		
No KRAS mutation	262, 131	8.0 (7.3–9.2)	5.7 (4.5–6.8)	0.62 (0.49–0.80)	<0.001			
Progression-free survival								
Unadjusted								
KRAS^{G12} mutation	185, 94	1.9 (1.9–2.0)	1.8 (1.7–1.8)	0.50 (0.38–0.65)	<0.001	0.97	0.39	0.88
No KRAS^{G12} mutation	306, 154	2.0 (1.9–2.5)	1.7 (1.7–1.8)	0.45 (0.37–0.55)	<0.001			
KRAS^{G13} mutation	40, 20	2.0 (1.9–3.7)	1.7 (1.6–1.9)	0.31 (0.16–0.58)	<0.001	0.24		
No KRAS mutation	262, 131	2.1 (1.9–2.8)	1.7 (1.7–1.8)	0.47 (0.37–0.59)	<0.001			
Adjusted								
KRAS^{G12} mutation	185, 94	1.9 (1.9–2.0)	1.8 (1.7–1.8)	0.45 (0.34–0.60)	<0.001	0.47	0.68	0.38
No KRAS^{G12} mutation	306, 154	2.0 (1.9–2.5)	1.7 (1.7–1.8)	0.46 (0.37–0.56)	<0.001			
KRAS^{G13} mutation	40, 20	2.0 (1.9–3.7)	1.7 (1.6–1.9)	0.34 (0.17–0.71)	0.004	0.25		
No KRAS mutation	262, 131	2.1 (1.9–2.8)	1.7 (1.7–1.8)	0.47 (0.37–0.60)	<0.001			

Figure 2. Associations of codon-specific KRAS mutation status with overall survival of mCRC patients treated with FTD/TPI or placebo in the RECOURSE trial.

A. Overall survival for patients with KRAS^{G12} mutations (upper left panel), without KRAS^{G12} mutations (upper right panel), with KRAS^{G13} mutations (lower left panel) and without KRAS mutations (lower right panel).

B. Forest plot of hazard ratios for overall and progression-free survival, stratified based on codon-specific KRAS mutation status. Adjusted hazard ratios are corrected for all prognostic factors prespecified in the RECOURSE trial. Two-sided p-values for interaction indicate if the survival benefit of FTD/TPI treatment was significantly different between subgroups, for which pairwise comparisons are indicated by the square brackets.

DISCUSSION

Using real-world data, supported by tumor organoid testing, and an independent validation in the global, double-blind, placebo-controlled, phase 3 RECOURSE trial, we demonstrated the predictive value of condon-specific KRAS mutations for the chemotherapeutic agent FTD/TPI in late-stage mCRC. Specifically, KRAS^{G12}-mutations mark patients who have no OS benefit of FTD/TPI, while the remaining population –and especially KRAS^{G13}-mutated patients– does. Testing mCRC patients for FTD/TPI treatment based on KRAS mutations could be readily adopted in the clinic, as these mutations are already routinely assessed in every mCRC patient[1,8].

In the RECOURSE trial, we observed a PFS benefit of FTD/TPI in KRAS^{G12}-mutated patients, which did not translate into an OS benefit. This is observed more regularly when the median PFS benefit is limited[20], as is the case in the RECOURSE trial (only 0.1 months for the KRAS^{G12}-mutated population). Regulatory agencies therefore consider OS to be the gold standard endpoint to assess treatment benefit. The main caveat of OS is that it may be confounded by later treatment lines, thereby obscuring a correlation between OS and PFS. However, the risk on such confounding in the RECOURSE trial is limited, as the patient population already exhausted the standard-of-care treatment options[3]. We thus consider OS to be the most appropriate endpoint to assess benefit from FTD/TPI in the RECOURSE trial.

Interestingly, our data show a profound contrast between KRAS^{G12}-mutated and KRAS^{G13}-mutated mCRC on two levels. First, on the prognostic level, as KRAS^{G13}-mutated patients have shorter OS in the placebo arm as compared to KRAS^{G12}-mutated patients. This finding is in line with previous results on an independent, smaller patient cohort[14]. Second, on the predictive level, as FTD/TPI clearly prolongs OS in KRAS^{G13}-mutated CRC, whereas this is not the case for KRAS^{G12}-mutated patients. We found no differential enrichments of the two mutations in different consensus molecular subtypes (**Fig. S4**)[19], suggesting that tumor subtype is not driving this differential treatment outcome. It is tempting to speculate that the prognostically poor KRAS^{G13} mutants may proliferate more quickly and incorporate more nucleoside analog into their genomes, increasing their sensitivity to FTD/TPI. However, our KRAS^{G13}-mutated patient-derived organoids did not have higher proliferation rates than their KRAS^{G12}-mutated counterparts, and yet they are still more sensitive to trifluridine.

Mechanistic studies are beyond the scope of our study, but could provide meaningful insight into the biology of KRAS mutations and their links to FTD/TPI response and prognosis. Our results also support the design of basket studies to assess the efficacy of FTD/TPI in non-CRC tumors with $KRAS^{G13}$ mutations[21].

As KRAS hotspot mutations outside of codon G12/13 were not consistently tested in the RECOURSE trial, it remains an open question how these mutations affect prognosis and survival benefit of FTD/TPI. The results on the discovery cohort suggest that these patients might more closely resemble $KRAS^{G13}$ mutated patients than those with $KRAS^{G12}$ mutations. Our data warrant a more systematic assessment of the prognostic and predictive nature of RAS mutations, and their impact on FTD/TPI efficacy.

Our study also has limitations. Although our RECOURSE trial-based analyses were hypothesis-driven and pre-specified in a formal data request before access to the data was granted, the analyses were not pre-planned in the study protocol of the RECOURSE trial. Second, the exceptionally strong OS benefit of FTD/TPI for patients with $KRAS^{G13}$ mutations was only found in an analysis of the RECOURSE trial data, as these genomic variants were absent in the discovery cohort. Finally, the interpretation of results obtained on the $KRAS^{WT}$ cohort of the RECOURSE study is complicated by the fact that it is unclear which fraction of this cohort was truly $KRAS^{WT}$ at the point of FTD/TPI therapy, for two reasons. First, the relatively rare KRAS hotspot mutations outside of codons G12/13 were only tested in part of the RECOURSE trial patient population. Second, *de novo* KRAS mutations are a known acquired resistance mechanism of $KRAS^{WT}$ mCRC treated with anti-EGFR therapy[22], and will have been missed if KRAS status is assessed at diagnosis, as is common clinical practice.

In conclusion, we report the first proof-of-concept for genomics-based personalized therapy for chemotherapy in mCRC. As $KRAS^{G12}$ and $KRAS^{G13}$ mutations occur respectively in ~28% and ~8% of patients with mCRC, a KRAS-guided clinical protocol has the potential to substantially improve patient selection for FTD/TPI therapy.

REFERENCES

1. Van Cutsem E, Cervantes A, Adam R, et al. ESMO consensus guidelines for the management of patients with metastatic colorectal cancer. Ann Oncol 2016;27:1386-422.
2. Marcus L, Lemery SJ, Khasar S, et al. FDA Approval Summary: TAS-102. Clin Cancer Res 2017;23:2924-7.
3. Mayer RJ, Van Cutsem E, Falcone A, et al. Randomized trial of TAS-102 for refractory metastatic colorectal cancer. N Engl J Med 2015;372:1909-19.
4. Van Cutsem E, Mayer RJ, Laurent S, et al. The subgroups of the phase III RECOURSE trial of trifluridine/tipiracil (TAS-102) versus placebo with best supportive care in patients with metastatic colorectal cancer. Eur J Cancer 2018;90:63-72.
5. Grothey A, Sargent D, Goldberg RM, Schmoll HJ. Survival of patients with advanced colorectal cancer improves with the availability of fluorouracil-leucovorin, irinotecan, and oxaliplatin in the course of treatment. J Clin Oncol 2004;22:1209-14.
6. Jonker DJ, O'Callaghan CJ, Karapetis CS, et al. Cetuximab for the treatment of colorectal cancer. N Engl J Med 2007;357:2040-8.
7. Allegra CJ, Jessup JM, Somerfield MR, et al. American Society of Clinical Oncology provisional clinical opinion: testing for KRAS gene mutations in patients with metastatic colorectal carcinoma to predict response to anti-epidermal growth factor receptor monoclonal antibody therapy. J Clin Oncol 2009;27:2091-6.
8. Allegra CJ, Rumble RB, Hamilton SR, et al. Extended RAS Gene Mutation Testing in Metastatic Colorectal Carcinoma to Predict Response to Anti-Epidermal Growth Factor Receptor Monoclonal Antibody Therapy: American Society of Clinical Oncology Provisional Clinical Opinion Update 2015. J Clin Oncol 2016;34:179-85.
9. Karapetis CS, Khambata-Ford S, Jonker DJ, et al. K-ras mutations and benefit from cetuximab in advanced colorectal cancer. N Engl J Med 2008;359:1757-65.
10. Zehir A, Benayed R, Shah RH, et al. Mutational landscape of metastatic cancer revealed from prospective clinical sequencing of 10,000 patients. Nat Med 2017;23:703-13.
11. Lu S, Jang H, Muratcioglu S, et al. Ras Conformational Ensembles, Allostery, and Signaling. Chem Rev 2016;116:6607-65.
12. Ostrem JM, Shokat KM. Direct small-molecule inhibitors of KRAS: from structural insights to mechanism-based design. Nat Rev Drug Discov 2016;15:771-85.
13. Li S, Balmain A, Counter CM. A model for RAS mutation patterns in cancers: finding the sweet spot. Nat Rev Cancer 2018;18:767-77.
14. De Roock W, Jonker DJ, Di Nicolantonio F, et al. Association of KRAS p.G13D mutation with outcome in patients with chemotherapy-refractory metastatic colorectal cancer treated with cetuximab. JAMA 2010;304:1812-20.
15. McFall T, Diedrich JK, Mengistu M, et al. A systems mechanism for KRAS mutant allele-specific responses to targeted therapy. Sci Signal 2019;12.
16. Rabara D, Tran TH, Dharmaiah S, et al. KRAS G13D sensitivity to neurofibromin-mediated GTP hydrolysis. Proc Natl Acad Sci U S A 2019;116:22122-31.
17. Priestley P, Baber J, Lolkema MP, et al. Pan-cancer whole-genome analyses of metastatic solid tumours. Nature

2019;575:210-6.

18. Ooft SN, Weeber F, Dijkstra KK, et al. Patient-derived organoids can predict response to chemotherapy in metastatic colorectal cancer patients. Sci Transl Med 2019;11.
19. Guinney J, Dienstmann R, Wang X, et al. The consensus molecular subtypes of colorectal cancer. Nat Med 2015;21:1350-6.
20. Johnson KR, Ringland C, Stokes BJ, et al. Response rate or time to progression as predictors of survival in trials of metastatic colorectal cancer or non-small-cell lung cancer: a meta-analysis. Lancet Oncol 2006;7:741-6.
21. van der Velden DL, Hoes LR, van der Wijngaart H, et al. The Drug Rediscovery protocol facilitates the expanded use of existing anticancer drugs. Nature 2019;574:127-31.
22. Misale S, Yaeger R, Hobor S, et al. Emergence of KRAS mutations and acquired resistance to anti-EGFR therapy in colorectal cancer. Nature 2012;486:532-6.

SUPPLEMENTARY MATERIALS

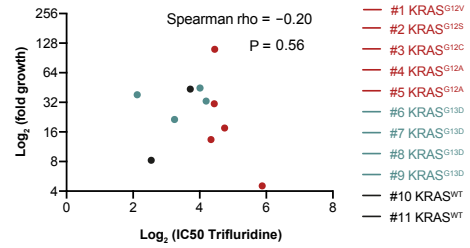

Figure S1. Lack of association between *in vitro* trifluridine sensitivity and growth rate of patient-derived mCRC organoids.

The *in vitro* growth rate of patient-derived mCRC organoids in the untreated condition is plotted against the half maximal inhibitory concentrations (IC50; $\log_2$) for trifluridine. Colors encode the codon-specific KRAS mutation status, as indicated in the legend. Spearman rho and corresponding two-sided p-value is shown.

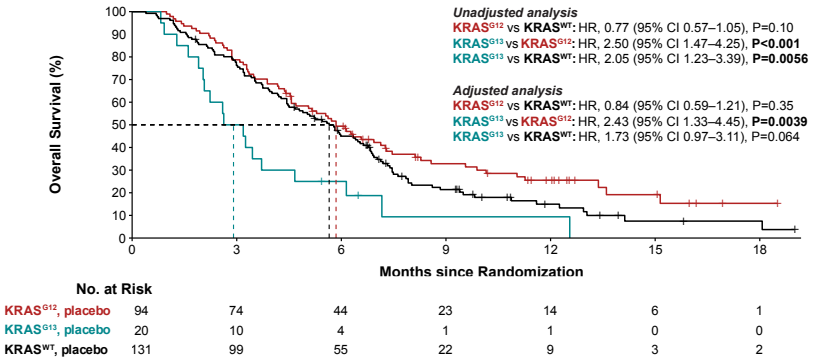

Figure S2. Overall survival of KRAS^{G12}-mutated, KRAS^{G13}-mutated and KRAS^{WT} patients in the placebo arm of the RECOURSE trial.

Cox regression-based hazard ratio (HR), 95% confidence interval (CI) and two-sided p-values are plotted for pairwise comparisons.

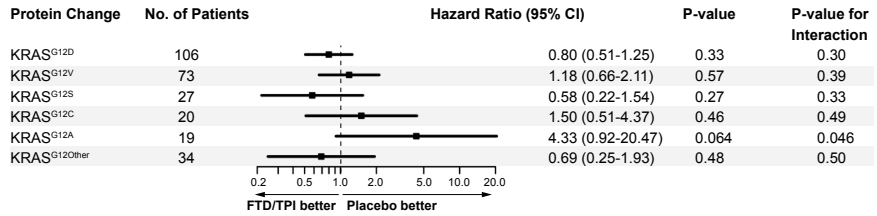

Figure S3. Forest plot of hazard ratios for overall survival for the KRAS^{G12}-mutated population, stratified based on the amino acid change.

The five most frequent KRAS^{G12} amino acid changes are shown as individual subgroups. KRAS^{G12Other} comprises all patients with KRAS^{G12} mutations that induce amino acid changes other than these five most frequent changes. Two-sided p-values for interaction indicate if the survival benefit of FTD/TPI treatment was significantly different for a specific subgroup, as compared to all patients with other KRAS^{G12} mutations.

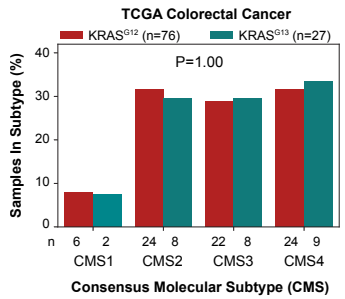

Figure S4. KRAS^{G12} and KRAS^{G13} mutations are not differentially enriched in Consensus Molecular Subtypes (CMS) in the colorectal cancer cohort of The Cancer Genome Atlas (TCGA).

The y-axis shows the percentage of samples with KRAS^{G12} mutations (red, n=76) or KRAS^{G13} mutations (dark cyan, n=27) in the different CMS (x-axis). Percentages are relative to the total number of samples with KRAS^{G12} or KRAS^{G13} mutations for red and dark cyan bars, respectively. Two-sided p-value for the c^2 test for differential enrichment is shown.

Table S1. Included patient IDs

Sheet 1: HMF cohort, Sheet 2: MSKCC cohort, Sheet 3: TCGA cohort.

Available online at https://bit.ly/3jz4hre

Table S2. Full list of candidate genomic biomarkers with at least one occurrence in the discovery cohort. Non-redundant drivers with at least five occurrences were tested for association to treatment outcome.

Somatic Driver Variant	Patients (n)	Level	Tested for association to treatment outcome	Reason for Exclusion
APC	31	GENE	NO	Full redundancy with more specific biomarker
APC_MUTATION	31	MUTATION	YES	
TP53	30	GENE	NO	Full redundancy with more specific biomarker
TP53_MUTATION	30	MUTATION	YES	
KRAS	24	GENE	NO	Full redundancy with more specific biomarker
KRAS_MUTATION	24	MUTATION	YES	
KRAS_MUT_Codon_12	20	CODON	YES	
SMAD4	7	GENE	YES	
KRAS_MUT_AA_Change_p.Gly12Asp	7	AA_CHANGE	YES	
ERBB2	5	GENE	YES	
PIK3CA_MUTATION	5	MUTATION	YES	
MACROD2_DEL	5	DEL	YES	
KRAS_MUT_AA_Change_p.Gly12Val	5	AA_CHANGE	YES	
NRAS_MUTATION	4	MUTATION	NO	<5 occurrences
SMAD4_MUTATION	4	MUTATION	NO	<5 occurrences
APC_MUT_Codon_1450	4	CODON	NO	<5 occurrences
KRAS_MUT_AA_Change_p.Gly12Cys	4	AA_CHANGE	NO	<5 occurrences
APC_MUT_AA_Change_p.Arg1450*	4	AA_CHANGE	NO	<5 occurrences
ERBB2_MUTATION	3	MUTATION	NO	<5 occurrences
TYMS_AMP	3	AMP	NO	<5 occurrences
FHIT_DEL	3	DEL	NO	<5 occurrences
PARK2_DEL	3	DEL	NO	<5 occurrences
SMAD4_DEL	3	DEL	NO	<5 occurrences
TP53_MUT_Codon_248	3	CODON	NO	<5 occurrences
APC_MUT_AA_Change_p.Arg876*	3	AA_CHANGE	NO	<5 occurrences
TP53_MUT_AA_Change_p.Arg175His	3	AA_CHANGE	NO	<5 occurrences
TP53_MUT_AA_Change_p.Arg282Trp	3	AA_CHANGE	NO	<5 occurrences
FGFR1	2	GENE	NO	<5 occurrences
ZFP36L2	2	GENE	NO	<5 occurrences
KLF5	2	GENE	NO	<5 occurrences
RNF43	2	GENE	NO	<5 occurrences
GNAS	2	GENE	NO	<5 occurrences
AMER1_MUTATION	2	MUTATION	NO	<5 occurrences
TCF7L2_MUTATION	2	MUTATION	NO	<5 occurrences
ZFP36L2_MUTATION	2	MUTATION	NO	<5 occurrences
MAP2K1_MUTATION	2	MUTATION	NO	<5 occurrences
BRAF_MUTATION	2	MUTATION	NO	<5 occurrences
RNF43_MUTATION	2	MUTATION	NO	<5 occurrences
ERBB2_AMP	2	AMP	NO	<5 occurrences
ITGAV_DEL	2	DEL	NO	<5 occurrences

Table S2 continued.

Somatic Driver Variant	Patients (n)	Level	Tested for association to treatment outcome	Reason for Exclusion
CCSER1_DEL	2	DEL	NO	<5 occurrences
NRAS_MUT_Codon_12	2	CODON	NO	<5 occurrences
TP53_MUT_Codon_220	2	CODON	NO	<5 occurrences
SMAD4_MUT_Codon_361	2	CODON	NO	<5 occurrences
APC_MUT_Codon_1309	2	CODON	NO	<5 occurrences
KRAS_MUT_Codon_61	2	CODON	NO	<5 occurrences
PIK3CA_MUT_Codon_1047	2	CODON	NO	<5 occurrences
GNAS_MUT_Codon_844	2	CODON	NO	<5 occurrences
KRAS_MUT_AA_Change_p.Gly12Ala	2	AA_CHANGE	NO	<5 occurrences
ERBB2_MUT_AA_Change_p.Val842Ile	2	AA_CHANGE	NO	<5 occurrences
KRAS_MUT_AA_Change_p.Gln61His	2	AA_CHANGE	NO	<5 occurrences
KRAS_MUT_AA_Change_p.Gly12Ser	2	AA_CHANGE	NO	<5 occurrences
TP53_MUT_AA_Change_p.Tyr220Cys	2	AA_CHANGE	NO	<5 occurrences
APC_MUT_AA_Change_p.Gln1378*	2	AA_CHANGE	NO	<5 occurrences
APC_MUT_AA_Change_p.Glu1309fs	2	AA_CHANGE	NO	<5 occurrences
GNAS_MUT_AA_Change_p.Arg844His	2	AA_CHANGE	NO	<5 occurrences
RPL22_MUT_AA_Change_p.Lys15fs	2	AA_CHANGE	NO	<5 occurrences
TP53_MUT_AA_Change_p.Arg248Gln	2	AA_CHANGE	NO	<5 occurrences
TP53_MUT_AA_Change_splice	2	AA_CHANGE	NO	<5 occurrences
CTNNB1	1	GENE	NO	<5 occurrences
JAK1	1	GENE	NO	<5 occurrences
CCND1	1	GENE	NO	<5 occurrences
MAP2K7	1	GENE	NO	<5 occurrences
STK11	1	GENE	NO	<5 occurrences
SOX9	1	GENE	NO	<5 occurrences
ZNRF3	1	GENE	NO	<5 occurrences
SMAD2	1	GENE	NO	<5 occurrences
PTEN	1	GENE	NO	<5 occurrences
JAK1_MUTATION	1	MUTATION	NO	<5 occurrences
ACVR2A_MUTATION	1	MUTATION	NO	<5 occurrences
KLF5_MUTATION	1	MUTATION	NO	<5 occurrences
STK11_MUTATION	1	MUTATION	NO	<5 occurrences
SOX9_MUTATION	1	MUTATION	NO	<5 occurrences
TSC1_MUTATION	1	MUTATION	NO	<5 occurrences
NSD1_MUTATION	1	MUTATION	NO	<5 occurrences
MAP2K7_MUTATION	1	MUTATION	NO	<5 occurrences
RBM10_MUTATION	1	MUTATION	NO	<5 occurrences
CD79B_AMP	1	AMP	NO	<5 occurrences
CDX2_AMP	1	AMP	NO	<5 occurrences
FGFR1_AMP	1	AMP	NO	<5 occurrences
FLT3_AMP	1	AMP	NO	<5 occurrences
CCND1_AMP	1	AMP	NO	<5 occurrences
IKBKB_AMP	1	AMP	NO	<5 occurrences
CCND2_AMP	1	AMP	NO	<5 occurrences
ANK1_AMP	1	AMP	NO	<5 occurrences
KLF5_AMP	1	AMP	NO	<5 occurrences

Table S2 continued.

Somatic Driver Variant	Patients (n)	Level	Tested for association to treatment outcome	Reason for Exclusion
TOP2A_AMP	1	AMP	NO	<5 occurrences
TG_AMP	1	AMP	NO	<5 occurrences
ZMIZ1_AMP	1	AMP	NO	<5 occurrences
ZBTB10_AMP	1	AMP	NO	<5 occurrences
MYC_AMP	1	AMP	NO	<5 occurrences
MDM2_AMP	1	AMP	NO	<5 occurrences
SEMG2_AMP	1	AMP	NO	<5 occurrences
CTNNB1_DEL	1	DEL	NO	<5 occurrences
GPHN_DEL	1	DEL	NO	<5 occurrences
TET2_DEL	1	DEL	NO	<5 occurrences
SPATA31A7_DEL	1	DEL	NO	<5 occurrences
OR4F21_DEL	1	DEL	NO	<5 occurrences
SMAD2_DEL	1	DEL	NO	<5 occurrences
SGCZ_DEL	1	DEL	NO	<5 occurrences
PTEN_DEL	1	DEL	NO	<5 occurrences
APC_MUT_Codon_1322	1	CODON	NO	<5 occurrences
APC_MUT_Codon_1492	1	CODON	NO	<5 occurrences
APC_MUT_Codon_1400	1	CODON	NO	<5 occurrences
APC_MUT_Codon_1315	1	CODON	NO	<5 occurrences
TP53_MUT_Codon_266	1	CODON	NO	<5 occurrences
TP53_MUT_Codon_245	1	CODON	NO	<5 occurrences
TP53_MUT_Codon_236	1	CODON	NO	<5 occurrences
TP53_MUT_Codon_173	1	CODON	NO	<5 occurrences
TP53_MUT_Codon_144	1	CODON	NO	<5 occurrences
TP53_MUT_Codon_127	1	CODON	NO	<5 occurrences
TP53_MUT_Codon_125	1	CODON	NO	<5 occurrences
NRAS_MUT_Codon_61	1	CODON	NO	<5 occurrences
NRAS_MUT_Codon_13	1	CODON	NO	<5 occurrences
KRAS_MUT_Codon_146	1	CODON	NO	<5 occurrences
PIK3CA_MUT_Codon_546	1	CODON	NO	<5 occurrences
PIK3CA_MUT_Codon_545	1	CODON	NO	<5 occurrences
ZNRF3_MUT_AA_Change_p.Gly612fs	1	AA_CHANGE	NO	<5 occurrences
ERBB2_MUT_AA_Change_p.Arg678Gln	1	AA_CHANGE	NO	<5 occurrences
FGFR1_MUT_AA_Change_p.Met698delinsIlePheAsnAspThr	1	AA_CHANGE	NO	<5 occurrences
GNAS_MUT_AA_Change_p.Arg999Cys	1	AA_CHANGE	NO	<5 occurrences
APC_MUT_AA_Change_p.Glu1379*	1	AA_CHANGE	NO	<5 occurrences
APC_MUT_AA_Change_p.Glu1057*	1	AA_CHANGE	NO	<5 occurrences
APC_MUT_AA_Change_p.Gln879*	1	AA_CHANGE	NO	<5 occurrences
APC_MUT_AA_Change_p.Gln349*	1	AA_CHANGE	NO	<5 occurrences
APC_MUT_AA_Change_p.Gln1367*	1	AA_CHANGE	NO	<5 occurrences
APC_MUT_AA_Change_p.Gln1294*	1	AA_CHANGE	NO	<5 occurrences
APC_MUT_AA_Change_p.Gln1291*	1	AA_CHANGE	NO	<5 occurrences
APC_MUT_AA_Change_p.Arg554*	1	AA_CHANGE	NO	<5 occurrences
APC_MUT_AA_Change_p.Arg499*	1	AA_CHANGE	NO	<5 occurrences
APC_MUT_AA_Change_p.Arg302*	1	AA_CHANGE	NO	<5 occurrences
APC_MUT_AA_Change_p.Arg216*	1	AA_CHANGE	NO	<5 occurrences

Table S2 continued.

Somatic Driver Variant	Patients (n)	Level	Tested for association to treatment outcome	Reason for Exclusion
APC_MUT_AA_Change_p.Arg213*	1	AA_CHANGE	NO	<5 occurrences
APC_MUT_AA_Change_p.Ala1492fs	1	AA_CHANGE	NO	<5 occurrences
AMER1_MUT_AA_Change_p.Asp307fs	1	AA_CHANGE	NO	<5 occurrences
AMER1_MUT_AA_Change_p.Arg631*	1	AA_CHANGE	NO	<5 occurrences
AKT1_MUT_AA_Change_p.Gly162Asp	1	AA_CHANGE	NO	<5 occurrences
AKT1_MUT_AA_Change_p.Glu17Lys	1	AA_CHANGE	NO	<5 occurrences
ACVR2A_MUT_AA_Change_p.Lys437fs	1	AA_CHANGE	NO	<5 occurrences
APC_MUT_AA_Change_p.Glu1286*	1	AA_CHANGE	NO	<5 occurrences
APC_MUT_AA_Change_p.Glu941*	1	AA_CHANGE	NO	<5 occurrences
BRAF_MUT_AA_Change_p.Val600Glu	1	AA_CHANGE	NO	<5 occurrences
APC_MUT_AA_Change_p.Glu984*	1	AA_CHANGE	NO	<5 occurrences
BRAF_MUT_AA_Change_p.Lys483Glu	1	AA_CHANGE	NO	<5 occurrences
BMPR2_MUT_AA_Change_p.Lys457fs	1	AA_CHANGE	NO	<5 occurrences
BMPR2_MUT_AA_Change_p.Asn583fs	1	AA_CHANGE	NO	<5 occurrences
APC_MUT_AA_Change_p.Val1472fs	1	AA_CHANGE	NO	<5 occurrences
APC_MUT_AA_Change_p.Thr1556fs	1	AA_CHANGE	NO	<5 occurrences
APC_MUT_AA_Change_p.Thr1388fs	1	AA_CHANGE	NO	<5 occurrences
APC_MUT_AA_Change_p.Ser836*	1	AA_CHANGE	NO	<5 occurrences
APC_MUT_AA_Change_p.Ser1400fs	1	AA_CHANGE	NO	<5 occurrences
APC_MUT_AA_Change_p.Ser1315*	1	AA_CHANGE	NO	<5 occurrences
APC_MUT_AA_Change_p.Ser1281*	1	AA_CHANGE	NO	<5 occurrences
APC_MUT_AA_Change_p.Ser1240fs	1	AA_CHANGE	NO	<5 occurrences
APC_MUT_AA_Change_p.Ser1068fs	1	AA_CHANGE	NO	<5 occurrences
APC_MUT_AA_Change_p.Leu1488fs	1	AA_CHANGE	NO	<5 occurrences
APC_MUT_AA_Change_p.Ile1580fs	1	AA_CHANGE	NO	<5 occurrences
APC_MUT_AA_Change_p.His913fs	1	AA_CHANGE	NO	<5 occurrences
KLF5_MUT_AA_Change_p.Pro305Arg	1	AA_CHANGE	NO	<5 occurrences
TP53_MUT_AA_Change_p.Pro151Ser	1	AA_CHANGE	NO	<5 occurrences
TP53_MUT_AA_Change_p.Gly266Glu	1	AA_CHANGE	NO	<5 occurrences
TP53_MUT_AA_Change_p.Gly245Ser	1	AA_CHANGE	NO	<5 occurrences
TP53_MUT_AA_Change_p.Glu286_Glu-287del	1	AA_CHANGE	NO	<5 occurrences
TP53_MUT_AA_Change_p.Gln167fs	1	AA_CHANGE	NO	<5 occurrences
TP53_MUT_AA_Change_p.Gln104*	1	AA_CHANGE	NO	<5 occurrences
TP53_MUT_AA_Change_p.Asp184fs	1	AA_CHANGE	NO	<5 occurrences
TP53_MUT_AA_Change_p.Arg306*	1	AA_CHANGE	NO	<5 occurrences
TP53_MUT_AA_Change_p.Arg248Trp	1	AA_CHANGE	NO	<5 occurrences
TP53_MUT_AA_Change_p.Arg196*	1	AA_CHANGE	NO	<5 occurrences
TCF7L2_MUT_AA_Change_p.Arg488His	1	AA_CHANGE	NO	<5 occurrences
STK11_MUT_AA_Change_p.Pro281fs	1	AA_CHANGE	NO	<5 occurrences
TP53_MUT_AA_Change_p.Leu308fs	1	AA_CHANGE	NO	<5 occurrences
TP53_MUT_AA_Change_p.Pro152Leu	1	AA_CHANGE	NO	<5 occurrences
TP53_MUT_AA_Change_p.Pro27fs	1	AA_CHANGE	NO	<5 occurrences
ZFP36L2_MUT_AA_Change_p.Gly108fs	1	AA_CHANGE	NO	<5 occurrences
ZFP36L2_MUT_AA_Change_p.Cys321fs	1	AA_CHANGE	NO	<5 occurrences
ZBTB20_MUT_AA_Change_p.Pro692fs	1	AA_CHANGE	NO	<5 occurrences

Table S2 continued.

Somatic Driver Variant	Patients (n)	Level	Tested for association to treatment outcome	Reason for Exclusion
TP53_MUT_AA_Change_p.Val173Leu	1	AA_CHANGE	NO	<5 occurrences
TP53_MUT_AA_Change_p.Tyr236His	1	AA_CHANGE	NO	<5 occurrences
TP53_MUT_AA_Change_p.Trp91*	1	AA_CHANGE	NO	<5 occurrences
TP53_MUT_AA_Change_p.Ser127Phe	1	AA_CHANGE	NO	<5 occurrences
SOX9_MUT_AA_Change_p.Glu293fs	1	AA_CHANGE	NO	<5 occurrences
KRAS_MUT_AA_Change_p.Ala146Thr	1	AA_CHANGE	NO	<5 occurrences
PIK3CA_MUT_AA_Change_p.Gln546Pro	1	AA_CHANGE	NO	<5 occurrences
NSD1_MUT_AA_Change_p.Pro1814fs	1	AA_CHANGE	NO	<5 occurrences
NRAS_MUT_AA_Change_p.Gly13Cys	1	AA_CHANGE	NO	<5 occurrences
NRAS_MUT_AA_Change_p.Gly12Ser	1	AA_CHANGE	NO	<5 occurrences
NRAS_MUT_AA_Change_p.Gly12Asp	1	AA_CHANGE	NO	<5 occurrences
NRAS_MUT_AA_Change_p.Gln61Lys	1	AA_CHANGE	NO	<5 occurrences
MAP2K7_MUT_AA_Change_p.Arg195His	1	AA_CHANGE	NO	<5 occurrences
MAP2K1_MUT_AA_Change_p.Glu203Lys	1	AA_CHANGE	NO	<5 occurrences
MAP2K1_MUT_AA_Change_p.Asp67Asn	1	AA_CHANGE	NO	<5 occurrences
KRAS_MUT_AA_Change_p.Pro34Arg	1	AA_CHANGE	NO	<5 occurrences
PIK3CA_MUT_AA_Change_p.Glu545Gln	1	AA_CHANGE	NO	<5 occurrences
SMAD4_MUT_AA_Change_p.Trp524Arg	1	AA_CHANGE	NO	<5 occurrences
PIK3CA_MUT_AA_Change_p.Gly1049Arg	1	AA_CHANGE	NO	<5 occurrences
SMAD4_MUT_AA_Change_p.Gln534del	1	AA_CHANGE	NO	<5 occurrences
SMAD4_MUT_AA_Change_p.Arg361Ser	1	AA_CHANGE	NO	<5 occurrences
SMAD4_MUT_AA_Change_p.Arg361His	1	AA_CHANGE	NO	<5 occurrences
RNF43_MUT_AA_Change_p.Lys125Asn	1	AA_CHANGE	NO	<5 occurrences
RNF43_MUT_AA_Change_p.Gly659fs	1	AA_CHANGE	NO	<5 occurrences
RBM10_MUT_AA_Change_p.Glu117_Glu-119del	1	AA_CHANGE	NO	<5 occurrences
PIK3CA_MUT_AA_Change_p.His1047Leu	1	AA_CHANGE	NO	<5 occurrences
PIK3CA_MUT_AA_Change_p.His1047Arg	1	AA_CHANGE	NO	<5 occurrences
ABL1_MUT_AA_Change_p.Lys266Arg	1	AA_CHANGE	NO	<5 occurrences

Table S3. Clinical and molecular characteristics of patient-derived organoids (PDOs) used for *in vitro* testing of Trifluridine sensitivity.

		PATIENT CHARACTERISTICS		TUMOR CHARACTERISTICS					REGIMENS PRIOR TO BIOPSY
Study number	Internal ID	Gender	Age at biopsy	Localization	Differentiation	Genetic profile		Biopsied lesion	Treatment regimen
						KRAS mutation-induced amino acid change	MSI status		
#1 KRAS^{G12V}	TUM010	M	69	Colon	Moderately	G12V	NA	Omentum	CAPOX-B/ Panitumumab
#2 KRAS^{G12S}	SNS026	F	51	Colon	Poorly	G12S	MSS	Lymph node	CAPOX
#3 KRAS^{G12C}	TUM052	M	63	Colon	Moderately	G12C	MSS	Liver	CAPOX-B
#4 KRAS^{G12A}	TUM003	M	72	Colon	Moderately	G12A	MSS	Liver	-
#5 KRAS^{G12A}	TUM101	M	54	Rectum	Moderately	G12A	MSS	Liver	CAPOX-B
#6 KRAS^{G13D}	SNS030	F	48	Colon	NA	G13D	MSS	Liver	FOLFIRI-B
#7 KRAS^{G13D}	TUM055	F	58	Colon	Undifferentiated	G13D	MSS	Lymph node	CAPOX (adjuvant)
#8 KRAS^{G13D}	SNS032	M	56	Rectum	Poorly	G13D	MSS	Lymph node	FOLFOX-B
#9 KRAS^{G13D}	TUM137	M	73	Colon	Well/moderately	G13D	MSS	Liver	-
#10 KRAS^{WT}	SNS005	M	55	Colon	NA	Wild type	MSS	Liver	CAPOX-B
#11 KRAS^{WT}	TUM050	M	56	Rectum	NA	Wild type	MSS	Lymph node	CAPOX-B

Table S4. Hazard ratios, two-sided p-values and Benjamini-Hochberg corrected false discovery rates (FDR) for associations between candidate biomarkers and treatment discontinuation in the discovery cohort.

biomarker	n positive	HR	lower	upper	pvalue	fdr
KRAS_MUT_Codon_12	20	4,594758383	1,974596974	10,6917031	0,000401805	0,004018049
KRAS_MUT_AA_Change_p.Gly12Val	5	2,810489829	1,031612963	7,656798971	0,04329747	0,14695828
PIK3CA_MUTATION	5	2,876913041	1,028367904	8,048314823	0,044087484	0,14695828
KRAS_MUT_AA_Change_p.Gly12Asp	7	2,294779719	0,96962645	5,430971855	0,0587861	0,14696525
KRAS_MUTATION	24	1,878031936	0,923061078	3,820986535	0,082026647	0,164053295
ERBB2	5	0,613445081	0,212920912	1,767392708	0,365404769	0,609007948
APC_MUTATION	31	0,803182635	0,325019491	1,984811257	0,634912706	0,907018151
SMAD4	7	0,870451605	0,378119166	2,003828591	0,744322901	0,930403626
MACROD2_DEL	5	1,09066904	0,419258559	2,837291997	0,858780992	0,954201102
TP53_MUTATION	30	0,991139638	0,429860788	2,285292846	0,983341042	0,983341042

Table S5. Hazard ratios, two-sided p-values and Benjamini-Hochberg corrected false discovery rates (FDR) for associations between candidate biomarkers and overall survival in the discovery cohort.

biomarker	n positive	HR	lower	upper	pvalue	fdr
KRAS_MUT_Codon_12	20	3,378401325	1,556161699	7,334453434	0,002083404	0,020834044
KRAS_MUTATION	24	2,769282378	1,241742875	6,175936293	0,012808575	0,064042877
KRAS_MUT_AA_Change_p.Gly12Asp	7	2,32368154	0,95688755	5,642769519	0,062517127	0,208390423
PIK3CA_MUTATION	5	2,389939608	0,883765926	6,463036376	0,086065707	0,215164268
KRAS_MUT_AA_Change_p.Gly12Val	5	1,601658769	0,613599091	4,180760456	0,335930781	0,633225026
ERBB2	5	0,624710292	0,218564388	1,78557428	0,379935016	0,633225026
SMAD4	7	1,327088645	0,574887462	3,063493967	0,507330188	0,635773861
MACROD2_DEL	5	1,380819523	0,530399771	3,594765043	0,508619089	0,635773861
TP53_MUTATION	30	1,099728765	0,47782569	2,531055532	0,823129909	0,905487514
APC_MUTATION	31	1,055177315	0,434792687	2,560758721	0,905487514	0,905487514

APPENDIX

Appendix 1. Bioinformatics analysis

Whole genome sequencing (median depths ~100 and ~40 for tumor and normal, respectively) and bioinformatics analysis of the discovery cohort were performed by HMF as previously described[17], with an optimized pipeline based on open source tools, which is freely available on GitHub (https://github.com/hartwigmedical/pipeline5). Somatic genomic drivers were identified as an integrated functionality of PURPLE v2.43[17]. Briefly, somatic mutations were considered drivers if they fulfilled one of the following criteria: 1) mutations in oncogenes located at –or within 5-bases of– known hotspots, 2) inframe indels in oncogenes with repeat count <8 repeats, 3) biallelic nonsense, splice or indel variants in tumor suppressor genes (TSG's), 4) mutations in oncogenes or TSG's with a sample-specific driver likelihood >80%, as calculated by PURPLE as previously described[17]. For this manuscript, we only considered TSG mutations to be drivers if 1) they were biallelic, or 2) in the case of multiple mutations in the gene for which the summed variant ploidies exceeded the gene ploidy within the sample minus 0.5 (e.g. the classical APC double hit). Amplifications were considered to be drivers if 1) they affected an oncogene with pan-cancer evidence for recurrent amplification[17], and 2) this oncogene had a copy number exceeding three times the sample ploidy. Deletions were considered to be drivers if 1) they affected TSG's with pan-cancer evidence for recurrent deletion[17], and 2) they were homozygous (absolute gene copy number <0.5).

Appendix 2. Candidate biomarker selection process

Somatic genomic driver variants (mutations and copy number alterations) were included as candidate biomarkers, at increasingly specific "levels": 1) gene-level biomarkers (e.g. "APC alteration", which could either be by mutation or copy number alteration), 2) variant class-level biomarkers (e.g. "APC mutation", or "APC deletion"), 3) codon-level biomarkers (e.g. "APC codon 1450 mutation"), and 4) amino acid change-specific biomarkers (e.g. "APC p.Thr562Met mutation"). In cases were biomarkers of different levels showed complete redundancy, only the most specific level was included. For example, all KRAS alterations in the cohort were mutations, leading to complete redundancy between "KRAS alteration" and "KRAS mutation". Hence, "KRAS mutation" was selected as the most specific level and included as a candidate biomarker, whereas "KRAS alteration" was excluded.

Appendix 3. Statistical packages

Application	Programming language	Package	Version	Function
Kaplan-Meier method	R	survminer	0.4.6	surv_median
Kaplan-Meier curve plotting	R	survminer	0.4.6	ggsurvplot
Cox regression	Python 3	lifelines	0.23.3	CoxPHFitter
Fisher's exact test	Python 3	scipy	1.4.1	stats.fisher_exact
c^2 test	Python 3	scipy	1.4.1	stats.chi2_contingency

CHAPTER 5

PROSPECTIVE EXPERIMENTAL TREATMENT OF COLORECTAL CANCER PATIENTS BASED ON ORGANOID DRUG RESPONSES

Salo Noël Ooft[1,*], Fleur Weeber[1,*], Luuk Schipper[1,#], Krijn Kristian Dijkstra[1,#], Chelsea Marie McLean[1], Sovann Kaing[1], Joris van de Haar[1,2], Warner Prevoo[3], Erik van Werkhoven[4], Petur Snaebjornsson[5], Louisa Hoes[1], Myriam Chalabi[1,6], Daphne van der Velden[1,6,7], Monqiue van Leerdam[6], Henk Boot[6], Cecile Grootscholte[6], Alwin Dagmar Redmar Huitema[8,9], Haiko Bloemendal[10], Edwin Cuppen[11,12,13], and Emile Voest[1,6,13,14]

[1]Department of Molecular Oncology and Immunology, The Netherlands Cancer Institute, 1066 CX Amsterdam, The Netherlands.
[2]Department of Molecular Carcinogenesis, The Netherlands Cancer Institute, 1066 CX Amsterdam, The Netherlands.
[3]Department of Radiology, The Netherlands Cancer Institute, 1066 CX Amsterdam, The Netherlands.
[4]Department of Biometrics, The Netherlands Cancer Institute, 1066 CX Amsterdam, The Netherlands.
[5]Department of Pathology, The Netherlands Cancer Institute, 1066 CX Amsterdam, The Netherlands.
[6]Department of Gastrointestinal Oncology, The Netherlands Cancer Institute, 1066 CX Amsterdam, The Netherlands.
[7]Department of Radiology and Nuclear Medicine, Amsterdam University Medical Center AMC, 1105 AZ Amsterdam, The Netherlands.
[8]Department of Pharmacy & Pharmacology, The Netherlands Cancer Institute, 1066 CX Amsterdam, The Netherlands.
[9]Department of Clinical Pharmacy, University Medical Centre Utrecht, 3584 CX Utrecht, The Netherlands.
[10]Department of Internal Medicine/Oncology, Radboud University Medical Center Nijmegen, 6525 GA Nijmegen, The Netherlands.
[11]Division of Biomedical Genetics, Centre for Molecular Medicine, University Medical Centre Utrecht, 3584 CX Utrecht, The Netherlands.
[12]Hartwig Medical Foundation, 1098 XH Amsterdam, The Netherlands.
[13]Oncode Institute, 3521 AL Utrecht, The Netherlands.
[14]Correspondence should be addressed to:
Prof. Emile E. Voest
Department of Gastrointestinal Oncology and Department of Molecular Oncology and Immunology, The Netherlands Cancer Institute
Plesmanlaan 121, 1066 CX, Amsterdam, the Netherlands
E.voest@nki.nl +31 20 512 6930
*,# These authors contributed equally to this work.

Journal of the National Cancer Institute (submitted)

ABSTRACT

Introduction

Organoid technology has recently emerged as a powerful tool to assess drug sensitivity of individual patient tumors in vitro. Organoids may therefore be an new avenue for precision medicine, as this circumvents many of the complexities associated DNA- or transcriptional-profiling.

Methods

The SENSOR trial was a single-arm, single-center, prospective, intervention trial to evaluate the feasibility of patient-derived organoids to allocate patients for treatment with off-label or investigational agents. The primary endpoint was an objective response rate of ≥20%. Patients underwent a biopsy for culture before commencing to their last round standard-of-care. Organoids were exposed to a panel of 8 drugs and patients were treated after progression on standard-of-care, and when a clear signal of anti-tumor activity was identified in vitro.

Results

Sixtyone patients were included and we generated 31 organoids of 54 eligible patients. Twentyfive cultures were subjected to drug screening and 19 organoids exhibited substantial responses to one or more drugs. Three patients underwent treatment with vistusertib and 3 with capivasertib. Despite drug sensitivity of organoid cultures, patients did not demonstrate objective clinical responses to the recommended treatment.

Conclusions

Organoid technology had limited value as tool for precision medicine in this patient population, because of the large fraction of patients could not undergo treatment, or because the recommended treatment did not elicit an objective response. We identified several essential parameters, such as the culture success rate, clinical deterioration of patients during standard-of-care and rational design of drug panels, that needs to be accounted for in organoid-guided clinical studies.

INTRODUCTION

The paradigm of personalized medicine revolves around allocating the right treatment to the right patient. As a consequence, most newly developed anti-cancer drugs have a defined, usually genomics-based, target. The implementation of personalized medicine in daily clinical practice has led to variable successes in the treatment of cancer patients[1-4]. Early experiences have identified several important challenges, including the tissue-specificity of cancer drivers, variants-of-unknown significance (VUS) and the context-dependency of genomic aberrations among the thousands found in cancer genomes[5]. These issues currently limit efficient use of new anti-cancer drugs and inspired us to explore other means (beyond genomics) to improve precision medicine[3,6].

Organoid technology allows culturing, expansion and drug screening of patient's individual tumors[7]. Organoids provide a morphological and genetic representation of a patient's tumor and several studies demonstrated that in vitro drug responses mirrored clinical responses of patient[8,9]. Organoids are therefore widely recognized as an novel opportunity to test a long-standing concept in the field of precision oncology: treatment based on individualized, ex vivo drug screening of patient tumor cells[6,10-15]. As such, many groups are now pursueing organoid-based drug screening of patient tumor cells to guide clinical decision-making[11,12,16]. Here, we present the first formal, prospective, intervention trial, the Selecting cancer patients for treatment using tumor organoids (SENSOR) trial, designed to evaluate the potential and feasibility to treat patients based on their *in vitro* organoid drug response profile.

METHODS

Study design

The SENSOR study was an open-label, single center, prospective, feasibility study (NL50400.031.14) at the Netherlands Cancer Institute between December 2016 and December 2018. The study was approved by the ethical review board of the Netherlands Cancer Institute and was designed in concordance with the Declaration of Helsinki for medical research involving human subjects, Dutch law, and Good Clinical Practice. The study objective was to evaluate the feasibility of organoids to allocate patients for treatment with specific targeted agents and the primary endpoint of the study was an objective response rate (ORR) of ≥20% according to Response Evaluation Criteria In Solid tumours (RECIST) 1.1[17]. Secondary and exploratory endpoints were to identify potential biomarkers of response, to identify mechanisms of primary and secondary resistance, and to determine whether any treatmentβ induced changes in organoids after failure of standard-of-care (SOC) in pre- and post-

treatment organoids were present. Patients with metastatic colorectal cancer (CRC) without curative treatment options were accrued at the Netherlands Cancer Institute before start of their last SOC treatment and refered to by their treating physicians. Patients underwent pre-treatment biopsies before start of their last round standard-of-care (SOC) treatment and second biopsy before start with experimental treatment to control for potential effect of intermittent SOC treatment. Treatment was provided for 5 patients per drug (vistusertib, capivasertib, selumetinib and gefitinib) by AstraZeneca and for 10 patients per drug (palbociclib, axitinib, gedatolisib, and glasdegib) by Pfizer.

Statistical analysis

RECIST response and progression free survival will be presented for the evaluable patient population. Adverse events will be presented separately for each safety population. As this is a feasibility study, there is no formal sample size calculation. All statistical tests were performed two-tailed in GraphPad Prism V7.03. P-values below 0.05 were considered statistically significant.

Patient material processing and organoid culture

Organoids for the decision model were derived from Wetering *et al.* 2015, our personal biobank, or our prior studies[13,18]. For patients included in the trial, we used one or two 18 Gauge tumour biopsies for both organoid culture and DNA-sequencing. Biopsies were collected and processed as previously described in Weeber *et al.* 2015 and Dijkstra, Cattaneo *et al.* 2018 (continued in the online methods)[9,18]. In case of eligibility and consent of the patient, cultures were also used in context of the TUMOROID study[13].

Drug screening

All drug screens were performed in duplicate by an independent researcher, blinded for all genetic (and clinical) data of patients. In case of discrepant results, the given drug was repeated a third time. Screens were performed as described previously by Ooft, Weeber *et al.* 2019 (see online methods for a description)[13]. Compounds were provided by Astra Zeneca and Pfizer, and dissolved in DMSO and plated using a Tecan D300e digital dispenser. The choice of concentrations used in drug screening was based on the maximum concentration (C_{max}) found in patients and concentrations 1-2 orders of magnitude lower[19-22]: 0.137, 0.249 and 2.49 µM vistusertib, 0.37, 0.825 and 3.7 µM capivasertib, 0.041, 0.26 and 2.6 µM selumetinib, 0.0531, 0.098 and 0.531 µM gefitinib, 0.0303, 0.147 and 0.303 µM palbociclib, 0.000815, 0.0163, 0.163 µM axitinib, 0.0069, 0.0407 and 0.407 µM gedatolisib, 0.1, 0.8 and 8.0 µM glasdegib. Organoid drug sensitivity was calculated using growth rate inhition metrics (scale 1 to -1). A score of 1 represents identical growth to non-treated condition, 0 represent a size identical to day 0 (no growth), and anything below 0 a degree of cytotoxicity after 6 days of exposure to the respective drug.

Study treatment

Organoid sensitivity, as defined by GR<0.1 (described in more detail in results), to one of the experimental compounds rendered patients eligible to treatment with that compound (continued in the online methods).

RESULTS

Development of a treatment-decision model

Five federal drug administration (FDA)-approved compounds and 3 drugs in advanced phase of clinical development were included in the study. This drug panel, made available by Astra Zeneca and Pfizer, consisted of vistusertib (mTOR), capivasertib (AKT) selumetinib (MEK), gefitinib (EGFR), palbociclib (CDK4/6) axitinib (VEGFR), gedatolisib (PI3K/mTOR) glasdegib (SMO). The panel was designed to target both frequent and sporadic genetic events in metastatic CRC, such as mutations or amplifications in EGFR (gefitinib), MEK (selumetinib), AKT (capivasertib) or SMO (glasdegib)[23]. To determine what would qualify as 'sensitive' or 'resistant', we amended our previously developed drug screening pipeline and screened a pilot cohort of organoids to construct a decision model for patient treatment[13]. The cohort consisted of 16 organoids, of which the genetic and clinical data are summarized in Table S1. We exposed all 16 organoids for 6 days to 3 concentrations per drug. The concentrations used in drug screening was guided by pharmacokinetic data from the investigator brochures or the published phase 1 studies each drug[19-22]. In order to use patient-relevant concentrations in the drug screens, we used the maximum drug concentration found in patients (C_{max}) and concentration 1-2 orders of magnitude lower[19-22]. Drug effects were quantified using GR metrics[24].

As expected, drug-response data demonstrated a dose-dependent pattern, in which the highest concentration (GR_{max}) generally elicted a substantial effect (Fig. S1). We decided that effects below 0.1 at these concentrations would be sufficiently stringent to qualify as *in vitro* hits, as this would nominate cultures in which we observe near-cytostatic effects at physiologically achievable concentrations. This criterium resulted in 'hits' on 4 drugs across the cohort targeting various oncogenic signaling nodes in CRC: vistusertib (mTOR), selumetinib (MEK), gefitinib (EGFR) and gedatolisib (PI3K/mTOR) (Fig. 1)[23]. To test whether our defined threshold would identify potential eligible patients, we assessed the predictive value for two known biomarker-drug combinations. Because EGFR inhibition is solely efficacious in EGF-pathway wild-type (EGF^{wt}) tumors and not in EGF-pathway mutated (EGF^{mut}) tumors, we expected that gefinitb in combination with our threshold can discriminate between these two genotypes. When we applied GR<0.1 as cut-off for potential responders, none of the EGF^{mut} organoids

were classified as hit. Analogous to the variable response rate of EGF^{wt} patients to the anti-EGFR monoclonal antibodies cetuximab and panitumumab, we observed a subset (2/4) of EGF^{wt} organoids responding to gefitinib treatment. This suggests that our model could not only discriminates between EGF^{wt} and EGF^{mut} organoids, but also identify differential responses within a genomically identical genotype (EGF^{wt})[25]. To further test ability of our model to exclude non-responders and prevent overtreatment, we also correlated organoids with gain-of-function mutations in KRAS (KRAS^{mut}) and the effects of selumetinib. (Pre)clinical evidence demonstrated that there is no benefit for selumetinib in KRAS^{mut} tumors, and we therefore expected this to be reflected in our organoid drug sensitivity data too[26,27]. Seven organoids harbored KRAS mutations (T10, T12, T14, T16, T2, T1 and T9), which were all classified as resistant by our pipeline in line with (pre)clinical data. These data suggest that, at least for gefitinib and selumetinib, organoid drug screening excludes genotypes that are known to be resistant to treatment (EGF/KRAS^{mut}; gefitinib/selumetinib). Conversely, organoids displayed differential responses within a genetically similar genotype-drug combination (EGF^{wt}; gefitinib), of which only a subset is known to respond well in the clinic to EGFR inhibition[25]. We therefore concluded that organoids can be used as a treatment selection step in addition to purely genomics-based approaches[25].

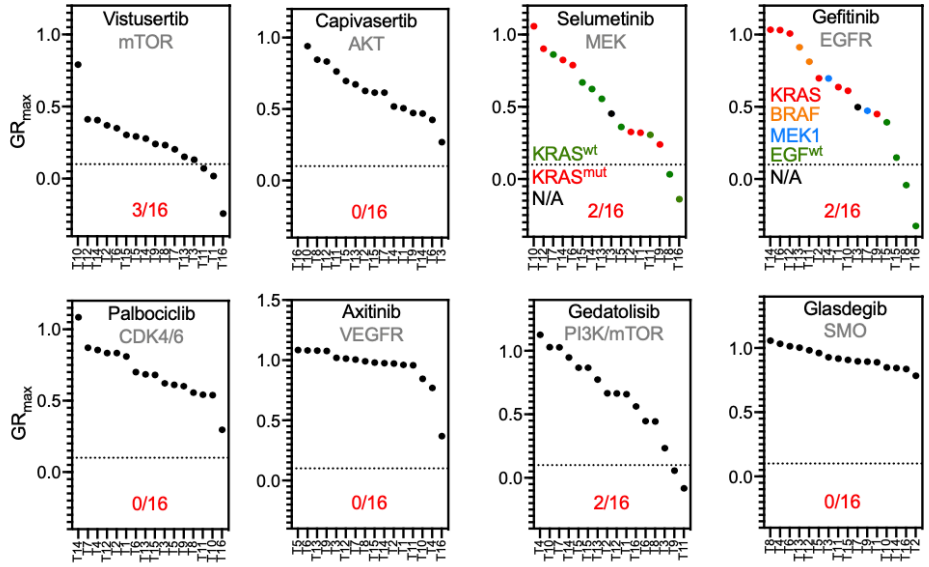

Fig. 1. Development of a decision model based on drug screening of 16 organoids.

The cohort of 16 organoids and their response to the GR_{max} concentration of each drug after 6 days. Effects were calculated using GR metrics. 1 equals no effect, 0 equals no growth and <0 a certain amount of cytotoxicity (up to -1). A cut-off of 0.1 was set, represented by the dotted line, discriminating between what

was considered a 'hit' versus 'no hit'. All organoids were plotted on the x-axis' and sorted from resistant to sensitive. All drug names were plotted in the top of each graph and the target(s) in grey below. In the bottom of each graph we noted the number of virtual hits per drug in red. For selumetinib and gefitinib additional, color-coded information on KRAS or the EGF-pathway status was added per organoid line. GR = growth-rate corrected metric, N/A = not available.

Prospective treatment of patients with metastatic colorectal cancer

Following validation of the decision model, we included patients of whom organoids were screened for responsiveness to our drug panel (Fig. 2a). All patients were included before they received their last SOC treatment line (irinotecan-based therapy or anti-EGFR mABs), while all had progressed on 1 or 2 prior lines of SOC treatment (containing 5-FU, with or without oxaliplatin and/or irinotecan) according to the SOC for palliative treatment of patients with metastatic CRC (Fig. 2a). Sixty-one patients were included in the trial, of which 54 underwent a succesful biopsy procedure as the biopsy failed to obtain tumor material in 7 cases (Fig. 2B; baseline characteristics of patients intended to treat are presented in Table 1). The remaining 54 biopsies were taken into culture and organoids were generated as previously described[9,13,18]. We obtained successful cultures for 31 patients, resulting in a culture success rate of 57% (31/54 biopsies). Twenty-three cultures failed due to either low epithelial/tumor cell content in the biopsy (n=14), infection (n=5), unknown (n=3) or quality control (n=1). Six patients dropped out before culture was succesful, of which 5 clinically deteriorated during their last line of SOC treatment. For these six patients we did not perform drug screening. In total, 25 drug screens were performed of patients for which all clinical and genetic parameters are presented in Table S2. Expansion of organoids from needle biopsies and drug screening was generally performed within 10 weeks after the biopsy and finished before the first evaluation of treatment response of SOC. Repeats were highly reproducible with a median Pearson r correlation between repeats of 0.937 (.1A and B). *In vitro* drug sensitivity to at least one drug was found for 19 patients, resulting in a patient-to-drug matching rate of 31% (19/61 patients). We identified hits to vistusertib (n = 16), capivasertib (n = 5), selumetinib (n = 3), gefitinib (n = 5), and gedatolisib (n = 2) (Fig. 2B). Of 19 patients eligible for study treatment (i.e. *in vitro* drug sensitivity), 6 patients started treatment based on the organoid assay. The other 13 patients did not start treatment mostly due to clinical deterioration under SOC (n = 6). For 3 patients we identified vistusertib as potential hit, but when the drug did not show superiority to everolimus in a randomized phase 2 study, AstraZeneca deprioritized further development of this drug[28]. We therefore also decided against further use of this drug. Two patients enrolled in other phase 1 studies (n = 2), 1 patient had an identical target of intermittent and experimental treatment (panitumumab/gefitinib targeting EGFR; n = 1) and another patient didn't receive follow-up (Fig. 2B).

Table 1. Baseline characteristics of all included patients in the SENSOR trial.

Baseline characteristics of all patients, patients with a successful organoid culture and subsequent drug screen, and patients that received an organoid-informed treatment. Differences in baseline characteristics were calculated using the Fisher's Exact test.Information not available for 4 (*), 6 (#), 9 (~), and 11 (>) patients. For 7 patients, no tissue for organoid culture was retrieved ($).

	All patients	Drug screen	Treated patients
	n = 61	n = 25	n = 6
Median age (range), years	59.5 (26 - 78)	57 (30 - 73)	57 (51 - 65)
Male :female n:n	35:26	11:14	3:3
WHO n (%)	#		
0	34 (61%)	14 (56%)	3 (50%)
1	20 (36%)	10 (40%)	3 (50%)
2	1 (2%)	1 (4%)	0
Localization of primary n (%)			
Colon	34 (55%)	16 (64%)	3 (50%)
Rectum	14 (23%)	5 (20%)	3 (50%)
Rectosigmoid	2 (3%)	2 (8%)	0
Colorectal NOS	12 (19%)	2 (8%)	0
Differentiation n%			
Well/moderately	38 (72%)	14 (67%)	5 (83%)
Poorly	12 (23%)	6 (29%)	1 (17%)
Mucineous	3 (6%)	1 (5%)	0
Undifferentiated	0	0	0
Biopsied lesion n (%)			
Liver	28 (51%)	18 (72%)	3 (50%)
Lymph node	11 (20%)	5 (20%)	2 (33%)
Peritoneum	5 (9%)	1 (4%)	0
Other	12 (22%)	1 (4%)	1 (17%)
Microsatellite status n (%)			
MSI	1 (2%)	1 (4%)	0
MSS	60 (99%)	24 (96%)	6 (100%)

Analogous to our test cohort, we also analyzed genotype-drug response relationships in the patient cohort. Drug sensitivity of P11 and P13 to gefitinib coincided with EGF^{wt} status, as found earlier in our test cohort (Fig. S2A; Fig. 1). In contrast, all other organoids harbored kinase gain-of-function mutations downstream of EGFR and did not respond to gefitinib *in vitro* (P12 harbored an $ARAF^{D24N}$ VUS located outside the kinase domain; Fig. S2A). We also assessed the effect of KRAS mutations and response to selumetinib, as done in our test cohort (Fig. 1). In line with (pre)clinical studies and the test cohort, all except one KRAS mutant culture in our patient cohort didn't respond to selumetinib (Fig. S2B)[26,27]. The exception, P7, harbored a $KRAS^{G13D}$ mutation in the context of an $EGFR^{G724V}$ VUS, located in the kinase domain. These complex genotype-drug relationships uncovered by organoid drug screening can therefore provide information complementary to DNA sequencing.

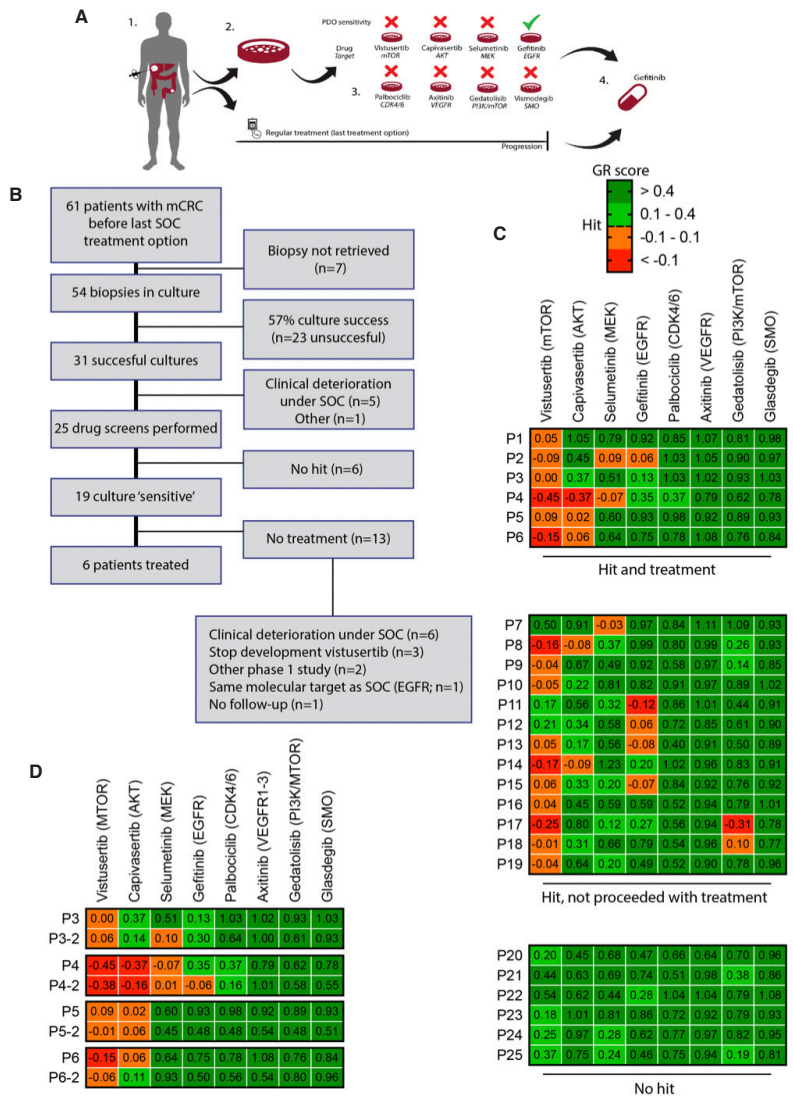

Fig. 2. Enrolment and organoid drug profiling of patients in the SENSOR trial.

(**A**) Outline of the SENSOR trial. Patients undergo a biopsy of a metastatic lesion for generation of organoids before start of their last line standard-of-care (SOC) treatment. Part of the biopsies were also used for DNA sequencing. 2. Organoid cultures are generated from biopsies and frozen in master and working biobanks at low passage. 3. Organoids are profiled for their response to 8 FDA-approved or investigational drugs. Patients received treatment when organoid drug response was qualified as 'hit' after two repeated experiments. In case organoids displayed sensitivity towards multiple drugs, treatment was proceeded with the strongest hit. 4. Patients received the drug identified in the drug

screen after progression on SOC or went off study when no treatment option was available. Patient underwent a mandatory second biopsy before start with experimental treatment, which was used for a second confirmatory organoid culture. These were subjected to the same drug screen as identified in step 3 to control for potential change in drug sensitivity due to intermittent SOC treatment. (**B**) Flow chart on inclusion and drop-out of patients in the SENSOR trial. (**C**) Heatmap with drug screening result of all organoids. Organoids were profiled for their drug response to the drug concentrations identified in fig. 1 (GR_{max}) and the average of two or, in case of discrepant results, three independent replicates is given in the heatmap per drug and organoid. In the top, hits in 6 organoids were identified that subsequently led to treatment of the respective patients. The hits in the middle 13 organoids did not lead to treatment due to various reasons stated in the bottom of the flowchart. In the bottom 6 organoids no hits were identified. (**D**) Patients that started treatment underwent a second biopsy after progression on SOC (represented by P#-2), and organoids were re-screened to control for potential shifts in drug sensitivity. mCRC = metastatic colorectal cancer, SOC = standard-of-care, GR = growth-rate corrected metric.

P1-3 started treatment with vistusertib and P4-6 with capivasertib after they underwent a second, post-SOC biopsy for organoid culture. Treatment-related and non-related adverse effects are described in Table S3. Post-SOC organoid cultures of 4 patients were successfully generated and could be re-screened to control for potential interference with drug sensitivity by intermittent SOC treatment. P3 retained sensitivity to vistusertib, and P4 and P5 remained sensitive to capivasertib (Fig. 2D). P6 had a marginal decrease in sensitivity to capivasertib (GR=0.106 post-SOC versus GR=0.05 pre-SOC; Fig. S2C).

Of the 6 patients that started treatment, P1 had a radiological stable disease at the first evaluation, but presented with neurological symptoms. The presence of symptomatic brain metastases was subsequently radiologically confirmed (Table 1 and S3). Also, cancer embryonic antigen (CEA; a surrogate tumor marker) levels did increase during treatment. P2 showed disease stabilization of both tumor masses at the first response evaluation, but had progressive disease two months later. P3 (vistusertib) and P6 (capivasertib) did not reach first evaluation due to clinical progression (symptomatic brain metastasis and intestinal obstruction with peritoneal carcinomatosis, which was unrelated to study treatment), despite a substantial decrease in CEA levels during treatment of P6. Both P4 and P5 showed disease progression at the first evaluation (Table 1). Notably, both vistusertib and capivasertib do not cross the blood-brain barrier. In conclusion, we did not observe durable clinical responses for organoid-informed treatment decision.

Because we observed limited clinical benefit in the 6 patients that underwent treatment, we decided to perform an unplanned interim analysis to evaluate the feasibility of organoid-

guided precision medicine in this patient population. We conluded there was substantial dropout (55/61 patients), mostly because of unsuccesfull cultures (n=23) and disease progression (n=11). Together with the absence of objective responses so far, we decided there was insufficient basis to continue the trial.

Table 2. Prospective, organoid-informed treatment of patients in the SENSOR trial.
Response to experimental was evaluated using RECIST 1.1 every 2 months. When available, the response in the biopsied lesion and levels of cancer embryonic antigen CEA; in ng/mL) were also recorded. Clinical disease progression was observed for patients P5 and P6 before the first response evaluation. The tumor measurements and CEA levels at 1st response evaluation correspond with the CT scan and blood withdrawal for clinical purposes, on day 20 after start treatment for both patients. *=2nd evaluation.

		Baseline			1st response evaluation			End of treatment	
Drug	Patient	Sum of RECIST lesions in mm	Biopsied lesion in mm	CEA (ng/mL)	Sum of RECIST lesions in mm (% relative to baseline)	Biopsied lesion in mm (% relative to baseline)	CEA (ng/mL)	Days after start treatment	Reason for end of treatment
Vistusertib	P1	101	30	253	107 (+6%)	29 (-3%)	1165	58	New symptomatic brain metastases
	P2	110	21	648	123 (+12%) 132 (+20%)*	22 (+5%) 26 (+24%)*	727 1119*	107	Progressive disease
	P3	300	9	923	351 (+17%)	11 (+22%)	652	57	New lesions at response evaluation
Capivasertib	P4	67			91 (+35%)			52	Progressive disease
	P5	46	22		47 (+2%)	25 (+14%)		20	Clinical progression
	P6	234	81	359	245 (+5%)	89 (+10%)	514	20	New symptomatic brain metastases

DISCUSSION

In this feasibility study we did not succeed to establish organoids as a means to improve response rates to off-label or investigational drugs. The major factor that prohibited testing of organoids as predictive tool for every individual patient was the culture success of 57%, which was slightly lower than our and others' prior success rate of 63-71%[9,11,13]. In our study we attempted to establish cultures of all included patients. However, we noted that the quantity of tumor material (number and size of the biopsies, and tumor/epithelial cell

content) were important indicators of culture success, which is a shared feature among other DNA-sequencing and primary cell culture methods alike[11,29-31]. Pre-selection of biopsies that contain sufficient material, as done for DNA-sequencing in large clinical studies, and further optimization of organoid culturing conditions from biopsies can be considered the major logistical and technical lessons learned from our prospective intervention clinical study[23,31]. In addition to the use of biopsies with with high cell content, other studies demonstrated that resection material can be an alternative source for organoid as this increases success rate and shortens time-to-establishment[14,15,30].

Secondly, organoids were expanded and subjected to the drug screen parallel to the last line of SOC treatment. Unfortunately, given the advanced stages of the disease of our patients, 11 patients deteriorated during SOC treatment or were considered to have progressive disease at the first evaluation after 8-10 weeks. Stricter patient selection at time of inclusion (i.e. earlier stages of treatment, better performance status) would potentially improve the likelihood for patients to start experimental treatment. An important finding is that there were no major shifts in drug sensitivity after SOC treatment in 4 paired biopsies, suggesting that the intermittent (chemo)therapy in our trial design does not significantly alter drug sensitivity and caused the lack of responses seen. This design can provide additional testing time and confirms our initial assumption.

In addition to increasing the success rate of biopsies and subsequent organoid cultures and the inclusion criteria, it may be beneficial to expand the number of drugs tested on organoids to increase the "hit rate". It could also allow for more stringent selection criteria as the numbers of options is larger. Our current threshold of 0.1 still could allow limited amount of growth *in vitro* rather than aiming for cell death, which could be an explanation for the ongoing, slow growth observed in most patients (Table 1). We have also chosen to select on the basis of single agent activity, although future efforts should also include combinatorial approaches as for a large fraction of patients we identified multiple 'active' drugs and combination therapy may increase the chance on clinical benefit[4,28,32-34]. We foresee that DNA-sequencing and other (pre)-clinical data, such as organoids established from clinical responders and/or preliminary evidence of activity in basket trials, can significantly contribute to a more streamlined design of drug (combination) panels[2,11].

The limited number of patients does not allow firm conclusions on whether organoid *in vitro* sensitivity predicts clinical response *in vivo*. P2 showed disease stabilization at the first evaluation, but this clinical benefit was not durable, as for the stable disease of P1; no clinical responses (e.g. partial or complete responses) were observed. Surprisingly, even when organoids predicted a strong effect, for instance P4 and the FDA-approved drug capivasertib

(GR = -0.35; Fig. S2C), the patient progressed rapidly. Although still anecdotal, it suggests organoids might not be universally predictive as we suggested earlier, and warrants careful design of drug panels[13].

In conclusion, the culture success rate and ineligibility of patients due to clinical deterioration during last line SOC treatment and the limited clinical efficacy of the proposed treatments are challenges for the use of organoids for precision medicine in patients with metastatic CRC who have exhausted SOC.

Acknowledgments

We would like to acknowledge all members of the Voest lab, Rene Bernards, Daniel Peeper, Piet Borst, Hans Clevers, Silvia Boj, Marc van de Wetering and Rene Overmeer for useful discussions and advice. We would like to acknowledge Stef van Lieshout and Ewart de Bruijn for performing WGS and profiling of organoids and Suzanne van der Kolk, Judith Westra and Sandra Visser for help with patient inclusion. We would also like to thank all the Netherlands Cancer Institute core facilities, with special thanks to Robotics and Screening, Molecular Pathology and Cryogenic storage their contribution and help. We would also like to acknowledge the NKI Department of Pharmacy & Pharmacology for the logistics and Manon Winter (Pfizer), Colin Glover and Peter Mortimer (both AstraZeneca) for their input and discussion. Furthermore, we would like to thank all participating centers, medical oncologists, and patients for contributing to the study. Rspondin-producing cells were a kind gift from C. Kuo (Stanford).

Funding

This study supported by grants of the KWF (EEV.; NKI2015-7732 and HUBR2014-7006) and the NWO gravitation program (EEV; 2012-2022)

Author contributions:

S.N.O. cultured organoids, designed and performed all experiments, and analyzed the data. F.W. wrote the study protocol, coordinated the clinical trial, included patients and analyzed data. L.S. coordinated the clinical trial, included patients and analyzed data. K.K.D. cultured organoids and contributed to experimental design and the conceptual basis of the study, and analyzed data. C.M.M. performed experiments and analyzed data. S.K. generated all organoids cultures and biobanks, J.v.d.H. contributed to the analysis and the decision model, W.P. and P.S. provided radiological and pathological expertise E.v.W. contributed to the statistical design of the study. L.H., M.C., D.v.d.V., H.B., C.G., A.D.R.H. and H.J.B. included patients. E.C. coordinated SNP profiling and WGS. E.E.V supervised the study. S.N.O., L.S. and E.E.V. wrote the manuscript.

Competing interests

E.E.V. is the medical director of the Netherlands Cancer Institute and legally responsible for all contracts with Astra Zeneca and Pfizer. Vistusertib, capivasertib, selumetinib and gefitinib for *in vitro* and clinical use were provided by AstraZenca. Palbociclib, axitinib, gedatolisib and glasdegib were provided by Pfizer. All other authors declare no conflict of interest.

Data and materials availability

Reagents used under material transfer agreement (MTA) are: Wnt-3a, Noggin (Hans Clevers, Hubrecht Institute) and R-spondin-1 producer lines (Calvin Kuo, Stanford). DNA sequencing data for T1, T5, T6 and T8 is published in the manuscript by Wetering *et al.* Cell 2015[8]. WGS data is published and deposited by Priestley, Baber *et al.* Nature 2019[35] Deposition of targeted-sequencing data and distribution of organoids and deposition of DNA sequencing data in publicly available databases are regulated by the informed consent that participants to this study signed. All materials and data on a per-patient level can be obtained through the Institutional Review Board of the Netherlands Cancer Institute (IRB@nki.nl). All other codes and materials used in this study are freely or commercially available.

REFERENCES

1. Le Tourneau C, Delord JP, Goncalves A, et al. Molecularly targeted therapy based on tumour molecular profiling versus conventional therapy for advanced cancer (SHIVA): a multicentre, open-label, proof-of-concept, randomised, controlled phase 2 trial. *The Lancet Oncology*. 2015;16(13):1324-1334.
2. van der Velden DL, Hoes LR, van der Wijngaart H, et al. The Drug Rediscovery protocol facilitates the expanded use of existing anticancer drugs. *Nature*. 2019;574(7776):127-131.
3. Friedman AA, Letai A, Fisher DE, Flaherty KT. Precision medicine for cancer with next-generation functional diagnostics. *Nature reviews Cancer*. 2015;15(12):747-756.
4. Sicklick JK, Kato S, Okamura R, et al. Molecular profiling of cancer patients enables personalized combination therapy: the I-PREDICT study. *Nature medicine*. 2019;25(5):744-750.
5. Hyman DM, Taylor BS, Baselga J. Implementing Genome-Driven Oncology. *Cell*. 2017;168(4):584-599.
6. Letai A. Functional precision cancer medicine-moving beyond pure genomics. *Nature medicine*. 2017;23(9):1028-1035.
7. Sato T, Stange DE, Ferrante M, et al. Long-term expansion of epithelial organoids from human colon, adenoma, adenocarcinoma, and Barrett's epithelium. *Gastroenterology*. 2011;141(5):1762-1772.
8. van de Wetering M, Francies HE, Francis JM, et al. Prospective derivation of a living organoid biobank of colorectal cancer patients. *Cell*. 2015;161(4):933-945.
9. Weeber F, van de Wetering M, Hoogstraat M, et al. Preserved genetic diversity in organoids cultured from biopsies of human colorectal cancer metastases. *Proceedings of the National Academy of Sciences of the United States of America*. 2015;112(43):13308-13311.
10. Sachs N, de Ligt J, Kopper O, et al. A Living Biobank of Breast Cancer Organoids Captures Disease Heterogeneity. *Cell*. 2018;172(1-2):373-386.e310.
11. Vlachogiannis G, Hedayat S, Vatsiou A, et al. Patient-derived organoids model treatment response of metastatic gastrointestinal cancers. *Science (New York, NY)*. 2018;359(6378):920-926.
12. Tiriac H, Belleau P, Engle DD, et al. Organoid Profiling Identifies Common Responders to Chemotherapy in Pancreatic Cancer. *Cancer discovery*. 2018;8(9):1112-1129.
13. Ooft SN, Weeber F, Dijkstra KK, et al. Patient-derived organoids can predict response to chemotherapy in metastatic colorectal cancer patients. *Science translational medicine*. 2019;11(513).
14. Yao Y, Xu X, Yang L, et al. Patient-Derived Organoids Predict Chemoradiation Responses of Locally Advanced Rectal Cancer. *Cell stem cell*. 2020;26(1):17-26.e16.
15. Ganesh K, Wu C, O'Rourke KP, et al. A rectal cancer organoid platform to study individual responses to chemoradiation. *Nature medicine*. 2019;25(10):1607-1614.
16. Tiriac H, Plenker D, Baker LA, Tuveson DA. Organoid models for translational pancreatic cancer research. *Current opinion in genetics & development*. 2019;54:7-11.
17. Eisenhauer EA, Therasse P, Bogaerts J, et al. New response evaluation criteria in solid tumours: revised RECIST guideline (version 1.1). *European journal of cancer (Oxford, England : 1990)*. 2009;45(2):228-247.
18. Dijkstra KK, Cattaneo CM, Weeber F, et al. Generation of Tumor-Reactive T Cells by Co-culture of Peripheral Blood

Lymphocytes and Tumor Organoids. *Cell*. 2018;174(6):1586-1598.e1512.

19. Basu B, Dean E, Puglisi M, et al. First-in-Human Pharmacokinetic and Pharmacodynamic Study of the Dual m-TORC 1/2 Inhibitor AZD2014. *Clinical cancer research : an official journal of the American Association for Cancer Research*. 2015;21(15):3412-3419.
20. Shapiro GI, Bell-McGuinn KM, Molina JR, et al. First-in-Human Study of PF-05212384 (PKI-587), a Small-Molecule, Intravenous, Dual Inhibitor of PI3K and mTOR in Patients with Advanced Cancer. *Clinical cancer research : an official journal of the American Association for Cancer Research*. 2015;21(8):1888-1895.
21. Banerji U, Camidge DR, Verheul HM, et al. The first-in-human study of the hydrogen sulfate (Hyd-sulfate) capsule of the MEK1/2 inhibitor AZD6244 (ARRY-142886): a phase I open-label multicenter trial in patients with advanced cancer. *Clinical cancer research : an official journal of the American Association for Cancer Research*. 2010;16(5):1613-1623.
22. Wagner AJ, Messersmith WA, Shaik MN, et al. A phase I study of PF-04449913, an oral hedgehog inhibitor, in patients with advanced solid tumors. *Clinical cancer research : an official journal of the American Association for Cancer Research*. 2015;21(5):1044-1051.
23. TCGA. Comprehensive molecular characterization of human colon and rectal cancer. *Nature*. 2012;487(7407):330-337.
24. Hafner M, Niepel M, Chung M, Sorger PK. Growth rate inhibition metrics correct for confounders in measuring sensitivity to cancer drugs. *Nature methods*. 2016;13(6):521-527.
25. Dahabreh IJ, Terasawa T, Castaldi PJ, Trikalinos TA. Systematic review: Anti-epidermal growth factor receptor treatment effect modification by KRAS mutations in advanced colorectal cancer. *Annals of internal medicine*. 2011;154(1):37-49.
26. Janne PA, van den Heuvel MM, Barlesi F, et al. Selumetinib Plus Docetaxel Compared With Docetaxel Alone and Progression-Free Survival in Patients With KRAS-Mutant Advanced Non-Small Cell Lung Cancer: The SELECT-1 Randomized Clinical Trial. *Jama*. 2017;317(18):1844-1853.
27. Sun C, Hobor S, Bertotti A, et al. Intrinsic resistance to MEK inhibition in KRAS mutant lung and colon cancer through transcriptional induction of ERBB3. *Cell reports*. 2014;7(1):86-93.
28. Schmid P, Zaiss M, Harper-Wynne C, et al. Fulvestrant Plus Vistusertib vs Fulvestrant Plus Everolimus vs Fulvestrant Alone for Women With Hormone Receptor-Positive Metastatic Breast Cancer: The MANTA Phase 2 Randomized Clinical Trial. *JAMA oncology*. 2019.
29. Kodack DP, Farago AF, Dastur A, et al. Primary Patient-Derived Cancer Cells and Their Potential for Personalized Cancer Patient Care. *Cell reports*. 2017;21(11):3298-3309.
30. Kim M, Mun H, Sung CO, et al. Patient-derived lung cancer organoids as in vitro cancer models for therapeutic screening. *Nature communications*. 2019;10(1):3991.
31. Comprehensive molecular characterization of gastric adenocarcinoma. *Nature*. 2014;513(7517):202-209.
32. Palmer AC, Sorger PK. Combination Cancer Therapy Can Confer Benefit via Patient-to-Patient Variability without Drug Additivity or Synergy. *Cell*. 2017;171(7):1678-1691.e1613.
33. Crystal AS, Shaw AT, Sequist LV, et al. Patient-derived models of acquired resistance can identify effective drug combinations for cancer. *Science (New York, NY)*. 2014;346(6216):1480-1486.
34. Schmid P, Abraham J, Chan S, et al. Capivasertib Plus Paclitaxel Versus Placebo Plus Paclitaxel As First-Line Therapy for Metastatic Triple-Negative Breast Cancer: The PAKT Trial. *Journal of clinical oncology : official journal of the American Society of Clinical Oncology*. 2020;38(5):423-433.
35. Priestley P, Baber J, Lolkema MP, et al. Pan-cancer whole-genome analyses of metastatic solid tumours. *Nature*. 2019;575(7781):210-216.

SUPPLEMENTARY METHODS, FIGURES AND TABLES

Inclusion criteria

Eligibility criteria were: an Eastern Cooperative Oncology Group (ECOG) performance status of ≤2; measurable disease according to RECIST 1.1 criteria[17]; histologic tumour biopsy feasible; age >18 years. Patients with a life expectancy of < 3 months due to tumor progression under standard of care, with symptomatic brain or leptomeningeal metastasis, with other malignancies within the last 5 years, or with a known HIV infection, and pregnant/nursing women were excluded from study participation. A written informed consent was provided before any study-specific procedures or assessments.

Patient material processing and organoid culture (continued)

In short: Biopsies were collected in Advanced Dulbecco's Modified Eagles Medium with Nutrient Mixture F-12 Hams (Ad-DF) (Invitrogen; #12634), supplemented with 1% penicillin/streptomycin (Invitrogen; #15140-122), 1% HEPES (Invitrogen; #15630-056) and 1% GlutaMAX (Invitrogen; #35050) (Ad-DF+++). Biopsies were mechanically dissociated with needles. Cells were washed with Ad-DF+++ and cultured in CRC medium as described previously[9,18]. PDOs were expanded into master and working biobanks, and PDOs from working biobanks were used for drug sensitivity testing, typically passage 4 or lower. Cultures were checked for mycoplasma contamination every month using the MycoAlert Mycoplasma Detection Kit (Lonza). As part of quality control, PDOs were authenticated using a Taqman-based SNParray targeting 26 SNPs (Hartwig Medical Foundation). PDOs with identity scores <0.9 (tumor vs. blood) were discarded[19].

Drug screening (continued)

Organoids were mechanically and enzymatically dissociated in TrypLE (Gibco, #12604-013) for 5-10 minutes, filtered for sizes <40 µm, and re-plated to allow for formation of organoids over the course of 4 days. After 4 days organoids were collected, incubated with 2 mg/ml dispase II (Sigma #D4693) for 15 minutes to remove Geltrex, and counted using a hemocytometer and trypan blue. Organoids were resuspended in 1:2 Ad-DF+++:Geltrex at a concentration of 20 organoids/µl. Five µl/well of the suspension was dispensed in clear-bottomed, white-walled 96-well plates (Corning, #3707) using an automated repeat pipet and overlaid with 200 µl CRC medium. Read-outs were performed at day 0 ('baseline') and at day 6 in the positive control (10 µM phenylarsine oxide), negative control, and the drug-treated wells. Quantification of cell viability was done by replacing medium with 50 µL Cell-TiterGlo 3D (Promega, #G9681) mixed with 50 µL Ad-DF+++ according to manufacturer instructions on an Infinite 200 Pro plate reader (Tecan Life Sciences).

DNA-sequencing

Part of the biopsied material for the trial was used for routine clinical or cancer panel sequencing (Illumina TruSeq; ABL1; AKT1; ALK; APC; ATM; BRAF; CDH1; CDKN2A; CSF1R; CTNNB1; EGFR; ERBB2; ERBB4; FBXW7; FGFR1; FGFR2; FGFR3; FLT3; GNA11; GNAQ; GNAS; HNF1A; HRAS; ADH1; JAK2; JAK3; KDR; KIT; KRAS; MET; MLH1; MPL; NOTCH1; NPM1; NRAS; PDGFRA; PIK3CA; PTEN; PTPN11; RB1; RET; SMAD; SMARCB1; SMO; SRC; STK11; TP53; VHL) for samples T2, T4, T7, T10-15, P2, P3, P7-10, P14-16, P18, P20 and P22-24 orl whole-genome sequencing (WGS) by the Hartwig Medical Foundation (HMF) for patients T9, P1, P4-6, P11-13. P17, P19 and P25. Both libraries were prepared according to manufactures instructions (targeted sequencing: FC-130-1008; WGS: Truseq Nano LT; FC-121-4001-3) and sequenced on Illumina MiSeq (panel) or HiSeqX paired-end 2x150bp (WGS) platform. Analysis of the targeted panel was performed with Somatic Variant Caller v1.3 (Illumina). Analysis of the WGS data by the HMF was performed using their standard pipeline.

Study treatment

In case patients were subsequently treated, additional in- and exclusion criteria applied and an additional written consent form was obtained. The in- and exclusion criteria, study-related procedures and assessments, and written consent were specific to each experimental treatment regimen. Disease assessment with CT or MRI was performed at baseline and every two treatment cycles (two months). Tumour measurements and treatment response were assessed according to RECIST 1.1[17]. Treatment was continued up until disease progression or withdrawal. Adverse events were registered and graded by the investigator according to the Common Terminology Criteria for Adverse Events (CTC version 4.0) untill 30 days after discontinuation of study treatment. Patients were treated with vistusertib or capivasertib according to investigator brochure at the recommended phase 2 dose: both orally and twice daily, at a dose of 480 mg in 28 days cycles using an intermittent dosing schedule (4 days on/3 days off) for vistusertib and 125 mg in 28 days cycles using an intermittent dosing schedule (2 days on/5 days) off for capivasertib.

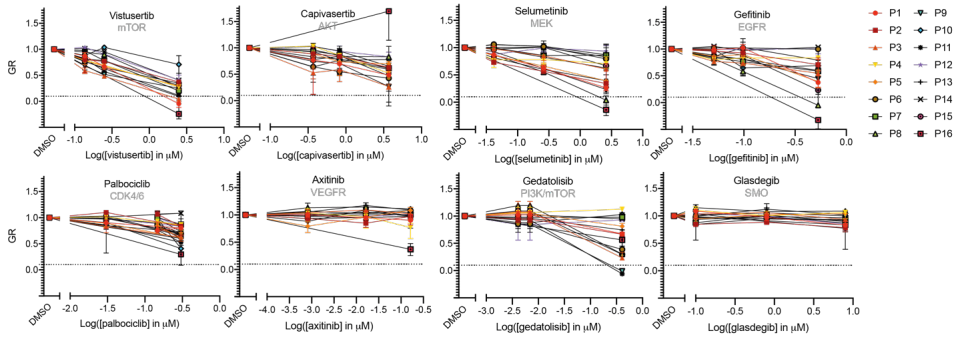

Fig. S1. Dose-responses of 16 organoids to 8 FDA-approved or investigational drugs.

16 organoids were exposed to 3 different concentrations of each drug and effects were calculated using GR metrics (P16 only had GR_{max} data available). Symbols depict the median and error bars represent the standard deviation of 3 technical replicates. The dotted line represents what was considered a 'hit'. GR = growth-rate corrected metric.

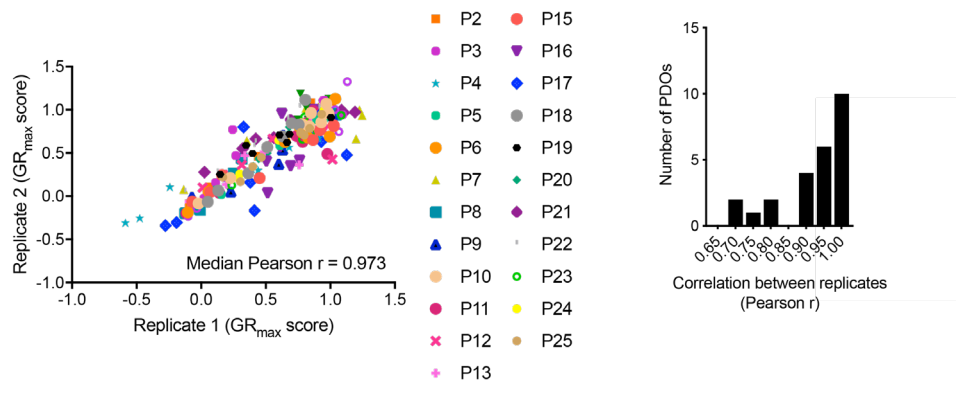

Fig. S2. Technical reproducibility of organoid drug screens.

(**A**) Scatterplot of all data points of screen 1 versus screen 2 per organoid culture. Pearson r was calculated between both replicates and the median over all organoid is reported in the bottom of the graph. (**B**) Histogram that summarizes all Pearson r's between replicates of organoid drug screens. On the x-axis the Pearson r bin center was plotted and on the y-axis the number organoid per bin.

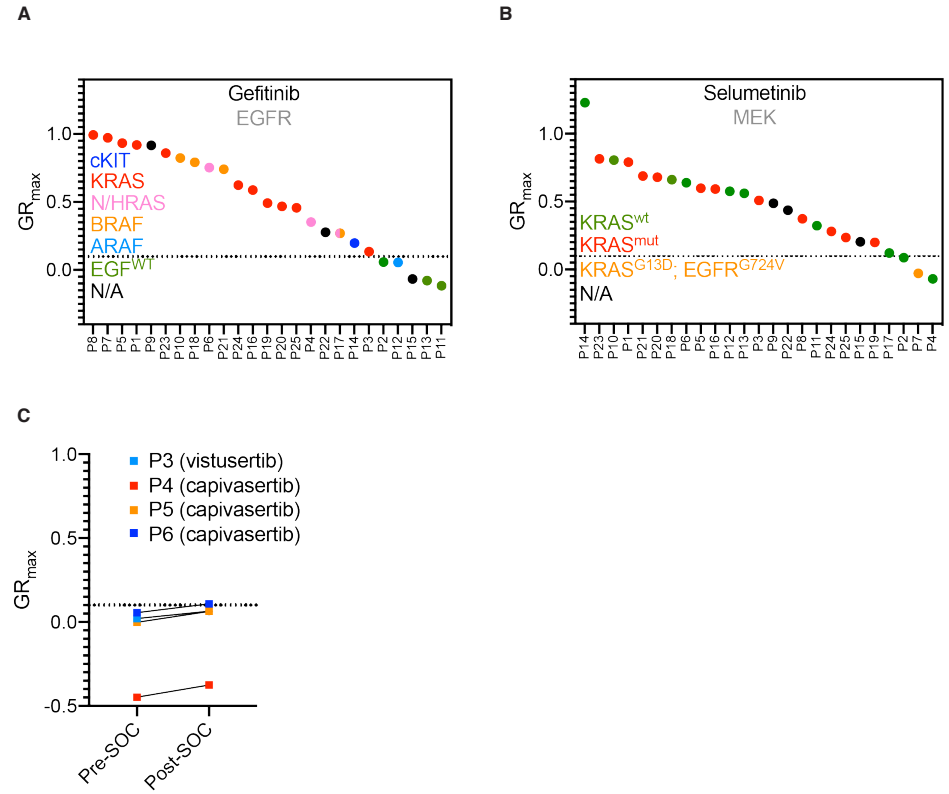

Fig. S3. Concordance between genetics and drug screen outcomes and between paired biopsies cultures.

(**A**) and (**B**) All 25 organoids were exposed to GR_{max} concentrations of each drug and effects were calculated using GR metrics. The dotted line represents what was considered a 'hit' versus 'no hit' (GR_{max}<0.1) All organoids were plotted on the x-axis and sorted from resistant to sensitive. Drug names were plotted in the top of each graph and the target(s) in grey below. Additional information on the tumor genotype was added per organoid on activating mutations in the EGF pathway (KRAS, H/NRAS, BRAF and ARAF). Organoids with gain-of-function mutations in KRAS are depicted in red (T14, T6, T23, T2, T1, T10 and T9), BRAF in orange (T13 and T11), MEK in blue (T7) and organoids with no detectable alterations in the EGF pathway in green ('EGF pathway wild-type' (T5, T15 and T8). N/A = not available. (C) Drug responses of pre- and post-SOC cultures of P3, P4, 5 and P6. The dotted line represents what was considered a 'hit' versus 'no hit' (GR_{max}<0.1). GR = growth-rate corrected metric.

Tables S1. Characteristics of 16 organoids used to generate the decision model.

Per patient the location of the primary tumor, the differentiation status, and the origin of the organoid culture is reported. Genetic profiles were already determined by *Wetering et al. 2015*[8] (T1, T5-6 and T8) or obtained through DNA-sequencing by us in Ooft, Weeber et al. 2019 (panel sequencing on T1, T4, T7, T10 and T13-14 or whole-genome sequencing on T9 and T12). MSS/MSI status for each patient was determined by immunohistochemistry. NOS = not otherwise specified, N/A = not available/sequencing unsuccesful, '-' indicates no mutations found, * = truncation, fs = frameshift, sdv = splice-donor variant, MSS = microsatellite stable, MSI = microsatellite instable.

Test organoids #	Localization	Differentiation	Genetic profile	MSS/MSI	Biopsied lesion
T1	Colorectal NOS	N/A	APC (T1487fs); TP53 (S215G); KRAS (A146T); PIK3CA (E545K)	MSS	Primary
T2	Colorectal NOS	N/A	TP53 (N/A); KRAS(N/A); PIKC3A (N/A)	MSS	Primary
T3	Colon	Moderately	N/A	MSS	Liver
T4	Colon	N/A	MEK1 (K57N)	MSS	Liver
T5	Colorectal NOS	N/A	APC (E1554fs); TP53 (Y234C); ARID1A (K1010fs); CTNNB1 (R582W)	MSS	Primary
T6	Colorectal NOS	N/A	APC (P1319fs); TP53 (T125sdv); KRAS (G12V); PIK3CA (E545Q_D939G); FBXW7 (K167sdv)	MSI	Primary
T7	Colon	Poorly	MEK (Q56P)	MSS	Lymph node
T8	Colon	N/A	APC (N/A)	MSS	Primary
T9	Colon	Moderately	PIK3CA (G545L); KRAS (G12C); APC (T1493R)	MSS	Liver
T10	Colon	Moderately	KRAS (G12A)	MSS	Liver
T11	Colorectal NOS	N/A	APC (T1556fs); BRAF (V600E)	MSI	Primary
T12	Colorectal NOS	N/A	APC (1378*); TP53 (R175H); KRAS (G12V); PIK3CA (R38C)	N/A	Liver
T13	Rectum	Moderately	BRAF (V600E)	MSS	Skin
T14	Colon	Moderately	FBXW7 (G437E/R278*); APC (T1459fs); KRAS (A146V); TP53 (G245S)	MSS	Liver
T15	Colorectal NOS	N/A	APC (C589Y) TP53 (C275Y)	MSI	Primary
T16	Rectosigmoid	N/A	-	MSS	Liver

Table S2. Characteristics of all patients/organoids subjected to drug screening.

For each patient the location of the primary tumor, the differentiation status, and the origin of the organoid culture is reported. Genetics profiles were determined by DNA-sequencing or whole-genome sequencing and MSS/MSI status for each patient was based on in-house pathology reports. Number of prior lines of systemic treatment was extracted from each electronic patient file. NOS = not otherwise specified, N/A = not available/sequencing unsuccesful, '-' indicates no mutations found, * = truncation, fs = frameshift, sdv = splice-donor variant, del = inframe deletion, MSS = microsatellite stable, MSI = microsatellite instable.

Patient #	Localization	Differentiation	Genetic profile	MSS/MSI	Biopsied lesion
P1	Rectum	Moderately	KRAS (A146T); BARD1 (P182L); APC (P2216T/G1367*); CSF1R (A150C); MET (A426H); PTCH1 (A497T); TP53 (A175H)	MSS	Lung
P2	Rectum	Moderately	-	MSS	Lymph node
P3	Colon	Poorly	APC (E1309fs); KRAS (G12S); TP53 (E286G)	MSS	Lymph node
P4	Colon	Moderately	NRAS (G12A); APC (R283*); ROS1 (R1182S); TP53 (W53*)	MSS	Liver
P5	Colon	Moderately	PIK3CA (G542K); KDS (A750P); APC (Q1429*); KRAS (G12V); TP53 (A161T/ R110C)	MSS	Liver
P6	Rectum	Well/moderately	HRAS (A59T); APC (E484*); TP53sdv; NF1 (R304*)	MSS	Liver
P7	Colon	Undifferentiated	TP53 (V173L); KRAS (G13D); EGFR (G724V)	MSS	Lymph node
P8	Colon	N/A	AKT1 (E17K); KRAS (A146T)	MSS	Liver
P9	Rectosigmoid	N/A	N/A	MSS	Liver
P10	Colon	Moderately	APC (R1450*); BRAF (V600E); PIK3CA (E545K)	MSS	Liver
P11	Colon	Moderately	APC (E988*) FANCI (H858N) TP53 (R282W)	MSS	Liver
P12	Rectosigmoid	Moderately	MSH2 (L92I); FBXW7 (G557V); APC (E1306*/E1353*); PALB2 (V425M); ARAF (D46N)	MSS	Liver
P13	Colon	Poorly	PIK3CA (E110del); TP53 (R209fs)	MSS	Liver
P14	Colorectal NOS	Poorly	KIT (exon 14); TP53 (exon 7); (TP53 exon 4)	MSS	Liver
P15	Colon	Moderately	N/A	MSS	Liver
P16	Colon	Moderately	KRAS (G12C); SMAD4 (Q245*); TP53 (R205D)	MSS	Liver
P17	Rectum	Well/moderately	NRAS (G12V); BRAF (G469V); BRCA2 (T2662M); FANCA (L316V); TP53 C238fs	MSS	Liver
P18	Colon	Poorly	BRAF (V600E)	MSS	Lymph node
P19	Colon	Mucineous	APC (E1345*) KRAS (G12V) SMAD4 (R135*)	MSS	Liver
P20	Colon	Well/moderately	KRAS (G12C); APC (S1411fs); TP53 (R282W); ERK2 (Y263F); BRCA2 (T2662M); FANCA (L316V); TP53(C238fs)	MSS	Liver
P21	Colorectal NOS	Poorly	BRAF (V600E)	MSI	Peritoneum
P22	Colon	N/A	N/A	MSS	Liver
P23	Colon	N/A	KRAS (G13D)	MSS	Liver
P24	Rectum	Poorly	KRAS (G13D)	MSS	Lymph node
P25	Colon	Moderately	APC (T1493R); KRAS (G12C); SMAD4 (R361C)	MSS	Liver

Table S3. Adverse events in the SENSOR trial.

All grade 3 adverse events (* = unlikely related to study treatment) and grade 1-2 adverse events possibly, probably or definitively related to study treatment in the six patients that were treated with an organoid-informed treatment. No grade 4 or 5 adverse events were reported. According to Common Terminology Criteria for Adverse Events (CTC version 4.0).

	Treatment	Adverse events	
		Grade 1-2	Grade 3
P1	Vistusertib	Diarrhoea, anorexia, fatigue	-
P2	Vistusertib	Fatigue, anorexia	-
P3	Vistusertib	Nausea	-
P4	Capivasertib	-	Hyperglycemia
P5	Capivasertib	Rash	Ileus*
P6	Capivasertib	Rash	Ataxia*

CHAPTER 6

MULTIPLE LOW DOSE THERAPY AS AN EFFECTIVE STRATEGY TO TREAT EGFR INHIBITOR-RESISTANT NSCLC TUMOURS

João M. Fernandes Neto[1], Ernest Nadal[2]*, Evert Bosdriesz[1,10]*, Salo N Ooft[3]*, Lourdes Farre[2,4], Chelsea McLean[3], Sjoerd Klarenbeek[5], Anouk Jurgens[1], Hannes Hagen[1], Liqin Wang[1], Enriqueta Felip[6,7], Alex Martinez-Marti[6,7], August Vidal[2], Emile Voest[3], Lodewyk F.A. Wessels[1], Olaf van Tellingen[8], Alberto Villanueva[2,9] and René Bernards[1#].

[1]Division of Molecular Carcinogenesis & Oncode Institute. The Netherlands Cancer Institute, Plesmanlaan 121, 1066 CX Amsterdam, The Netherlands.

[2]Group of Chemoresistance and Predictive Factors, Subprogram Against Cancer Therapeutic Resistance (ProCURE), ICO, Oncobell Program, IDIBELL, L'Hospitalet del Llobregat, Barcelona, Spain.

[3]Division of Molecular Oncology and Immunology, The Netherlands Cancer Institute, 1066 CX Amsterdam, The Netherlands.

[4]Institute Gonçalo Moniz. Fundaçao Oswaldo Cruz (FIOCRUZ), Brasil.

[5]Experimental Animal Pathology, The Netherlands Cancer Institute, 1066 CX Amsterdam, The Netherlands.

[6]Department of Medical Oncology, Vall d'Hebron University Hospital and Vall d'Hebron Institute of Oncology (VHIO), Barcelona, Spain.

[7]Autonomous University of Barcelona (UAB), Barcelona, Spain.

[8]Division of Clinical Pharmacology, The Netherlands Cancer Institute, 1066 CX Amsterdam, The Netherlands.

[9]Xenopat S.L., Business Bioincubator, Bellvitge Health Science Campus, Barcelona, Spain.

[10]Department of Computer Science, Faculty of Science, Vrije Universiteit, Amsterdam, The Netherlands

Corresponding author: R. Bernards

* These authors contributed equally to this work.

Nature Communications 2020 Jun 22;11(1):3157.

ABSTRACT

Resistance to targeted cancer drugs is thought to result from selective pressure exerted by a high drug dose. Partial inhibition of multiple components in the same oncogenic signalling pathway may add up to complete pathway inhibition, while decreasing the selective pressure on each component to acquire a resistance mutation. We report here testing of this Multiple Low Dose (MLD) therapy model in *EGFR* mutant NSCLC. We show that as little as 20% of the individual effective drug doses is sufficient to completely block MAPK signalling and proliferation when used in 3D (RAF+MEK+ERK) or 4D (EGFR+RAF+MEK+ERK) inhibitor combinations. Importantly, *EGFR* mutant NSCLC cells treated with MLD therapy do not develop resistance. Using several animal models, we find durable responses to MLD therapy without associated toxicity. Our data support the notion that MLD therapy could deliver clinical benefit, even for those having acquired resistance to third generation EGFR inhibitor therapy.

INTRODUCTION

Inhibition of signalling pathways that are activated by oncogenic mutations elicit therapeutic responses due to "addiction" of the cancer to the activated pathway[1]. However, in advanced cancers, development of resistance is practically inevitable due to secondary mutations that restore signalling through the drug-inhibited pathway. Such acquired resistance mutations affect either the drug target itself or components that act upstream, downstream or parallel to the activated signalling component[2,3]. In *BRAF* mutant melanoma and non-small cell lung cancer (NSCLC), inhibition of two components of the same oncogenic pathway (BRAF+MEK, referred to as "vertical targeting") has been shown to provide more lasting clinical benefit compared to inhibition of only BRAF[4,5]. More recently, both clinical[6,7] and pre-clinical[8] studies have shown that inhibition of three components of the same oncogenic pathway further increases therapeutic benefit. In these scenarios the drugs are usually administered at maximum tolerated dose (MTD). The increase in the number of drugs being used in combination is often accompanied by an increase in toxicity and to this date virtually no studies have been done to assess the efficacy of using drugs below-MTD. In a preclinical model, multiple drugs used at low dose also demonstrated promising activity in ovarian clear cell carcinoma[9]. In this study we explore the use of a Multiple Low Dose (MLD) strategy in *EGFR* mutant NSCLC. In this approach, multiple drugs that act in the same oncogenic signalling pathway are combined at low concentration. We hypothesized that this might add up to complete pathway inhibition without causing prohibitive toxicity. Further, by using low drug concentrations, the pressure exerted on each node of the pathway should greatly diminish, reducing the selective pressure on each node and therefore diminishing the chances of acquiring resistance.

RESULTS

MLD therapy blocks MAPK pathway and proliferation in PC9 cells.

The mechanisms of resistance to EGFR inhibition (standard-of-care) in *EGFR* mutant NSCLC are well understood. We therefore compared the efficacy of MLD therapy to standard-of-care MTD therapies in this indication. We used PC9 NSCLC cells, which harbour an activating mutation in the gene encoding EGFR[10]. We used four drugs, each inhibiting a different node in the MAPK pathway: gefitinib (EGFR inhibitor), LY3009120 (pan-RAF inhibitor[11]), trametinib (MEK inhibitor) and SCH772984 (ERK inhibitor[12]), as shown schematically in **Fig. 1a**. We established dose-response curves for each of the four drugs using 5-day culture assays (**Fig. 1b**). From these data, we inferred for all 4 inhibitors the IC_{20} dose, *i.e.* a drug concentration that inhibits cell viability by 20% - henceforth referred as Low Dose (LD). To assess the efficacy of the MLD

strategy we then tested the impact of all possible drug combinations of the 4 drugs at LD on cell viability (assessed by CellTiter-Blue® assay), on cell proliferation (assessed by long-term colony formation assay) and on pathway activity (measured by p-RSK levels[13] using Western Blotting) (**Figs. 1c-e**). The expected viability and the synergy scores were calculated using the Bliss independence model[14]. We found that PC9 cells treated with the single drugs at low dose were only minimally affected, as expected. However, some of the drug combinations showed a striking combination effect, much higher than expected based on drug additivity. In particular, the combination of RAF+MEK+ERK inhibitors at low dose (henceforth called 3D combination) and the combination of EGFR+RAF+MEK+ERK inhibitors at low dose (henceforth called 4D combination) showed an almost complete inhibition of cell viability and proliferation, along with a complete blockade of MAPK pathway signalling. Due to these notable findings we pursued the MLD study focusing on the 3D and 4D combinations. To address if we could further reduce the drug concentrations, we diluted the 4D combination. When the drugs were reduced to half of the IC_{20} concentrations, the 4D combination was no longer able to achieve complete inhibition of proliferation and was similarly unable to mediate complete MAPK pathway inhibition, indicating that there is a threshold that limits efficacy (Supplementary **Figs. 1a, b**). Based on this, we continued our MLD studies using the IC_{20} concentrations as "Low Dose". To make sure our findings were not drug-specific, we tested the MLD approach using different inhibitors for each of the nodes in the MAPK pathway (erlotinib as EGFRi, BGB-283 as RAFi, selumetinib as MEKi and LY-3214996 as ERKi). **Supplementary Figs. 1c, d** show that we obtained essentially the same effect with these drugs in 3D and 4D combinations. This, together with the notion that each drug is used at low dose, makes it very unlikely that off target effects of the four drugs are responsible for the observed effects.

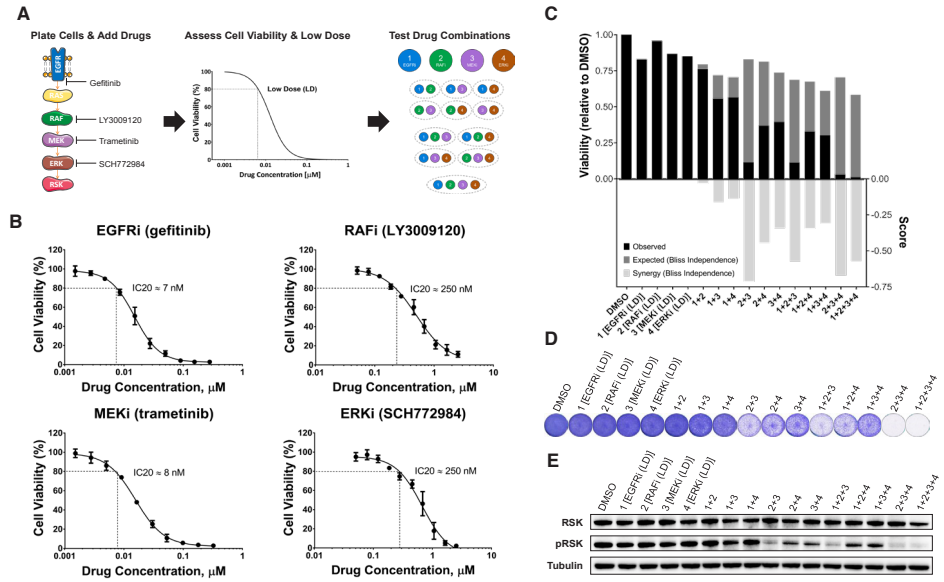

Figure 1. Multiple Low Dose therapy blocks MAPK pathway and proliferation in PC9 cells.

A, Schematic of the Multiple Low Dose (MLD) efficacy determination. After plating, cells are treated with increasing drug concentrations. Four days later cell viability is measured and the low dose (LD) is assessed. At last, the efficacy of all the possible combinations at LD is determined. **B,** Dose-response curves of EGFR, RAF, MEK and ERK inhibitors in PC9 cells. PC9 cells were cultured with increasing concentrations of EGFRi Gefitinib, RAFi LY3009120, MEKi Trametinib or ERKi SCH772984 for 4 days, after which cell viability was measured using CellTiter-Blue®. Standard deviation (SD) from 3 biologically independent replicates (each with 3 technical replicates) is plotted. Low doses (IC_{20}s) were then determined: gefitinib=7nM, LY3009120=250 nM, 292 trametinib=8nM and SCH772984=250nM**. C-E,** Determination of the efficacy of all the possible combinations of EGFR, RAF, MEK and ERK inhibitors at LD in PC9 cells. PC9 cells were cultured with all possible drug combinations of EGFR, RAF, MEK and ERK inhibitors at the low doses determined in **B**. In **C** cell viability from 3 biologically independent replicates (each with at least 3 technical replicates) was measured by CellTiter-Blue® assay after 4 days of treatment; In black the observed experimental viability; In dark-grey the expected viability and in light-grey the synergy scores, calculated using the Bliss independence model, are plotted. In **D** cells were treated for 10 days, after which plates were stained and scanned; A representative image from the 3 biologically independent replicates performed is displayed. In **E** protein for western blotting was harvested after 24 hours of treatment; The level of pathway inhibition was determined by examining pRSK protein levels in the western blot. Tubulin was used as loading control.

MLD therapy minimizes therapeutic resistance.

Next, we tested how MLD therapy compares to standard-of-care high dose therapy in terms of resistance development. To mimic high dose therapy, we treated PC9 cells with a concentration of EGFR inhibitor gefitinib that inhibited cell viability by ~99% in a 5-day culture assay – henceforth referred as High Dose (HD). We found that 3D and 4D combinations inhibit cell proliferation and induce apoptosis at comparable levels to cells treated with HD of gefitinib (**Fig. 2a and Supplementary Fig. 2a, b**). The level of pathway inhibition is also similar between cells treated with 3D and 4D combinations and HD of gefitinib (**Fig. 2d**). Additionally, we performed RNA-Seq transcriptome analyses in cells treated with 4D combination (**Supplementary Fig. 2c, d**). These data showed that 4D combo treated cells displayed a significant downregulation of MYC and E2F target genes as well as cell cycle genes. Moreover, MAPK activity markers[15] were significantly downregulated and several pro-apoptotic genes were found to be upregulated, while anti-apoptotic genes were downregulated. To study how MLD therapy compares to HD therapy regarding resistance, we treated PC9 cells with 3D or 4D combinations and with HD of gefitinib or osimertinib for one month (**Fig. 2b**). As seen by others previously[16,17], cells treated with HD of gefitinib or osimertinib quickly developed resistance, but the cells treated with 3D or 4D combinations did not. Additionally, we treated PC9 cells for 16 days with high dose of gefitinib or with 3D or with 4D MLD combinations; we then either removed the drugs, continued to treat with the original drug, or treated with 4D MLD combination for another 16 days (**Supplementary Fig. 2e**). We observed resistant colonies after 32 days of gefitinib treatment, but not in the cells treated with 3D or 4D combinations. Apparently, 16 day-treatment with 3D or 4D combinations had killed all cells, as continued culturing for another 16 days in media without drugs did not yield any colonies. Importantly, PC9 cells that had developed resistance to high dose EGFR inhibitor, were still responsive to 4D MLD combination. This striking result indicates that EGFR inhibitor-resistant cells remain sensitive to 3D and 4D combinations. This suggests that MLD therapy might be an option for patients having developed resistance to standard-of-care EGFR inhibitor therapy.

MLD therapy is effective in EGFRi-resistant PC9 cells.

To study further if EGFRi-resistant cells are indeed sensitive to 3D and 4D combinations, we generated PC9 cells resistant to clinically-used EGFR inhibitors. We cultured PC9 cells in the presence of gefitinib (PC9-GR) or osimertinib (PC9-OR) until cells were no longer responsive to the inhibitors (see methods). We performed exome sequencing of the two resistant cell populations to gain insight into the mechanisms of acquired resistance. These data showed acquisition of the well-known T790M mutation in the PC9-GR cells and a number of mutations in the PC9-OR cells, none of which has been previously associated with resistance to osimertinib (**Supplementary Table 2**). We then tested the sensitivity of the resistant lines to 3D and 4D combinations. In both resistant cell populations, we saw an almost complete

inhibition of cell viability after only 4 days of MLD therapy treatment and a complete MAPK pathway signalling blockade (**Fig. 2c, d**).

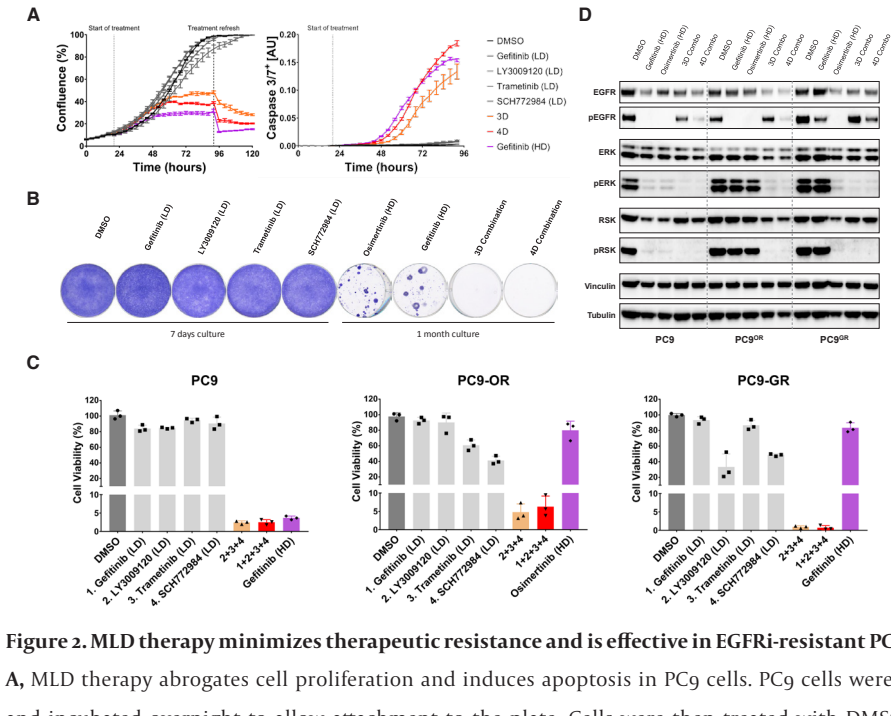

Figure 2. MLD therapy minimizes therapeutic resistance and is effective in EGFRi-resistant PC9 cells. **A,** MLD therapy abrogates cell proliferation and induces apoptosis in PC9 cells. PC9 cells were plated and incubated overnight to allow attachment to the plate. Cells were then treated with DMSO, with EGFR, RAF, MEK, ERK inhibitors at low dose, with 3D Combo (RAF+MEK+ERK inhibitors at LD) or with 4D Combo (EGFR+RAF+MEK+ERK inhibitors at LD) and placed in the IncuCyte®. Confluence (left) and caspase 3/7 activation (right) over time was measured by the IncuCyte®. Standard error of the mean (SEM) from 3 replicates is plotted. **B,** MLD therapy prevents the acquisition of drug resistance in PC9 cells. PC9 cells were cultured with DMSO, with EGFR, RAF, MEK and ERK inhibitors at low dose (for 7 days) and with high dose (HD) of Osimertinib (200 nM), HD of Gefitinib (280 nM) and with 3D and 4D Combinations (for 1 month), after which plates were stained and scanned; A representative image from 3 biologically independent replicates is displayed. **C,** EGFRi-resistant PC9 cells remain sensitive to MLD therapy. PC9, PC9-OR (Osimertinib-resistant) and PC9-GR (Gefitinib-resistant) cells (see methods) were cultured with DMSO, with low doses of EGFR, RAF, MEK or ERK inhibitors, with 3D or 4D combinations or with HD of Gefitinib or Osimertinib for 4 days, after which cell viability was measured using CellTiter-Blue®. Standard deviation (SD) from 3 biologically independent replicates is plotted. **D,** MLD therapy blocks MAPK pathway in EGFRi-resistant PC9 cells. PC9, PC9-OR and PC9-GR cells were cultured with DMSO, HD of Osimertinib, HD of Gefitinib or with 3D or 4D combinations. Protein for western blotting was harvested after 24 hours of treatment; The level of pathway inhibition was measured by examining

pERK and pRSK protein levels and the level of EGFR inhibition was measured by examining pEGFR protein levels in the western blot. Tubulin and Vinculin were used as loading control.

MLD therapy is effective in multiple tumour models.

We then tested if the MLD strategy would also be effective in additional *in vitro* tumour models. After low dose determination (**Supplementary Figs. 3a-c and Supplementary Table 1**) we tested the MLD strategy in patient-derived (colorectal and NSCLC) organoids. Treatment with 3D and 4D combinations resulted in a major reduction in cell viability (**Fig. 3a**). In addition, we tested 6 different MAPK pathway addicted cell lines: HCC827 and H3255 (*EGFR* mutant lung cancer), H2228 and H3122 (*EML4-ALK* translocated lung cancer, in which EGFRi was replaced with ALK inhibitor crizotinib in the 4D combination), DiFi and Lim1215 (EGFR dependent colorectal cancer) and in 2 different PI3K pathway addicted cell lines: SKBR3 and HCC1954 (*HER2* amplified breast cancer, in which 4D combination consisted of HER2, PI3K, AKT and mTOR inhibitors). When treated with 4D combination, proliferation of all cell lines was inhibited, regardless of the tumour type/driver/genotype, pointing towards a broad applicability of the MLD treatment strategy (**Supplementary Fig. 3d**).

MLD therapy is tolerated by non-tumorigenic cell lines.

One of the major concerns when using multiple drugs in combination is the possible toxicity to normal tissues[18]. To test the effect of the MLD strategy on "normal" (non-tumorigenic) cell lines we used primary human BJ (fibroblast) and RPE1 (retinal pigment epithelium) cells. Upon 3D and 4D MLD drug combination treatment, cell viability was reduced, but to a much lesser extent than in cancer cells. This indicates that the MLD strategy might be tolerated by normal tissues (**Fig. 3b**). Since the MAPK pathway is rich in cross-talk and feedback control circuits[19,20], we also tested how a pulse of signalling through the EGFR pathway would be affected by 3D or 4D MLD treatment. We serum-starved BJ cells overnight and then incubated with 3D or 4D MLD drug combinations for two hours. After this, cells were stimulated with 100 ng/ml of EGF in the presence of 3D or 4D drug combinations. Twenty minutes after EGF stimulation, a significant amount of p-RSK was detected, which was no longer detected at 4 hours post EGF stimulation (**Fig. 4c**). These data suggest that the efficient inhibition of MAPK signalling exerted by 3D and 4D MLD treatment is the result of an effect of these drugs on homeostatic feedback/cross-talk signalling[19,21], as pulsatile signalling through the MAPK pathway seems to be much less affected than persistent signalling through an oncogene-activated MAPK pathway.

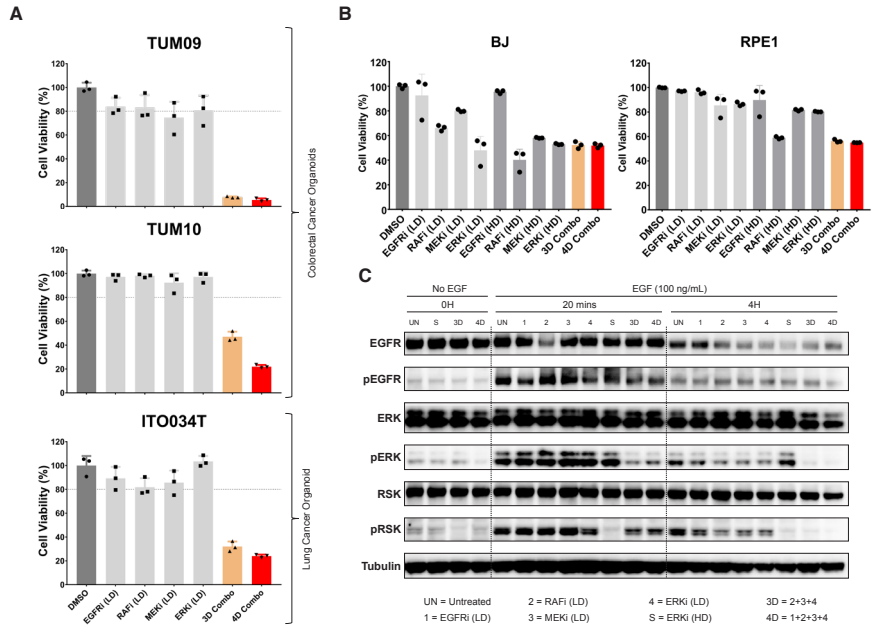

Figure 3. MLD therapy is effective in patient-derived organoids and is tolerated by normal cell lines. **A,** MLD therapy is effective in several colorectal and lung cancer patient-derived organoids. Organoids were cultured with DMSO, with EGFR, RAF, MEK and ERK inhibitors at LD and with 3D and 4D combos. After 5 days of drug treatment cell viability was measured using CellTiter-Glo®. Standard deviation (SD) from 3 biologically independent replicates is plotted. **B,** Cell viability of normal cells is much less affected by MLD therapy than tumour cells. BJ and RPE1 cells were treated with DMSO, with EGFR, RAF, MEK and ERK inhibitors at low and high doses and with 3D and 4D Combos (using the LD and HD concentrations determined for PC9 cells). After 4 days of drug treatment cell viability was measured. SD from 3 replicates is plotted. **C,** MLD therapy allows pulsed signaling in normal cells. BJ cells, after overnight starvation, were treated with the indicated inhibitors/concentrations for 2 hours, after which EGF (100 ng/mL) was added. Cells were harvested before, 20 minutes and 4 hours after EGF stimulation. The level of pathway inhibition was measured by examining pERK and pRSK protein levels. The level of EGFR inhibition was measured by examining pEGFR protein levels in the western blot. Tubulin was used as loading control.

MLD therapy induces tumour regression without toxicity in vivo.

To address if the MLD strategy is effective *in vivo*, we used patient derived xenograft (PDX) tumours from four different patients who had developed resistance to first- or second-line therapy with EGFR inhibitors erlotinib or osimertinib[22] in the clinic by acquiring EGFR T790M mutation, *KRAS* mutation or *MET* amplification (**Supplementary Table 3**). For the *in vivo* studies we defined LD as 20% (for gefitinib and trametinib) and 30% (for LY3009120 and

SCH772984 – due to the shorter half-lives) of the published maximum tolerated dose (MTD) in mice for each of the individual drugs[11,12,23,24]. Osimertinib-resistant PDX-1 was implanted subcutaneously and orthotopically in the lungs. In both models, treatment with 3D or 4D combination resulted in a reduction in tumour volume, without associated toxicity (**Fig. 4a-d**). Interestingly however, treatment with 4D combo was slightly more effective than 3D combo. Due to this finding we focused the *in vivo* studies that followed on the 4D combination. In all PDX models tested we observed similar results to PDX-1, i.e., a reduction in tumour volume, without significant toxicity (**Figs. 4e, f and Supplementary Fig. 4e**). Additionally, in gefitinib-resistant models PDX-2 and PDX-3 we tested if it would be possible to acquire resistance to the 4D MLD combination therapy during a drug holiday. In both PDX models, re-starting of 4D MLD therapy after a drug holiday resulted in a second response to the drug combination, indicating that overt resistance had not developed *in vivo* (**Figs. 4e, f**).

We also implanted PC9 cells in nude mice and treated them with vehicle, with EGFR, RAF, MEK and ERK inhibitors individually at low dose and with 4D combination. The use of low dose regimens was inadequate to suppress PC9 tumour growth when used as single agents, but when used in combination we observed a sustained reduction in the tumour volume of PC9 xenografts over a period of 70 days, which was associated with an extended survival (**Supplementary Fig. 4a, b**). These observations are also supported by immunohistochemical staining of the tumours, which show decreased Ki67 (a proliferation marker) and pERK (MAPK activation) levels in the tumours treated with 4D combination (**Fig. 4g**). Significantly, mice treated with 4D combination did not show any significant signs of toxicity, assessed by the weight of the mice over time and by the morphology of the GI tract and bone marrow (S**upplementary Figs. 4c, f**). In the clinic, the T790M mutation is already present (at very low percentages) in the majority of the tumours before undergoing anti-EGFR treatment[25,26]. To mimic this scenario, we implanted in nude mice a mix of PC9 cells and PC9-GR cells (which are T790M positive) in a 9:1 ratio, respectively. Mice were treated with vehicle, with MTD of gefitinib and with 4D combination. Treatment with MTD of gefitinib resulted in a quick reduction of tumour volume which was followed by outgrowth of resistant cells, unlike the mice treated with 4D combination, where a sustained tumour control was observed (**Supplementary Fig. 4d**).

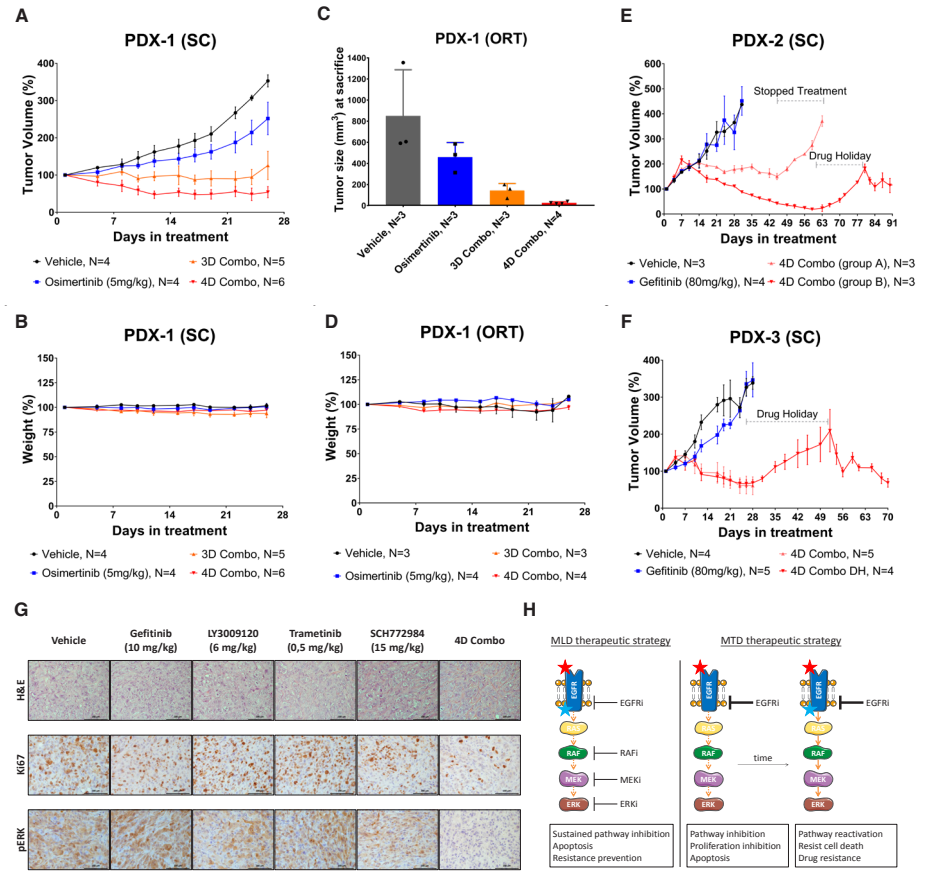

Figure 4. MLD therapy induces tumour regression without toxicity *in vivo*.

a-f, Patient derived xenografts (PDX) are sensitive to MLD therapy. PDX tumours (see Supplementary Table 3) were implanted subcutaneously (**a**, **e**, **f**) or orthotopically in the lungs (**c**) of Crl:NU-Foxn1nu mice. PDX1 was implanted both subcutaneously (**a**) and orthotopically in the lungs (**c**). We defined the in vivo LD as 20-30% of the MTD for each of the individual drugs - gefitinib (10 mg/kg), LY3009120 (6 mg/kg), trametinib (0.5 mg/kg) and SCH772984 (15 mg/kg). In **a-d** after tumour establishment, mice were treated 5 days/week with vehicle, with osimertinib (5 mg/kg) and with 3D or with 4D Combos for 26 days, after which mice were sacrificed. In **a** tumour volume percentages ± SEM is shown, in **c** tumour size (mm3) at sacrifice ± SEM is shown and in **b** and **d** the mice weight percentages ± SEM is shown. **e**, After tumour establishment, mice were treated 5 days/week with Vehicle (N=3), with gefitinib (80 mg/kg) (N=4) or with 4D Combo for 6 weeks (group A, N=3) or with 4D Combo for 8 weeks (group B, N=3). Mice treated with vehicle and gefitinib were sacrificed when tumours reached ~2000mm3. After 6 weeks, Group A was taken off treatment and mice were sacrificed when tumours reached ~2000mm3. After 8 weeks Group B was taken off treatment and was given 3 weeks of drug holiday. Mice were then treated for another 2 weeks with 4D combo, after which they were sacrificed. Tumour volume percentages ± SEM is shown. **f**,

After tumour establishment, mice were treated 5 days/week with vehicle (N=4), with gefitinib (80 mg/kg) (N=5) or with 4D Combo (N=9) for 4 weeks, after which mice were sacrificed, except for 4 animals from the 4D Combo group. These 4 mice were spared and were given 3 weeks drug holiday (4D Combo DH group), followed by another 3 weeks of treatment, after which they were sacrificed. Tumour volume percentages ± SEM is shown. **g**, H&E, Ki67 and pERK stainings from tumour sections of PC9 xenografts. A representative staining image from each cohort (N≥6) is displayed. Scale bars 100µm. **h**, Schematic representation of the MLD therapy for the treatment of EGFR mutant NSCLC.

Despite the significant tumour regressions observed in the *in vivo* experiments none of the mice were fully cured, unlike in the *in vitro* data where all the cells were killed by the 3D or 4D combinations. To study why this is the case we studied the pharmacokinetics and pharmacodynamics of the four drugs *in vivo* over time. We found that drug plasma concentrations of gefitinib and trametinib dropped relatively slowly ($T_{1/2}$ 8 hours), but the pan-RAF and ERK inhibitors were less stable in plasma ($T_{1/2}$ of 5 and 4 hours, respectively). A similar difference was seen for intra-tumoural drug concentrations (**Supplementary Figs. 5a, b**). Consistent with this, we observed a complete inhibition of pRSK in tumour biopsies two hours after 4D combination drug administration, which progressively decreased after 8 and 24 hours (**Supplementary Fig. 5c**). These data indicate that, unlike in the *in vitro* experiments, two of the four drugs were not present at a significant concentration during at least 12 hours of the 24-hour treatment cycle. As a result of this, a sustained MAPK pathway inhibition was not achieved *in vivo*, possibly explaining why we didn't achieve full tumour regressions. We tested this hypothesis *in vitro*, by removing RAF and ERK inhibitors from the treatment for approximately 8 hours every day. We found that, as hypothesized, when the drugs in the 3D or 4D combination were not present continuously the MLD therapy became less effective (**Supplementary Fig. 5d**). Finally, we tested whether there was any drug-drug interaction by measuring the half-lives of the drugs when given alone or in combination (**Supplementary Fig. 5e**). Overall, there is not any apparent drug-drug interaction, except for LY3009120, for which the half-life increases when given in the 4D Combo.

DISCUSSION

We report here that treatment of *EGFR* mutant NSCLCs with MLD therapy effectively suppresses development of drug resistance, without associated toxicity. As such, our data challenge the common paradigm that patients should be treated with the MTD of a targeted agent. Our data are consistent with a model in which diffuse inhibition of an oncogenic pathway at multiple nodes reduces selective pressure on each of the nodes to mutate and

thereby increase response time (**Fig 4h**). Our findings also challenge the current model for MAPK pathway signalling, which postulates that the MAPK kinase cascade functions to amplify signals. Such amplification cascade model is clearly at odds with the data obtained here in which a very partial inhibition of each of 4 nodes in this cascade adds up to complete pathway inhibition. Further mechanistic studies are required to better understand the efficacy of the MLD strategy.

Importantly, we show that tumours having the most common mechanisms of clinically-observed resistance to high dose standard of care EGFR inhibitors still respond to MLD therapy. Therefore, MLD treatment strategy appears especially promising for patients that have already developed resistance to all clinically used EGFR inhibitors, including osimertinib. In such resistant tumours, multiple metastases may be present having different resistance mutations. In this study we have shown that MLD therapy is effective in PDX models having diverse EGFR inhibitor resistance mechanisms, including EGFR T790M mutation, *KRAS* mutation, *MET* amplification and even SCLC transformation, highlighting that MLD therapy could apply to a diverse range of EGFR TKI resistant tumours. However, not all the resistance mechanisms have been tested and it is possible that some might not respond to MLD therapy. Indeed, in clinical practice, an MLD treatment strategy can only be tested in patients having developed resistance to standard-of-care EGFR inhibitors. We find in PDX models that 4D MLD is consistently somewhat better than 3D MLD, which may relate to the notion that not all *EGFR* alleles in the tumour may have acquired resistance mutations to the EGFR inhibitor therapy. Furthermore, it will be important to maintain osimertinib in an experimental MLD therapy trial, as this drug crosses the blood-brain barrier, and such late-stage patients may have (latent) brain metastases. We therefore suggest that clinical testing of the MLD strategy should include osimertinib.

While we never observed development of resistance to MLD therapy *in vivo*, even after long drug exposure, we did not achieve complete tumour regressions. This is most likely due to the short half-lives of the RAF and ERK inhibitors used in this study, which resulted in a situation in which we did not achieve a continuous pathway blockade. This may be improved by using continuous release formulations of these drugs, or by using drugs with longer half-lives.

The MLD therapy described here is fundamentally different from metronomic chemotherapy[27,28]. In this latter scenario, low doses of chemotherapy are given at high frequency with the aim to suppress division of endothelial cells of the tumour vasculature. In the present MLD schedule, we target the MAPK pathway of the tumour itself, as growth inhibition in all cases parallels inhibition of the MAPK pathway (as judged by pRSK). Three-drug combinations given at MTD have been used before in pre-clinical[8] and clinical studies[6,7]

for *BRAF*^{V600E} mutant tumours, showing clear therapeutic benefits, but such regimen have an associated cost of toxicity.

The lack of significant toxicity of the MLD therapy in mice may be explained by the fundamentally different nature of MAPK pathway signalling between normal and EGFR mutant cancer cells. In the former, signalling is transiently activated when growth factors are present. In the latter, oncogenic mutations result in persistent activation of the pathway. Importantly, we show here that transient signalling in normal cells is, at least initially, not interrupted by MLD treatment (Fig. 3c). This may explain why long-term exposure of mice to MLD treatment is without major toxicity, as judged by lack of weight loss and lack of toxicity to gut epithelium and bone marrow. However, mice and human are fundamentally different with respect to drug toxicity. Especially skin toxicity following MAPK inhibition therapy is often underestimated in mice. Therefore, only a phase I clinical trial will be able to fully assess the toxicity of this strategy in humans.

Extrapolation of dose from animals to humans based only on mg/kg conversion is difficult, since body surface area and differences in pharmacokinetics should also be taken into consideration. To convert the animal dose in mg/kg to human equivalent doses (HED) in mg/kg, it is recommended to divide by 12.3[29]. If we estimate the HED based on the low-doses used in our in vivo experiments for Gefitinib and Trametinib (where dosing in humans is known) using this approach then Gefitinib (10mg/kg in mice) corresponds to 57mg once daily in patients, which is approximately one quarter of the dose used in patients (250mg qd). And Trametinib (0.5mg/kg in mice) corresponds to 2,8mg once daily in patients, which is a bit higher than the dose used in patients (2mg qd). However, we also we performed an in vivo experiment using lower concentrations of Gefitinib (1mg/kg) and Trametinib (0.1mg/kg) (**Supplementary Figure 4d**). These drug concentrations correspond to 2,5% of the human daily dose for gefitinib and 28% of the daily human dose of trametinib, using the calculation method of Nair mentioned above. These data indicate that with these further reduced concentrations of Gefitinib and Trametinib we still have a significant anti-tumor effect in vivo. Due to the difficulty in translating drug doses from mice to human we feel that only a well-designed phase 1 trial can help assess the potential clinical utility of the MLD strategy proposed here.

Even though we focused mostly on EGFR mutant NSCLC, we have also shown that the MLD strategy can potentially be effective in other tumour types. Overall, our findings challenge the current paradigm of using the maximum tolerated dose of single targeted cancer drugs and suggest that, instead, it might be more beneficial to use a combination of multiple drugs that target the oncogenically activated pathway using sub-optimal drug concentrations.

METHODS

Cell lines culture and drug-response assays

The PC9 cell line was obtained from ATCC. PC9^{OR} (osimertinib-resistant) and PC9^{GR} (gefitinib-resistant) cells were made by continuous (2 months) drug exposure of PC9 cells to 1µM osimertinib (AZD9291) and to 2µM gefitinib, respectively. Exome sequencing was performed to determine if any *de novo* genetic alterations had occurred (**Supplementary Table 2**). The HCC827, H3255, H3122, H2228, SKBR3, HCC1954, BJ and RPE1 cell lines were obtained from ATCC. And DiFi and Lim1215 cell lines were a gift from A. Bardelli (Torino, Italy). BJ and RPE1 cells were cultured in DMEM (Gibco 41966029). SKBR3 and HCC1954 which were cultured in DMEM/F-12 medium (Gibco 31331028). All the other cell lines were cultured in RPMI medium (Gibco 21875034). All the cell lines media were supplemented with 10% FBS (Serana), 1% penicillin/streptomycin (Gibco 15140122) and 2mM L-glutamine (Gibco 25030024). All cell lines were cultured at 37°C and with 5% CO_2. All cell lines were validated by STR profiling and mycoplasma tests were performed every 2-3 months.

All drug-response assays were performed in triplicate, using black-walled 384-well plates (Greiner 781091). Cells were plated at the optimal seeding density (Supplementary Table 1) and incubated for approximately 24 hours to allow attachment to the plate. Drugs were then added to the plates using the Tecan D300e digital dispenser. 10 µM phenylarsine oxide was used as positive control (0% cell viability) and DMSO was used as negative control (100% cell viability). Four days later, culture medium was removed and CellTiter-Blue (Promega G8081) was added to the plates. After 1-4 hours incubation, measurements were performed according to manufacturer's instructions using the EnVision (Perkin Elmer).

Organoid culture and drug-response assays

Colorectal (CRC) and non-small cell lung cancer (NSCLC) organoids were established and handled as previously described[30]. All drug-response assays were performed in replicate, each by independent researchers. PDOs were mechanically and enzymatically dissociated into single cells, pipetted through a 40 µM cell strainer, and re-plated to allow for organoids formation. At day 4 PDOs were collected, Cultrex was removed by incubation of the cell pellet in 1 mg/ml dispase II (Sigma D4693) for 15 minutes. Whole organoids were counted using a hemocytometer and trypan blue. PDOs were resuspended in 1:3 Advanced Dulbecco's Modified Eagles Medium with Nutrient Mixture F-12 Hams (Ad-DF) (Invitrogen 12634), supplemented with 1% penicillin/streptomycin (Invitrogen 15140122), 1% HEPES (Invitrogen 15630056) and 1% GlutaMAX (Invitrogen 35050) (Ad-DF+++):Cultrex at a concentration of 20 organoids/µl. Five µl/well was dispensed in clear-bottomed, white-walled 96-well plates (Greiner Bio-One 655098) and overlaid with 200 µl CRC or NSCLC culture medium. We

generated 10-step dose response curves using the Tecan D300e digital dispenser, interpolated IC_{20} values and re-screened organoids in presence of a range of concentration around the IC_{20} of each drug separately and in 3D and 4D Combos. In addition, we re-performed the dose-response curves to control for variation between experiments. Read-out was performed at day 10 in the positive control (10 µM phenylarsine oxide), negative control (DMSO), and the drug-treated wells. Quantification of cell viability was done by replacing the CRC medium with 50 µL Cell-TiterGlo 3D (Promega G9681) mixed with 50 µL Ad-F+++. Measurements were performed according to manufacturer's instructions on an Infinite 200 Pro plate reader (Tecan Life Sciences) with an integration time of 100 ms.

Compounds, reagents and antibodies

Gefitinib (100140), LY3009120 (206161), trametinib (201458), SCH772984 (406578), osimertinib (206426), crizotinib (202222), lapatinib (100946), BKM120 (204690), MK2206 (201913) and AZD8055 (200312) were purchased from MedKoo Biosciences. Erlotinib (S7786), BGB-283 (S7926), selumetinib (S1008) and LY-3214996 (S8534) were purchased from Selleckchem. Annexin V-FITC Apoptosis Staining Detection Kit was purchased from Abcam (ab14085).

Antibodies against Tubulin (T9026) and Vinculin (V9131) were purchased from Sigma; antibodies against EGFR (4267), pERK (4377), ERK (9102) and RSK (8408) were purchased from Cell Signalling; antibody against pRSK (04-419) was purchased from Millipore; antibody against pEGFR (ab5644) was purchased from Abcam. Secondary antibodies Goat Anti-Rabbit IgG (H + L)-HRP Conjugate (1706515) and Goat Anti-Mouse IgG (H + L)-HRP Conjugate (1706516) were purchased from Bio Rad.

Colony formation and IncuCyte cell proliferation assays

Cells were seeded in the appropriate density (Supplementary Table 1) in 6-well plates. Cells were incubated for approximately 24 hours to allow attachment to the plates, after which drugs were added to the cells using the Tecan D300e digital dispenser as indicated. The culture media/drugs were refreshed every 3/4 days. When control wells (DMSO) were confluent (unless otherwise stated in the text) cells were fixed using a solution of 2% formaldehyde (Millipore 104002) diluted in phosphate-buffered saline (PBS). Two hours later, they were stained, using a solution of 0.1% crystal violet (Sigma HT90132) diluted in water. Not more than 10 minutes later the staining solution was removed, plates were washed with water left to dry overnight. Finally, plates were scanned and stored.

For IncuCyte proliferation assays, cells were seeded in 96-well plates and incubated overnight to allow attachment to the plates. Drugs were added to the cells using the Tecan D300e digital dispenser. Cells were imaged every 4 hours in the IncuCyte ZOOM (Essen Bioscience).

Phase-contrast images were collected and analysed to detect cell proliferation based on cell confluence. For cell apoptosis, IncuCyte® Caspase-3/7 green apoptosis assay reagent (Essen Bioscience 4440) was also added to culture medium and cell apoptosis was analysed based on green fluorescent staining of apoptotic cells.

Western Blots

After the indicated culture period, cells were washed with chilled PBS and then lysed with RIPA buffer (25mM Tris - HCl pH 7.6, 150mM NaCl, 1% NP-40, 1% sodium deoxycholate, 0.1% SDS) containing protease inhibitors (Complete (Roche) and phosphatase inhibitor cocktails II and III). Samples were then centrifuged for 10 minutes at 14.000 rpm at 4°C and supernatant was collected. Protein concentration of the samples was normalized after performing a Bicinchoninic Acid (BCA) assay (Pierce BCA, Thermo Scientific), according to the manufacturer's instructions.

Protein samples (denatured with DTT followed by 5 minutes heating at 95°C) were then loaded in a 4-12% polyacrylamide gel. Gels were run (SDS-PAGE) for approximately 60 minutes at 165 volts. Proteins were then transferred from the gel to a polyvinylidene fluoride (PVDF) membrane, using 330 mA for 90 minutes.

After the transfer, membranes were placed in blocking solution (5% bovine serum albumin (BSA) in PBS with 0,1% Tween-20 (PBS-T). Subsequently, membranes were probed with primary antibody in blocking solution (1:1000) and left shaking overnight at 4°C. Membranes were then washed 3 times for 10 minutes with PBS-T, followed by one hour incubation at room temperature with the secondary antibody (HRP conjugated, 1:10000) in blocking solution. Membranes were again washed 3 times for 10 minutes in PBS-T. Finally, a chemiluminescence substrate (ECL, Bio-Rad) was added to the membranes and the Western Blot was resolved using the ChemiDoc (Bio-Rad).

Mouse xenografts studies

All animal experiments were approved by the Animal Ethics Committee of the Netherlands Cancer Institute or by the Animal Ethics Committee of the Institut Català d'Oncologia and performed in accordance with institutional, national and European guidelines for Animal Care and Use.

PC9 cell line xenografts: One million PC9 cells were resuspended in PBS and mixed 1:1 with matrigel (Corning 354230). Cells were injected subcutaneously into the posterior flanks of 7-week-old immunodeficient BALB/cAnNRj-Foxn1nu mice (half male and half female; Janvier Laboratories, The Netherlands). Tumour formation was monitored twice a week. Tumour

volume, based on calliper measurements, was calculated by the modified ellipsoidal formula (tumour volume = 1/2(length × width2)). When tumours reached a volume of approximately 200 mm^3, mice were randomized into the indicated treatment arms. Vehicle, gefitinib, LY3009120, trametinib, SCH772984 or the combination of the 4 inhibitors were formulated in DMSO: Kolliphor EL (Sigma 27963): Saline solution, in a ratio of (1:1:8). Mice were treated 5 days a week (Monday to Friday) at the indicated doses by intraperitoneal injection.

Patient-derived xenografts (PDX) and orthotopic xenograft (PDOX): Primary tumours were obtained from Bellvitge Hospital (HUB) and the Catalan Institute of Oncology (ICO) with approval by the Ethical Committee. Ethical and legal protection guidelines of human subjects, including informed consent from the patient to implant the tumour in mice, were followed. PDX-1 was generated from a lung adenocarcinoma biopsy from a patient who was treated with Erlotinib (first line), Gefitinib + Capmatinib (second line) and Cisplatin+Pemetrexed (third line). This tumour has an EGFR mutation (del19) and *MET* amplification. PDX-2 was generated from a lung adenocarcinoma biopsy from a patient who was treated with Erlotinib (first line), Gefitinib + Capmatinib (second line) and Carboplatin+Gemcitabine and Nivolumab (third line). This tumour has an EGFR mutation (L858R) and *MET* amplification. PDX-3[30] was generated from a lung adenocarcinoma biopsy of a brain metastasis from a patient who was treated with Erlotinib (first line) and Osimertinib (second line). PDX-4 was generated from a lung adenocarcinoma biopsy from a patient who was treated with Afatinib (first line) and CBDCA + pemetrexed (second line). This tumour has a germline p53 mutation and an EGFR mutation (del19). Tumours were isolated and implanted subcutaneously (or orthotopically, in the lungs, in the case of PDX-3) into Crl:NU-Foxn1nu mice by following previously reported procedures[22,31]. In the subcutaneous models, tumour volume was monitored twice a week by a digital caliper. When tumours reached a volume of approximately 200-600 mm^3, mice were randomized into the indicated treatment arms. In the orthotopic model, tumours were left to grow for 2 weeks, followed by 26 days of treatment. Vehicle, gefitinib, osimertinib or the 3D and 4D Combos were formulated in DMSO: Kolliphor EL (Sigma 27963): Saline solution, in a ratio of (1:1:8). Mice were treated 5 days a week (Monday to Friday) at the indicated doses by intraperitoneal injection.

***In vivo* pharmacokinetics and pharmacodynamics studies**

Plasma and tumour samples were assayed by liquid chromatography triple quadrupole mass spectrometry (LC-MS/MS) using an API4000 detector (Sciex) for the simultaneous determination of Gefitinib (MRM: 447.4/128.1), LY3009120 MRM: 425.5/324.2), Trametinib (616.3/491.2) and SCH772984 (MRM: 588.4/320.2). Gefitinib-d8 (MRM: 455.4/136.3) was used as internal standard. LC separation was achieved using a Zorbax Extend C18 column (100 × 2.0 mm; ID). Mobile phase A and B comprised 0.1% formic acid in water and methanol,

respectively. The flow rate was 0.4 ml/min and a linear gradient from 20%B to 95%B in 2.5 min, followed by 95%B for 2 min, followed by re-equilibration at 20%B for 10 min was used for elution. Sample pre-treatment was accomplished by mixing 5 ul (plasma) or 25 ul (tumour homogenate) with 30 or 150 ul, respectively, of formic acid in acetonitrile (1+99) containing the internal standard. After centrifugation, the clear supernatant was diluted 1+4 with water and 50 ul was injected into the LC-MS/MS system.

The plasma/tumour samples were harvested at the time points indicated in **Supplementary figure 5**. Blood samples were obtained by tail cut (at 2h and 8h time points) and by cardiac puncture at the 24h time point. Samples were collected on ice in tubes containing potassium EDTA as anticoagulant. The tubes were immediately cooled in melting ice and centrifuged (10 minutes, 5000g, 4°C) to separate the plasma fraction, which was transferred into clean vials. For the tumours samples, the mice were sacrificed by cervical dislocation, the tumour was dissected and frozen at -80°C. Half of the tumour was then lysed mechanically with RIPA buffer and lysates were analysed by Western blot. The other half was weighed and homogenized in 1 ml of ice-cold 1% of BSA in water and stored at −20°C until further analysis.

Data availability

All relevant data are available from the corresponding author upon request. Full scans of the gels and blots are available in Supplementary Figure 7. All the other data supporting the findings of this study are available within the article and its supplementary information files. A reporting summary for this article is available as a Supplementary Information file. RNAseq data can be accessed with the GEO assession GSE144258. Most raw data can be assessed at https://doi.org/10.6084/m9.figshare.12408803.v1.

Acknowledgements

We thank A. Bardelli (Torino, Italy) for gift of cell lines, the facilities of The Netherlands Cancer Institute: Mouse Clinic – Intervention Unice (Natalie Proost, Bjorn Siteur, Bas van Gerwen, Charlotte Baak, Renske Grimmerink, Rebecca Theeuwsen and Marieke van de Ven), Robotics and Screening Center (Ben Morris and Roderick Beijersbergen), Clinical Pharmacology (Levi Buil and Artur Burylo), Experimental Animal Pathology, Flow Cytometry and Sequencing. We also thank Richard Marais for discussions. This work was supported by a grant from the Dutch Cancer Society through the Oncode Institute.

Alberto Villanueva was supported by the Fondo de Investigaciones Sanitarias, FIS (PI16-01898 (to A.V.), and by the Spanish Association Against Cancer, AECC (CGB14142035THOM) and Ideas Semilla project (IDEAS098VILL-IDEAS16) and Generalitat de Catalunya (2014SGR364) (to A.V.). L.F received a European Union's Horizon 2020 research and innovation programme under the Marie Sklodowska-Curie, grant agreement number 799850 (L.F). E.N. was funded by

Instituto Carlos III through the project PI18/00920. We thank CERCA Program / Generalitat de Catalunya for their institutional support and grant 2017SGR448.

Authors' Contributions:
R.B. supervised all research. J.N., A.V., O.vT, and R.B., wrote the manuscript. J.N., E.N., S.O., E.B., L.F., C.M., S.K., A.J., H.H., L.W., Au.V. designed, performed and analysed the experiments. E.V., A.V., E.F., A.M-M and Lo.W. provided advice for the project. All authors commented on the manuscript.

Conflicts of interest:
A.V. is co-founder of Xenopat S.L.. The remaining authors declare no competing interests.

REFERENCES

1. Weinstein, I. B. Addiction to Oncogenes--the Achilles Heal of Cancer. *Sci.* **297**, 63–64 (2002).
2. Konieczkowski, D. J., Johannessen, C. M. & Garraway, L. A. A Convergence-Based Framework for Cancer Drug Resistance. *Cancer Cell* **33**, 801–815 (2018).
3. Sun, C. & Bernards, R. Feedback and redundancy in receptor tyrosine kinase signaling: relevance to cancer therapies. *Trends Biochem. Sci.* **39**, 465–474 (2014).
4. Flaherty, K. T. *et al.* Combined BRAF and MEK inhibition in melanoma with BRAF V600 mutations. *N. Engl. J. Med.* **367**, 1694–1703 (2012).
5. Khunger, A., Khunger, M. & Velcheti, V. Dabrafenib in combination with trametinib in the treatment of patients with BRAF V600-positive advanced or metastatic non-small cell lung cancer: clinical evidence and experience. *Ther. Adv. Respir. Dis.* **12**, 1753466618767611 (2018).
6. Kopetz, S. *et al.* Encorafenib, Binimetinib, and Cetuximab in BRAF V600E-Mutated Colorectal Cancer. *N. Engl. J. Med.* (2019). doi:10.1056/NEJMoa1908075
7. Corcoran, R. B. *et al.* Combined BRAF, EGFR, and MEK Inhibition in Patients with BRAF(V600E)-Mutant Colorectal Cancer. *Cancer Discov.* **8**, 428–443 (2018).
8. Xue, Y. *et al.* An approach to suppress the evolution of resistance in BRAF(V600E)-mutant cancer. *Nat. Med.* **23**, 929–937 (2017).
9. Caumanns, J. J. *et al.* Low-dose triple drug combination targeting the PI3K/AKT/mTOR pathway and the MAPK pathway is an effective approach in ovarian clear cell carcinoma. *Cancer Lett.* **461**, 102–111 (2019).
10. Sharma, S. V *et al.* A chromatin-mediated reversible drug-tolerant state in cancer cell subpopulations. *Cell* **141**, 69–80 (2010).
11. Peng, S.-B. *et al.* Inhibition of RAF Isoforms and Active Dimers by LY3009120 Leads to Anti-tumor Activities in RAS or BRAF Mutant Cancers. *Cancer Cell* **28**, 384–398 (2015).
12. Morris, E. J. *et al.* Discovery of a novel ERK inhibitor with activity in models of acquired resistance to BRAF and MEK inhibitors. *Cancer Discov.* **3**, 742–750 (2013).
13. Anjum, R. & Blenis, J. The RSK family of kinases: emerging roles in cellular signalling. *Nat. Rev. Mol. Cell Biol.* **9**, 747–758 (2008).
14. Russ, D. & Kishony, R. Additivity of inhibitory effects in multidrug combinations. *Nat. Microbiol.* **3**, 1339–1345 (2018).
15. Brant, R. *et al.* Clinically Viable Gene Expression Assays with Potential for Predicting Benefit from MEK Inhibitors. *Clin. Cancer Res.* **23**, 1471–1480 (2017).
16. Hata, A. N. *et al.* Tumor cells can follow distinct evolutionary paths to become resistant to epidermal growth factor receptor inhibition. *Nat. Med.* **22**, 262–269 (2016).
17. Eberlein, C. A. *et al.* Acquired Resistance to the Mutant-Selective EGFR Inhibitor AZD9291 Is Associated with Increased Dependence on RAS Signaling in Preclinical Models. *Cancer Res.* **75**, 2489–2500 (2015).
18. Park, S. R., Davis, M., Doroshow, J. H. & Kummar, S. Safety and feasibility of targeted agent combinations in solid tumours. *Nat. Rev. Clin. Oncol.* **10**, 154–168 (2013).
19. Mendoza, M. C., Er, E. E. & Blenis, J. The Ras-ERK and PI3K-mTOR pathways: cross-talk and compensation. *Trends*

Biochem. Sci. **36**, 320–328 (2011).

20. Fey, D., Croucher, D., Kolch, W. & Kholodenko, B. Crosstalk and Signaling Switches in Mitogen-Activated Protein Kinase Cascades . *Frontiers in Physiology* **3**, 355 (2012).
21. Lake, D., Correa, S. A. L. & Muller, J. Negative feedback regulation of the ERK1/2 MAPK pathway. *Cell. Mol. Life Sci.* **73**, 4397–4413 (2016).
22. Martinez-Marti, A. *et al.* Dual MET and ERBB inhibition overcomes intratumor plasticity in osimertinib-resistant-advanced non-small-cell lung cancer (NSCLC). *Ann. Oncol. Off. J. Eur. Soc. Med. Oncol.* **28**, 2451–2457 (2017).
23. Hayakawa, H. *et al.* Lower gefitinib dose led to earlier resistance acquisition before emergence of T790M mutation in epidermal growth factor receptor-mutated lung cancer model. *Cancer Sci.* **104**, 1440–1446 (2013).
24. Tricker, E. M. *et al.* Combined EGFR/MEK Inhibition Prevents the Emergence of Resistance in EGFR-Mutant Lung Cancer. *Cancer Discov.* **5**, 960–971 (2015).
25. Ichihara, E. *et al.* Clinical significance of repeat rebiopsy in detecting the EGFR T790M secondary mutation in patients with non-small cell lung cancer. *Oncotarget* **9**, 29525–29531 (2018).
26. Vendrell, J. A. *et al.* Ultra-sensitive EGFR (T790M) Detection as an Independent Prognostic Marker for Lung Cancer Patients Harboring EGFR (del19) Mutations and Treated with First-generation TKIs. *Clin. Cancer Res.* **25**, 4280–4289 (2019).
27. Kerbel, R. S. & Kamen, B. A. The anti-angiogenic basis of metronomic chemotherapy. *Nat. Rev. Cancer* **4**, 423–436 (2004).
28. Scharovsky, O. G., Mainetti, L. E. & Rozados, V. R. Metronomic chemotherapy: changing the paradigm that more is better. *Curr. Oncol.* **16**, 7–15 (2009).
29. Nair, A. B. & Jacob, S. A simple practice guide for dose conversion between animals and human. *J. basic Clin. Pharm.* **7**, 27–31 (2016).
30. Dijkstra, K. K. *et al.* Generation of Tumor-Reactive T Cells by Co-culture of Peripheral Blood Lymphocytes and Tumor Organoids. *Cell* **174**, 1586–1598.e12 (2018).
31. Ambrogio, C. *et al.* Combined inhibition of DDR1 and Notch signaling is a therapeutic strategy for KRAS-driven lung adenocarcinoma. *Nat. Med.* **22**, 270–277 (2016).

SUPPLEMENTARY FILES

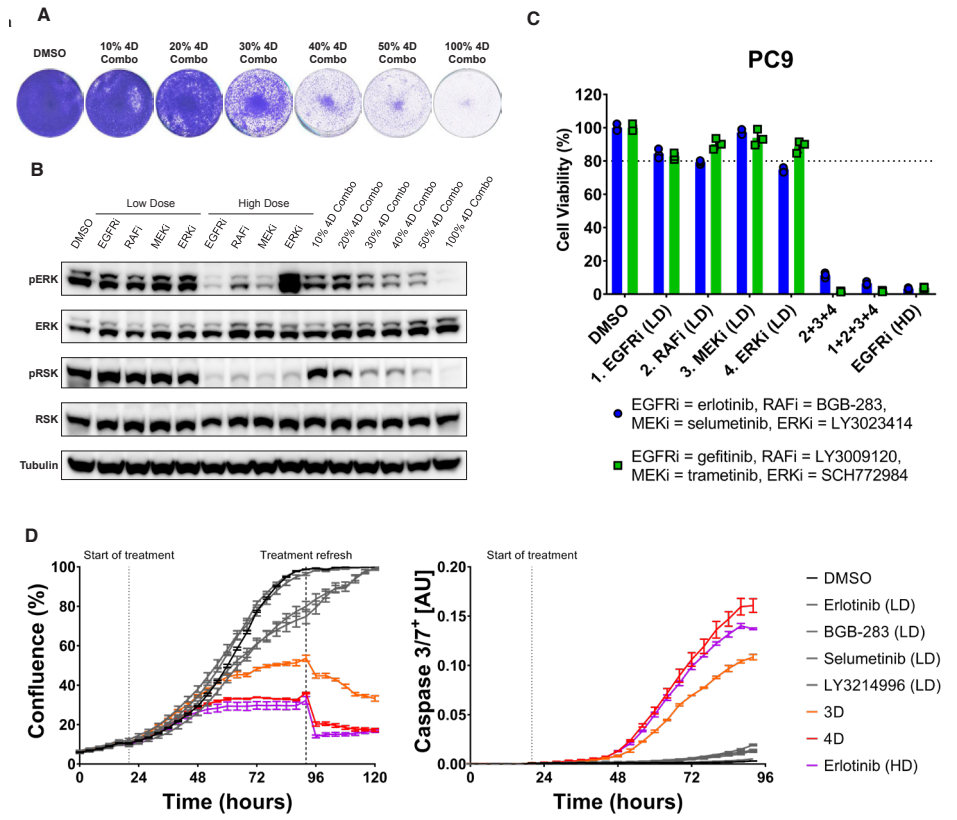

Supplementary Figure 1. A drug concentration threshold is necessary for the efficacy of MLD therapy, which is not drug-specific.

A, Dilution of 4D Combo results in incomplete inhibition of proliferation. PC9 cells were plated and incubated overnight to allow attachment to the plate. Cells were then treated with DMSO, with 4D Combo and with the indicated dilutions of 4D Combo. Cells were cultured for 7 days, after which plates were stained and scanned; A representative image from 3 biologically independent replicates is displayed. **B,** Dilution of 4D Combo results in incomplete MAPK pathway inhibition. PC9 cells were cultured with DMSO, with EGFR, RAF, MEK and ERK inhibitors both at low and at high doses, with 4D Combo and with different dilutions of 4D combo. Protein for western blotting was harvested after 24 hours of treatment. The level of pathway inhibition was measured by examining pERK and pRSK protein levels; Tubulin was used as loading control. **C, D,** MLD therapy efficacy is not drug-specific. PC9 cells were plated and incubated overnight to allow attachment to the plate; Cells were then treated with two different inhibitors for each of the nodes in the MAPK pathway (gefitinib or erlotinib as EGFRi, LY3009120 or BGB-283 as RAFi, Trametinib or selumetinib as MEK and SCH772984 or LY-3214996 as ERKi) as indicated.

In c cell viability was measured using CellTiter-Blue® after 4 days of treatment. Standard deviation (SD) from 3 replicates is plotted. In d the confluence (left) and caspase 3/7 activation (right) over time was measured by the IncuCyte®; 3 days after the first treatment the drugs and media were refreshed. SEM from 3 replicates is plotted.

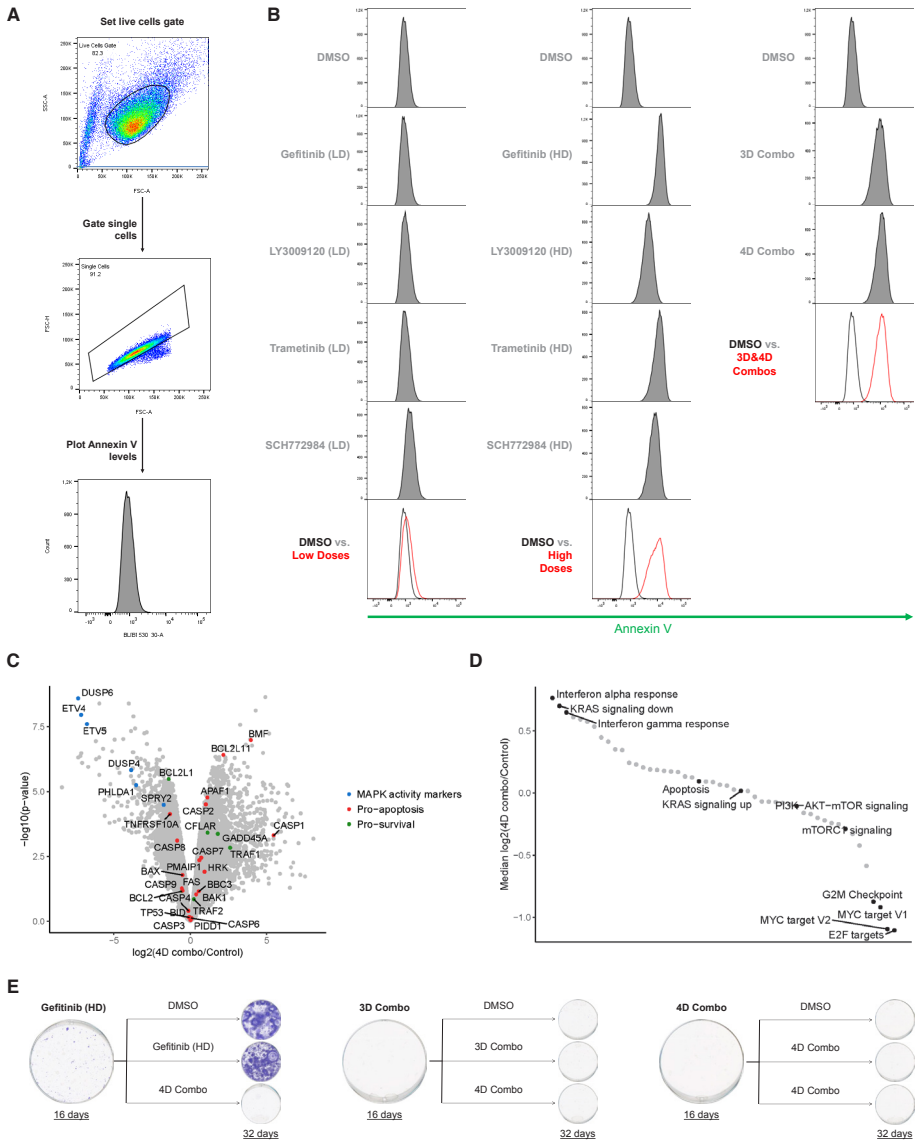

Supplementary Figure 2. MLD therapy induces apoptosis and prevents drug resistance.

A, Gating strategy used in b. Live cells were gated from all events; then single cells were gated from the

live cells and, finally, Annexin V levels were plotted from the single cells. **B,** 3D and 4D Combos induce apoptosis at comparable levels as high doses of each inhibitor in PC9 cells. PC9 cells were stained with Annexin V-FITC Apoptosis Staining/Detection kit (ab14085) after 48 hours of drug treatment. The Annexin V levels were measured by flow cytometry (BD LSRFortessa) and analysed using FlowJo V10. c, d, Transcriptome analysis of PC9 cells treated with 4D combo. **C,** Volcano plot of differential gene expression analysis. **D,** Median log2-fold change of the MSigDB hallmark gene-sets, ranked from high to low. For c and d PC9 cells were treated with DMSO for 48 hours or with 4D combo for 48 or 72 hours. Experiments were performed in duplicates. Because the difference between 48 and 72 hour 4D combo treatment was comparable to the variability between replicates, the four MLD treated samples were considered replicates. Differential expression analysis was performed using the R-package limma [Ritchie et al, 2015] and the MSigDB hallmark gene-sets analysis was performed using version 6.2 of MSigDB [Liberzon et al, 2015]. **E,** MLD therapy prevents the acquisition of drug resistance in PC9 cells. PC9 cells were cultured with high dose of gefitinib (280 nM) and with 3D and 4D Combos (4 plates per condition). After 16 days in culture, one plate was fixed and stained. From the remaining three plates (per condition) one was switched to DMSO treatment, the other was switched to 4D Combo and the third one continued with the previous treatment. Sixteen days later (after 32 days of “treatment” in total) cells were fixed and stained and then plates were scanned.

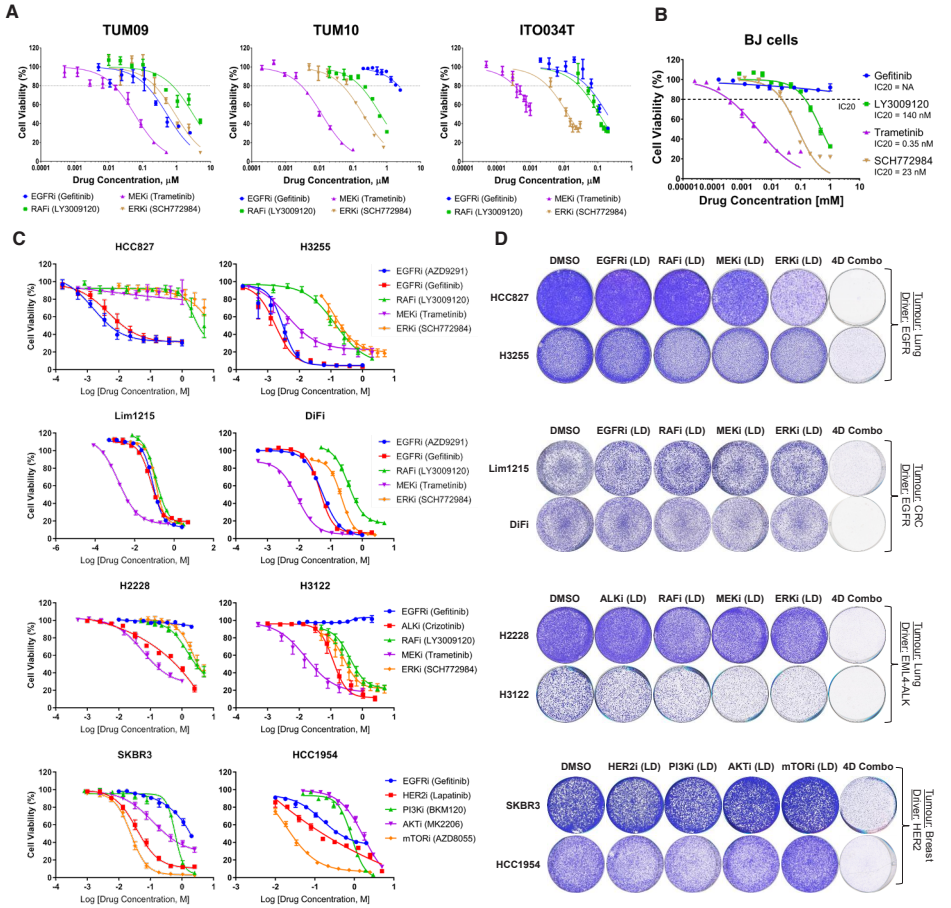

Supplementary Figure 3. MLD therapy is effective in multiple cancer cell lines.

A-C, Dose-response curves across the organoid and cell line panel. **A,** Organoids were cultured with DMSO or with the different inhibitors and after 5 days of drug treatment cell viability was measured using CellTiter-Glo®. SEM from 3 replicates is plotted. **B, C,** Cells were plated in 384-well plates. Drugs were added ~24h after plating; after 4 days of exposure to the drugs cell viability was measured using CellTiter-Blue®. SEM from 3 replicates is plotted. Low doses (IC20s) were then determined (see Supplemental Table 1). **D,** MLD therapy is effective in several cell lines/tumour types. HCC827, H3255, Lim1215, DiFi, H2228, H3122, SKBR3 and HCC1954 cell lines were treated with DMSO, with the indicated pathway inhibitors at low dose and with their combination (4D Combo). After 10 days of treatment plates were stained and scanned.

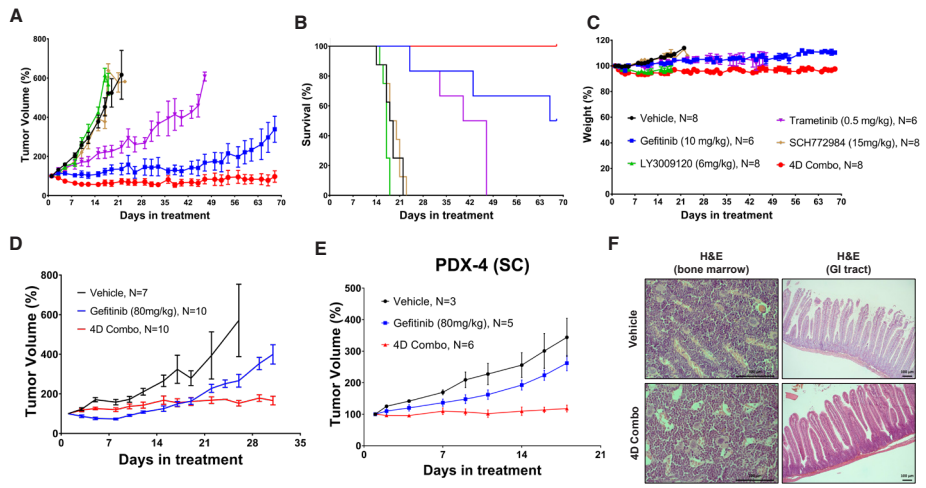

Supplemental Figure 4. MLD therapy reduces tumour volume in vivo without toxicity.

A-D, PC9 xenografts are sensitive to 4D Combo without toxicity. (**A-C**) PC9 cells were grown as tumour xenografts in BALB/cAnNRj-Foxn1nu mice. After tumour establishment (200–250 mm3), mice were treated 5 days/week with vehicle (N=8), gefitinib (10 mg/kg) (N=6), LY3009120 (6 mg/kg) (N=8), trametinib (0.5 mg/kg) (N=6), SCH772984 (15 mg/kg) (N=8) or the combination of the 4 inhibitors (4D Combo) (N=8) for 10 weeks. In a the mean tumour volume percentages ± SEM is shown; In **B** the Kaplan-Meier survival curve is shown and in c the mice weight percentages ± SEM is shown. **D,** PC9 cells and PC9GR cells were mixed in a 9:1 ratio, respectively, and were grown as tumour xenografts in BALB/cAnNRj-Foxn1nu mice. After tumour establishment (200–250 mm3), mice were treated 5 days/week with vehicle, with the MTD of gefitinib (80 mg/kg) and with 4D Combo – cocktail containing gefitinib (1 mg/kg), LY3009120 (6 mg/kg), trametinib (0.1 mg/kg), SCH772984 (15 mg/kg) for 30 days. The mean tumour volume percentages ± SEM is shown. **E,** EGFR and p53 mutant PDX responds to 4D Combo. PDX-4 was generated from a biopsy of patient with EGFR and TP53 mutation that progressed after afatinib and chemotherapy treatment. After tumour establishment, mice were treated 5 days/week with Vehicle (N=3), with gefitinib (80 mg/kg) (N=5) or with 4D combo (N=6) – cocktail containing gefitinib (10 mg/kg), LY3009120 (6 mg/kg), trametinib (0.5 mg/kg) and SCH772984 (15 mg/kg) (N=6) for 18 days. Tumour volume percentages ± SEM is shown. **F,** H&E stainings from the GI tract and the bone marrow of the PC9 xenografts in a. A representative staining image from the vehicle and 4D combo cohorts (N=8) is displayed. Scale bars 100µm.

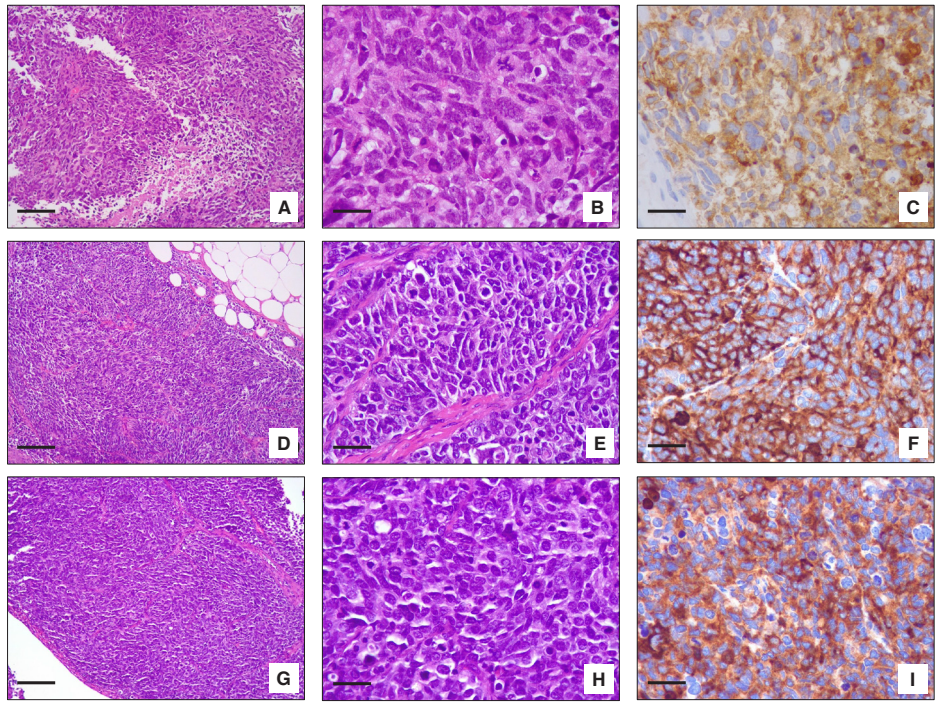

Supplemental Figure 5. Small cell lung cancer transformation of PDX4.

Biopsy samples from either the primary human lung cancer (**A-C**), the subcutaneous xenograft of this tumor (**D-F**) or the orthotopic xenograft of this tumor (**G-I**) were fixed and stained with H&E. Immunohistochemical staining with synaptophysin antibody was performed to assess small cell lung cancer transformation.

A-C: Small cell carcinoma metastatic to a mediastinal lymph node. The tumor has a sheet-like growth pattern. The tumor cells have ovoid or spindled nuclei and scant cytoplasm. Nuclear chromatin is finely granular and nucleoli are absent. There are brisk mitotic activity with atypical mitotic figures. **D-F:** subcutaneous xenograft of lung cancer shown in **A-C**. **G-I:** orthotopic xenograft of lung cancer shown in **A-C**. **A, D** and **G:** original magnification 100X, scale bars 200 µm. **B, C, E, F, H, I:** original magnification 400X, scale bars 50 µm. **A, B, D ,E, G, H:** H&E stain. **C, F, I:** immunohistochemical stain for synaptophysin. A representative staining image is displayed from the patient biopsy (**A-C**), from a total of 8 blocks from 8 different mice (**D-F**) and from 6 blocks from 6 different mice (**G-I**).

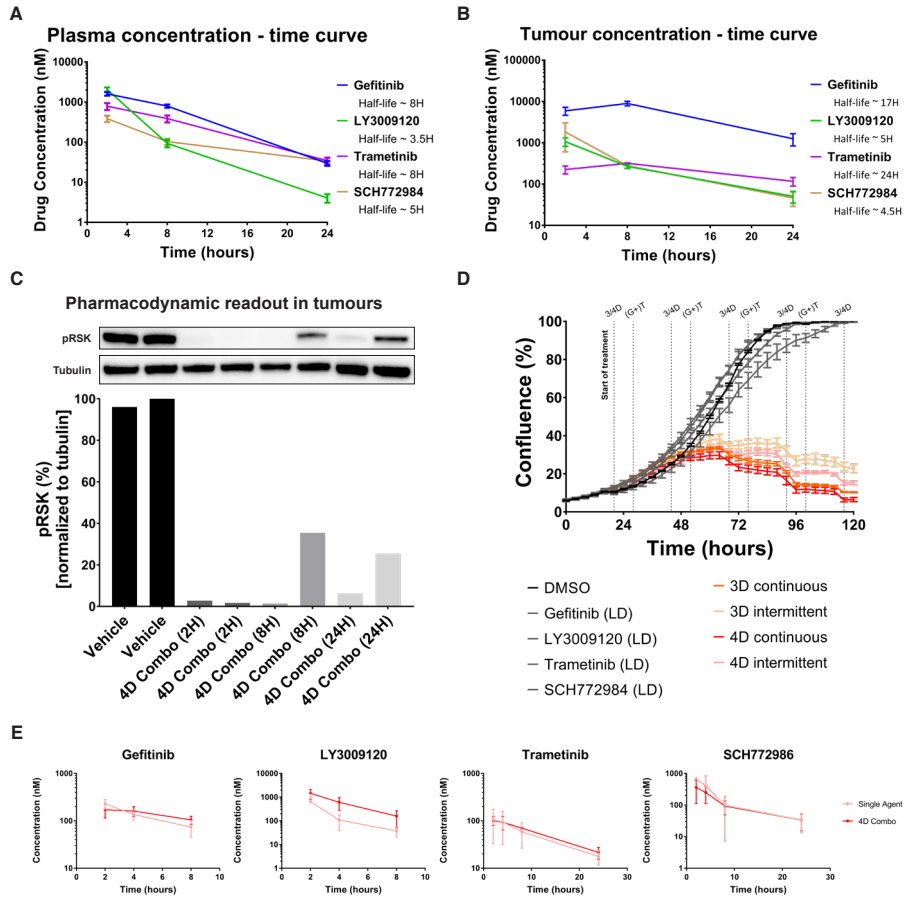

Supplementary Figure 6. PK-PD studies in PC9 xenografts reveal different half-lives of the inhibitors.

A-D, Pharmacokinetic and pharmacodynamics studies in PC9 xenografts. In **A-C** PC9 cells were injected (bilaterally) subcutaneously in BALB/cAnNRj-Foxn1nu mice. After tumour establishment (~200 mm3), mice were treated with vehicle (N=4) or 4D Combo (N=12). Vehicle mice were sacrificed 2H after treatment; Mice treated with 4D combo were sacrificed 2, 8 and 24h after treatment, respectively; 4 mice were sacrificed per time point. Blood and tumours were harvested; half of the tumour was used for the PD study and the other half was used for biochemical analysis. The drug concentrations in the blood and in the tumours were determined by mass spectrometry. In **A** the concentration of the individual drugs in the plasma is displayed and in **B** the concentration of the individual drugs in the tumours is displayed; SEM is plotted. In c the level of pathway inhibition in the tumours was measured by examining pRSK protein levels in the western blot (WB). Tubulin was used as loading control. WB was quantified using the Image Lab V5.2.1 software, from Bio Rad. **D,** Intermittent MLD therapy is less efficient in reducing cell growth in PC9 cells. PC9 cells were plated and incubated overnight to allow attachment to the plate. Cells were then treated with DMSO, with EGFR, RAF, MEK, ERK inhibitors at low dose, with 3D Combo or with

4D Combo. To mimic the availability of the drugs in vivo, in some of the 3D and 4D combo replicates the RAF and ERK inhibitors were removed from the culture media for approximately 8 hours every day (called intermittent MLD therapy). Confluence over time was measured by the IncuCyte®. SEM from 3 replicates is plotted. **E,** BALB/cAnNRj-Foxn1nu mice were treated with gefitinib (1mg/kg, N=3), LY3009120 (6mg/kg, N=3), trametinib (0,1mg/kg, N=3), SCH772984 (15mg/kg, N=3) or 4D Combo (N=3) and blood was harvested 2, 4, 8 and 24h after treatment. The drug concentrations in the blood was determined by mass spectrometry. The concentration of the drugs in the plasma given as single agent or in the 4D Combo ± SEM is displayed.

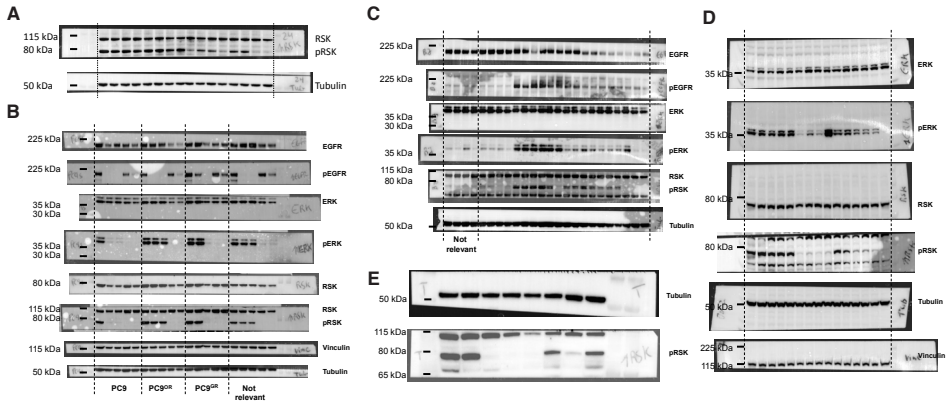

Supplementary Figure 7. Full blots images.

A, Figure 1e. **B,** Figure 2d. **C,** Figure 3c. **D,** Supplemental Figure 1b. **E,** Supplemental Figure 6c.

Supplementary Table 1. Compendium of drivers, plating density, low doses and high doses of the cell lines and organoids used in the study.

						Drug concentrations used in the study (μM)							
						Low Doses				High Doses			
Cell Line Name	**Tissue of Origin**	**Driver**	**Plating density (384-well plates)**	**Plating density (96-well plates)**	**Plating density (6-well plates)**	**EGFRi (Gefitinib)**	**RAFi (LY3009120)**	**MEKi (Trametinib)**	**ERKi (SCH772984)**	**EGFRi (Gefitinib)**	**RAFi (LY3009120)**	**MEKi (Trametinib)**	**ERKi (SCH772984)**
PC9/PC9^{GR}/PC9^{GR}	Lung	EGFR	150 cells	2000 cells	20000 cells	0.007	0.25	0.008	0.25	0.28	2.8	0.32	2.5
HCC827		EGFR	350 cells	NA	40000 cells	0.0025	0.5	0.1	0.75	1	5	1	5
H3255		EGFR	750 cells	NA	50000 cells	0.001	0.03	0.001	0.04	1	2	2	5
Cell Line Name	**Tissue of Origin**	**Driver**	**Plating density (384-well plates)**	**Plating density (96-well plates)**	**Plating density (6-well plates)**	**ALKi (Crizotinib)**	**RAFi (LY3009120)**	**MEKi (Trametinib)**	**ERKi (SCH772984)**	**ALKi (Crizotinib)**	**RAFi (LY3009120)**	**MEKi (Trametinib)**	**ERKi (SCH772984)**
H3122	Lung	EML4-ALK	1000 cells	NA	60000 cells	0.075	0.11	0.0038	0.084	2.5	5	1	5
H2228		EML4-ALK	1500 cells	NA	80000 cells	0.046	0.5	0.01	0.75	2.5	5	1	5
Cell Line Name	**Tissue of Origin**	**Driver**	**Plating density (384-well plates)**	**Plating density (96-well plates)**	**Plating density (6-well plates)**	**EGFRi (Gefitinib)**	**RAFi (LY3009120)**	**MEKi (Trametinib)**	**ERKi (SCH772984)**	**EGFRi (Gefitinib)**	**RAFi (LY3009120)**	**MEKi (Trametinib)**	**ERKi (SCH772984)**
DiFi	CRC	EGFR	1000 cells	NA	60000 cells	0.02	0.17	0.0025	0.095	2	5	0.5	2.5
Lim1215		EGFR	1250 cells	NA	40000 cells	0.04	0.06	0.0006	0.075	5	3	0.5	2.5
Cell Line Name	**Tissue of Origin**	**Driver**	**Plating density (384-well plates)**	**Plating density (96-well plates)**	**Plating density (6-well plates)**	**HER2i (Lapatinib)**	**PI3Ki (BKM120)**	**AKTi (MK2206)**	**mTORi (AZD8055)**	**HER2i (Lapatinib)**	**PI3Ki (BKM120)**	**AKTi (MK2206)**	**mTORi (AZD8055)**
SKBR3	Breast	HER2	2500 cells	NA	100000 cells	0.025	0.3	0.05	0.025	2.5	2.5	2.5	2.5
HCC1954		HER2	500 cells	NA	40000 cells	0.0125	0.4	0.5	0.025	5	3	5	2.5
Organoid Name	**Tissue of Origin**	**Driver**	**Plating density (384-well plates)**	**Plating density (96-well plates)**	**Plating density (6-well plates)**	**EGFRi (Gefitinib)**	**RAFi (LY3009120)**	**MEKi (Trametinib)**	**ERKi (SCH772984)**	**EGFRi (Gefitinib)**	**RAFi (LY3009120)**	**MEKi (Trametinib)**	**ERKi (SCH772984)**
ITO034T	Lung	KRAS	NA	NA	NA	0.065	0.035	0.0003	0.004	NA	NA	NA	NA
TUM09	CRC	MEK	NA	NA	NA	0.125	0.76	0.014	0.225	NA	NA	NA	NA
TUM10		KRAS	NA	NA	NA	2.2	0.16	0.003	0.05	NA	NA	NA	NA

Supplementary Table 2. Compendium of de *novo* mutations found in PC9^{OR} and PC9^{GR} by Exome Sequencing.

For the characters nomenclature please check http://varnomen.hgvs.org/recommendations/general/

PC9^{OR}						PC9^{GR}					
#	Gene	Mutation	#	Gene	Mutation	#	Gene	Mutation	#	Gene	Mutation
1	ABHD12	c.*489C>A	56	NCOA6	c.514+43T>G	1	ABCA10	c.2344G>A	56	NTRK2	c.917C>A
2	ADAM19	c.*1650C>T	57	NDNF	c.1399G>A	2	ACAD8	c.742T>G	57	OAS2	c.*744C>T
3	AFF2	c.48-9T>G	58	NEURL2	c.480G>A	3	ALK	c.4146G>C	58	OR2M2	c.366C>T
4	ANKLE2	c.9G>A	59	NF2	c.1331C>T	4	AMY1C	c.-37T>C	59	OR4D6	c.85G>A
5	ARAP1	c.264C>T	60	NRG1	c.1163_1164delGTinsAG	5	ARID3A	c.766+5G>C	60	PIEZO1	c.3582C>G
6	ARHGEF11	c.3068-30G>A	61	NWD1	c.891G>C	6	ARMCX3	c.307C>T	61	PPP1R17	c.449G>A
7	ASTN2	c.1878G>A	62	OLFM4	c.357+38G>C	7	BAAT	c.829C>T	62	PROSER2	c.51G>A
8	B4GALNT3	c.-48C>A	63	OR10A2	c.259C>G	8	BBX	c.1028A>G	63	PRPF40A	c.834_869dupTGCTGTTGTTGCAGCAGCAGCAGCGGCAGCAGCAGC
9	BPTF	c.5303+23G>T	64	OR1S2	c.483G>A	9	BCL11A	c.1175T>C	64	PSG7	c.430+40G>C
10	BTBD17	c.*106G>T	65	PCDHB16	c.416C>A	10	CANX	c.1023T>C	65	RARA	c.179-5998C>T
11	CALY	c.440C>T	66	PCDHB4	c.2124G>T	11	CASP7	c.682+24G>C	66	RN7SKP187	n.-1759C>G
12	CASP1	c.818T>G	67	PCED1B	c.115A>G	12	CCDC149	c.1418G>A	67	RP11-195L15.2	n.-468G>C
13	CDC34	c.588G>A	68	PCLO	c.4529A>G	13	CCL21	c.68-34C>A	68	RP11-44F14.1	n.412C>G
14	CDH12	c.361G>C	69	PDE10A	c.198T>C	14	CEACAM4	c.*13G>A	69	SCFD2	c.1962+46G>A
15	CEBPZ	c.1983G>A	70	PLEC	c.8311G>C	15	CENPO	c.207G>A	70	SCN11A	c.1472delA
16	CEP120	c.*1003-7A>T	71	PMCH	c.438A>G	16	CHRNA3	c.1392T>C	71	SLC17A7	c.-887A>G
17	CLTC	n.-1471G>T	72	POLA2	c.204+34A>G	17	CIC	c.4203T>G	72	SMG7	c.1828C>T
18	CORO7	c.2422C>T	73	POM121	c.2975C>T	18	CRYBG3	c.5554G>T	73	SUSD3	c.231delG
19	DNMT3A	c.*4A>G	74	PPP4R1	c.2032A>G	19	CYP26B1	c.1040C>G	74	TBXAS1	c.1326+5G>A
20	EIF2B1	c.-52G>C	75	PRKAR2A	c.262+5G>T	20	DCAF1	c.493G>T	75	TG	c.7710G>T
21	EPHA6	c.500T>C	76	RAB34	c.-464_-447delCGCGCCCCGGGCCGCTC	21	DDX59	c.1258A>C	76	THAP9	c.581-13T>C
22	F3	c.279C>A	77	RP1-170O19.17	n.-2249C>T	22	DEPDC5	c.*438C>T	77	THUMPD2	c.907G>A
23	FAM184B	c.2456G>A	78	RSPH6A	c.58A>G	23	DTHD1	c.825T>C	78	TINF2	c.225T>C
24	FCRL4	c.722delG	79	RTN1	c.1587G>A	24	EGFR	c.2369C>T	79	TM6SF2	c.1008C>T
25	FCRL4	c.721A>T	80	RUNX1T1	c.88+13146C>G	25	EMCN	c.415+1474C>A	80	TNS1	c.150delA
26	GLI3	c.3372C>T	81	RYR2	c.7552C>A	26	ENAM	c.2492A>C	81	TRIM48	c.604C>G
27	GPRIN3	c.1489G>C	82	SARS2	n.-2409G>A	27	FEZ1	c.*114T>A	82	TRIO	c.4189A>C
28	GSTK1	c.*12G>A	83	SLC2A10	c.1447G>A	28	GFM1	c.153C>A	83	TRIO	c.4191A>T
29	GSTM2	c.230T>C	84	SLIT3	c.2108A>G	29	GLI3	n.1334-26C>G	84	TRMT2B	c.1071G>A
30	GUCA1C	c.132G>C	85	SPAG17	c.2907G>A	30	GLI3	c.2681C>G	85	UNCX	c.348G>C
31	HYAL4	c.334C>T	86	SPTB	c.2890G>A	31	GNAS	c.842A>G	86	VEPH1	c.1034_1047delAGAGCAGAGACATC
32	IL4R	c.1318A>G	87	STIP1	c.666C>G	32	GRIK3	c.1828C>A	87	XRN2	c.623T>C
33	IRS4	c.63_65delGGC	88	TM9SF2	c.974C>A	33	GSTK1	c.*12G>A	88	ZIC2	c.364C>T
34	KSR1	c.54C>G	89	TMEM108	c.1532C>T	34	GSTM2	c.230T>C	89	ZNF467	c.754C>G
35	KSR1	n.-1100C>T	90	TNXB	n.-732T>C	35	JAG2	c.2467G>C	90	ZNF644	c.1058A>G
36	LFNG	c.108A>G	91	TONSL	c.1590G>T	36	JAK3	c.3060C>T			
37	LINC01006	n.-4236delT	92	TRIP12	c.3483C>G	37	KCNK13	c.-1564C>G			
38	LIX1L	c.784_787dupCATT	93	TSHR	c.615-5308A>G	38	KIAA1109	c.3324-495T>C			
39	LPAR4	c.279T>A	94	TUBGCP2	c.2402G>T	39	KIAA1109	c.6763-58G>A			
40	LRRK1	c.590C>T	95	UNC93B1	n.-3171G>C	40	KIF1B	c.4400C>T			
41	MADCAM1	c.790C>T	96	UTRN	c.8337G>A	41	KIFAP3	c.41C>G			
42	MADCAM1	c.800_801delAGinsCC	97	WDR6	c.1012G>C	42	KMT2C	c.10898C>G			
43	MCF2	c.-278C>A	98	YDJC	c.362C>T	43	LRP4	c.199+14C>A			
44	MED28	c.150+6A>G	99	ZBTB25	c.*1322G>A	44	LTBP3	c.1978+15G>T			
45	MKNK2	c.*1725T>G	100	ZFHX4	c.1295C>G	45	MAEA	n.-82A>G			
46	MON1B	c.901C>T	101	ZNF423	c.-165+3206C>A	46	MAGEL2	c.1623_1624insT			
47	MTRR	c.1850+4T>A	102	ZNF451	c.*879G>C	47	MAGEL2	c.1623G>A			
48	MTRR	c.1850+6G>C	103	ZNF467	c.740C>T	48	MIOS	c.2608G>T			
49	MTUS2	c.634C>A	104	ZNF469	c.7162A>T	49	MYH2	c.2388C>T			
50	MUC16	c.40783+19G>A	105	ZNF479	c.806A>G	50	MYOC	c.630G>T			
51	MYH13	c.1973A>G	106	ZNF568	c.1161G>A	51	NARS2	c.-2497delT			
52	MYO18A	c.1002G>A	107	ZNF586	c.987A>G	52	NCOA7	c.573-41C>G			
53	NCAM2	c.738-2A>G	108	ZNF665	c.1597C>T	53	NDUFS3	c.157G>C			
54	NCKAP5	c.874A>T	109	ZWINT	c.-1_1delGAinsTT	54	NEMP2	c.564A>T			
55	NCOA6	c.5893+48_5893+52delCCTAA				55	NSL1	c.191-453G>T			

Supplementary Table 3. Compendium of patient, tumour, treatments and mutations information for all the PDXs used in the study.

	PDX name			
	PDX-1	**PDX-2**	**PDX-3**	**PDX-4**
Age	46	69	44	39
Gender	Female	Male	Female	Female
Smoking Info	Former	Smoker	Former	Never
Diagnostic	Lung Adenocarcinoma	Lung Adenocarcinoma	Lung Adenocarcinoma	Lung Adenocarcinoma
EGFR mutation	Exon 19 deletion	Exon 19 deletion	L858R	Exon 19 deletion
Treatment 1 (T1)	Erlotinib	Erlotinib	Erlotinib	Afatinib
Alterations after T1	T790M positive	MET amplification	MET overexpression	Unknown
Treatment 2	Osimertinib	Gefitinib + Capmatinib	Gefitinib + Capmatinib	CBDCA + Pemetrexed
Treatment 3	Osimertinib + Capmatinib	CDDP + Pemetrexed	Carboplatin + Gemcitabine + Nivolumab	CDDP + VP-16
Source of PDX	After progressing to 2 lines	After progressing to 3 lines	After progressing to >3 lines	After progressing to 2 lines
Known alterations in the PDX	EGFR (T790M) and KRAS G12C	EGFR (del19) and METamp	EGFR (L858R) and METamp	TP53 mutation and SCLC transformation

CHAPTER 7

GENERAL DISCUSSION

GENERAL DISCUSSION

The coming-of-age of precision medicine for cancer treatment has been a rocky road. The draft of the human genome in the early '00 in combination with the successes of the first targeted agents (Gleevec, Herceptin) could be considered the biomedical milestones that laid the foundation for precision medicine for cancer treatment as we know it[1]. The concept of cancer as a consequence of genetic mistakes, and the ability to effectively inhibit those missteps, fueled the idea that cancer treatment would now quickly shift from an one-drug-fits-all approach to a patient-tailored approach[2]. Now, a decade later, we learned that this was more complicated than acknowledged at the time, and that the timelines were overoptimistic[3,4]. There are multiple reasons for the initial disappointing results, but they all converge on the staggering complexity of cancer genomes. In this thesis we demonstrate that clever and integrative use of genome-wide sequencing technologies, patient-derived organoids (PDOs), novel anti-cancer treatments, patient studies and clinically-annotated databases have the potential to dramatically improve anti-cancer treatment. Below I would like to touch upon the various concepts introduced in this thesis and their future outlooks.

Feasibility of organoid-based precision medicine

In this thesis we have extensively evaluated the predictive value of PDOs for patients with metastasized cancer. However, predictive value is not the only parameter that warrants clinical utility. The usefulness of a strategy depends on an array of factors that ultimately weigh into its feasibility. These factors constitute, but are not limited to: predictive value, success rate, turn-around time and adoptability. Therefore, I will discuss the clinical feasibility of organoids for precision medicine in the context of these parameters.

First and most important, a strategy or method should return a precise prediction of patient outcome and yield high sensitivity and/or high specificity, depending on whether the model is used to predict outcome for standard-of-care (SOC) or experimental treatment, respectively. Because it is ethically undesirable to miss patients that would have benefitted from SOC (i.e. proven to be effective) treatment, precision medicine strategies for SOC should be designed in such a way that they return sensitive prediction for sensitivity, and/or, conversely, high specificity for resistance (high confidence to detect all potential responders). The opposite is true for experimental treatment, because the clinical usefulness is still unknown. In this case predictive models should be skewed towards high specificity for sensitivity (high confidence that all detected responders are true responders) in order to prevent overtreatment. In chapter 2 we demonstrated that, in two cohorts, PDO drug screening can return highly sensitive predictions for response to irinotecan-based regimens. This has important implications as this is world-wide SOC and tens of thousands of patients with advanced CRC

undergo this often ineffective treatment due to the absence of powerful biomarkers. To date Individualized tumor cell screening never gained foothold in the realm of clinical oncology, because of a lack in sensitivity (i.e. ability to reliably detect all responders)[5]. This could be true for PDOs, as another study on rectal cancer organoids and predictive value for neoadjuvant 5-FU, irinotecan and radiation also reported high predictive value in terms of area-under-the-curve (AUC) and specificity (0.88 and 91.97%, respectively), but a modest sensitivity of 78.3%[6]. Unfortunately, it is unknown whether the authors were unaware of this essential rule for SOC prediction, and did not optimize their sensitivity as such, or whether 78.3% represents the sensitivity of an optimized prediction model, as we have done chapter 2.

A limitation of PDO-based precision medicine is that PDOs are not universally predictive for clinical outcome to chemotherapy, as illustrated by the lack of predictive value for 5-FU and oxaliplatin. This is an important finding as PDOs are often used to model responses to this combination in smaller studies and underscores the need for sufficiently powered PDO avatar cohorts and validation used matched clinical data of patients[7-9]. We also demonstrate in chapter 4 that '*de novo*' predictions for off-label drugs is challenging. The reason for this is multifactorial, but the observation that a strong *in vitro* response does not necessarily translate into a clinical response suggests that PDOs, like other tumor model systems, can yield false-positive findings. Preliminary clinical evidence from phase 1 or basket studies in combination with organoids from these patients as benchmark could aid in the development of these predictive models. All in all, clinical studies are key to determine, validate and optimize PDO-based predictions for individual treatments using clinical outcome data.

Second, the proportion of patients for which a test van be successfully employed s a clear determinant for its clinical utility. Compared to the 85% success rate of clinical sequencing, the current 57-71% rate for PDO culture is slightly lower[10,11]. In line with others studies we found tumor or epithelial cell content is the major determinant for successful generation of PDO culture[6,10,12,13]. Logical solutions include the preselection of patients for which the biopsy cellularity or epithelial content is sufficient, as suggested in chapter 5 and in large-scale sequencing studies, or the use of resection material as source material[14,15]. A more thorough study on this is needed for organoids, as most reports are still descriptive or retrospective[6,10,12,13]. Alternatively, PDO-based precision medicine can be employed in the adjuvant setting (post-surgery therapy) demonstrated by two other studies, because of the abundance of material and time in this setting, and an equal clinical need to prevent overtreatment[6,7]

Third, the speed by which a predictive test can be employed is essential for its clinical potential. Although mCRC patients can generally wait up to four weeks, early start of treatment is generally preferred. Sequencing in clinical context takes approx. 2-4 weeks

and in chapter 2 we estimated that these turnaround times should be achievable for PDOs too[10,16,17]. Admittedly, sequencing of DNA can be 'rushed' in some cases and this is not possible for PDO drug screening. Testing in an earlier stage of treatment, as done in chapter 4, is possible although intermittent, major clinical responses could alter the landscape of the tumor and, as a consequence, the accuracy of the prediction[18,19]. Turnaround times of PDO-based precision medicine may improve if tests can be further miniaturized. In chapter 2 and 5 we demonstrate that predictive value can be captured by a single drug concentration instead of a full dose-response curves or matrices. Further downscaling of cell numbers per condition by microfluidics or single-cell techniques could improve the current turnaround times even more.

Fourth, adoptability is an important factor for the success of a precision medicine approach. Classical approaches such as IHC and sequencing technologies are widely adopted by most comprehensive cancer centers or can even be outsourced to third parties. Classically, obtaining clinically-grade results by novel technologies, such as (single-cell) transcriptomics, can be challenging as sources of variation have simply not extensively studied[20]. PDO culture is no exception to this, but in this thesis we demonstrate that this can be done in a reproducible manner. We do note that functional screening of patient material has a steep learning curve. We would argue that, for now, implementation of organoid culture and drug screening in standard pathology practice would be challenging, both practically and financially, and initial validation studies should be performed as done currently: the testing of PDOs can be performed centrally by experienced technicians/scientists according to strict standard-operating procedures, as done in chapter 2 and 5. Organoid-based testing is currently done for CFTR patients in such an academic context[21,22]. The first formal experiences will likely stem from this initiative. In short: obtaining initial, clinically-grade testing results will likely be first achieved in a centralized and academic fashion.

Though promising, we have identified several additional questions on the clinical utility of PDOs for precision medicine. The most prominent one is that predictive value for treatments likely differs between treatment modalities, implying that predictive capacity of PDOs has to be determined and validated for each one individually. Clinical data of patients treated with SOC or enrolled in basket studies will be instrumental for this.

Genomics-based precision medicine for chemotherapy

Chemotherapy will remain part of the SOC for late-stage cancer in the foreseeable future, and so does the need for auxiliary diagnostics. Genomics has steadily made its ways in nearly all fields of cancer research. So why has it been so challenging to integrate personalized medicine into the realm of chemotherapy? As I briefly suggested earlier, the pleotropic

mechanism of action of chemotherapy and its complex metabolism are likely factors in this, as evidenced by largely discrepant results in clinical studies seeking predictive biomarkers for chemotherapy[23-25]. Even for drugs with an ostensibly clear target and mechanism of action, like irinotecan and Topoisomerase 1, complex drug metabolism, redundancy between DNA damage pathways, and even protein isoforms, have frustrated the identification of clinically-viable biomarkers[26].

Apart from the complex mechanism of action of chemotherapy, there are no to very few initiatives that systematically document patient and tumor genomics and outcome to chemotherapy. To fill that niche, the Center for Personalized Therapy (CPCT), and later the Hartwig Medical Foundation (HMF) database, was initiated to fill that void. We are now reaping the first fruits as a consequence of these efforts: In chapter 4 we describe the first genomic biomarker for a chemotherapeutic regimen that reliably predicts both resistance and sensitivity. Surprisingly, the biomarker depends on merely 2 amino acids (glycine12 and glycine13) in the 2nd codon of arguably the most infamous and illusive oncogene: KRAS. The mechanism that explains this finding has been equally elusive. The observation that G12 and G13 mutants have a different prognosis implies a more complex biology than clinically appreciated[27-29].

Can we expect to find genomic predictors for other chemotherapeutics in the near future? This remains speculative, but it is not unthinkable as the HMF database provides a wealth of genomics data linked to clinical responses on a variety of chemotherapeutics, and –in addition-- is now also supplemented with RNA-sequencing data. Nonetheless, an essential aspect will be validating findings in independent and sufficiently powered datasets. We were fortunate that KRAS status is tested for nearly every patient with late-stage CRC, which allowed us to validate the finding in the original patient cohorts of a large international, randomized, placebo-controlled phase 3 trial. For other biomarkers extracted from the HMF database, a validation cohort might not be readily available. Additional evidence can be sought in patient models and/or mechanistic data. For these purposes, we found that PDOs were particularly useful, as drug screening of a geno- and phenotype matched avatar patient cohort returned a similar outcome as the 'real-world' patient data. Conversely, such a cohort can also serve as the initial discovery set, which can be validated in the HMF database, demonstrating the power of complementary data types and/or patient models to generate and validate translational research questions[9].

Higher-order combinations to overcome drug resistance

A major challenge for use of small-molecular inhibitors in the clinic is the rapid onset of drug resistance. Pathway re-activation represents the dominant mechanism by which cancer cells

overcome drug pressure[30]. Rationally-designed (dual) drug combinations have now made their way into the clinic and can provide additional survival benefit[31]. However, resistance through pathway re-engagement can still occur[30,32].

In chapter 6 we describe that multiple low-dose (MLD) inhibition of a single oncogenic pathway reverts or delays drug resistance, thereby addressing an unmet clinical need. The concept is appealing because of its modular approach: it can be amended to any other (approved) drug (combination) that targets the IGF- or EGF-pathway. For instance, the first evidence has surfaced that inhibition of $KRAS^{G12C}$ leads to objective responses in the clinic, but so have the first data that describe adaptive resistance swiftly emerges through pathway reactivation and by-pass[33,34]. This should come as no surprise, as it is well established that monotherapy treatment can be easily bypassed. With this in mind, pre-clinical studies should focus on testing additional compounds targeting up- and downstream signaling nodes in similar vein as chapter 6. Because most anti-cancer drugs are developed for increasingly narrow patient groups, PDOs could prove themselves useful as they allow establishment of patient avatars from rare disease subtypes[35-37].

Our data demonstrated long-term disease stabilization, even on an intermittent dosing schedule, and no signs of resistance. Despite these data generated in human cancer models, these models may be insufficient to truly recapitulate the plethora of mechanisms through which cancer cells achieve drug resistance[30]. Well-designed, exploratory, objectives in the efficacy study might provide insight into the mechanisms by which human tumor overcome the therapeutic effect of MLD treatment

An obvious criticism of the MLD approach is the expected treatment-associated toxicity. While several experiment were undertaken to assess the adverse effects, mouse toxicity profiles have been poor predictors of toxicity in humans[38]. Several studies have suggested human 'healthy' organoids as vehicles to assess treatment-associated toxicities[39]. Although this is a promising approach to alleviate patient-exposure to potentially harmful drugs in phase 1/2 studies, formal proof for this approach is still lacking. For now, formal clinical studies are needed to evaluate toxicity profiles (and efficacy). The FDA-approval of a triple drug combination to treat $BRAF^{V600E}$ mCRC has set a hopeful precedent for concept of vertical inhibition of essential signaling pathways, as it is equally tolerated and effective[40].

FINAL REMARKS

Recent years have seen a surge in available (anti-cancer) drugs and health care costs alike. In light of these developments, personalized medicine will take an increasingly prominent position in patient care. We demonstrate that integrative use of genomics, organoids, clinical studies and patient outcome can identify more sophisticated treatment strategies for advanced cancer, even for therapies that were long deemed too complex to tailor to individual patients.

REFERENCES

1 Moscow, J. A., Fojo, T. & Schilsky, R. L. The evidence framework for precision cancer medicine. *Nature reviews. Clinical oncology* **15**, 183-192, doi:10.1038/nrclinonc.2017.186 (2018).

2 La Thangue, N. B. & Kerr, D. J. Predictive biomarkers: a paradigm shift towards personalized cancer medicine. *Nature reviews. Clinical oncology* **8**, 587-596, doi:10.1038/nrclinonc.2011.121 (2011).

3 Hyman, D. M., Taylor, B. S. & Baselga, J. Implementing Genome-Driven Oncology. *Cell* **168**, 584-599, doi:10.1016/j.cell.2016.12.015 (2017).

4 Prasad, V. Perspective: The precision-oncology illusion. *Nature* **537**, S63, doi:10.1038/537S63a (2016).

5 Unger, F. T., Witte, I. & David, K. A. Prediction of individual response to anticancer therapy: historical and future perspectives. *Cellular and molecular life sciences : CMLS* **72**, 729-757, doi:10.1007/s00018-014-1772-3 (2015).

6 Yao, Y. *et al.* Patient-Derived Organoids Predict Chemoradiation Responses of Locally Advanced Rectal Cancer. *Cell stem cell* **26**, 17-26.e16, doi:10.1016/j.stem.2019.10.010 (2020).

7 Ganesh, K. *et al.* A rectal cancer organoid platform to study individual responses to chemoradiation. *Nature medicine* **25**, 1607-1614, doi:10.1038/s41591-019-0584-2 (2019).

8 Pauli, C. *et al.* Personalized In Vitro and In Vivo Cancer Models to Guide Precision Medicine. *Cancer discovery* **7**, 462-477, doi:10.1158/2159-8290.Cd-16-1154 (2017).

9 Hidalgo, M. *et al.* Patient-derived xenograft models: an emerging platform for translational cancer research. *Cancer discovery* **4**, 998-1013, doi:10.1158/2159-8290.Cd-14-0001 (2014).

10 Zehir, A. *et al.* Mutational landscape of metastatic cancer revealed from prospective clinical sequencing of 10,000 patients. *Nature medicine* **23**, 703-713, doi:10.1038/nm.4333 (2017).

11 Weeber, F. *et al.* Preserved genetic diversity in organoids cultured from biopsies of human colorectal cancer metastases. *Proceedings of the National Academy of Sciences of the United States of America* **112**, 13308-13311, doi:10.1073/pnas.1516689112 (2015).

12 Vlachogiannis, G. *et al.* Patient-derived organoids model treatment response of metastatic gastrointestinal cancers. *Science (New York, N.Y.)* **359**, 920-926, doi:10.1126/science.aao2774 (2018).

13 Kim, M. *et al.* Patient-derived lung cancer organoids as in vitro cancer models for therapeutic screening. *Nature communications* **10**, 3991, doi:10.1038/s41467-019-11867-6 (2019).

14 TCGA. Comprehensive molecular characterization of human colon and rectal cancer. *Nature* **487**, 330-337, doi:10.1038/nature11252 (2012).

15 Comprehensive molecular characterization of gastric adenocarcinoma. *Nature* **513**, 202-209, doi:10.1038/nature13480 (2014).

16 Sicklick, J. K. *et al.* Molecular profiling of cancer patients enables personalized combination therapy: the I-PREDICT study. *Nature medicine* **25**, 744-750, doi:10.1038/s41591-019-0407-5 (2019).

17 van der Velden, D. L. *et al.* The Drug Rediscovery protocol facilitates the expanded use of existing anticancer drugs. *Nature* **574**, 127-131, doi:10.1038/s41586-019-1600-x (2019).

18 Kim, C. *et al.* Chemoresistance Evolution in Triple-Negative Breast Cancer Delineated by Single-Cell Sequencing. *Cell* **173**, 879-893.e813, doi:10.1016/j.cell.2018.03.041 (2018).

19 Riaz, N. *et al.* Tumor and Microenvironment Evolution during Immunotherapy with Nivolumab. *Cell* **171**, 934-949.e916, doi:10.1016/j.cell.2017.09.028 (2017).

20 Shalek, A. K. & Benson, M. Single-cell analyses to tailor treatments. *Science translational medicine* **9**, doi:10.1126/scitranslmed.aan4730 (2017).

21 Berkers, G. *et al.* Rectal Organoids Enable Personalized Treatment of Cystic Fibrosis. *Cell reports* **26**, 1701-1708.e1703, doi:10.1016/j.celrep.2019.01.068 (2019).

22 Dekkers, J. F. *et al.* Characterizing responses to CFTR-modulating drugs using rectal organoids derived from subjects with cystic fibrosis. *Science translational medicine* **8**, 344ra384, doi:10.1126/scitranslmed.aad8278 (2016).

23 Obeid, M. *et al.* Calreticulin exposure dictates the immunogenicity of cancer cell death. *Nature medicine* **13**, 54-61, doi:10.1038/nm1523 (2007).

24 Zitvogel, L., Apetoh, L., Ghiringhelli, F. & Kroemer, G. Immunological aspects of cancer chemotherapy. *Nature reviews. Immunology* **8**, 59-73, doi:10.1038/nri2216 (2008).

25 Koopman, M., Venderbosch, S., Nagtegaal, I. D., van Krieken, J. H. & Punt, C. J. A review on the use of molecular markers of cytotoxic therapy for colorectal cancer, what have we learned? *European journal of cancer (Oxford, England : 1990)* **45**, 1935-1949, doi:10.1016/j.ejca.2009.04.023 (2009).

26 Friboulet, L. *et al.* ERCC1 isoform expression and DNA repair in non-small-cell lung cancer. *The New England journal of medicine* **368**, 1101-1110, doi:10.1056/NEJMoa1214271 (2013).

27 De Roock, W. *et al.* Association of KRAS p.G13D mutation with outcome in patients with chemotherapy-refractory metastatic colorectal cancer treated with cetuximab. *Jama* **304**, 1812-1820, doi:10.1001/jama.2010.1535 (2010).

28 McFall, T. *et al.* A systems mechanism for KRAS mutant allele-specific responses to targeted therapy. *Science signaling* **12**, doi:10.1126/scisignal.aaw8288 (2019).

29 Rabara, D. *et al.* KRAS G13D sensitivity to neurofibromin-mediated GTP hydrolysis. *Proceedings of the National Academy of Sciences of the United States of America* **116**, 22122-22131, doi:10.1073/pnas.1908353116 (2019).

30 Konieczkowski, D. J., Johannessen, C. M. & Garraway, L. A. A Convergence-Based Framework for Cancer Drug Resistance. *Cancer cell* **33**, 801-815, doi:10.1016/j.ccell.2018.03.025 (2018).

31 Robert, C. *et al.* Five-Year Outcomes with Dabrafenib plus Trametinib in Metastatic Melanoma. *The New England journal of medicine* **381**, 626-636, doi:10.1056/NEJMoa1904059 (2019).

32 Kong, X. *et al.* Cancer drug addiction is relayed by an ERK2-dependent phenotype switch. *Nature* **550**, 270-274, doi:10.1038/nature24037 (2017).

33 Hallin, J. *et al.* The KRAS(G12C) Inhibitor MRTX849 Provides Insight toward Therapeutic Susceptibility of KRAS-Mutant Cancers in Mouse Models and Patients. *Cancer discovery* **10**, 54-71, doi:10.1158/2159-8290.Cd-19-1167 (2020).

34 Xue, J. Y. *et al.* Rapid non-uniform adaptation to conformation-specific KRAS(G12C) inhibition. *Nature* **577**, 421-425, doi:10.1038/s41586-019-1884-x (2020).

35 Puca, L. *et al.* Patient derived organoids to model rare prostate cancer phenotypes. *Nature communications* **9**, 2404, doi:10.1038/s41467-018-04495-z (2018).

36 Fujii, M. *et al.* A Colorectal Tumor Organoid Library Demonstrates Progressive Loss of Niche Factor Requirements during Tumorigenesis. *Cell stem cell* **18**, 827-838, doi:10.1016/j.stem.2016.04.003 (2016).

37 van de Wetering, M. *et al.* Prospective derivation of a living organoid biobank of colorectal cancer patients. *Cell* **161**,

933-945, doi:10.1016/j.cell.2015.03.053 (2015).

38 Van Norman, G. A. Limitations of Animal Studies for Predicting Toxicity in Clinical Trials: Is it Time to Rethink Our Current Approach? *JACC. Basic to translational science* **4**, 845-854, doi:10.1016/j.jacbts.2019.10.008 (2019).

39 Fatehullah, A., Tan, S. H. & Barker, N. Organoids as an in vitro model of human development and disease. *Nature cell biology* **18**, 246-254, doi:10.1038/ncb3312 (2016).

40 Kopetz, S. *et al.* Encorafenib, Binimetinib, and Cetuximab in BRAF V600E-Mutated Colorectal Cancer. *The New England journal of medicine* **381**, 1632-1643, doi:10.1056/NEJMoa1908075 (2019).

APPENDIX

SUMMARY IN DUTCH /
SAMENVATTING IN HET NEDERLANDS

DANKWOORD

CURRICULUM VITAE AND LIST OF PUBLICATIONS

SAMENVATTING IN HET NEDERLANDS

Voor patiënten met uitgezaaide kanker zijn er tegenwoordig meerdere, levensrekkende behandelopties beschikbaar. Helaas slaat niet elke behandelingen aan en ondervinden patiënten alleen de nadelige effecten van een behandeling. Enerzijds is dit een onwenselijke situatie voor patiënten die in een fase zitten waar kwaliteit van leven prioriteit heeft. Anderzijds is dit onwenselijk vanwege de hoge kosten van deze behandelingen. Om dit probleem te ondervangen wordt geprobeerd een behandeling beter toe te spitsen op individuele patiënten. Dit concept wordt 'precision medicine', 'personalized medicine' of gepersonaliseerde behandeling genoemd. Het doel van personalized medicine is een balans te vinden tussen de effectiviteit van een behandeling, de kwaliteit van leven van een patiënt en de (zorg)kosten.

Onderzoek naar gepersonaliseerde behandeling richt zich onder andere op de ontwikkeling van meer 'gerichte' geneesmiddelen (i.e., het geneesmiddel maakt een mutatie in een tumor onschadelijk), door een behandeling afstemmen op het tumor DNA, een subgroep patiënten te identificeren die geen baat hebben bij een behandeling (of juist wel) of door geneesmiddelen slim te combineren en zo de effectiviteit te waarborgen of verlengen. In de kliniek wordt nu routinematig voor elke patiënt het tumor DNA geanalyseerd om zo te achterhalen welke mutaties de kanker veroorzaken. Op basis van deze data kan er in veel gevallen een (gerichte) behandeling worden voorgesteld die het effect van een of meer mutaties in de tumor remt. De combinatie DNA-analyse en gerichte behandeling heeft voor een aantal tumortypes en behandelopties geleid tot spectaculaire resultaten en wordt beschouwd als een van de succesverhalen van kankeronderzoek. Mede daarom wordt personalized medicine in één adem genoemd met gerichte behandeling en (klinische) DNA-analyse. Een tumor reduceren tot een serie mutaties doet echter geen recht aan de complexiteit van kanker, hetgeen terug is te zien in de statistiek: Ondanks een sterke rationale om een patiënt te behandelen, slaan de meeste behandelingen niet aan of is de effectiviteit maar van korte duur. Een reden hiervoor is de context-afhankelijke effecten van de duizenden mutaties die worden gevonden in het DNA van een tumor. Omdat er een oneindig aantal combinaties mogelijk is van deze mutaties, is geen tumor hetzelfde en is het effect op de behandeluitkomst dus lastig te voorspellen; De complexiteit van tumor DNA maakt universeel gebruik van gerichte therapie en DNA-analyse onmogelijk. Voor chemotherapie is dit probleem nog complexer. Chemotherapie is een type behandeling dat stamt uit de jaren '50 en maakt deel uit van de standaardbehandeling voor bijna elk tumortype. Omdat voor dit type behandeling onbekend is welke mutaties voorspellend zijn voor de effectiviteit van de behandeling en de bijwerkingen ernstiger zijn dan bij de nieuwere generatie geneesmiddelen, is de klinische nood voor gepersonaliseerde behandelstrategieën nog groter.

Het is duidelijk dat DNA-analyse alleen te kort schiet om een gepersonaliseerde behandeling te realiseren voor elke patiënt en voor elk type behandeling. Een nieuwe kweekmethode ('organoids'), geavanceerde DNA-analyse van patiënt tumoren ('whole-genome sequencing') en databases met tumor DNA en (behandel) data van patiënten zijn recentelijk beschikbaar gekomen en bieden de mogelijkheid om personalized medicine vanuit een ander perspectief te benaderen. De vraag is hoe we dit soort technologieën en data op een slimme manier kunnen combineren om (langlopende) klinische vraagstukken te beantwoorden. In dit proefschrift confronteren we de eerdergenoemde uitdagingen die personalized medicine kent door integraal gebruik te maken van de bovenstaande technologieën, patiënt data en klinische studies.

In **hoofdstuk 1** worden de voor- en nadelen van de huidige pre-klinische model systemen van kanker en de ontwikkeling van 'organoids', een nieuwe methode om patiënten tumoren in het lab op te kweken, besproken. Ook wordt er een veelbelovend concept uitgelicht: het testen van medicijnen op tumorcellen van patiënten in het lab om zo de meest effectieve behandeling te selecteren.

Hoofdstuk 2 beschrijft de resultaten van een observationele, klinische studie, uitgevoerd in meerdere ziekenhuizen in Nederland, waarin we de voorspellende waarde van organoids testen voor chemotherapie. Gebaseerd op chemotherapiegevoeligheidtests in het lab op organoids van patiënten ontwikkelen we een voorspellend model voor irinotecan-bevattende chemotherapie en laten we zien dat organoids uitstekende voorspellende waarde kunnen hebben voor een therapielijn die notoir ineffectief is in een groot gedeelte van de darmkankerpatiënten. Er is echter een nuance: organoids lijken niet universeel voorspellend te zijn voor elk soort therapie. Er is namelijk geen voorspellende waarde voor de chemotherapiecombinatie 5-FU en oxaliplatin.

Hoofdstuk 3 beschrijft een follow-up waarom organoids niet voorspellend zijn voor 5-FU en oxaliplatin. We maken gebruik van een populair muismodel in kankeronderzoek: een subcutaan, tumormuismodel, waarin verschillende parameters aanwezig zijn, zoals systemische metabolisme van chemotherapie en tumor stroma, die in vitro afwezig zijn. Het gebruik van dit muismodel laat echter geen verbetering zien van de voorspellende waarde van de organoids en we concluderen daarom dat er weinig waarde is om dit model te gebruiken voor biomarkerstudies of de voorspelling van behandeluitkomsten van patiënten. Opvallend genoeg komen de behandeluitkomsten in het muismodel en in het lab sterk overeen.

In **Hoofstuk 4** worden twee subgroepen darmkanker patiënten geïdentificeerd die of veel of

weinig baat hebben bij behandeling met een nieuw soort chemotherapie, TAS-102 (Lon-surf). Met behulp van patiëntdata en organoids laten we zien dat de aanwezigheid van $KRAS^{G12}$ mutatie in het tumor DNA voorspelt dat een patiënt weinig baat heeft bij de behandeling. Omgekeerd laten we zien dat $KRAS^{G13}$-gemuteerde patiënten, slechts één aminozuur verschillende, een slechtere prognose hebben dan $KRAS^{G12}$-gemuteerde patiënten. Echter, juist deze patiënten hebben veel baat hebben bij behandeling met Lon-surf. Omdat deze mutaties al routinematig worden getest in de kliniek voorzien we dat patiënten direct baat hebben bij deze gepersonaliseerde behandelstrategie

In **hoofdstuk 5** wordt organoid technologie toe in een tweede klinische studie toegepast. Het doel van deze interventie studie was om een extra behandeloptie voor te stellen voor patiënten die uitbehandeld zijn. Echter, gebruik van deze technologie in deze reeds zwaar behandelde patiëntpopulatie is een uitdaging, mede door het lagere kweeksucces van patiënttumoren in het lab, de uitval van patiënten door het vergevorderde stadium van de ziekte en de ineffectiviteit van de voorgestelde behandelingen. De observatie dat een sterk effect in een kweekbakje geen sterk effect in patiënt garandeert geeft stof tot nadenken.

In **hoofdstuk 6** wordt het ontwerp van een nieuwe behandelstrategie voor klein-cellige longkanker en darmkanker beschreven. Door 4 verschillende geneesmiddelen te gebruiken op lage dosis, elk aangrijpend op een verschillend punt in EGF-signalering, wordt resistentie voorkomen of vertraagd. Deze vierdubbele therapie lijkt zelfs aan te slaan in kweekmodellen van patiënten die eerder resistent waren op monotherapiebehandeling van EGF-signalering. Het synergetische effect van de vierdubbele combinatie lijkt te gelden voor verschillende EGF-remmende therapieën beschikbar in de kliniek en voor verschillende tumortypes. De modulaire aard van deze behandelstrategie maakt het een aantrekkelijk concept dat breed inzetbaar lijkt.

In **hoofdstuk 7** plaatsen we de bevindingen in een bredere context en doen we een aantal aanbevelingen voor vervolgonderzoek.

DANKWOORD

Werp een snelle blik op de lange auteurslijsten die de wetenschappelijke hoofdstukken voorgaan, en u begrijpt dat dit proefschrift tot stand is gekomen met hulp van een zeer groot aantal mensen. Even belangrijk zijn de onderonsjes met collega's, vrienden en familie die je steunen, aan het denken zetten of van gedachte doen veranderen. Hieronder zou ik graag de ruimte nemen deze mensen persoonlijk te bedanken.

Emile, het traject begon op een nogal opmerkelijke en typerende manier: een Ph.D.'er aannemen op basis van een krakerig telefoongesprek uit Laos. Je sms een paar dagen later sprak boekdelen: 'De wonderen zijn de wereld nog niet uit, maar ik zou je graag via deze weg de positie aanbieden'. Ik heb gedurende mijn Ph.D. een diepe bewondering gekregen voor je visie op wetenschap en hoe je de onderzoeksgroep op het NKI leidt, naast talloze andere bezigheden die het equivalent zijn van drie fulltimebanen. De manier waarop je een diverse groep mensen bij elkaar brengt, de juiste vragen laat stellen, weet te motiveren, en je oog strak op het einddoel houdt is niet alleen uniek maar ook extreem succesvol gebleken. Focus is voor mij het toverwoord gebleken, en ik denk dat ik je flink hebt uitgedaagd om dat voor elkaar te krijgen bij mij. Maar het is gelukt, het boekje ligt voor je en zonder jouw mentorschap had deze thesis nooit tot stand gekomen. Ik ben er trots op deel uit te hebben gemaakt van de Voest groep en kijk terug op een periode waarin ik nog nooit zoveel hebt geleerd én nog nooit zo vaak van mening ben veranderd (met als kers op de taart tijdens mijn eerste werkbespreking: 'Immunotherapie? Pff, dat werkt toch helemaal niet').

Fleur, jouw enthousiasme, drive en organisatie skills waren essentieel om de SENSOR en TUMOROID (en dus eigenlijk mijn hele Ph.D.) in goede banen te leiden. Je klinische denkwijze en oog voor de patiënt hebben mij als wetenschapper heel anders naar (kanker)onderzoek laten kijken en daar ben ik je erg dankbaar voor. Ik denk dat we elkaar perfect aanvulde: chaos vs. organisatie, 'creatieve' (aka wilde en ondoordachte) ideeën vs. praktische oplossingen, fundamenteel onderzoek vs. klinische realiteit. Van successen, naar dieptepunten en weer terug naar successen, we hebben het allemaal samen meegemaakt en het resultaat mag er zijn: een fijne en vaak hilarische samenwerking. Ik ben er trots op dat we dit hebben kunnen vereeuwigen in een serie manuscripten (een oeuvre?), waarin we samen organoids zowel de hemel in prijzen als flink onder vuur nemen. Weeber F, Ooft SN et al. is een combinatie die hopelijk veel geciteerd wordt komende jaren.

Krijn, het begon allemaal met anderhalf uur durend telefoongesprek waarin het relatief kort over wetenschap ging, want het was duidelijk dat we veel meer raakvlakken hadden. Je was gedurende mijn Ph.D., op gelegen en ongelegen tijden, mijn go-to klankbord voor een

onhaalbaar en vergezocht idee, een grap, een sterk verhaal of het ontwerp van een experiment. Ik kan je blik op wetenschap en alles daar omheen erg waarderen, want het is vaak doordacht, slim en genuanceerd. Tot er een keer speciaalbier in ging, want toen waren we je kwijt. Je integriteit en correctheid zijn typerend, maar wie houdt zich in godsnaam netjes aan de spelregels tijdens een drankspelletje (met speciaalbier ook..). Los van dit incident weet ik zeker dat je het fantastisch zal doen in Londen, want daar schenken ze immers 'normale' pints.

David, **Errol**, ik kan aan ieder van jullie een volledige thesis wijden. Misschien is het wel mooier dat ik hier eigenlijk geen woorden meer voor nodig hebben. We weten namelijk precies wat we aan elkaar hebben. Ik ben er trots op dat jullie mijn paranimfen zijn en we deze once-in-a-lifetime gebeurtenis samen mogen vieren.

Chelsea, ik zou dit eigenlijk in het Engels moeten schrijven maar dat doe ik lekker niet, want, of je het nu wilt of niet, je bent inmiddels gewoon een Nederlander. Je wetenschappelijke ervaring, rust en humor hebben ervoor gezorgd dat ik altijd met beide benen op de grond bleef, niet (teveel) afdwaalde of ik het even niet meer zag zitten. Als Nederlands-Amerikaans blok hebben we ons door wetenschappelijke problemen heen geslagen en ons collectief geschaamd voor de (soms erbarmelijke) Nederlandse/Amerikaanse cultuur, mensen of politiek. Ik denk dat we een perfect team vormde, wetenschappelijk of op een kruistocht tegen slecht eten.

Joris, gelukkig wordt er ook nog een beetje gelachen tijdens het Ph.D.'en. Door jou heeft de wereld officieel kennis gemaakt met obscure concepten als 'mutual exclusivity' en 'schroeven', en dat is natuurlijk een fantastische prestatie. Of je nu 5 projecten compleet tot leven wekt en in een stroomversnelling brengt of 5 bier schroeft; het gaat allemaal met overtuiging en humor. De combinatie van humor, een scherpe geest en talent voor (bio-informatisch) onderzoek zijn erg zeldzaam in de wetenschap, je zou het 'mutually exclusive' mogen noemen ($P<0.001$), en de reden dat ik ervan overtuigd ben dat je het ver gaat schoppen.

Sovann, ma dude. The Voest group (or the culture room, it's basically the same) wouldn't be the same without you. Some people consider Ph.D.'ing boring, but they probably didn't have a 'Sovann' in their group. For some reason you pulling off being a scientist, dad, successful(!) investor, our lab pet, and the single most cynical person ever (probably not true, but what are you going to do about it). I would like to thank you for laughs, the support and also the last months rounding up all experiments, based on limited instructions from my side (classic).

Chiara, voor jouw schrijf ik de tekst gewoon in het Nederlands, omdat je zo diepe waardering

koestert voor Nederlandse taal en cultuur. En omdat je je Nederlands nog wel een beetje mag bijspijkeren. Kidding, I'll do it English, in part because you'll probably kill me if I wouldn't. Your cheerful personality, strong opinion and Italian genes are exactly what a research group needs to spice up the atmosphere. The internet movies, chonky animal pictures and the pastries you brought were some of the many highlights. Also, I never have to eat macarons again, which will save me a lot of money and time, so thanks for that too. Enjoy your wedding and let me know when you are pargant gregnant pergent pregonet, pegnet purgenent pregnan pregnart preget pargnet pregernet peegnant fregnant pragnent pregenant, pregnante pregnant… Whatever, I meant that thing with children, so we can celebrate accordingly.

Louisa, promoveren is af en toe zwaar, maar om nu te zeggen dat het ondragelijk was. Er waren ook retreats, borrels en congressen en daar hebben we ons erg goed vermaakt. Ik dacht even dat we beide tegelijkertijd zouden promoveren, maar je plakte er toch nog even wat tijd aan vast. Dit is een gemiste kans, want het gezamenlijke feestje was gegarandeerd een klapper geworden.

Luuk, ik dacht dat ik redelijk kon koken, maar jouw bbq-skills zijn ongeëvenaard (volgende keer niet direct na Lowlands aub). Hoewel onze formele samenwerking van kortere duur was dan gepland, denk ik dat we er samen alsnog iets moois van hebben gebrouwen. (woordgrappen doe je trouwens ook beter dan ik). Anyway, ik vond het fijn samenwerken en ben heel blij dat je de studies door de kafkaëske bureaucratie hebt genavigeerd.

Myriam, 'even' promoveren op een rits klinische studies naast een fulltimebaan als specialist, ik doe het je niet na. Ik vond het jammer dat je maar één dag per week bij ons in het kantoor zat. Desondanks heb ik genoten van je verhalen over (culinaire) uitstapjes of de verhitte telefoongesprekken die je voerde in het kantoor met mensen die niet deden wat je ze vriendelijk had opgedragen te doen.

Christina, heel even dacht ik dat onze NKI-groep een waardevolle aanwinst had, maar helaas vertrok je weer naar het UMC. Het is namelijk erg fijn werken met iemand die altijd vrolijke en positief is. Petje af hoe je je als onderzoeker staande hebt gehouden onder (tijds)druk en met een aantal taaie projecten.

Daphne, je bent al eventjes weg, maar zeker niet vergeten want we worden elke dag herinnerd aan de fantastische DRUP studie (waar de groep nog vele jaren vruchten van gaat plukken).

Alice, er is geen Voestgroep zonder jouw organisatietalent. Ik weet niet precies hoe je Emile's agenda balanceert tussen ons en zijn vele andere verplichtingen, maar er was altijd wel tijd

en dat is een prestatie. Heel erg bedankt voor je hulp, tijd en moeite voor de ondersteuning bij alle formaliteiten rondom het promotietraject en de fantastische retreats.

Joao, it was great collaborating on the MLD-project, but maybe the IPSCC in London and Amsterdam were the real highlights. I'm pretty sure we'll meet again sometime in the future and we can reflect back on a sometimes hectic, but mostly fun time at the NKI.

Vivien, I think you made the right decision to come back to our group. Also for us, because you can't have enough people that are talented, smart, down-to-earth and up-to-date on all the latest intel. Good luck keeping our group with both feet on the ground and finding a new chocolate donor.

Steven, het duurde niet lang of je was officieel geadopteerd als Voestie. Het is aan jou om de kantoortraditie van sterke verhalen op maandag door te zetten, maar daar heb ik alle vertrouwen in.

Mike, de weekenden samen in Londen had ik hard nodig om even weg te zijn van alle hectiek, net als iemand die me af en toe de waarheid vertelt (zelfs als ik die ik liever niet wil horen). Dat de IPSCC 2018 in Londen plaatsvond was uiteraard de kat(ten) op het spek binden.

Luèn, **Monique**, **Capri**, **Lima**, onze gezamenlijk vakanties en feestdagen zijn altijd lichtpuntjes geweest na hectische periodes en de perfecte reset. Ik vind het fijn dat we zo'n hechte familie zijn en dit soort dingen nog steeds samen delen.

Tom, **Pim**, **Laurien**, **Lyndsay**, ik heb jullie helaas kort of van een afstandje meegemaakt, maar ik ben ervan overtuigd dat er in de Voestgroep geen gebrek zal zijn aan sfeer, droge humor (of code..) en wetenschap van hoog niveau. Ik kijk uit naar jullie eerste successen op Pubmed!

Daniel P., ik wil je bedanken voor je scherpe advies bij het starten van de projecten op H5, het leiden van de afdeling en plaatsnemen in mijn begeleidingscommissie. Ik ben er trots op deel uit te hebben gemaakt van zo'n sterke divisie.

René B., **Jelle**, ik wil jullie heel erg bedanken voor de begeleiding gedurende mijn promotie, en dat jullie mijn ogen strak op het einddoel hielden. **Onno**, **René M**. **Geert**, **Jacco**, **Roderick**, fantastisch dat jullie plaats willen nemen in mijn beoordelingscommissie. Ik kijk uit naar een mooie gedachtewisseling,

Erik, een mailtje met een omslachtig geformuleerd, statistisch probleem van mij en je had altijd tijd om ernaar te kijken, én een waardevol antwoord paraat. Ik ben je zeer dankbaar voor je creatieve blik op en gigantische kennis van statistiek. Wie had gedacht dat statistiek eigenlijk best leuk is.

Ji-Ying, je expertise en scherpe oog zijn een aanwinst voor het NKI. Ik wil je hierbij bedanken voor de tijd die je inruimde in je (overvolle) agenda) om gezamenlijk door coupes heen te gaan en me de fijne kneepjes van pathologie bij te brengen.

Sandra, **Suzanne**, **Judith**, dank voor jullie hulp bij de klinische studies. Excuus als we weer eens verstoppertje speelden op het lab.

Marieke, heel erg bedankt voor het plannen en begeleiden van de grote experimenten. Dit was niet gelukt zonder jouw kennis en expertise, en heeft me in korte tijd heel veel geleerd over muisexperimenten.

Begoña, organoids culture has a steep learning curve and your early experiences were very valuable. **Sara**, **Liqin**, many thanks I could use your knowledge and repository of cell lines, so any wild idea or project could be started immediately.

Edwin Cuppen, **Warner**, **Petur**, **Hans Clevers**, **Alwin**, jullie expertise was van onschatbare waarde voor onze (klinische) studies. **Haiko**, **Henk**, **Cecile**, **Laurens**, ik wil jullie heel erg bedanken voor de inclusie van de patiënten in de studies.

Minze, **Edwin**, **Jufry**, **Cryobase** is de faciliteit waar ik 5 jaar lang het zwaarst op heb geleund en daarom wil ik jullie bedanken voor het logistiek ondersteunen van onze biobanken en experimenten.

Henri en **Elise**, helaas verhuisde wij naar H5, maar gelukkig was daar nog de organisatie van de IPSCC op de NKI en waar ik (na enig aandringen) aan meedeed. Dank voor jullie hulp en ondersteuning, het eindresultaat was fantastisch. **Ziva**, **Kevin**, **Lisette**, ik ben genoten van de IPSCC en hopelijk lopen we elkaar nog eens tegen het lijf op een congres voor een biertje.

Ton, **John**, **Christian**, **Pia**, **Daniela**, **Marleen**, jullie scherpe commentaar en expertises is altijd zeer waardevol geweest. Het hoge wetenschappelijk niveau van de B6-afdeling is grotendeels aan jullie te danken, en ik ben er trots op dat ik daar deel van mocht uitmaken.

Piet en **Daniel V**, dank voor jullie hulp, tijd en kritisch blik op onze data en projecten.

Ron, **Els**, bedankt jullie hulp bij het opvragen en sequencen van onze samples.

Michelle, gelukkig had je al een flink portie zelfstandigheid, want mij vinden was niet altijd eenvoudig. Jouw begeleiden was niet alleen leerzaam, maar ook gewoon heel leuk.

Julia, **David**, **Pierre**, **Georgie**, **Kong**, **Thomas**, **Maarten**, ik heb genoten van jullie op de afdeling, de discussies en het hoge niveau van het onderzoek. Ik hoop jullie te zien op het feestje begin oktober!

Bob, **Laurens**, hartelijk dankjewel voor alle gezelligheid op de CB, de dinertjes en het opsporen van kromme Nederlandse zinnen. Hartstikke dankjewel.

Hilje, **Marloes**, ik vond het leuk en erg leerzaam dat jullie me de kans hebben gegeven mijn onderzoek aan een breder publiek uit te leggen. Het NKI zou het NKI niet zijn zonder zo sterke PR-afdeling.

CURRICULUM VITAE AND LIST OF PUBLICATIONS

Salo Noël Ooft was born on January 29th 1991 in Spijkenisse. He attended primary school in Brielle at the RKBS St. Leonardusschool and VWO Gymnasium at 't Maerlant College, majoring in nature and health. Following his biology thesis on cancer he moved to Utrecht to study Biomedical Sciences at Utrecht University. During his last year of the bachelor program he attended Lund University in Sweden as part of the EU Erasmus exchange program, which was followed by a master in Cancer, Genomics and Development Biology back at Utrecht University. He performed research internships in the labs of Prof. Saskia van Mil (UMC Utrecht) and Prof. Jacco van Rheenen (Hubrecht Institute) on intestine-liver signaling and cancer biophysics, respectively, and wrote his thesis on repurposing the heralded CRISPR-Cas9 technology to answer fundamental questions on causality in gene regulation in the lab of Prof. Wouter de Laat at the Hubrecht Institute. His literature and research studies at the Hubrecht Institute brought him in close contact with the organoids culture system of Prof. Hans Clevers. He moved to Amsterdam and joined the lab of Prof. Emile Voest at the Antoni van Leeuwenhoek-Netherlands Cancer Institute to exploit the organoid culture technology for personalized treatment of cancer patients. The results of these efforts are described in this thesis.

Currently, he is part of the National Thinktank 2020. The National ThinkTank Foundation was founded in 2005 and aims to positively impact Dutch society by presenting an independent vision, thorough analyses and innovative solutions. The National ThinkTank 2020 will focus on the resilience of the Dutch middle class, which is under pressure due to – among others – flexibilisation of the labour market and the lack of affordable housing. The project is facilitated by McKinsey & Company and supported by a large number of partner universities, private companies and public institutions.

Published

Kloosterman WP, Coebergh van den Braak RRJ*, Pieterse M*, van Roosmalen MJ*, Sieuwerts AM, Stangl C, Brunekreef R, Lalmahomed ZS, Ooft SN, van Galen A, Smid M, Lefebvre A, Zwartkruis F, Martens JWM, Foekens JA, Biermann K, Koudijs MJ, Ijzermans JNM, Voest EE.
A systematic analysis of oncogenic gene fusions in primary colon cancer. Cancer Res. 2017 Jul 15;77(14):3814-3822.

Weeber F*, Cirkel GA*, Hoogstraat M, Bins S, Gadellaa-van Hooijdonk CGM, Ooft SN, Van Werkhoven E, Willems SM, Van Stralen M, Veldhuis WB, Besselink NJM, Horlings HM, Steeghs N, De Jonge MJ, Langenberg MHG, Wessels LFA, Cuppen EPJG, Schellens JH, Sleijfer S, Lolkema MP, Voest EE. Predicting clinical benefit from everolimus in patients with advanced solid tumors, the CPCT-03 study. Oncotarget 2017 Aug 15; 8(33): 55582–55592.

Weeber F*, Ooft SN*, Dijkstra KK, Voest EE. Tumor organoids as a pre-clinical cancer model for drug discovery. Cell Chem Biol. 2017 Sep 21;24(9):1092-1100

Ooft SN*, Weeber F*, Dijkstra KK#, McLean CM#, Kaing S, van Werkhoven E, Schipper L, Hoes L, Vis DJ, van de Haar J, Prevoo W, Snaebjornsson P, van der Velden D, Klein M, Chalabi M, Boot H, van Leerdam M, Bloemendal HJ, Beerepoot LV, Wessels L, Cuppen E, Clevers H, Voest EE. Patient-derived organoids can predict response to chemotherapy in metastatic colorectal cancer patients. Sci Transl Med. 2019 Oct 9;11(513).

Neto J, Nadal E*, Bosdriesz E*, Ooft SN*, McLean CM, Klarenbeek S, Jurgens A, Hagen H, Wang L, Voest EE, Van Tellingen O, Villanueva A, Bernards R. Multiple low dose therapy as an effective strategy to treat EGFR inhibitor-resistant NSCLC tumours. Nat Commun. 2020 Jun 22;11(1):3157.

Submitted

Ooft SN*, Weeber F*, Schipper L#, Dijkstra KK#, McLean CM, Kaing S, Van de Haar J, Prevoo W, Van Werkhoven W, Snaebjornsson P, Hoes L, Chalabi M, Van der Velden D,, Van Leerdam M, Boot H, Grootscholten C, Huitema ADR, Bloemendal HJ, Cuppen EPJG, Voest EE. Prospective experimental treatment of colorectal cancer patients based on organoid drug responses
(submitted at the Journal of the National Cancer Institute)

Ooft SN, Weeber F, Dijkstra KK, Kaing S, Proost N, Van Gerwen B, Siteur B, De Korte-Grimmerink R, Cattaneo CM, Song J, Van Werkhoven E, Boot H, Van Leerdam M, Bloemendal HJ, Chalabi M, Van der Ven M, Voest EE. In vivo modeling of patient-derived organoids and matched clinical responses
(submitted at Cancer Research)

Van de Haar J*, Ooft SN*, Hoes L, Yoshino T, Van Cutsem E, Mayer RJ, Wessels LFA, Voest EE. Robust genomics-based personalized medicine for TAS-102 (Lonsurf) in metastatic colorectal cancer
(submitted at New England Journal of Medicine)
*/# = equal contribution